



Involvement of Autophagy and Mitophagy in the Pathogenesis of Hepatic Encephalopathy

Inaugural dissertation

for the attainment of the title of doctor

in the Faculty of Mathematics and Natural Sciences

at the Heinrich Heine University Düsseldorf

presented by

Kaihui Lu

from Fujian

Düsseldorf, April 2018

from the Institute of Biochemistry and Molecular Biology I
at the Heinrich Heine University Düsseldorf

Published by permission of the
Faculty of Mathematics and Natural Sciences at
Heinrich Heine University Düsseldorf

Supervisor: Prof. Dr. Andreas Reichert

Co-supervisor: Prof. Dr. Lutz Schmitt

Date of the oral examination: June 19th, 2018

獻給我的母親和父親

遊子吟

(唐) 孟郊

慈母手中線，遊子身上衣。
臨行密密縫，意恐遲遲歸。
誰言寸草心，報得三春暉。

Table of Contents

Table of Contents	I
1. Introduction	1
1.1 Mitochondria	1
1.1.1 Mitochondrial structure and function	1
1.1.2 Mitochondrial dynamics	5
1.1.3 Mitochondrial dysfunction and diseases.....	7
1.1.4 Mitochondrial quality control.....	11
1.2 Autophagy	12
1.2.1 Classification of autophagy and selective types of autophagy	13
1.2.2 The core machinery of autophagy in mammals.....	17
1.2.3 Major pathways regulating autophagy in mammals.....	21
1.2.4 Biological function of autophagy	24
1.2.5 Transglutaminase 2.....	25
1.3 Mitophagy	27
1.3.1 Molecular mechanism of mitophagy in mammals.....	28
1.3.2 Major pathways regulating mitophagy in mammals	31
1.3.3 Biological function of mitophagy in mammals	33
1.3.4 Mitophagy in <i>S. cerevisiae</i>	34
1.4 Hepatic encephalopathy.....	37
1.4.1 Diagnostic and therapy strategies of hepatic encephalopathy	37
1.4.2 The pathogenesis of hepatic encephalopathy	39
1.4.3 Oxidative/Nitrosative stress in hepatic encephalopathy	40
1.4.4 Functional consequences of osmotic and oxidative/nitrosative stress in astrocytes	41
1.5 Working hypothesis: mitochondrial quality control pathways are involved in the pathogenesis of hepatic encephalopathy	45
1.6 Aims of the study	47
2. Materials and Methods	48
2.1 Material	48
2.1.1 Chemicals and materials.....	48
2.1.2 Equipment	50
2.1.3 Consumables	52
2.1.4 Culture mediums and buffers	53
2.1.5 Mammalian cells and <i>E. coli</i> strains.....	55
2.1.6 siRNAs	56
2.1.7 Plasmids	56

2.1.8 Antibodies.....	57
2.1.9 Software	59
2.1.10 Animal tissue lysates	60
2.2 Methods.....	61
2.2.1 Preparation and cultivation of primary rat astrocytes.....	61
2.2.2 Cultivation of human cell lines.....	61
2.2.3 MTT assay.....	62
2.2.4 Trypan blue staining.....	62
2.2.5 Preparation of plasmids from <i>E. coli</i> cells.....	63
2.2.6 siRNA transfection	64
2.2.7 Crude mitochondria isolation	64
2.2.8 TCA precipitation.....	65
2.2.9 SDS-PAGE	65
2.2.10 Western blot.....	66
2.2.11 Immunofluorescence	67
2.2.12 Evaluation of mitochondrial membrane potential via TMRM	67
2.2.13 Fluorescence microscopy	68
2.2.14 Spinning disk confocal microscopy.....	68
2.2.15 Transmission electron microscopy	69
2.2.16 Validation of paNP functionality by pH measurement	69
2.2.17 LysoSensor™ staining and image analysis	70
2.2.18 Magic red cathepsin L activity assay.....	70
2.2.19 Nanoparticle treatment and UV exposure.....	71
2.2.20 Rat models of acute ammonium intoxication	71
2.2.21 <i>Post Mortem</i> human brain tissue	72
2.2.22 Array-based human transcriptome analysis.....	72
2.2.23 Statistical analysis	73
3. Results	74
3.1 Autophagy is partially inhibited by ammonia in cultured rat astrocytes	74
3.1.1 Dual role of ammonia on autophagy in cultured rat astrocytes	74
3.1.2 High concentrations of ammonium treatment inhibit autophagy in various cell lines	76
3.2 Inhibition of autophagy by ammonium is time- and dose-dependent, fast and reversible	76
3.3 Inhibition of autophagy by ammonia is mainly mediated via pH alteration and is decreased by ROS scavengers.....	78
3.3.1 Autophagy inhibition induced by ammonium treatment is mainly mediated by pH alteration	78
3.3.2 Inhibition of autophagy by methylammonium chloride is similar to that induced by ammonium chloride.....	79
3.3.3 Autophagy inhibition can be largely alleviated by intracellular ROS scavengers.....	81
3.3.4 Autophagy inhibition is not dependent on glutamine synthetase or p38MAPK activity.....	83

3.4 Autophagy is impaired in the brains of rats acutely intoxicated by ammonium acetate and the impairment is alleviated by taurine	83
3.4.1 Ammonium treatment results in autophagy inhibition in an <i>in vivo</i> model of HE	83
3.4.2 Taurine treatment reduces the degree of autophagy inhibition in a rat model of HE	85
3.4.3 Taurine treatment reduces the degree of autophagy inhibition induced by ammonia in cultured rat astrocytes.....	85
3.5 TGM2 is upregulated in response to ammonia.....	87
3.5.1 Ammonium treatment leads to upregulation of TGM2 in cultured rat astrocytes	87
3.5.2 Elevated expression level of TGM2 is observed in multiple cell lines.....	88
3.5.3 Elevated expression level of TGM2 is observed in a rat model of HE.....	88
3.5.4 TGM2 mRNA is upregulated in the human cerebral cortex of patients with HE.....	89
3.6 Mitochondrial dysfunction is increased by ammonia in cultured rat astrocytes.....	90
3.6.1 Ammonium treatment leads to mitochondrial fragmentation.....	90
3.6.2 Ammonium treatment results in loss of mitochondrial membrane potential.....	92
3.6.3 High concentrations of ammonia decrease cristae number per mitochondrion	92
3.6.4 Both l-OPA1 and s-OPA1 are accumulated after ammonium treatment.....	94
3.7 Ammonium treatment leads to enhanced Parkin-mediated mitophagy initiation in cultured rat astrocytes.....	95
3.7.1 Ammonium treatment induces Parkin-mediated mitophagy	96
3.7.2 Parkin-mediated mitophagy can also be induced by methylammonium chloride	98
3.8 Ammonium treatment increases NIX-mediated mitophagy initiation in cultured rat astrocytes.....	99
3.8.1 Ammonium treatment induces NIX-mediated mitophagy in non-cancerous cells	99
3.8.2 NIX accumulation is mainly dependent on pH and is affected by ROS level	100
3.9 Ammonia induces PGC-1 α -mediated mitochondrial biogenesis in cultured rat astrocytes	101
3.9.1 Elevation of PGC-1 α expression induced by ammonia is dose- and time-dependent	101
3.9.2 Elevated expression level of PGC-1 α is observed in non-cancerous cells	103
3.10 Knockdown of key autophagy/mitophagy machinery genes sensitizes cells at high concentrations of ammonia.....	103
3.10.1 Ammonia reduces MTT assay activity in cultured rat astrocytes.....	103
3.10.2 Autophagy and mitophagy inhibition do not further sensitize astrocytes to cell death after ammonium treatment.....	106
3.11 Photoactivatable acidifying nanoparticles (paNP) restore autophagic flux in cultured rat astrocytes	107
3.11.1 Quality control of paNP and optimization of treatment conditions	107
3.11.2 paNP relieve ammonia-induced autophagy inhibition in cultured rat astrocytes.....	109
3.11.3 paNP restore cathepsin L activity in cultured rat astrocytes treated with ammonium	111

4. Discussion	112
4.1 Current model.....	112
4.2 Ammonia aggravates mitochondrial dysfunction in the pathogenesis of HE.....	113
4.3 Various mQC degradation pathways are involved in the pathogenesis of HE	115
4.4 Common regulatory mechanisms are underlying ammonia-altered autophagy and mitophagy....	119
4.5 Compensatory mechanisms are possibly triggered in response to ammonia.....	121
4.6 Taurine, NAC, and paNP may serve as bases for future therapeutics against HE.....	125
Summary	128
Zusammenfassung	131
References	134
List of Figures	150
List of Tables	152
Abbreviations	153
Acknowledgements	159
Eidesstattliche Erklärung	161

1. Introduction

1.1 Mitochondria

Mitochondria, usually regarded as the cellular energy powerhouse, are evolutionarily conserved double membrane organelles which perform multiple fundamental cellular processes including oxidative phosphorylation (Mitchell 1961, Saraste 1999), iron-sulfur cluster formation (Lill and Kispal 2000), the biosynthesis of heme and β -oxidation of fatty acids (Scheffler 1999). The origin of mitochondria in eukaryotes is widely accepted to be an α -proteobacterial endosymbiont that was endocytosed by an amitochondriate pro-eukaryotic host (Margulis 1971, Lane and Martin 2010). An important evidence supporting this notion is that in mammals, as distinct from other organelles, mitochondria have their own genome, the mitochondrial DNA (mtDNA), together with independent protein synthesis. Mammalian mtDNAs, almost exclusively inherited maternally, are circular double-stranded molecules which consist of 15,000-17,000 base pairs (Birky 1995, Al Rawi et al. 2011). Human mtDNA only encode for 37 genes (13 oxidative phosphorylation-related protein subunits, 22 mitochondrial tRNAs, and 2 mitochondrial rRNAs) as most of the α -proteobacterial genes are thought to be transferred to the nucleus during evolution (Boore 1999). Thus, after being synthesized in the cytosol, the majority of mitochondrial proteins need to be sorted and imported into mitochondria via highly conserved protein translocation machinery (Mokranjac and Neupert 2009, Schmidt et al. 2010).

1.1.1 Mitochondrial structure and function

Mitochondria exhibit a membrane-enclosed structure that is similar to their bacterial ancestors (Palade 1953). The two membranes separating the cytosol from the mitochondrial matrix consist of phospholipid bilayers and proteins, however, they are quite different structurally and functionally (Mannella et al. 1997).

The outer mitochondrial membrane (OMM) is permeable to small molecules (< 5000 daltons) while larger proteins can pass the outer membrane only with the help of translocases, such as the translocase of the outer membrane (TOM) complex (Neupert 1997) and the topogenesis of mitochondrial outer-membrane beta-barrel proteins (TOB) complex (Waizenegger et al. 2004). Besides being the location of numerous enzymes and receptors, the OMM is also associated with the endoplasmic reticulum (ER) membrane via a structure called mitochondria-associated membrane (MAM) which is crucial for the regulation of mitochondrial morphology, calcium signaling, lipid transfer, autophagy and mitophagy (van Vliet et al. 2014). The inner mitochondrial membrane (IMM) is rich in proteins and cardiolipin. As it is impermeable to most molecules, special membrane transporters are required for proteins, lipids, and metabolites to enter or exit the matrix. Proteins located in the IMM or matrix are transferred via Oxa1 and translocases of the inner mitochondrial membrane (TIM), *i.e.*, the TIM22 and TIM23 complexes (Stojanovski et al. 2012). In normal mitochondria, the IMM is uniquely compartmentalized into many cristae which further divide the IMM into crista membrane (CM) and inner boundary membrane (IBM). Cristae host various enzymes involved in the electron transport chain (ETC) which also generates a membrane potential. This unique membrane potential is required for many essential mitochondrial functions, for example, mitochondrial protein import. The number and size of cristae are proposed to be highly correlated with the energy demand of individual cells. Crista junctions (CJs) which connect the cristae and IBM are rather small with a diameter of 12 to 40 nm, yet they are considered to be responsible for controlling the profile of cristae components and cristae remodeling (Anand et al. 2016). Abnormal cristae morphology is observed in several human diseases such as Barth syndrome (Finsterer and Frank 2013). Between the two membranes, there is a small aqueous space termed the intermembrane space (IMS). The matrix, enclosed by the IMM, is the site for the ATP production and mtDNA-related protein synthesis. The ultrastructure of mitochondria is schematically depicted in Figure 1.1.

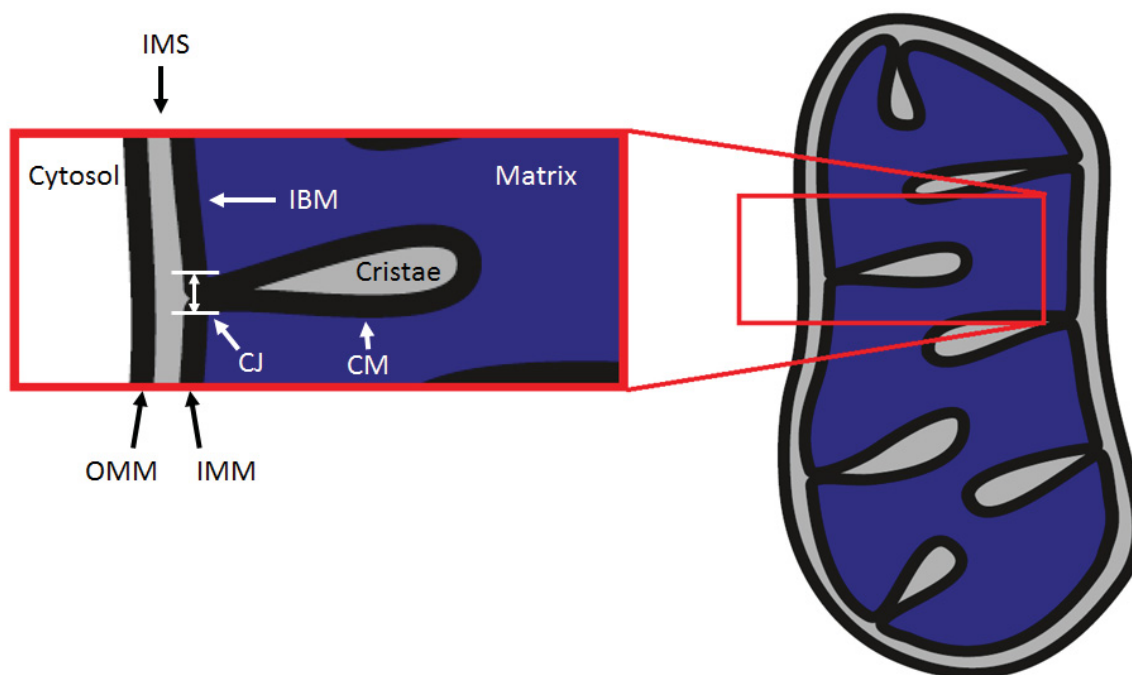


Figure 1.1 Ultrastructure of mitochondria. CJ: crista junction; CM: crista membrane; IBM: inner boundary membrane; IMM: the inner mitochondrial membrane; IMS: intermembrane space; OMM: the outer mitochondrial membrane.

Oxidative phosphorylation probably is the most well-known function of mitochondria, through the cooperation of complex I-V, mitochondria elegantly convert the energy stored in nutrients into the energy stored in ATP. Besides energy production, mitochondria also serve as a hub for controlling various stress responses related to cellular and organellar health. Upon apoptosis-inducing conditions, the release of cytochrome *c* from the mitochondrial IMS marks the initiation of the intrinsic apoptotic pathway which subsequently leads to the activation of caspases and programmed cell death (Jiang and Wang 2004). Mitochondria can also affect ageing via multiple pathways, one fundamental example is that dysfunctional mtDNA polymerase γ can result in the accumulation of mtDNA mutations which occur in various tissues during the ageing process (Trifunovic et al. 2004).

Apart from these functions, mitochondria are also the sole or major player in many intracellular processes including formation and export of iron-sulfur clusters (Lill and Kispal 2000), the TCA cycle, the synthesis of heme and β -oxidation of fatty acids (Scheffler 1999), calcium homeostasis (Rizzuto et al. 2004) and production of signalling reactive oxygen species/reactive

nitrogen species (ROS/RNS) (Newmeyer and Ferguson-Miller 2003). In addition, many mitochondrial proteins are involved in processes relevant to the functionality of mitochondria such as mitochondrial protein translocation, assembly, and degradation, mitochondrial fusion and fission, as well as mitophagy (Reichert and Neupert 2004) (Figure 1.2). Emerging evidence also points out that mitochondria may actively participate in epigenetic control as mitochondria provide various intermediate metabolites required for DNA methylation as well as histone acetylation and methylation. Interesting to note, mtDNA is also methylated under ageing and some pathological conditions, although the functional relevance is still unknown (Matilainen et al. 2017).

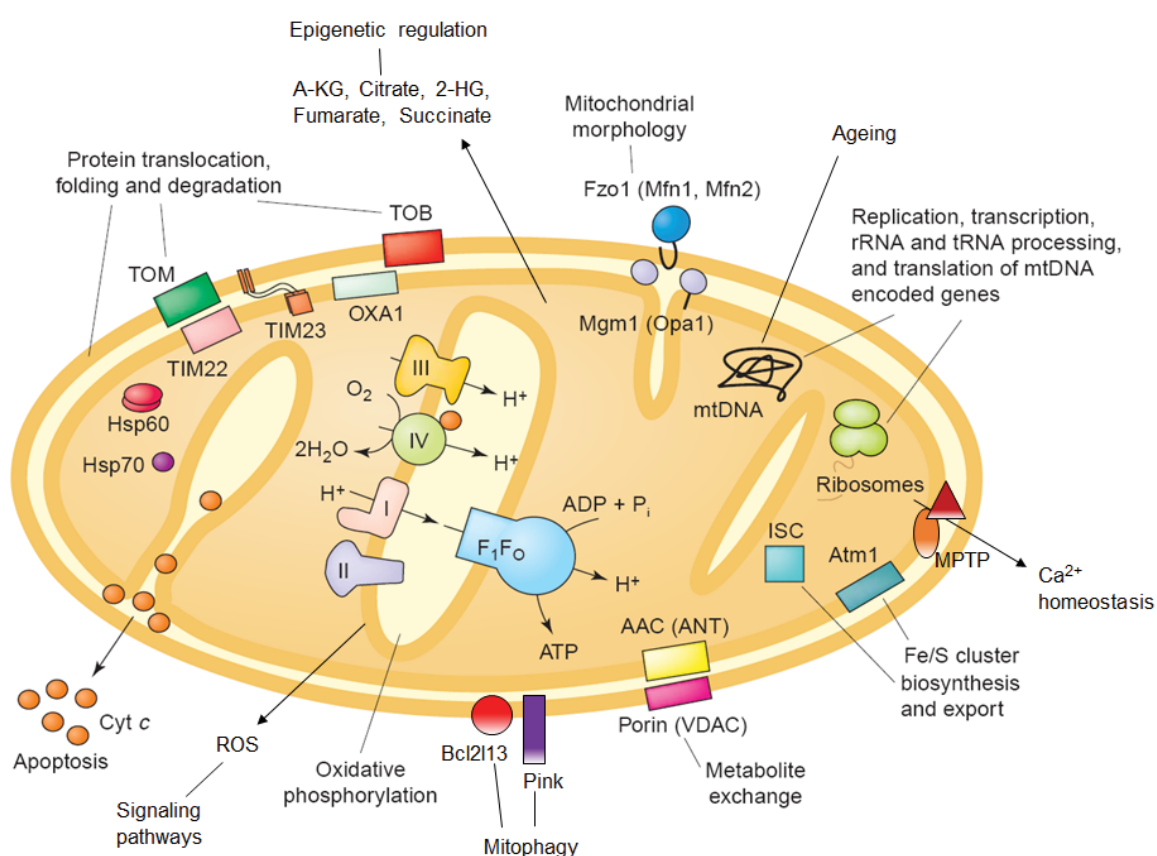


Figure 1.2 The major functions of mitochondria. Overview of the major cellular processes relevant to mitochondria and the key mitochondrial components involved in the respective process (modified from Reichert and Neupert 2004). Yeast proteins are shown with their mammalian counterparts (in parenthesis). Basic mechanisms such as metabolism of certain lipids and amino acids are not shown.

In order to gain a more comprehensive understanding of mitochondrial functions, the scientific community have employed multiple bioinformatic, genetic, transcriptomic, proteomic and

metabolomic approaches to systematically investigate the total number, the sub-mitochondrial location and the relevant function of mitochondrial proteins (Sickmann et al. 2003, Reichert and Neupert 2004, Williams et al. 2016). Currently, it is claimed that there are at least around 700 different proteins residing in the mitochondria of *S. cerevisiae*, and the existence of orthologous kinases in plant and human mitochondria indicates that the number of mitochondrial protein in higher eukaryotes is much larger (Pflieger et al. 2002, Reichert and Neupert 2004).

The versatile functions of mitochondria maybe explained structurally by the facts that (1) compared with other organelles, mitochondria host a large amount as well as a wide range of proteins with distinct functions; (2) the relative complex architecture of mitochondria creates multiple interconnected and compartmented spaces which facilitate the execution of many cellular processes. However from an evolutionary view, it seems reasonable that increased intracellular communication and interaction among mitochondria, cytosol, and other organelles are expected for a better adaptation, thus functionally distinct but not isolated subcompartments need to be created and a large amount of adaptors, carriers, transporters, receptors, as well as channels are required to distribute into these different regions of mitochondria.

1.1.2 Mitochondrial dynamics

Mitochondria are highly dynamic organelles which constantly undergo fusion and fission processes, forming a large plastic interconnected network with many branches surrounding the nucleus region of the cell (Figure 1.3). Besides fusion and fission, mitochondrial movement through the cytoskeleton is recently considered another perspective of mitochondrial dynamics (Ni et al. 2015). Mitochondrial dynamics was proposed to be necessary for synaptic signaling and proper mitochondria and mitochondrial genome distribution during cell growth, division and differentiation (van der Bliek et al. 2013).

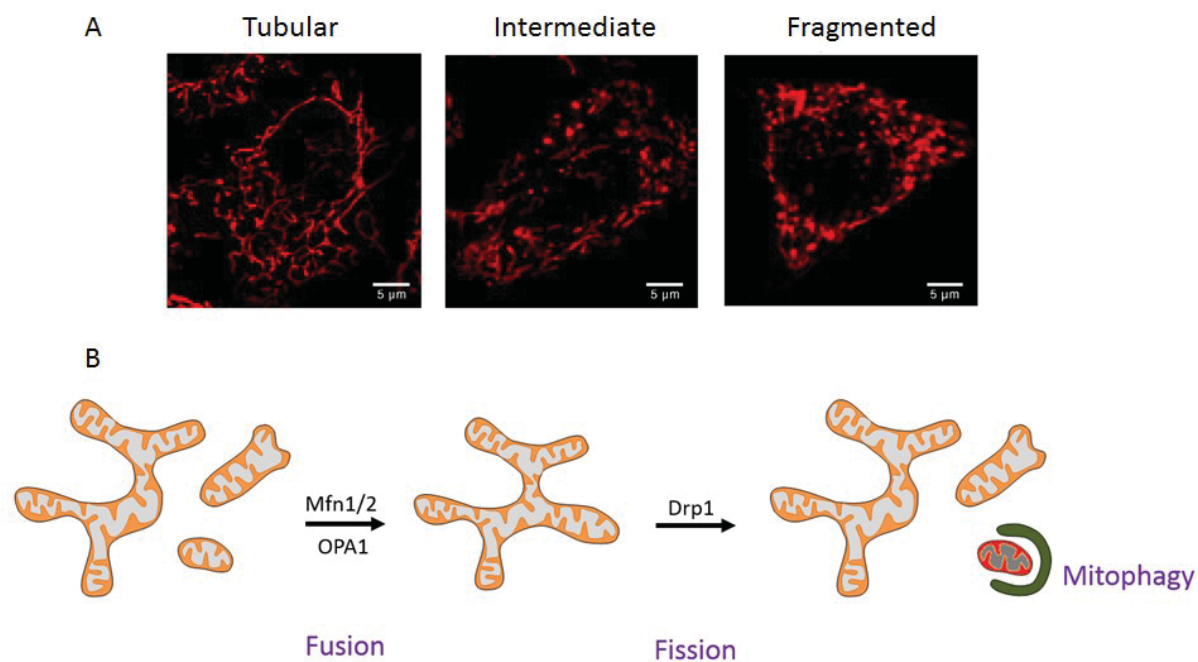


Figure 1.3 Fusion and fission of mammalian mitochondria. (A) Representative images of different mitochondrial morphologies in HeLa cells labeled mitoDsRed (adapted from Frank et al. 2012). (B) A schematic drawing of mitochondrial fusion and fission.

Studies in *S. cerevisiae* uncovered the core components involved in mitochondrial fission and fusion (Hoppins et al. 2007). Following mammalian studies confirmed the evolutionary conservation and identified essential orthologs for the majority of this fission and fusion machinery (Westermann 2010).

Fission in mammalian mitochondria is mediated via the interaction between dynamin-related protein 1 (Drp1) and several mitochondrial receptor proteins such as fission 1 (Fis1) and mitochondrial fission factor (Mff) (Loson et al. 2013). Post-translational modifications of Drp1 were reported to be the key regulatory processes for mitochondrial fission. Phosphorylation of Drp1 at Ser637 by cyclic AMP-dependent protein kinase (PKA) inhibits fission while its dephosphorylation by calcineurin or phosphorylation of Drp1 at Ser616 by Cdk1/cyclin B stimulates fission (Cereghetti et al. 2008, Knott et al. 2008). Besides, ubiquitination of Drp1 by a mitochondrial E3 ligase, MARCH V, regulates its stability while SUMOylation of Drp1 enhances mitochondrial fission (Zunino et al. 2007).

Fusion in mammalian mitochondria is mediated via three dynamin-related GTPases, namely,

mitofusin 1 & 2 (Mfn1 & 2) and optic atrophy 1 (OPA1). Mfn1 & 2 are responsible for the OMM fusion while OPA1 is responsible for the IMM fusion. OPA1 exists in two categories of isoforms: uncleaved l-OPA1 and cleaved s-OPA1. l-OPA1 is essential for mitochondrial IMM fusion while the accumulation of s-OPA1 leads to mitochondrial fragmentation (Duvezin-Caubet et al. 2007). OPA1 processing is executed via the proteases presenilin-associated rhomboid-like (PARL), paraplegin, as well as Yme (Cipolat et al. 2006, Duvezin-Caubet et al. 2007, Griparic et al. 2007). As reviewed by Schäfer and Reichert., OPA1 cleavage has been proposed to be a key process linking mitochondrial morphology to its bioenergetic functionality (Schafer and Reichert 2009).

Mitochondrial fission and fusion have been suggested to be an important quality control mechanism for safeguarding the functionality of mitochondria as damaged mitochondria, separated by the fission mechanism, could not fuse back to the tubular intact mitochondrial network (Twig et al. 2008). In particular, in mammalian systems, on the one hand, mitochondrial fission alone was shown to be not sufficient for triggering mitophagy (Ni et al. 2015), while on the other hand, mitochondrial fission was proved to be a prerequisite for mitophagy under stress conditions (Frank et al. 2012).

1.1.3 Mitochondrial dysfunction and diseases

As mitochondria play a fundamental role in life, it is not surprising that mitochondrial dysfunction is associated with many pathological conditions. One classic view, regarding mitochondrial dysfunction, is that as a result of oxidative phosphorylation, mitochondria are not only the major generators but also direct victims, of excessive ROS (Wallace 2005). The harmful effects of ROS affecting the mitochondrial genome, proteome and mitochondrial quality control systems include massive protein modification, lipid peroxidation, and DNA damage. Indeed, increased oxidative stress was proved to be a cause of decreased mitochondrial membrane potential and increased cell death (Tatsuta and Langer 2008).

Human mitochondrial disorders are associated with a myriad of diseases and pathological

conditions including a variety of neurodegenerative diseases, cancers, ageing, cardiomyopathies, diabetes, and obesity (Gerbitz et al. 1995, Schafer and Reichert 2009, Nunnari and Suomalainen 2012, Boland et al. 2013). Of particular interest, mitochondrial dysfunction is also observed frequently in organs requiring a higher energy demand such as liver and brain (Table 1.1, generated from mitomap.org database). One of the explanations may be that since the liver is the major organ for detoxification, liver cells encounter a higher dose of toxic substances which aggregate the oxidative stress. Besides, long-lived brain cells like neurons strongly depend on mitochondria to execute their normal function. In neurons, mitochondria not only synthesize lipids and supply the metabolite intermediates for GABA as well as glutamate neurotransmitter synthesis, but also control neurotransmission and neurogenesis via modulating Ca^{2+} flux (Waagepetersen et al. 2001, Mayr et al. 2011). These functions are directly or indirectly dependent on the mitochondrial oxidative phosphorylation system (OXPHOS) which composes an essential portion of mtDNA-encoded subunits, thus neurons are susceptible to any pathogenic mtDNA mutations (Schafer and Reichert 2009, Nunnari and Suomalainen 2012).

Table 1.1 List of liver and brain diseases associated with mitochondrial dysfunction.

Component	Dysfunction	Encoded	Clinical phenotype
16S rRNA	Mutation	mtDNA	MELAS, Rett syndrome, Alzheimer's disease, Parkinson's disease
APTX	COQ10 biosynthesis	nDNA	Cerebellar ataxia oculomotor apraxia
BOLA3	Iron homeostasis	nDNA	Encephalomyopathy
CABC1	COQ10 biosynthesis	nDNA	Cerebellar ataxia
Complex I	Assembly	nDNA	Cardioencephalomyopathy, early onset progressive encephalopathy, neonatal/infantile encephalopathy, LS, encephalomyopathy, hypertrophic cardiopathy encephalopathy
	NADH:Ubiquinone Oxidoreductase	mtDNA	Leber's hereditary optic neuropathy
	NADH:Ubiquinone Oxidoreductase	nDNA	LS, encephalopathy
Complex II	Assembly	nDNA	Leukoencephalopathy
	Succinate dehydrogenase complex	nDNA	LS, phaeochromocytoma
Complex III	Assembly	nDNA	Encephalopathy, hepatic failure, LS
	Cytochrome <i>b-c1</i> complex	mtDNA	Leber's hereditary optic neuropathy
	Cytochrome oxidase	mtDNA	Leber's hereditary optic neuropathy
	Electron transfer	nDNA	Severe neurological phenotype
Complex IV	Apoptosis	nDNA	Encephalomyopathy
	Assembly	nDNA	LS
	Copper transport	nDNA	Neonatal hepatic failure and encephalopathy, neonatal cardioencephalomyopathy
	COX1 translation	nDNA	LS
	Cytochrome oxidase	nDNA	Encephalomyopathy
	Heme A farnesyltransferase	nDNA	Neonatal encephalopathy, LS
Complex V	Assembly	nDNA	Early-onset encephalopathy, neonatal encephalopathy
	ATPase	nDNA	Mental retardation, peripheral neuropathy
	ATP synthase	mtDNA	Leber's hereditary optic neuropathy
COQ2	COQ10 biosynthesis	nDNA	Encephalomyopathy, nephropathy
COQ4	COQ10 biosynthesis	nDNA	Encephalomyopathy, mental retardation

DARS2	Mitochondrial translation	nDNA	Leukoencephalopathy and lactic acidosis
DDP	Protein import	nDNA	Mohr-Tranebjaerg syndrome
EFG1	Mitochondrial translation	nDNA	Severe hepatoencephalopathy and lactic acidosis
ETHE1	Ethylmalonic acid metabolism	nDNA	Encephalopathy
FRDA	Iron homeostasis	nDNA	Neuropathy
MFN2	Fusion	nDNA	Charcot-Marie-Tooth disease
mtDNA	Stability	nDNA	Alpers syndrome, SANDO syndrome, hepatocerebral MDDS, MNGIE, encephalomyopathy
PDHA1	Pyruvate dehydrogenase	nDNA	LS
PDSS1	COQ10 biosynthesis	nDNA	Mental retardation
PDSS2	COQ10 biosynthesis	nDNA	LS, nephrotic syndrome
RARS2	Mitochondrial translation	nDNA	Pontocerebellar hypoplasia
tRNA Arg	Mutation	mtDNA	Encephalopathy
tRNA Asn	Mutation	mtDNA	Encephalomyopathy, multi-organ failure
tRNA Asp	Mutation	mtDNA	Encephalomyopathy
tRNA Cys	Mutation	mtDNA	Encephalomyopathy
tRNA Gln	Mutation	mtDNA	MELAS, Alzheimer's disease, Parkinson's disease, migraine
tRNA Glu	Mutation	mtDNA	Encephalopathy
tRNA Gly	Mutation	mtDNA	Encephalomyopathy
tRNA His	Mutation	mtDNA	Encephalomyopathy, MERRF
tRNA Ile	Mutation	mtDNA	Encephalomyopathy, multisystem disease
tRNA Leu	Mutation	mtDNA	MELAS, MERRF
tRNA Lys	Mutation	mtDNA	Encephalomyopathy, MERRF
tRNA Phe	Mutation	mtDNA	MELAS, MERRF
tRNA Pro	Mutation	mtDNA	Encephalopathy
tRNA Ser	Mutation	mtDNA	Encephalomyopathy
tRNA Thr	Mutation	mtDNA	Encephalomyopathy
tRNA Trp	Mutation	mtDNA	LS, dementia, chorea
tRNA Val	Mutation	mtDNA	Encephalomyopathy, ataxia, LS, MELAS, movement disorder
TFSM	Mitochondrial translation	nDNA	Encephalomyopathy

LS: leigh syndrome; MDDS: mtDNA depletion syndrome; MELAS: mitochondrial encephalomyopathy, lactic acidosis and stroke-like episodes; MERRF: myoclonic epilepsy and ragged red fiber disease; MNGIE:

mitochondrial neurogastrointestinal encephalopathy; SANDO: sensory ataxic neuropathy, dysarthria, and ophthalmoparesis.

More details of the listed mitochondria-associated diseases can be found at <http://www.mitomap.org>. Unfortunately, therapeutics are still lacking for these mitochondrial disorders (Nunnari and Suomalainen 2012).

1.1.4 Mitochondrial quality control

Mitochondrial quality control (mQC) describes a pleiotropy of pathways that, executed at multiple levels, counteract the accumulation of mitochondrial dysfunction. First, at the molecular level, mitochondria can degrade those imported misfolded or damaged mitochondrial proteins via their own proteolytic system (Baker and Haynes 2011) while the damaged proteins anchored in the OMM can be degraded by the ubiquitin-proteasome system (UPS) (Karbowski and Youle 2011). At the sub-organellar level, under various stress conditions, damaged mitochondria can be separated for degradation via the mitochondrial fission machinery (Frank et al. 2012) or the formation of mitochondria-derived vesicles (MDV) (Soubannier et al. 2012). Formation of mitochondrial spheroids and subsequent lysosomal markers-incorporated structures was reported to be an alternative pathway for maintaining mitochondrial homeostasis (Ni et al. 2015). At the organellar level, damaged mitochondria can be degraded via general autophagy or the more specific mitophagy (Youle and Narendra 2011). Finally, when the damage is too severe, apoptosis can be induced via the intrinsic pathway as a final means of mQC at the cellular level (Maiuri et al. 2007).

Inside cells, it is expected that mQC is ensured by the coordination of multiple mQC degradation pathways. Indeed, proteins of different sub-mitochondrial locations exhibit distinct degradation rates during dysfunctional mitochondrial removal (Yoshii et al. 2011, Abeliovich et al. 2013).

Among the numerous means by which a cell ensures its mitochondrial quality, autophagy and

selective mitophagy represent two important mitochondrial degradation pathways at the organelle level. The importance of these pathways is well documented in various neurodegenerative diseases such as Parkinson's disease, but not for hepatic encephalopathy.

Important to note, to compensate for the loss of mitochondrial mass and functionality due to mitochondrial degradation, a mitochondrial biogenesis mechanism is necessary for maintaining the mitochondrial homeostasis. Peroxisome proliferator-activated receptor gamma coactivator 1 alpha (PGC-1 α) was reported to be mainly responsible for the mitochondrial biogenesis, in response to environmental changes. Under starvation or mitochondrial disease conditions, increased NAD⁺:NADH or AMP:ATP ratios would activate the key nutrient sensors, Sirtuin 1 (Sirt1) and AMP-activated kinase (AMPK) which subsequently activate the transcription factor, PGC-1 α , to stimulate mitochondrial biogenesis while in nutrient-rich conditions, the lysine acetyltransferase 2A (GCN5) would be activated which would inactivate PGC-1 α via acetylation (Canto and Auwerx 2009, Jeninga et al. 2010). Mitochondrial biogenesis was inhibited in mouse models with long-term OXPHOS dysfunction, increased mitochondrial biogenesis was shown to delay relevant pathogenesis of mitochondrial diseases (Viscomi et al. 2011). These evidence indicate the potential of therapies enhancing mitochondrial biogenesis.

1.2 Autophagy

Autophagy, whose molecular mechanism was discovered and elucidated by Prof. Yoshinori Ohsumi, describes a degradation process via which a cell digests its unwanted organelles and components in autolysosomes to eliminate toxic components and provide additional nutrients and energy under various stress conditions (Okamoto 2014, Yin et al. 2016). Prof. Yoshinori Ohsumi was awarded the Nobel Prize in Physiology or Medicine 2016 “for his discoveries of mechanisms for autophagy”. Evidence gained during the last decades emphasizes the significance of autophagy in various cellular processes including stress response, cellular/organelle homeostasis, cell death, inflammation and maturation (Yin et al. 2016).

1.2.1 Classification of autophagy and selective types of autophagy

Depending on the substrates, autophagy can be categorized into two major classes, non-selective autophagy and selective types of autophagy. Depending on the mechanisms of action, autophagy can be further divided into three types, namely, macroautophagy, microautophagy and chaperone-mediated autophagy (CMA), based on morphological characteristics (Okamoto 2014) (Fig. 1.4). Macroautophagy (hereafter referred to as autophagy) is the most well-studied form of autophagy. It describes a process in which cytoplasmic components are engulfed in the *de novo* synthesized double-membrane-encapsulated autophagosomes, delivered to and finally degraded in autolysosomes via fusion of autophagosomes and lysosomes. The term 'microautophagy' coins a process through which proteins and organelles are directly taken up via invagination of lysosomal membranes, leading to break down of the cargos. Distinct from the above mentioned two forms of non-selective autophagy, chaperone-mediated autophagy (CMA) is only found in mammals and only digests proteins. In CMA, substrates are degraded with the participation of the core autophagy machinery, proteins first need to be associated with the molecular chaperone Hsc70 in order to be taken up into the lysosome lumen by the receptor Lamp-2A (Kaushik and Cuervo 2012).

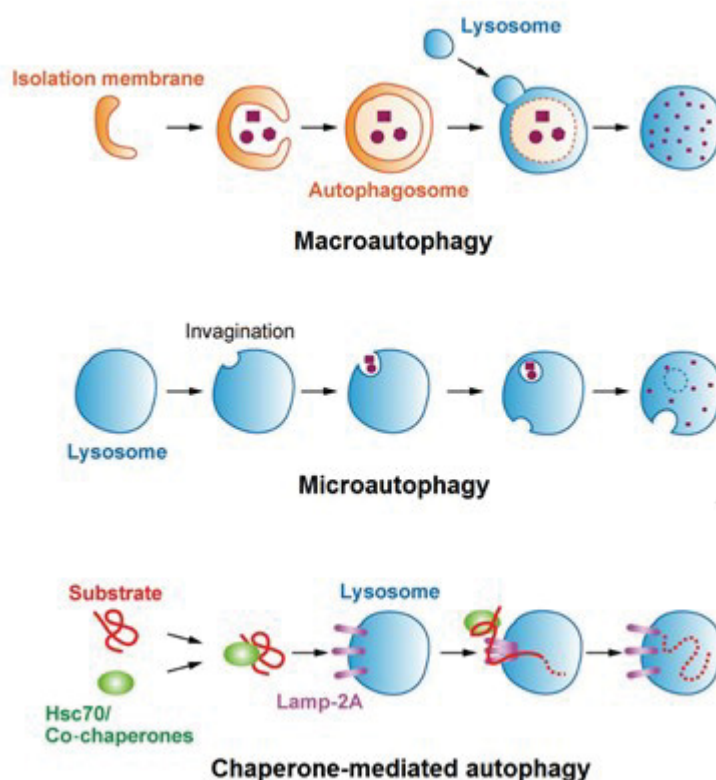


Figure 1.4 Major types of autophagy in mammals. Based on different mechanisms of action, autophagy can be mainly divided into three distinct forms, namely, macroautophagy, microautophagy and chaperone-mediated autophagy (adapted from Okamoto 2014).

Selective types of autophagy describe a series of pathways in which specific cellular components are delivered to lysosomes with the help of autophagy receptors, autophagy adaptors, and isolation membranes. Numerous selective types of autophagy have been discovered and named after the specific cargo they degrade (Khaminets et al. 2016).

Among them, mitophagy represents the relevant pathways that specifically target and degrade surplus or dysfunctional mitochondria, which will be described in detail in Chapter 1.3. Interesting to note, except Golgi apparatus, it seems that all other major cellular organelles have their respective selective degradation pathways. The hallmark of these selective pathways is the recognition of the particular cargoes for specific degradation, which is usually mediated by autophagy receptors and organellar landmark molecules in a ubiquitin (Ub)-dependent or ubiquitin-independent manner (Khaminets et al. 2016), thus ubiquitination and phosphorylation are the major two post-translational regulators in selective types of autophagy (Fig. 1.5).

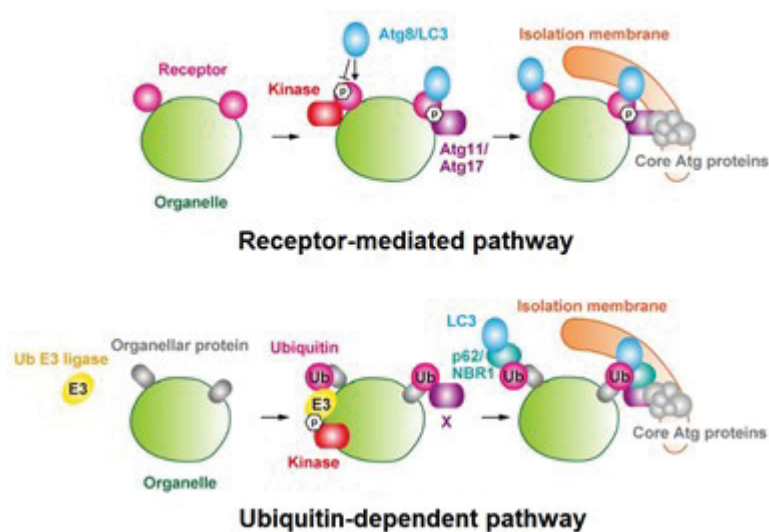


Figure 1.5 Two common modes of selective types of autophagy in mammals. There are two common molecular mechanisms underlying cargo recognition in various selective types of autophagy, namely, receptor- and ubiquitin-mediated pathways (adapted from Okamoto 2014).

Table 1.2 summarizes currently known receptors that are involved in respective selective types of autophagy. Despite the poor conservation of respective autophagy receptors from yeast to human, functional homologs are present for most of the selective types of autophagy, highlighting the highly-conserved basic principle for selective types of autophagy. Considering the bacterial ancestry of mitochondria, there may be evolutionarily conserved connections between mitophagy and xenophagy, as discussed by Lazarou (Lazarou 2015).

Table 1.2 List of selective types of autophagy.

Pathway	Substrate	Receptor, Ub- dependent pathway	Receptor, Ub- independent pathway	Y	M	Reference
Aggrephagy	Protein aggregate	p62, NBR1, OPTN, Cue5, TOLLIP	-	√	√	(Pankiv et al. 2007, Lu et al. 2014)
Cvt targeting	Ape1, Ams1	-	Atg19, Atg34	√	-	(Suzuki et al. 2010)
ER-phagy	ER	-	FAM134B, Atg40	√	√	(Khaminets et al. 2015, Mochida et al. 2015)
Fatty acid synthase disposal	FAS	-	FAS	√	-	(Shpilka et al. 2015)
Ferritinophagy	Ferritin	-	NCOA4	-	√	(Mancias et al. 2014)
Glycophagy	Glycogen	-	Stbd1	-	√	(Jiang et al. 2011)
Granulophagy	Stress granule	-	-	√	√	(Buchan et al. 2013)
Lipophagy	Lipid droplet	-	-	-	√	(Singh et al. 2009)
Lysophagy	Lysosome	-	Galectin-8	-	√	(Thurston et al. 2012)
Midbody disposal	Midbody	p62, NBR1	-	-	√	(Kuo et al. 2011)
Mitophagy	Mitochondrion	OPTN, NDP52, Tax1BP1	NIX, BNIP3, FUNDC1, Atg32	√	√	(Kanki et al. 2009, Quinsay et al. 2010, Liu et al. 2012, Sarraf et al. 2013, Wong and Holzbaur 2014, Lazarou et al. 2015)
Myelinophagy	Myelin	-	-	-	√	(Gomez-Sanchez et al. 2015)
Nucleic acid disposal	Nucleic acid	p62, NDP52	-	-	√	(Guo et al. 2014)
Nucleophagy	Nuclear envelop	-	Atg39	√	√	(Mijaljica and Devenish 2013, Mochida et al. 2015)

Pexophagy	Peroxisome	NBR1	NBR1, Atg30, Atg36	√	√	(Farre et al. 2008, Motley et al. 2012, Deosaran et al. 2013)
Proteaphagy	Proteasome	RPN10, Cue5,p62	-	√	√	(Marshall et al. 2015, Cohen- Kaplan et al. 2016, Marshall et al. 2016)
Ribophagy	Ribosome	-	-	√	√	(Kraft et al. 2008, Cebollero et al. 2012)
Signalophagy	Src	-	c-Cbl	-	√	(Sandilands et al. 2011)
Virophagy	Viral component	-	TRIM5 α , SMURF1	-	√	(Orvedahl et al. 2011, Mandell et al. 2014)
Xenophagy	Bacteria	p62, NDP52, OPTN	Galectin-8	-	√	(Thurston et al. 2009, Wild et al. 2011, Thurston et al. 2012)
Zymophagy	Zymogen	p62	-	-	√	(Grasso et al. 2011)

Y: yeast; M: mammal; √: reported; -: not reported.

1.2.2 The core machinery of autophagy in mammals

Through yeast/fungi genetic studies, scientists currently identified around 40 AuTophagy-related (ATG) genes (Araki et al. 2013, Yao et al. 2015), among which around 20 Atg genes are responsible for autophagosome biogenesis in non-selective and selective autophagy, forming the core autophagy machinery. Of note, some Atg genes (e.g. Atg32) are only involved in a certain selective autophagy pathway. As autophagy is an evolutionarily conserved process, homologs of the majority of these Atg genes also exist in mammalian cells and can be further divided into at least four subgroups: first, the Ulk1 & 2 complexes; second, two ubiquitin-like protein (Atg12 and LC3) conjugation systems; third, the class III PI3K complex; and fourth, two transmembrane proteins (mATG9 and VMP1) and their associated proteins (Yang and

Klionsky 2010).

Autophagy is a highly structured process and classically can be divided into five sequential steps: induction, nucleation, expansion, fusion and cargo degradation (Yang and Klionsky 2010). Components of the core autophagy machinery participate in each of these steps (Fig. 1.6), which is elaborated briefly in the following sections.

Induction and Ulk1 & 2 complexes

In yeast, induction of autophagy is mediated via activation of a complex consisting of the serine/threonine kinase Atg1, Atg13, and Atg17, which act directly downstream of the target of rapamycin complex 1 (TORC1). Inhibition of TORC1 dephosphorylates Atg13, enhances formation of the Atg1-Atg13-Atg17 complex and thus activates autophagy (Suzuki et al. 2007). Ulk1 & 2 are the mammalian homologs of Atg1, which also form a complex with the mammalian homolog of Atg13 and the mammalian ortholog of Atg17, FIP200. Mammalian TORC1 (mTORC1) is associated with the Ulk1-Atg13-FIP200 complex under nutrient-rich conditions, however, under nutrient deprivation, mTORC1 quickly dissociates from the Ulk1-Atg13-FIP200 complex, leading to dephosphorylation and activation of Ulk1 & 2 which subsequently phosphorylates Atg13 and FIP200 to initiate autophagy (Hosokawa et al. 2009, Jung et al. 2009). Atg101, another gene essential for autophagy, was found to be associated with Ulk1 in an Atg13-dependent manner (Mercer et al. 2009).

Nucleation and class III PI3K complex

Nucleation refers to the process of delivering a small group of molecules to the autophagosome formation sites (the mammalian counterpart of yeast phagophore assembly sites, PAS). Upon induction of autophagy, one of the key processes facilitating nucleation is the recruitment of class III PI3K complex to the autophagosome formation site. Similar to their yeast counterpart, the mammalian class III PI3K complex also includes five distinct proteins, Vps34, p150 (mammalian homolog of Vps15), Beclin1 (mammalian homolog of Atg6), Atg14L and

UVRAG (mammalian ortholog of Vps38) (Itakura et al. 2008). Briefly, the class III PI3K complex amplifies the recruitment of other Atg proteins to the autophagosome formation site via synthesis of phosphatidylinositol 3-phosphate (PtdIns3P) which is responsible for the correct trafficking of some Atg proteins (Burman and Ktistakis 2010). Of note, Rubicon, a protein able to decrease hVps34 activity, inhibits autophagy via forming a complex with UVRAG, Beclin 1, hVps34 and p150 which later places an unfavorable impact on autophagosome maturation (Matsunaga et al. 2009). Emerging evidence has continuously highlighted the different regulatory effects of class III PI3K complex on autophagy, during both autophagosomes formation and maturation processes (Yang and Klionsky 2010).

Expansion and ubiquitin-like conjugation systems

Formation of autophagosome via expansion is a main characteristic of autophagy, which requires the participation of two highly conserved ubiquitin-like conjugation systems, the Atg5-Atg12-Atg16L complex, and the Atg3-Atg7-LC3 system. Atg12, a ubiquitin-like protein, is conjugated with Atg5 via the E1 enzyme activity of Atg7 and the E2 enzyme activity of Atg10, then this Atg5-Atg12 conjugate further interacts and oligomerizes with Atg16L, forming a large multimeric complex. By contrast, LC3 (mammalian homolog of Atg8), the other ubiquitin-like protein, is conjugated in a different mode. LC3 is first cleaved by the protease Atg4 to generate the cytosolic LC3-I. The covalent conjugation of phosphatidylethanolamine (PE) to LC3-I is then executed with the help of the E1 enzyme Atg7, the E2 enzyme Atg3, and the E3 enzyme, the Atg5-Atg12-Atg16L complex, converting LC3-I to the autophagosome membrane-localized LC3-II (Ohsumi 2001).

Trafficking, fusion and transmembrane protein mAtg9

In mammalian cells, mammalian Atg9 (mAtg9) has been proposed to be the major contributor to membrane shuttling as it is the only multi-spanning membrane member of the Atg proteins (Yang and Klionsky 2010). Upon starvation or treatment of rapamycin, mAtg9 translocates from the trans-Golgi network (TGN) and late endosomes to the peripheral pool and colocalizes with LC3. Similar to the yeast Atg9 trafficking, the mammalian process has also been proved

to be mediated via Ulk1 and Vps34 (Young et al. 2006). Recent studies revealed more regulators of Atg9 trafficking and subsequent autophagosome formation, including two RABGAPs, TBC1D5 and TBC1D14 as well as the Src kinase (Popovic and Dikic 2014, Lamb et al. 2016, Zhou et al. 2017). Of note, besides Atg9, vacuole membrane protein 1 (VMP1), a transmembrane protein interacting with Beclin1, was also identified as another transmembrane protein required for the membrane trafficking (Ropolo et al. 2007). Once the formation is completed, the autophagosome targets to and fuses with the lysosome to become the autolysosome in which the delivered cytosolic contents are degraded.

Cargo degradation and Atg15, Atg22

The core autophagy machinery has also been proved to be involved in the final step of autophagy, the degradation process, in *S. cerevisiae*. Atg15, a putative lipase, controls the degradation of autophagic body membrane while Atg22, a permease, assists in recycling the macromolecules produced from digestion back to the cytosol (Teter et al. 2001, Yang et al. 2006). However, currently, the mammalian homologs/orthologs of Atg15 and Atg22 have not been discovered yet.

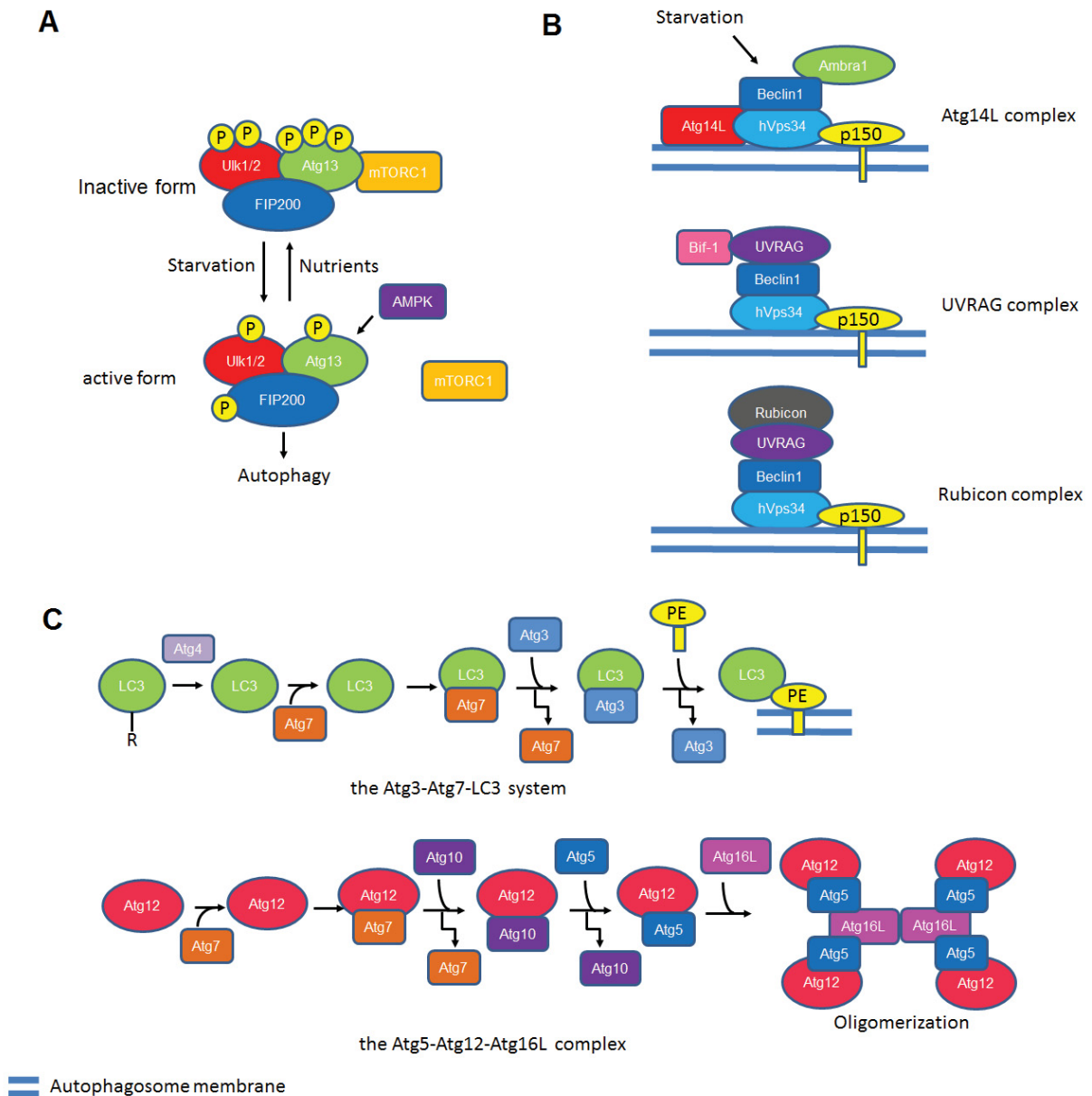


Figure 1.6 The core machinery of mammalian autophagy. (A) The Ulk1 complex in autophagy induction. (B) The class III PI3K complex in nucleation and autophagosome maturation. The Atg14L complex and the UVRAG complex enhance autophagy induction while the Rubicon complex hinders autophagosome maturation. (C) The two ubiquitin-like conjugation systems in membrane expansion.

1.2.3 Major pathways regulating autophagy in mammals

Autophagy, as one of the two major intracellular degradation pathways (the other being the ubiquitin-proteasome system, UPS), is consistently maintained at the basal level in normal,

healthy cells to eliminate damaged or excessive proteins and organelles. However, it can be dramatically evoked as a cytoprotective process by various stress stimuli including starvation, growth factor withdrawal, hypoxia, ER stress and iron depletion (Yin et al. 2016). Moreover, when autophagy is deregulated or excessive, it could also lead to autophagic cell death. Thus, autophagy as a crucial intracellular process needs to be tightly regulated. In mammals, autophagy is regulated by multiple signaling pathways, among which, the mechanistic target of rapamycin (mTOR) and protein kinase A (PKA) are impressive negative regulators while the AMP-activated protein kinase (AMPK) is a potent positive regulator.

Nitrogen-dependent mechanisms

In mammals, mTOR, a conserved serine/threonine kinase which senses and integrates multiple nutrition-related signals to coordinate cellular catabolism and growth, serves as the major negative regulator of autophagy. In response to amino acids, mTORC1 is translocated to the lysosomal membrane with the help of RAG proteins and the Ragulator complex and subsequently activated by the GTPase RHEB (Sancak et al. 2010). Upon nitrogen starvation, mTORC1 is inactivated, resulting in the dephosphorylation of Ulk1 through protein phosphatase 2A and the translocation of unphosphorylated transcription factor EB (TFEB) to the nucleus which activates transcription of numerous genes in autophagy (Settembre et al. 2011, B'Chir et al. 2013). Important to note, rapamycin, a macrolide compound isolated from the bacterium *Streptomyces hygroscopicus*, can also stimulate autophagy by inhibiting the mTORC1, independent of the nutrition status (Heitman et al. 1991). In addition, upon nitrogen starvation, the acetylated Atg7, Atg8, Atg12 and Atg5 dissociate from the acetyltransferase p300 and are deacetylated by Sirt1, increasing the autophagosome biogenesis (Lee and Finkel 2009).

Glucose/Energy-dependent mechanisms

AMPK is a major bioenergetic sensor activated by an increased AMP/ATP ratio. In mammalian

cells, glucose/energy depletion causes activation of AMPK which stimulates autophagy via mTORC1 inhibition through direct phosphorylation of Raptor, a mTORC1 subunit or phosphorylation and activation of the TSC1/2 complex, a negative regulator of mTORC1 (Russell et al. 2014). Furthermore, AMPK can also directly phosphorylate and activate Ulk1 (Kim et al. 2011). Besides the AMPK pathway, FOXO1/3, two transcription factors that are responsible for the transcription of several Atg genes, were reported to be deacetylated and thus activated upon glucose depletion (Feng et al. 2015).

Ubiquitination and autophagy

Ubiquitin (Ub), serves not only as a signal in the recognition of cargoes destined for the UPS or autophagic degradation but also controls the rate of autophagosome biogenesis via direct targeting of the core autophagy machinery and the key upstream signaling pathway components. For instance, ubiquitination of optineurin (OPTN) by the E3 ligase HACE1 increases its affinity to p62, thus enhancing the production of the autophagy receptor complex and affecting the intracellular autophagic activity (Liu et al. 2014).

Regulation of lysosomal degradation

Autophagy is also regulated at the final degradation stage via modulation of the lysosomal function. Since almost all lysosomal hydrolases which degrade the cytosolic content in autolysosomes are only active at an acidic pH which is maintained via proton pumps consuming ATP, there are mainly two modes of lysosomal dysfunction which lead to blockage of autophagy: defective expression or transport of lysosomal enzymes as well as defects in the lysosome acidification (Koike et al. 2005, Yogalingam and Pendergast 2008). Thus, an elevated lysosomal pH caused by various neutralizers is usually associated with the blockage of intracellular autophagic flux. Besides the above mentioned regulatory pathways, autophagy also shares some common regulators with apoptosis such as p53 and the Bcl-2 family proteins (Yang and Klionsky 2010).

1.2.4 Biological function of autophagy

Under physiological conditions, autophagy is vital for a wide range of processes such as cellular homeostasis, ageing, development and cell death. Generally speaking, autophagy serves as a housekeeper in the cell, conducting quality control and homeostasis maintenance at multiple levels. At the molecular level, unlike the UPS system which mainly deals with the degradation of short-lived proteins, autophagy is primarily responsible for massive turnover of long-lived proteins. At the organelle level, autophagy is responsible for clearing old, dysfunctional, damaged and excessive organelles, as reviewed in chapter 1.1.4. Modulation of autophagy was proposed as a promising anti-ageing strategy as enhanced autophagy at the whole body level is connected with longer lifespan in different organisms while defective autophagy associates with pathological ageing (Rubinsztein et al. 2011). Autophagy also participates in multiple developmental processes by eliminating unwanted cells or structures. A good example is that part of the sperm mitochondria are degraded through the autophagy machinery after fertilization, leading to the maternal inheritance of mitochondria (Song et al. 2016). Besides specific xenophagy, autophagy also plays fundamental roles in various perspectives of immunity such as antigen presentation, control of the pro-inflammatory response, and maintenance of the adaptive immune system (Deretic et al. 2013).

As autophagy has extensive interplay with other cell death mechanisms such as apoptosis, autophagy is regarded as an important factor in determining cell fate decisions. The double-edged sword effect of autophagy on cell survival is widely discussed. On the one hand, in most organisms, autophagy is initiated primarily as a protective mechanism alleviating various stresses, thus mainly placing a pro-survival effect; but on the other hand, under certain situations, death mechanisms can also be triggered by and executed through autophagy, resulting in so-called autophagic cell death (Yin et al. 2016). For instance, autophagic cell death is caused by autophagy elimination of the iron storage protein ferritin which leads to accumulation of intracellular liable iron and excessive ROS (Gao et al. 2016).

In pathological conditions, deficient autophagy is frequently observed in the background of a

wide range of human diseases, especially cancers and neurodegenerative diseases (Mizushima et al. 2008, Yin et al. 2016). Neuronal cell death in many neurodegenerative diseases is triggered by the accumulation of toxic protein aggregates, indicating a direct linkage between defective autophagy and the disease phenotype (Shibata et al. 2006). Mouse models with reduced autophagy activity in the central nervous system indeed showed symptoms of neurodegeneration (Komatsu et al. 2006). In line with this, marks of insufficient autophagy such as decreased autophagosome biogenesis and inhibited autolysosome degradation were also observed in patient samples of neurodegenerative diseases including Alzheimer's disease and Parkinson's disease (Nixon et al. 2005, Wang et al. 2016). Nevertheless, caution should be taken when using autophagy as a therapeutic strategy since autophagy may also promote some harmful consequences under certain pathological conditions (Yin et al. 2016).

1.2.5 Transglutaminase 2

Transglutaminase 2 (TGM2, TG2, tissue transglutaminase) is a thiol-dependent and Ca^{2+} -dependent crosslinking enzyme which regulates multiple intracellular process via its transglutaminase crosslinking, G protein signaling and kinase activity (Lai and Greenberg 2013). Regulated by alternative splicing, TGM2 mRNA is processed into at least four isoforms which have distinct biological functions (Lai and Greenberg 2013).

As a stress-responsive gene, TGM2 is upregulated under various stress conditions including tissue injury, inflammation, and oxidative stress (D'Eletto et al. 2009, Zhang and Ney 2009, Feng et al. 2010). Ablation of TGM2 leads to an increase in vulnerability towards stress as well as a reduction in mitochondrial complex I activity (Battaglia et al. 2007).

Recently, TGM2 has been linked to autophagy (Akar et al. 2007, D'Eletto et al. 2009, Cao and Huang 2016, Yeo et al. 2016, Zhang et al. 2016) (Fig. 1.7). Akar et al. reported that TGM2, whose expression was regulated by protein kinase C- δ (PKC δ), placed an inhibitory effect on autophagy as knockout of TGM2 resulted in a significant increase in autophagy in pancreatic cells (Akar et al. 2007). However, D'Eletto et al. demonstrated that knockout of TGM2 led to a

dramatic accumulation of LC3-II and a significant decrease in the formation of acidic autolysosomes, suggesting TGM2 plays a positive role in the autophagosome maturation process, possibly via post-translational modification of the cytoskeleton (D'Eletto et al. 2009). In line with this, Yeo et al. also revealed a positive regulation of TGM2 on protein degradation during the late stages of autophagic process. In addition, they identified TGM2 as a downstream target gene of TP53 (Yeo et al. 2016). Besides, TGM2 was frequently seen in couple with NF- κ B to form a self-amplifying loop under autophagy inducing conditions (Ai et al. 2012, Zhang et al. 2016).

Considering the multiple functions of TGM2 and its involvement in autophagy, it is not surprising that abnormality of TGM2 is indicated in many diseases including various cancers, atherosclerosis, neurodegenerative diseases, and autoimmunity (Lai and Greenberg 2013, Cao and Huang 2016). Regarding cancer and autophagy, different effects of TGM2 on oncogenesis have been reported. Some studies found that overexpression/compensatory upregulation of TGM2 resulted in cell survival and chemotherapy resistance (e.g. rapamycin treatment) in cancer cells possibly through autophagy while others find TGM2-associated autophagy placed an inhibitory effect on oncogenic transformation (Cao and Huang 2016, Yeo et al. 2016, Zhang et al. 2016). In neurodegenerative diseases, TGM2 has been proved to be capable of crosslinking proteins such as tau, huntingtin, and α -synuclein, generating neurotoxic aggregates or insoluble inclusions (Lai and Greenberg 2013). Nevertheless, future efforts are needed to elucidate the role of TGM2-mediated autophagy in the pathogenesis of neurodegenerative diseases.

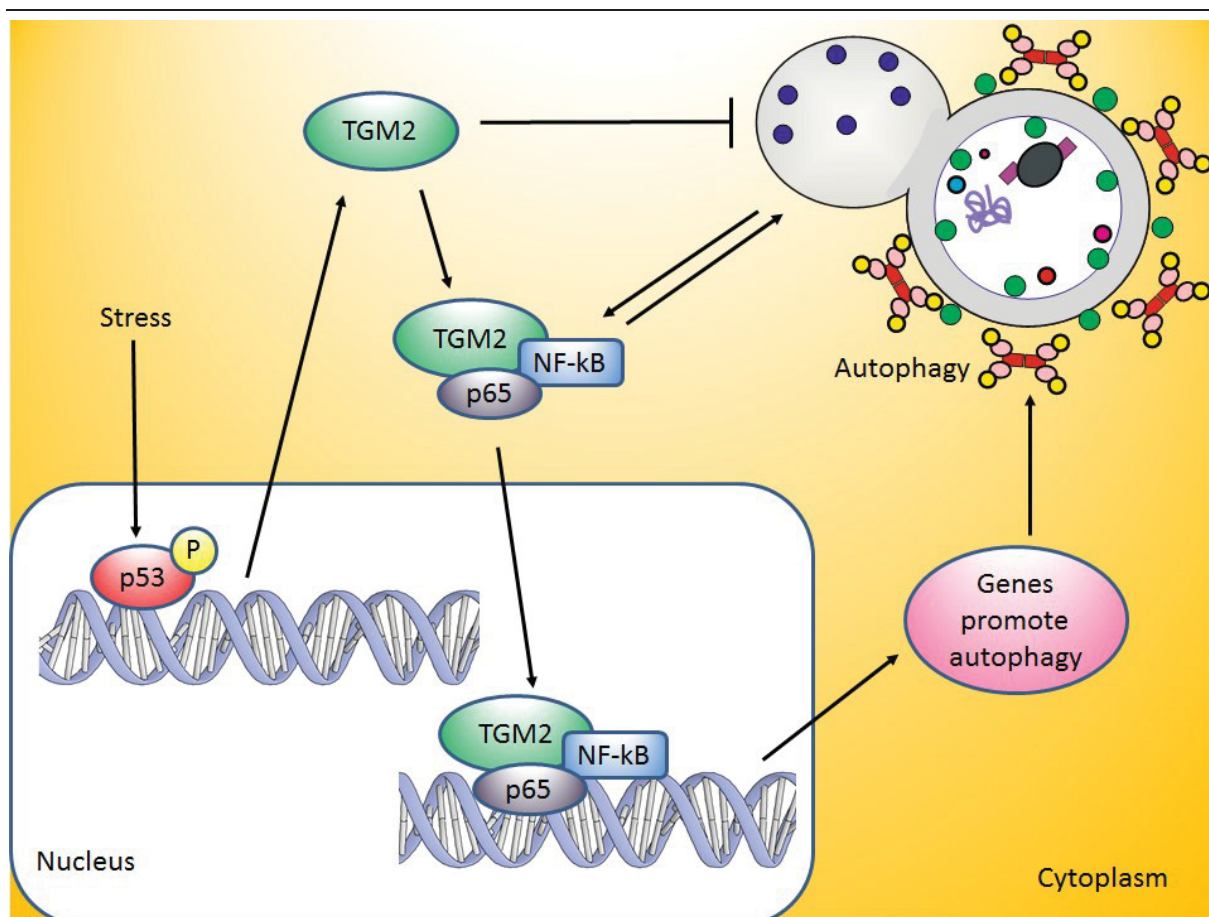


Figure 1.7 Regulation of TGM2 on autophagy. TGM2, a downstream gene of TP53, was mainly reported to place a favourable effect towards autophagy by forming a self-amplifying loop with NF- κ B as well as stimulating transcription of autophagy-prone genes.

1.3 Mitophagy

Lysosomal degradation of mitochondria was first observed in mammalian cells via electron microscopy in the 1960s (Ashford and Porter 1962, De Duve and Wattiaux 1966) and “mitophagy” as a definite concept describing the selective removal of mitochondria via autophagy machinery was developed by John Lemasters in 2005 (Lemasters 2005). The last decade has witnessed a tremendous advance in our knowledge of functions and mechanisms of mitophagy in both yeast and higher eukaryotes, however there are still plenty of open questions in this field.

1.3.1 Molecular mechanism of mitophagy in mammals

As reviewed in Chapter 1.2.1, similar to other selective types of autophagy, mitophagy can be executed through both ubiquitin-dependent and ubiquitin-independent pathways.

Ubiquitin-dependent pathways

Currently, the PTEN-induced putative kinase 1 (PINK1)/Parkin-mediated mitophagy pathway is the best-characterized mechanism for mammalian mitophagy, with its putative purpose being proposed as an mQC pathway to specifically eliminate dysfunctional mitochondria. Briefly, both PINK1 and Parkin, whose abnormalities cause early onset hereditary forms of Parkinson's disease, target the dysfunctional mitochondria to autophagosome (Narendra et al. 2008, Narendra et al. 2010). PINK1, a mitochondrial serine/threonine kinase, is usually internalized into the IMS, cleaved by PARL and then degraded by peptidase in the healthy mitochondria (Jin et al. 2010). Upon mitochondrial membrane potential loss, PINK1 retains its full length and stays on the OMM where it dimerizes and recruits the E3 ubiquitin ligase, Parkin, to the OMM. Phosphorylated by PINK1, Parkin is activated and ubiquitylates various mitochondrial proteins including mitofusins, TOMM20, mitochondrial Rho GTPase (Miro) and voltage-dependent anion channel (VDAC) which leads to mitochondrial fragmentation, aggregation, and mitophagy initiation (Kim et al. 2008, Sha et al. 2010). Nevertheless, PINK1 also phosphorylates other substrates such as ubiquitin to further activate the E3 ubiquitin ligase activity of Parkin (Kane et al. 2014, Koyano et al. 2014).

Once the OMM proteins are ubiquitinated by Parkin, autophagy receptors and associated proteins such as p62, OPTN, NDP52, and Ambra1 are recruited to mitochondria to trigger autophagosome formation (Geisler et al. 2010, Van Humbeeck et al. 2011, Wong and Holzbaur 2014, Lazarou et al. 2015). Besides, following Parkin translocation and ubiquitination, histone deacetylase 6 (HDAC6) which promotes autolysosome formation via a cytoskeleton-remodeling machinery dependent on acetylation, is also recruited to mitochondria to facilitate mitophagy (Lee et al. 2010). Thus, Parkin translocation is regarded as a hallmark for mitophagy

initiation.

OPTN and NDP52, two primary mitophagy receptors, rely on their Ub-binding domains for removing damaged mitochondria during the PINK1/Parkin-mediated mitophagy (Lazarou et al. 2015). Besides PINK1, the other four E2 co-enzymes, UBE2D, UBE2L3, UBE2N and UBE2R1, have also been shown to affect the translocation and activation of Parkin during mitophagy (Fiesel et al. 2014). In addition to Parkin, other E3 ligases capable to induce mitophagy have been discovered, including mitochondrial ubiquitin ligase 1 (MUL1) and gp78 (Fu et al. 2013, Yun et al. 2014). However, SMURF1, another E3 ubiquitin ligase, places a favorable effect on mitophagy not through the ligase activity, but via its C2 domain which is essential for the mitochondrial engulfment into autophagosome (Orvedahl et al. 2011).

Ubiquitin-independent pathways

Several ubiquitin-independent mitophagy pathways have been discovered so far, most of them proved to be receptor-mediated and require the participation of an LC3 interacting region (LIR). These autophagy receptor proteins include Bcl2/adenovirus E1B 19 kDa protein-interacting protein 3 (BNIP3), NIX (also called Bnip3L), and Fun14 Domain containing 1 (FUNDC1). They locate to mitochondria and initiate mitochondrial degradation via interaction with LC3 and subsequent autophagosome formation (Zhang et al. 2008, Liu et al. 2012).

Under hypoxic conditions, BNIP3 and NIX, two hypoxia-inducing factor-1 (HIF-1) target genes that are functionally complementary in binding Bcl2, activate autophagy through dissociating Bcl2 from Beclin-1 as well as interacting directly with LC3 via their LIR to recruit autophagosomes (Bellot et al. 2009). Besides hypoxia-induced mitophagy, NIX has also been reported to be involved in terminal erythrocyte differentiation as a mitophagy receptor (Schweers et al. 2007). FUNDC1, an outer mitochondrial membrane protein containing an LIR, also plays a role in the mitophagy induction during hypoxia. PGAM5-mediated dephosphorylation of FUNDC1 is essential for this mitophagy induction while Bcl2-like 1 (BCL2L1) can negatively affect this process via inhibiting PGAM5 (Liu et al. 2012, Wu et al. 2014). Recently, FKBP8, another OMM proteins, was also shown to recruit autophagosomes to

clear the damaged mitochondria in an LIR-dependent way (Bhujabal et al. 2017). Moreover, BCL2L13 was recently identified as the mammalian homolog of the yeast mitophagy receptor Atg32. Interesting to note, BCL2L13 induces mitochondrial fragmentation and mitophagy in a Drp1-independent and Park-independent manner (Otsu et al. 2015).

Besides receptor-mediated mitophagy, lipid-mediated mitophagy was also reported. Cardiolipin, a phospholipid dimer located in the IMM is translocated to the OMM to trigger mitophagy via interaction with LC3 upon mitochondrial depolarization in neuronal cells (Chu et al. 2013, Chu et al. 2014). Important to note, the ubiquitin-dependent and ubiquitin-independent mitophagy pathways are not necessarily mutually exclusive.

Representative pathways involved in mammalian mitophagy are summarized in Figure 1.8.

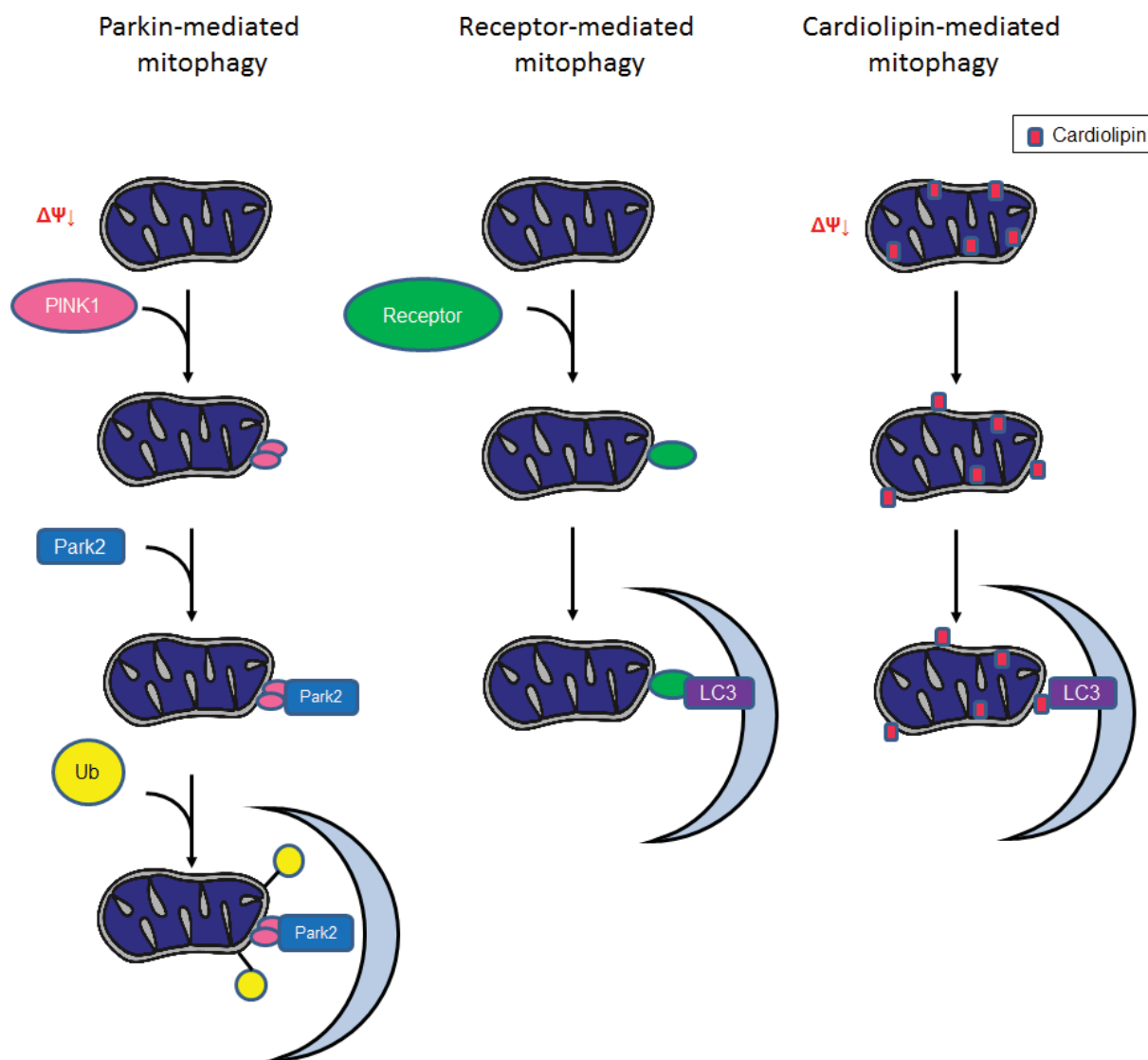


Figure 1.8 Major pathways underlying mammalian mitophagy. As depicted, there are three major mammalian mitophagy pathways. In the Parkin-mediated mitophagy, Parkin is recruited by dimerized PINK1 onto mitochondria, upon mitochondrial membrane potential loss. Parkin then ubiquitinates many mitochondrial proteins to initiate mitophagy. In the receptor-mediated or lipid-mediated mitophagy, upon mitochondrial dysfunction, mitochondrial-localized receptor proteins or lipids interact with LC3 to initiate mitophagy (modified from Youle and Narendra 2011).

1.3.2 Major pathways regulating mitophagy in mammals

The fact that mitophagy can be executed via either macroautophagy or microautophagy, indicates the importance of different induction modes as well as the complex network regarding regulation of mitophagy (Müller et al. 2015).

Mitochondrial fission and fusion

It has been proposed that mitochondrial fission should precede mitophagy as autophagosomes can only encapsulate mitochondria of a manageable size (Westermann 2010). Indeed, Drp1-mediated mitochondrial fission has been proved to be a prerequisite for mitophagy in mammalian cells (Twig et al. 2008). Along with this line, mitophagy was shown to be inhibited when excessive mitochondrial fusion is induced (Twig and Shirihai 2011). Whereas mitochondrial fission was demonstrated to be not essential for yeast mitophagy, perhaps owing to the relatively small size of the mitochondrial network in yeast (Mendl et al. 2011).

Ubiquitination and deubiquitination

Multiple levels of ubiquitination-related regulation have been observed for mammalian mitophagy. First, Ubiquitin-specific peptidase 30 (USP30), a mitochondrial deubiquitinase, was shown to be able to decrease Parkin-mediated mitophagy via directly antagonizing Parkin's ubiquitination of OMM proteins (Bingol et al. 2014). Second, the ubiquitination and proteasomal degradation of Parkin could be affected by an E3 ubiquitin ligase, neuregulin receptor degradation protein 1 (Nrdp1) (Soleimanpour et al. 2014). Third, FUNDC1-mediated mitophagy is also affected by mitochondrial E3 ligase MARCH5 as it controls the UPS degradation of FUNDC1 (Chen et al. 2017). Fourth, ubiquitination of multiple fusion and fission factors governs mitochondrial dynamics (Escobar-Henriques and Langer 2014).

Phosphorylation pathways

Observed by various studies, protein kinases and phosphatases, which determine the stability of interaction between mitophagy receptor proteins and LC3, place huge impacts on yeast as well as mammalian mitophagy (Aoki et al. 2011, Liu et al. 2012, Farre et al. 2013, Kanki et al. 2013, Zhu et al. 2013). For example, phosphorylation of a Ser residue near the LIR of BNIP3 is crucial for LC3 binding and efficient mitophagy (Zhu et al. 2013) while the Src family kinase-conducted phosphorylation of Tyr and casein kinase-2 (CK2)-conducted phosphorylation of Ser

near the LIR of FUNDC1 inhibit LC3 binding and subsequent mitophagy (Liu et al. 2012, Chen et al. 2014). Upon hypoxia or FCCP treatment, PGAM5 was shown to dephosphorylate FUNDC1 to initiate mitophagy (Chen et al. 2014). In addition, Phosphorylation of FUNDC1 by Ulk1 was demonstrated to enhance the FUNDC1-LC3 interaction (Wu et al. 2014).

Other types of regulation

Several proteins have been shown to be potent in affecting Parkin-mediated mitophagy by stabilizing/destabilizing PINK1 on the OMM (e.g. TOMM7, SIAH3, BAG2) or by disrupting the Parkin mitochondrial translocation (e.g. HSPA1L, BAG4) (Hasson et al. 2013, Qu et al. 2015). Furthermore, TBC1D15, a Rab GTPase-activating protein, has been shown to control the autophagosome formation downstream of Parkin activation via interacting with both Fis1 and the LC3/GABARAP family members (Yamano et al. 2014).

1.3.3 Biological function of mitophagy in mammals

Mitophagy can be induced by various stresses such as nutrient deprivation, photodamage, and membrane potential disruption (Ni et al. 2015). As described previously, the primary function of mitophagy is to selectively remove dysfunctional mitochondria, performing mQC (Twig et al. 2008, Ashrafi and Schwarz 2013). Apart from this fundamental role, mitophagy is also actively involved in the steady-state mitochondrial turnover as well as the mitochondrial degradation induced by metabolic change (Kissova et al. 2004, Tal et al. 2007, Youle and Narendra 2011). What is more, the role of mitophagy in development is recently capturing more and more attention. During early embryogenesis, the paternal mtDNA is cleared via mitophagy in fertilized oocytes. Strikingly, in mammals, this specific mitophagy also associates with ubiquitination of prohibitin (PHB), an IMM protein (Sutovsky et al. 1999). During red blood cell maturation, mitochondria are cleared by the NIX/Bnip3L pathway as previously reviewed. In addition, Ulk1 and Atg7 are also implicated in this mitophagy as delayed clearance or

accumulation of damaged mitochondria was observed in both Ulk1-deficient and Atg7-deficient reticulocytes (Lu et al. 2013). Mitophagy is also linked to white adipose tissue development and differentiation. During the early stage of adipogenesis, 3T3-L1 cell with defective autophagy machinery failed to complete the differentiation and eliminate excessive mitochondria generated by the increased mitochondrial biogenesis (Singh et al. 2009).

Defective mitophagy is present in many pathological conditions including Parkinson's disease, Alzheimer's disease, various human cancers and more specific mitochondrial diseases such as Barth syndrome (Lu et al. 2013). For instance, altered mitochondrial ultrastructure is a major characteristic of Barth syndrome and defective mitophagy was reported to be essential for the pathogenesis. Yme1, a highly conserved i-AAA protease, was shown to control mitophagy in the Barth syndrome models, highlighting the therapeutic potential of enhancing mQC machinery for curing this disease (Gaspard and McMaster 2015). Furthermore, Okamoto also reported that in mammals, decreased expression of mitophagy machinery components led to a defective inflammation (Okamoto 2014). However, the current understanding regarding the pathological role of mitophagy is still very limited.

1.3.4 Mitophagy in *S. cerevisiae*

Studies using *S. cerevisiae* (baker's yeast) have tremendously deepened our understanding towards the molecular mechanisms as well as the regulatory networks of mitophagy (Müller et al. 2015). In yeast cells, mitophagy was shown to be induced by rapamycin treatment, nitrogen starvation, stationary phase non-fermentable media, and mitochondrial dysfunction due to either deletion of Mdm38 or mutation of Fmc1. However, CCCP was shown to be incapable of inducing mitophagy in yeast (Priault et al. 2005, Nowikovsky et al. 2007, Kanki and Klionsky 2008, Mendl et al. 2011). Interestingly, N-acetyl-L-cysteine (NAC) was shown to alleviate the rapamycin-induced and nitrogen starvation-induced mitophagy without impacting on autophagy, presumably through suppressing Atg32 expression (Deffieu et al. 2009, Okamoto et al. 2009). Still, it should be noted that for yeast mitophagy studies, there is still no described

method for specific induction of mitophagy in yeast (Müller et al. 2015).

In yeast, similar to other selective types of autophagy, mitophagy is also executed via the interaction between autophagy receptors and adaptor proteins. Atg11, the common autophagy adaptor involved in pexophagy and the Cytoplasm-to-vacuole targeting (Cvt) pathway, also connects damaged mitochondria and the core autophagy machinery in a specialized PAS (Kanki and Klionsky 2008, Kanki et al. 2009). Atg32, a transmembrane protein located on the OMM, was identified by two genome-wide screens to be the first mitophagy-specific receptor (Kanki et al. 2009, Okamoto et al. 2009). Besides interacting with Atg8 via its Atg8 family interacting motif (AIM) directly, the cytosolic N-terminus of Atg32 can also be phosphorylated by CK2 at Ser114 & Ser119 to interact with Atg11 under mitophagy-inducing conditions (Okamoto et al. 2009, Kanki et al. 2013). Yme1-mediated procession of the IMS-located C-terminus of Atg32 was reported to be crucial for these interactions (Wang et al. 2013) (Fig. 1.9). Of note, FIP200 was hypothesized to be a functional Atg17 ortholog in mammals and BCL2L13 was proposed as a mammalian Atg32 ortholog (Hara and Mizushima 2009, Otsu et al. 2015). Furthermore, Atg33 was also identified as another mitophagy-specific protein (Kanki et al. 2009).

Apart from CK2, the phosphorylation of Atg32 was also reported to be under control of Atg1 as well as two mitogen activated protein kinases (MAPK), Slt2 and Hog1 (Aoki et al. 2011, Mao et al. 2011, Hirota et al. 2012, Kondo-Okamoto et al. 2012). Besides, TOR and its downstream Ume6-Sin3-Rpd3 complex were reported to be able to repress the Atg32 expression (Aihara et al. 2014). Other modulators of yeast mitophagy include the Ubp3-Bre5 deubiquitination complex, UTH1, Aup1 and Whi2 (Kissova et al. 2007, Tal et al. 2007, Müller et al. 2015, Müller et al. 2015).

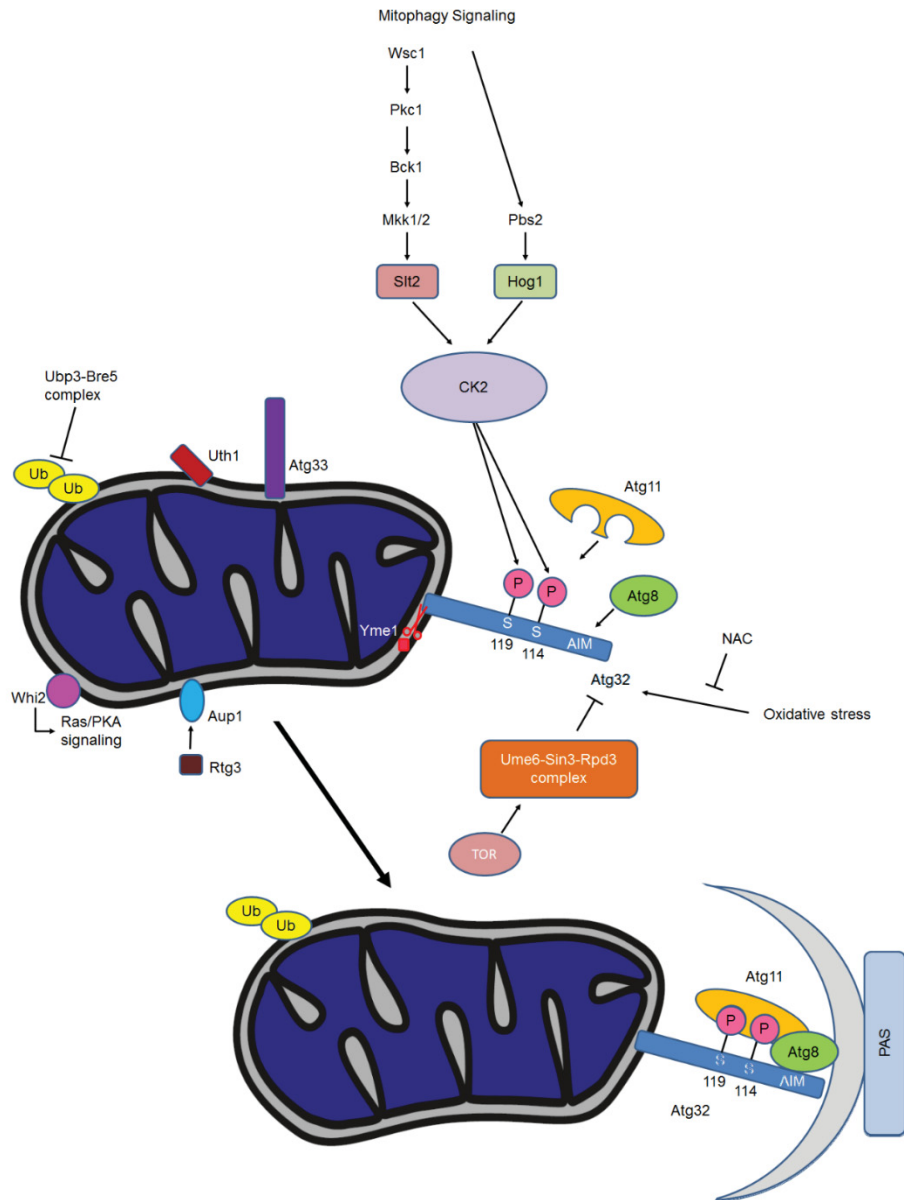


Figure 1.9 A schematic model of mitophagy in *S. cerevisiae*. The mitochondrial outer membrane protein Atg32 is phosphorylated at its cytosolic N-terminus under mitophagy-inducing conditions. Atg11 binds specifically to phosphorylated Atg32 on the surface of mitochondria. Atg32 also interacts with Atg8 via a conserved AIM motif. Yme1-mediated processing of the C-terminal domain in the intermembrane space regulates these interactions. The Atg32-Atg11-Atg8 ternary complex is generated upon mitophagy induction, leading to the recruitment of mitochondria to the PAS (modified from Hirota, Kang et al. 2012).

Whi2, a stress response factor able to impact the Ras/PKA pathway, was shown to be specifically required for mitophagy as deletion of Whi2 led to an around 50% decrease in the

rapamycin-induced mitophagy activity and no impacts on non-selective autophagy activity or the Cvt pathway activity (Mendl et al. 2011, Müller and Reichert 2011). Other studies also pointed out various mitochondrial dysfunction indicators such as actin aggregation, mitochondrial fragmentation, membrane potential loss, ROS accumulation, and growth defect in *Whi2* deletion strains during diauxic shift (Leadsham et al. 2009). Our recent data suggest that *Whi2* seems to serve as a double-edged sword in the mitophagy regulation, possibly through the Ras/PKA pathway. However, the detailed molecular mechanisms of *Whi2*-regulated mitophagy still need to be further elucidated.

1.4 Hepatic encephalopathy

Hepatic encephalopathy (HE) is a major neuropsychiatric syndrome of acute or chronic liver failure manifested by many consciousness changes, ranging from subtle abnormal behavior to deep coma and death. Although acute HE has a high mortality rate, current research focuses on chronic HE as 97% of HE cases were diagnosed in patients with liver cirrhosis (Häussinger and Sies 2013). In Germany, it was reported that approximately 30-70% of liver cirrhosis patients also developed HE (Pietrowsky et al. 1991).

1.4.1 Diagnostic and therapy strategies of hepatic encephalopathy

Clinically, HE can be categorized into two classes based on symptomatology: minimal HE (MHE) which does not present overt symptoms and manifest HE which can be further divided in four different grades with the West Haven criteria (Table 1.3) (Zhan and Stremmel 2012). As MHE is only detectable by neuropsychological test, it is hard to standardize the diagnostic for MHE. Thus a concept termed “low-grade HE” is coined to collectively represents MHE as well as manifest HE grade I and II, while manifest HE grade III and IV are regarded as “high-grade HE” (Häussinger and Sies 2013). Of note, even MHE patients suffer from inaccurate actions

and attention deficits, rendering an impaired driving fitness (Kircheis et al. 2009). In particular, in patients with liver cirrhosis, HE is claimed to be a low-grade edema which is triggered by a wide range of precipitating factors such as bleeding, infections and high oral protein intake. *In vivo* proton magnetic resonance and quantitative water mapping of patients' brain supported this notion (Häussinger et al. 1994, Shah et al. 2008).

Table 1.3 Severity-based classification of hepatic encephalopathy (adopted from Zhan and Stremmel 2012).

Severity	Grade	Level of consciousness	Neuropsychiatric symptoms	Neurological symptoms
Low-grade	0 (MHE)	Normal	Aggression, marked disorientation to time and place	None
	I (manifest HE)	Slight mental slowing down	Eu-/dysphoria, irritability and anxiety, shortened attention span	Fine motor skills disturbed (impaired ability to write, finger tremor)
	II (manifest HE)	Increased fatigue, apathy or lethargy	Slight personality disorder, slight disorientation to time and place	Flapping tremor, ataxia, slurred speech
High-grade	III (manifest HE)	Somnolence	Aggression, marked disorientation to time and place	Rigor, clonus, asterixis
	IV (manifest HE)	Coma	–	Signs of increased intracranial pressure

Current therapies towards HE consist of multiple ammonia-lowering strategies (e.g. protein restriction) as well as therapies targeting the gut microbiome and dealing with treatment and prevention of the harmful effect of precipitation factors including electrolyte disturbance, infection elimination (e.g. Rifaximin). However, the therapeutic strategies directly aiming at the low-grade edema or the associated oxidative stress have not been incorporated into clinical treatment yet, although animal studies supported the promising outcome of applying such strategies (Häussinger and Sies 2013). Liver transplantation thus represents the only therapeutic approach to permanently improve the symptoms, yet persistent cognitive impairment after

transplantation has been reported (Atluri et al. 2010, Riggio et al. 2011).

1.4.2 The pathogenesis of hepatic encephalopathy

Various studies have pointed out that increased blood and brain ammonia play a central role in the pathogenesis of HE (Butterworth 2002, Häussinger and Sies 2013). As ammonia in the brain is detoxified by the glutamine synthetase (GS) expressed only in astrocytes (Martinez-Hernandez et al. 1977, Schliess et al. 2002), astrocyte dysfunction is regarded as the core mechanism in this pathogenesis.

The well-accepted HE pathogenetic model is depicted in Figure 1.10. Briefly, liver dysfunctions cause significant abnormalities in the nitrogen metabolism, leading to an increased concentration of ammonia in the blood which also bypasses the blood-brain barrier (Depending on the environment pH, ammonia is protonated to NH_4^+ or stays un-ionized as NH_3). The increased brain ammonia which induces an intensified accumulation of glutamine in astrocytes, together with other heterogeneous precipitation factors including inflammatory cytokines, benzodiazepines, and hyponatremia, causes astrocyte swelling and associated damage in the brain (Lachmann et al. 2013). Importantly, astrocyte swelling induces oxidative/nitrosative stress which can positively feedback to reinforce swelling (Görg et al. 2013). Thus the formation of a self-amplifying signaling loop between astrocyte swelling and oxidative/nitrosative stress could result in many destructive processes including protein tyrosine nitration, RNA oxidation, and abnormal signal transduction. The accumulation of these harmful effects lead to astrocyte & neuronal dysfunction, which can further impair synaptic plasticity, disturb oscillatory networks, and ultimately render various cognitive and motoric symptoms observed in HE (Häussinger and Görg 2010, Häussinger and Sies 2013). Of note, HE was also reported to be fully or partially reversible in patients receiving treatment (Atluri et al. 2010).

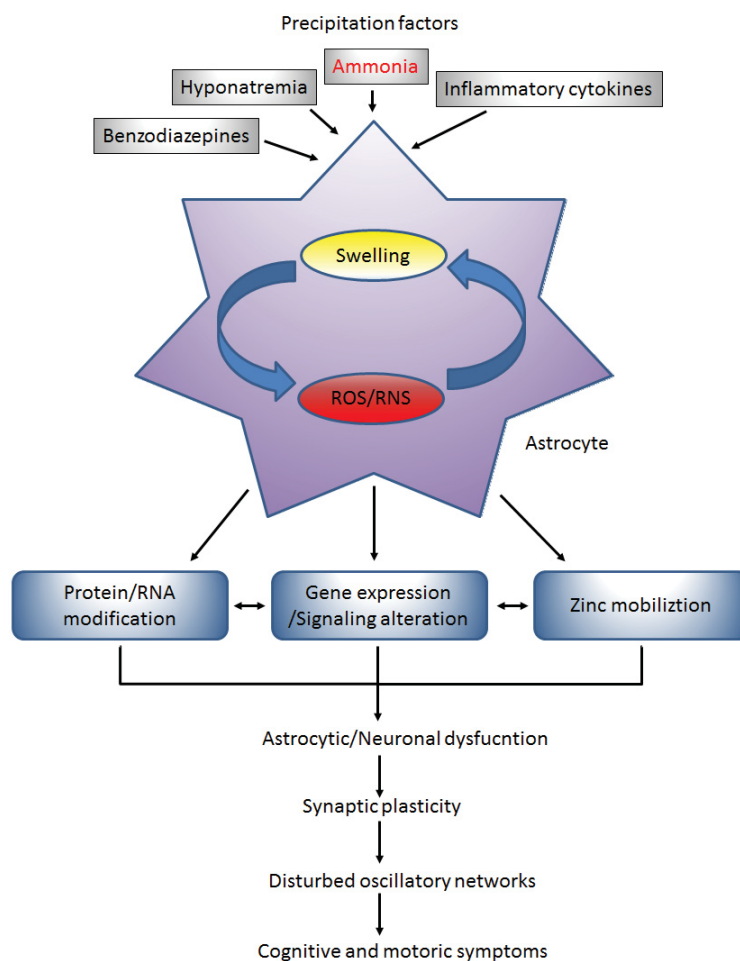


Figure 1.10 The pathogenic model of hepatic encephalopathy. Under hyperammonemic conditions, ammonia, together with other precipitation factors, causes astrocyte swelling. Astrocyte swelling then stimulates ROS/RNS generation which further reinforces astrocyte swelling. This self-amplifying loop then leads to a variety of harmful alterations that accumulatively result in astrocyte & neuron dysfunction and development of more severe symptoms (modified from Häussinger and Schliess 2008, Häussinger and Sies 2013).

1.4.3 Oxidative/Nitrosative stress in hepatic encephalopathy

Oxidative/Nitrosative stress induced by ammonia and astrocyte swelling was frequently observed in many cell and animal studies addressing the pathogenesis of HE (Häussinger and Schliess 2008, Häussinger and Görg 2010). Ammonia triggers astrocyte swelling via activation and overexpression of the Na-K-Cl cotransporter-1 (NKCC1) (Jayakumar et al. 2008, Kelly et al. 2009). Besides, ammonia induces glutamate release from astrocytes which activates *N*-

methyl-D-aspartate (NMDA) receptors (Ohara et al. 2009). These further not only generate a gradient of the intracellular Ca^{2+} concentration which stimulates calmodulin-dependent nitric oxide synthase but also stimulates NADPH oxidases which account for the major production of the early ROS (Schliess et al. 2004, Kruczek et al. 2009). Of note, swelling and increased ROS in astrocyte may evoke other players in oxidative stress response like p53, Nrf2, and NF- κ B (Sinke et al. 2008, Panickar et al. 2009, Oenarto et al. 2016).

Based on the observation that ammonia-induced oxidative stress can be reduced by substances such as histidine and cyclosporine A, Albrecht and Norenberg proposed the "Trojan horse" hypothesis, connecting ammonia toxicity with mitochondrial metabolism via glutamine (Albrecht and Norenberg 2006). In this hypothesis, newly synthesized glutamine serves as an ammonia carrier from cytoplasm to mitochondria. Its subsequent cleavage by phosphate-activated glutaminase inside mitochondria, yielding an increased concentration of mitochondrial ammonia which stimulates ROS production and mitochondrial dysfunction such as mitochondrial membrane potential loss (Bai et al. 2001, Jayakumar et al. 2004).

Notably, in patients with liver cirrhosis, increased levels of biomarkers for oxidative stress were only observed in the cerebral cortexes from patients co-diagnosed with HE, indicating that oxidative/nitrosative stress is mainly a characteristic of HE but not a characteristic of liver cirrhosis (Görg et al. 2013).

1.4.4 Functional consequences of osmotic and oxidative/nitrosative stress in astrocytes

As described previously, osmotic and oxidative/nitrosative stresses lead to multiple functional consequences. The major effects are summarized in Fig. 1.11.

Protein tyrosine nitration

One of the most pronounced consequences in perivascular astrocytes is protein tyrosine nitration (PTN) (Häussinger and Görg 2010, Häussinger and Sies 2013). Induced by various

precipitation factors like ammonia, inflammatory cytokines, and benzodiazepines, PTN modifies many proteins involved in the pathogenesis of HE including glutamine synthetase, NKCC1, GAPDH and peripheral benzodiazepine receptor (PBR) (Schliess et al. 2002, Häussinger and Görg 2010). 3-nitro-tyrosine in serum has already been incorporated as a biomarker for low-grade HE (Llansola et al. 2013).

Protein O-GlcNAcylation

Reversible O-GlcNAcylation at serine and threonine residues were also observed recently after NH₄Cl treatment in cultured rat astrocytes, GAPDH was identified as a target for this post-translational protein modification (Karababa et al. 2014).

RNA oxidation

Another consequence of oxidative stress is RNA oxidation which is detected in both animal astrocytes and neurons. Importantly, RNA oxidation in response to precipitation factors like ammonia was proved to be a selective process (Häussinger and Sies 2013). The ribosomal 28S and 18S RNA as well as the glutamate/aspartate transporter (GLAST) were among the oxidized RNAs, indicating RNA species involved in local postsynaptic protein synthesis were modified by oxidative stress under HE pathological conditions, which may ultimately affect learning skills and long-term memory (Görg et al. 2008, Häussinger and Sies 2013).

Gene expression/signal alteration

Microarray analysis conducted in HE experiment models as well as human patient samples revealed multiple levels of alternation and regulation regarding gene expression under HE pathological conditions (Görg et al. 2013, Oenarto et al. 2016, Karababa et al. 2017). For example, heme oxygenase I (HO-1), a key enzyme in the intracellular antioxidant mechanism, was found to be upregulated in ammonia-treated cultured rat astrocytes and in rat brains after

ammonium-acetate administration (Warskulat et al. 2002). Upregulation of HO-1 mRNA was also confirmed via mRNA microarray analysis, at least 6 miRNA were identified as regulators contributing to this upregulation (Oenarto et al. 2016).

Zinc mobilization

Increased zinc mobilization and nucleus accumulation of the transcription factors MTF-1 and SP1 were seen as another pathophysiological relevant consequence (Kruczek et al. 2009). SP1 enhances the expression of the peripheral benzodiazepine receptor (PBR) which subsequently increases synthesis of neurosteroids (Giatzakis and Papadopoulos 2004). These neurosteroids not only positively regulate GABA_A-receptor function but also have a high affinity towards the G-protein-coupled receptor TGR5 which is involved in HE pathogenesis (Keitel et al. 2010). Interestingly, TGR5 downregulation was reported in both ammonia-treated astrocytes and the brain of HE patients with liver cirrhosis (Keitel et al. 2010).

Senescence

Another functional consequence of oxidative/nitrosative stress is cellular senescence observed in astrocytes treated with NH₄Cl (5 mM, 72 h) (Görg et al. 2015, Oenarto et al. 2016). Characterized by increased senescence-associated β-galactosidase activity, increased nuclear accumulation of activated p53 and upregulation of its downstream genes, GADD45a and p21, senescence was shown to be sensitive to the GS inhibitor MSO, NADPH oxidase inhibitor apocynin, and the p38MAPK inhibitor SB203580. Interesting to note, upregulation of senescence-associated genes was also found in patients' brain samples (Görg et al. 2015).

Mitochondrial and bioenergetic changes

Oxidative/Nitrosative stress can cause tremendous mitochondrial damages and alterations in the cellular bioenergetic status. Many forms of mitochondrial dysfunction have already been

associated with pathological conditions of HE including mitochondrial fragmentation, swelling of mitochondria, and loss of mitochondrial membrane potential (Drewes and Leino 1985, Bai et al. 2001, Görg et al. 2015). An observation supporting the connection between HE-associated oxidative stress and energy mechanism is that application of the ROS scavenger, NAC, significantly alleviated the inhibition on ETC enzyme activities in the brain of CCl₄-intoxicated rats (Boer et al. 2009). Recently, Niknahad et al. detected lipid peroxidation as well as glutathione and ATP depletion in isolated mice liver and brain mitochondria upon high concentrations of ammonium treatment (Niknahad et al. 2017). Dhanda et al. also found impaired respiratory chain activity of the brain mitochondria in a rat model of HE (Dhanda et al. 2018). However, the detailed mechanism of how energy metabolism contributes to the pathogenesis of HE is largely unknown.

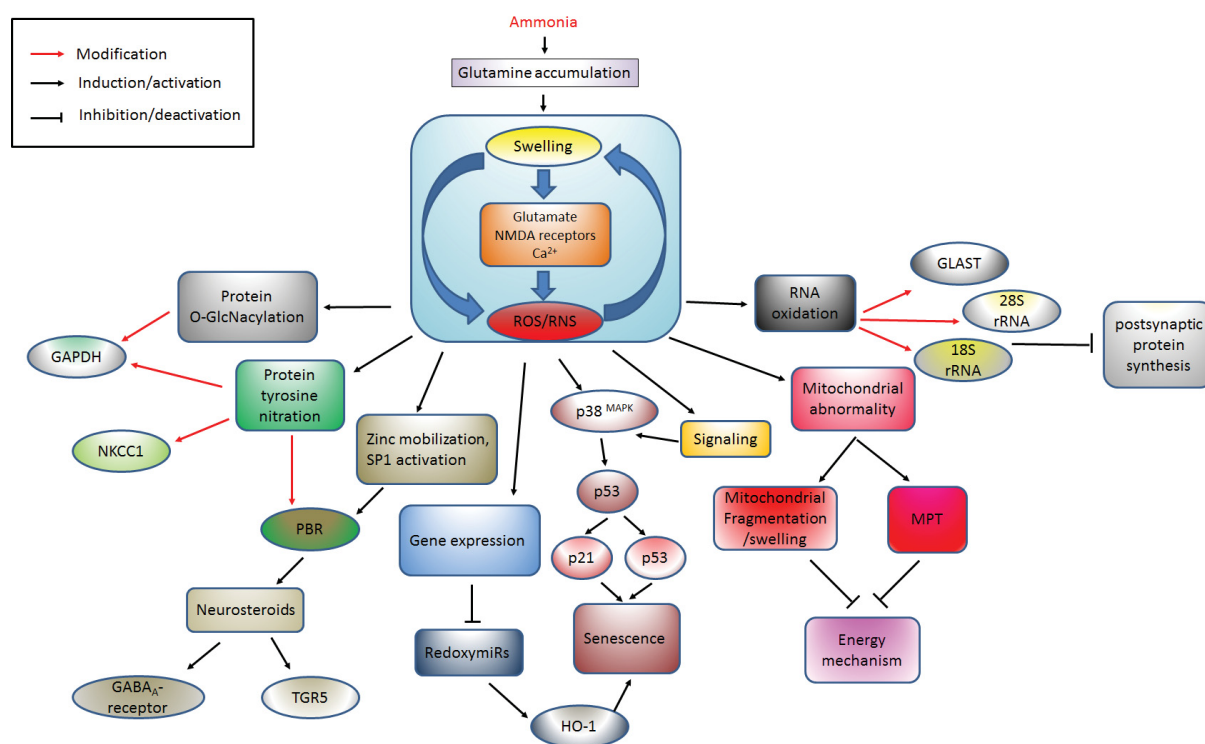


Figure 1.11 Major functional consequences of osmotic and oxidative/nitrosative stress in astrocytes. In the pathogenesis of HE, glutamine accumulation induced by ammonia causes astrocyte swelling which forms a strong self-amplifying loop with the accompanied increases in oxidative/nitrosative stress. This self-amplifying loop alters multiple intracellular processes and signaling pathways such as RNA oxidation, protein tyrosine nitration, and the p38MAPK pathway. MPT: mitochondrial permeability transition.

1.5 Working hypothesis: mitochondrial quality control pathways are involved in the pathogenesis of hepatic encephalopathy

Despite the interesting observations that mitochondrial morphology and functions are altered by high concentrations of ammonia in astrocytes (Drewes and Leino 1985, Bai et al. 2001, Rama Rao and Norenberg 2012), there were no studies reporting the involvement of mitochondrial quality control (mQC) in the pathogenesis of HE when this project started.

mQC processes at the organellar level consist of biogenesis as well as degradation of mitochondria. Removal of mitochondria is performed specifically by means of mitophagy or more generally by means of autophagy, both can be induced by increased ROS/RNS, the major trigger of HE. Defects of autophagy and mitophagy have been indicated in various forms of liver and neurodegeneration diseases and can thus be targets of new therapeutic approaches. (Nunnari and Suomalainen 2012, Czaja et al. 2013). It is likely that besides oxidative stress, autophagy and mitophagy also play an important role in astrocyte dysfunction induced by hyperammonemia. Indeed, a recent study suggests mitophagy is also stimulated by NH₄Cl treatment (Polletta et al. 2015), however, it is unclear whether this effect can also be observed in models of HE and whether ROS/RNS regulates autophagy and/or mitophagy in the pathogenesis of HE.

Hence the hypothesis needed to be tested is that autophagy and mitophagy, two important degradation pathways ensuring mitochondrial homeostasis, are involved in the pathogenesis of HE (Fig. 1.12).

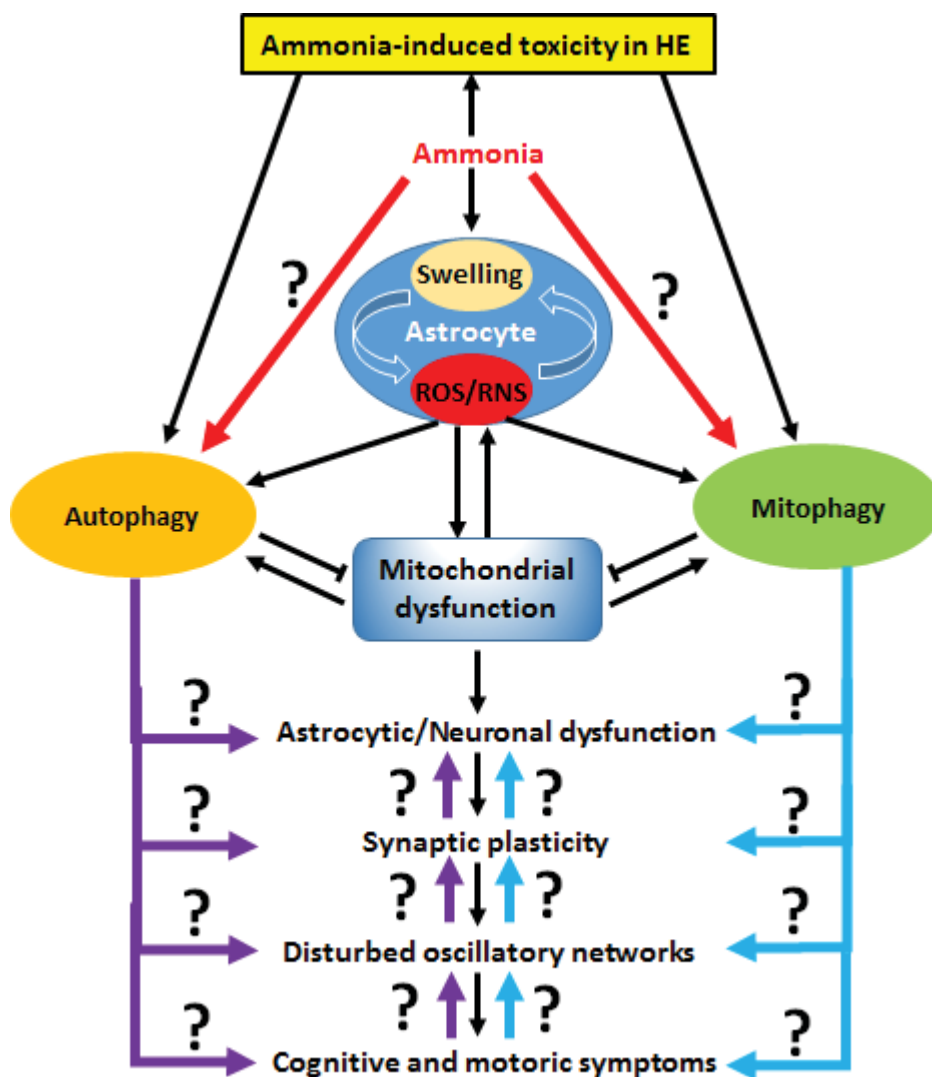


Figure 1.12 Working hypothesis: involvement of mitochondrial quality control pathways in the pathogenesis of hepatic encephalopathy. Mitochondrial dysfunction has been documented in the pathological models of HE (modified from Haussinger and Sies 2013), indicating the demand for a proper mitochondrial quality control. Cellular quality control pathways that are responsible for the clearance of dysfunctional mitochondria mainly consist of autophagy and the more specific mitophagy. Major contributing factors in the pathogenesis of HE such as ammonia have been reported to affect both autophagy and mitophagy under various pathological conditions. However, whether autophagy and mitophagy are critically involved in HE pathogenesis and whether they are modulated by ammonia in a similar manner as previously reported remain unclear. In the present work, we aim to answer these questions.

1.6 Aims of the study

The aim of the present doctoral thesis is to investigate the involvement of autophagy and mitophagy in the pathogenesis of HE. Autophagy, mitophagy as well as their functional roles in HE are mechanistically analyzed using established markers in cultured rat astrocytes. Verification of the *in vivo* relevance is conducted with rat brain samples from an acute ammonia intoxication HE model.

Long-term general aims:

- 1) Obtaining a mechanistic understanding of the roles of autophagy & mitophagy in the pathogenesis of HE.
- 2) Establishing strategies to improve mQC as potential therapeutic approaches for the treatment of HE.

Specific aims:

- 1) Determining the functional role of ammonia on mitochondrial quality.
- 2) Determining the involvement of mitophagy in the pathogenesis of HE & elucidating the relevant molecular mechanisms.
- 3) Determining the involvement of autophagy in the pathogenesis of HE & elucidating the relevant molecular mechanisms.
- 4) Analyzing the impacts of autophagy and mitophagy on ammonia-induced processes in astrocytes.

2. Materials and Methods

2.1 Material

2.1.1 Chemicals and materials

Table 2.1 List of chemicals, enzymes and kits.

Name	Company
2-Mercaptoethanol	<i>AppliChem, Darmstadt</i>
Acetic acid	<i>Sigma-Aldrich, Taufkirchen</i>
Agar	<i>AppliChem, Darmstadt</i>
Agarose	<i>Biozym Scientific, Hessisch Oldendorf</i>
Ammonium acetate	<i>AppliChem, Darmstadt</i>
Ammonium chloride	<i>VWR International, Langenfeld</i>
Ammonium persulfate	<i>Carl Roth, Karlsruhe</i>
Ampicillin sodium salt	<i>Carl Roth, Karlsruhe</i>
Apocynin	<i>Sigma-Aldrich, Taufkirchen</i>
Bradford reagent	<i>Sigma-Aldrich, Taufkirchen</i>
Bromophenol blue	<i>AppliChem, Darmstadt</i>
BSA, 98%	<i>Sigma-Aldrich, Taufkirchen</i>
Calcium chloride	<i>AppliChem, Darmstadt</i>
CCCP	<i>Sigma-Aldrich, Taufkirchen</i>
Cellular ROS/RNS detection assay kit	<i>Abcam, Cambridge, UK</i>
Chloroquine	<i>AppliChem, Darmstadt</i>
COmplete protease inhibitor tablets, EDTA-free	<i>Roche, Rotkreuz, Switzerland</i>
D-(+)-Trehalose dihydrate	<i>Sigma-Aldrich, Taufkirchen</i>
DAPI	<i>Sigma-Aldrich, Taufkirchen</i>
Deoxynucleotide (dNTP) solution mix	<i>New England Biolabs, Frankfurt am Main</i>
DMEM	<i>Sigma-Aldrich, Taufkirchen</i>
DMSO	<i>AppliChem, Darmstadt</i>
DTT	<i>AppliChem, Darmstadt</i>
EDTA	<i>AppliChem, Darmstadt</i>
Effectene transfection reagent	<i>Qiagen, Hilden</i>
Ethanol	<i>Carl Roth, Karlsruhe</i>
Ethidium bromide solution, 1%	<i>Carl Roth, Karlsruhe</i>
FBS	<i>PAN-Biotech, Aidenbach</i>
Formaldehyde, 37%	<i>AppliChem, Darmstadt</i>
GelRed nucleic acid gel stain	<i>Biotium, Fremont, USA</i>
GeneRuler 1 Kb DNA ladder	<i>Thermo Fisher Scientific, Langenselbold</i>
Gibco GlutaMAX	<i>Life Technologies, Ober-Olm</i>

Glutaraldehyde	<i>Sigma-Aldrich, Taufkirchen</i>
Glycine	<i>Sigma-Aldrich, Taufkirchen</i>
H ₂ O ₂	<i>Sigma-Aldrich, Taufkirchen</i>
HEPES sodium salt, 99%	<i>Sigma-Aldrich, Taufkirchen</i>
HiPerFect transfection reagent	<i>Qiagen, Hilden</i>
Hydrochloric acid, 32%	<i>Carl Roth, Karlsruhe</i>
Hydrogen peroxide, 30%	<i>Merck, Darmstadt</i>
Isopropanol	<i>Sigma-Aldrich, Taufkirchen</i>
Lipofectamine RNAiMAX	<i>Invitrogen, Karlsruhe</i>
LysoSensor™ Green DND-189	<i>Invitrogen, Karlsruhe</i>
Magic red cathepsin L assay kit	<i>Immunochemistry, Bloomington, USA</i>
Magnesium chloride hexahydrate	<i>Carl Roth, Karlsruhe</i>
Mannitol	<i>Carl Roth, Karlsruhe</i>
Methanol	<i>VWR International, Langenfeld</i>
Methylammonium chloride	<i>Merck, Darmstadt</i>
MSO	<i>Sigma-Aldrich, Taufkirchen</i>
NAC	<i>Sigma-Aldrich, Taufkirchen</i>
p-Cumaric acid	<i>Sigma-Aldrich, Taufkirchen</i>
paNP	<i>AG Orian S. Shirihai, Los Angeles, USA</i>
PageRuler prestained protein ladder	<i>Thermo Fisher Scientific, Langenselbold</i>
Paraformaldehyde	<i>Sigma-Aldrich, Taufkirchen</i>
Penicillin/Streptomycin	<i>PAA Laboratories, Cölbe</i>
Phosphate buffered saline with Ca ²⁺ and Mg ²⁺	<i>Sigma-Aldrich, Taufkirchen</i>
Phosphate buffered saline without Ca ²⁺ and Mg ²⁺	<i>Sigma-Aldrich, Taufkirchen</i>
Phusion high-fidelity DNA polymerase	<i>New England Biolabs, Frankfurt am Main</i>
PIPES	<i>Carl Roth, Karlsruhe</i>
PMSF	<i>Carl Roth, Karlsruhe</i>
Polyethylene glycol (PEG 4000)	<i>Sigma-Aldrich, Taufkirchen</i>
Ponceau S	<i>AppliChem, Darmstadt</i>
Potassium chloride	<i>AppliChem, Darmstadt</i>
Potassium hydroxide	<i>Merck, Darmstadt</i>
Potassium phosphate, monobasic	<i>Sigma-Aldrich, Taufkirchen</i>
PureLink HiPure plasmid midiprep kit	<i>Life Technologies, Ober-Olm</i>
Pyruvat	<i>Invitrogen, Karlsruhe</i>
QIAprep spin miniprep kit	<i>Qiagen, Hilden</i>
QIAquick gel extraction kit	<i>Qiagen, Hilden, Hilden</i>
QuantiNova reverse transcription kit	<i>Qiagen, Hilden</i>
QuantiNova SYBR Green PCR kit	<i>Qiagen, Hilden</i>
Rapamycin	<i>LC Laboratories, Woburn, USA</i>
RNase A	<i>AppliChem, Darmstadt</i>
Rotiphorese gel 40 (40% acrylamide/bisacrylamide, 29 : 1)	<i>Carl Roth, Karlsruhe</i>
SB203580	<i>Merck, Darmstadt</i>

SDS	<i>Carl Roth, Karlsruhe</i>
SignalFire ECL reagent	<i>Cell Signaling Technology, Danvers, USA</i>
Skim milk powder	<i>Carl Roth, Karlsruhe</i>
Sodium chloride	<i>Sigma-Aldrich, Taufkirchen</i>
Sodium deoxycholate	<i>Sigma-Aldrich, Taufkirchen</i>
Sodium hydroxide	<i>Carl Roth, Karlsruhe</i>
Sodium phosphate, dibasic	<i>Sigma-Aldrich, Taufkirchen</i>
Sucrose	<i>Sigma-Aldrich, Taufkirchen</i>
Taurine	<i>Sigma-Aldrich, Taufkirchen</i>
TEMED	<i>Carl Roth, Karlsruhe</i>
TMRM	<i>Thermo Fisher Scientific, Langenselbold</i>
Trichloroacetic acid	<i>Sigma-Aldrich, Taufkirchen</i>
Tris	<i>AppliChem, Darmstadt</i>
Triton X-100	<i>AppliChem, Darmstadt</i>
Trizol reagent	<i>Invitrogen, Karlsruhe</i>
Trypan blue	<i>Sigma-Aldrich, Taufkirchen</i>
Trypsin/EDTA solution	<i>Biochrom, Berlin</i>
Tryptone	<i>Sigma-Aldrich, Taufkirchen</i>
Tween 20	<i>Carl Roth, Karlsruhe</i>
Venor GeM classic mycoplasma detection kit	<i>Minerva Biolabs, Berlin</i>
Xylene Cyanol	<i>Sigma-Aldrich, Taufkirchen</i>

2.1.2 Equipment

Table 2.2 List of equipment.

Type	Name	Company
Autoclave	VX-95	<i>Systec, Wetztenberg</i>
Biosafety cabinet	Biological safety cabinet safe 2020	<i>Thermo Fisher Scientific, Langenselbold</i>
Cell counting device	Countess automated cell counter Neubauer chamber	<i>Invitrogen, Karlsruhe</i> <i>Brand, Wertheim</i>
Centrifuge	Allegra X-15R	<i>Beckman Coulter, Krefeld</i>
	Centrifuge 5417C	<i>Eppendorf, Hamburg</i>
	Centrifuge 5424	<i>Eppendorf, Hamburg</i>
	Heraeus megafuge 8R	<i>Thermo Fisher Scientific, Langenselbold</i>
CO ₂ incubator	Sanyo MCO-18AIC CO ₂ incubator	<i>Panasonic, Hamburg</i>

Electrophoresis equipment	Gel electrophoresis chambers, glass plates, spacers & gel combs	<i>P. Reiser, Munich</i>
Electrophoresis power supply	EV 265 PowerPac HC High-Current Power Supply	<i>Consort bvba, Turnhout, Belgium</i> <i>Bio-Rad Laboratories, München</i>
Gel imaging and documentation	FUSION SL chemiluminescence system UV transilluminator	<i>Vilber Lourmat, Eberhardzell</i> <i>PEQLAB Biotechnologie, Erlangen</i>
Heating block	neoBlock 1 2-2503 Peqlab HX-1	<i>neoLab Migge Laborbedarf-Vertriebs, Heidelberg</i> <i>PEQLAB Biotechnologie, Erlangen</i>
Incubator	Heraeus incubator B12 Incubation shaker multitron standard	<i>Thermo Fisher Scientific, Langenselbold</i> <i>Infors, Bottmingen/Basel, Switzerland</i>
Microscopy	Axio observer D1 fluorescence microscopy Eclipse Ti microscope Eclipse TS100 microscope LSM520 meta confocal laser scanning microscopy UltraVIEW VoX spinning disk confocal system	<i>Carl Zeiss, Jena</i> <i>Nikon, Düsseldorf</i> <i>Nikon, Düsseldorf</i> <i>Carl Zeiss, Jena</i> <i>PerkinElmer LAS, Solingen</i>
pH meter	pH-Meter HI221	<i>Hanna instruments, Kehl am Rhein</i>
Photometer	Biospectrometer basic Fluoroskan Ascent FL Microplate reader infinite 200 PRO	<i>Eppendorf, Hamburg</i> <i>Thermo Fisher Scientific, Langenselbold</i> <i>Tecan Group, Männedorf, Switzerland</i>
Pipette	Pipet aid Reference pipettes	<i>IBS Integra Biosciences, Fernwald</i> <i>Eppendorf, Hamburg</i>
Scale	Analytical balance TE124S TE612 talent	<i>Sartorius, Göttingen</i> <i>Sartorius, Göttingen</i>
Shaker	Orbital shaker 410 x 297 mm	<i>neoLab Migge Laborbedarf-Vertriebs, Heidelberg</i>
Stirrer	Magnetic stirrer	<i>IKA-Werke, Staufen</i>
Thermal cycler	Peqstar 2x gradient thermocycler Rotor-Gene 6000 Tprofessional trio thermocycler	<i>VWR International, Langenfeld</i> <i>Qiagen, Hilden</i> <i>Biometra, Göttingen</i>
Thermomixer	Thriller	<i>PEQLAB Biotechnologie, Erlangen</i>
Vacuum pump	KNF LABOPORT pump	<i>KNF Neuberger, Freiburg</i>

Vortex mixer and homogeniser	MS1 minishaker Vortex genie 2	<i>IKA-Werke, Staufen</i> <i>Scientific Industries, New York, USA</i>
Water bath	Aqualine AL 25 water bath	<i>Lauda, Lauda-Königshofen</i>
Water treatment	Milli-Q academic system	<i>Merck, Darmstadt</i>
Western blot equipment	Roller RM-5-Assistant	<i>B. Braun Melsungen, Melsungen</i>
	Semi-dry blotting system	<i>P. Reiser, Munich</i>
	Trans-Blot SD semi-dry transfer cell	<i>Bio-Rad Laboratories, München</i>
	XCell sureLock mini-cell electrophoresis system	<i>Thermo Fisher Scientific, Langenselbold</i>

2.1.3 Consumables

Table 2.3 List of consumables.

Name	Company	Usage
Cellstar cell culture dishes (3 cm, 6 cm, 10cm)	<i>Greiner bio-one, Frickenhausen</i>	Cell/bacteria culture
Cellstar cell culture flasks (175 cm ²)	<i>Greiner bio-one, Frickenhausen</i>	Cell culture
Cellstar, centrifuge tubes (15 mL, 50 mL)	<i>Greiner bio-one, Frickenhausen</i>	Cell culture/chemical preparation
Cellstar pipettes (5 mL, 10 mL, 25 mL)	<i>Greiner bio-one, Frickenhausen</i>	Cell culture/chemical preparation
Cuvettes	<i>Sarstedt, Nümbrecht</i>	Photometer measurement
Glass pasteur pipettes	<i>Brand, Wertheim</i>	Cell culture
Gel cassette (1.5 mm)	<i>Invitrogen, Karlsruhe</i>	Western blot
Cell culture plates (6 well, 24 well, 96 well)	<i>Greiner bio-one, Frickenhausen</i>	Cell culture
Eppendorf tubes (1.5 mL, 2 mL)	<i>Eppendorf, Hamburg</i>	Cell culture/chemical preparation
TipOne filtertips (10 µL, 100 µL, 1000 µL)	<i>Starlabs, Hamburg</i>	Cell culture/chemical preparation
Whatman paper	<i>Whatman, Dassel</i>	Chemical preparation
Nitrocellulose membranes	<i>Sigma-Aldrich, Taufkirchen</i>	Western blot
PVDF membranes	<i>GE Healthcare, Freiburg</i>	Western blot
MatTek dish (55 mm, plastic, glass)	<i>MatTek Corporation, Ashland, USA</i>	Bioimaging
Ibidi dish (35 mm, plastic, glass)	<i>Ibidi, Planegg</i>	Bioimaging

Steril filter (0,20 µm)	<i>Sartorius, Göttingen</i>	Cell culture/chemical preparation
Parafilm M labfilm	<i>Pechiney, Chicago, USA</i>	Cell culture/chemical preparation
Filter paper for western blot	<i>GE Healthcare, Chicago, USA</i>	Western blot

2.1.4 Culture mediums and buffers

Table 2.4 List of mammalian cell culture mediums.

Name	Component	Company	Cat. No.	Type
DMEM culture medium	With 1 g/L glucose (low glucose), supplemented with penicillin (100 U/mL)/ streptomycin (100 µg/mL), GlutaMAX™ (2 mM) and FBS (0 or 10%)	<i>Sigma-Aldrich, Taufkirchen</i>	D5546	Culture medium
DMEM without phenol red	With 1 g/L glucose (low glucose), supplemented with penicillin (100 U/mL)/ streptomycin (100 µg/mL), GlutaMAX™ (2 mM) and FBS (10%)	<i>Sigma-Aldrich, Taufkirchen</i>	D5921	Culture medium
Opti-MEM medium	Reduced serum medium with L-glutamine, without phenol red	<i>Life Technologies, Ober-Olm</i>	11058-021	Culture medium
Cryopreservation medium	50% (v/v) DMEM with 40% (v/v) FCS, 10% (v/v) DMSO	-	-	Freezing medium

Table 2.5 List of *E. Coli* culture mediums.

Name	Component	Concentration	Type
LB medium	Tryptone	1% (w/v)	Culture medium
	Yeast extract	0.5% (w/v)	
	Sodium chloride	1% (w/v)	
LB ^{Amp} medium	LB medium Ampicillin (added after autoclaving)	- 100 µg/mL	Selection medium

Table 2.6 List of buffers.

Name	Componentent	Concentration	Usage
Dulbecco's phosphate buffered saline	Sodium chloride	8 g/L	Cell culture
	Potassium phosphate, monobasic	0.2 g/L	
	Sodium phosphate, dibasic	1.15 g/L	
	Potassium chloride	0.2 g/L	
Blocking solution	Milk powder in 1x TBST	5%	Western blot
1X Blotting buffer	Tris	20 mM	Western blot
	Glycine	150 mM	
	Ethanol	20% [v/v]	
	SDS	0.08% [w/v]	
	adjust pH to 8.3 with HCl		
10X SDS running buffer	SDS	10 g/L	Western blot
	Tris	30.3 g/L	
	Glycine	144.1 g/L	
	adjust pH to 8.3 with HCl		
1X TBST buffer	Tris	50 mM	Western blot
	Sodium chloride	150 mM	
	Tween 20	0.1% [v/v]	
	adjust pH to 7.6 with HCl		
4x Lämmli buffer	Glycerol	40% [v/v]	Western blot
	2-mercaptoethanol	20% [v/v]	
	SDS	12% [v/v]	
	Bromophenol blue	0.4% [w/v]	
1X RIPA-lysis buffer	Tris	1 mM	Cell lysis
	Sodium chloride	150 mM	
	Triton X-100	1% [v/v]	
	Sodium deoxycholate	0.05% [w/v]	
	SDS	0.1% [w/v]	
	EDTA	1 mM	
Stripping buffer	Tris	62.5 mM	Western blot
	SDS	2% [w/v]	
	2-mercaptoethanol	0.7% [v/v]	
	adjust pH to 6.8 with HCl		
10X TAE	Tris	400 mM	Agarose gel electrophoresis
	Acetic acid	11.4 mL/L	
	EDTA	10 mM	
	adjust pH to 8 with HCl		

10x DNA loading buffer	Glycerol	6% [v/v]	Agarose gel electrophoresis
	Bromophenol blue	0.05% [w/v]	
	Xylene cyanol	0.05% [w/v]	
Mitoisolation buffer	Mannitol	210 mM	Mammalian mitochondrial isolation
	Sucrose	70 mM	
	EDTA	0.5 mM	
	HEPES	10 mM	
	Protease inhibitor	1 tablet/50 mL	
Mitoiso freezing buffer	Trehalose	300 mM	Mammalian mitochondrial isolation
	Potassium chloride	10 mM	
	EDTA	1 mM	
	Fatty acid free BSA	0.1% [w/v]	
	HEPES	10 mM	

2.1.5 Mammalian cells and *E. coli* strains

Table 2.7 List of mammalian cells.

Name	Species	Tissue	Disease	Origin
Primary astrocytes	Rattus norvegicus	Brain	-	AG Häussinger/Görg, Düsseldorf
HEK293	Homo sapiens	Kidney	-	AG Reichert, Frankfurt
HeLa	Homo sapiens	Cervix	Adenocarcinoma	ATCC, Manassas, USA
HeLa mCherry-Parkin	Homo sapiens	Cervix	Adenocarcinoma	AG Reichert, Frankfurt
HepG2	Homo sapiens	Liver	Hepatocyte carcinoma	ECACC, Salisbury, UK
MOG-G-CCM	Homo sapiens	Brain	Astrocytoma	ECACC, Salisbury, UK
SH-SY5Y	Homo sapiens	Bone marrow	Neuroblastoma	DSMZ, Braunschweig

Table 2.8 List of *E. coli* strains.

Name	Genotype	Origin
<i>E. coli</i> DH5 α	F ⁻ Φ 80lacZ Δ M15 Δ (lacZYA-argF) U169 recA1 endA1 hsdR17 (rK ⁻ , mK ⁺) phoA supE44 λ ⁻ thi-1 gyrA96 relA1	Life Technology
<i>E. coli</i> XL1-Blue	recA1 endA1 gyrA96 thi-1 hsdR17 supE44 relA1 lac [F' proAB lacI Δ M15 Tn10 (Tet ^r)]	AG Reihert, Düsseldorf

2.1.6 siRNAs

Table 2.9 List of siRNAs.

Name	Company	Catalogue No.	Reference
Control siRNA	<i>Thermo Fisher Scientific, Langensfeld</i>	AM4611	<i>(Cui et al. 2010)</i>
siPARK2	<i>GE Dharmacon, Lafayette, USA</i>	L-090709-02-0005	<i>(Cui et al. 2010)</i>
siPINK1	<i>Thermo Fisher Scientific, Langensfeld</i>	180640	<i>(Cui et al. 2010)</i>
siATG5	<i>GE Dharmacon, Lafayette, USA</i>	M-095125-01-0005	<i>(Kim et al. 2013)</i>
siNIX	<i>GE Dharmacon, Lafayette, USA</i>	L-094497-02-0005	<i>This study</i>

Table 2.10 Sequences of siRNAs.

Name	Sequence (5'-3')
Control siRNA	Not available (trade secret) <i>(Cui et al. 2010) (Cui, Tang et al. 2010)</i>
siPARK2	UCGCUUAGCAACCACUCC,UUCGCAGGUGACUUUCCUC,UGUUUUCGUGACUUUCCUC,UUCCCAUGAFFUCGUGCG
siPINK1	Not available (trade secret) <i>(Cui et al. 2010) (Cui, Tang et al. 2010)</i>
siATG5	UCUGAAUGAAAGGCCGUUC,AAAUCUCACUAACAUCUUC,UAUUCCAUGAGUUUCCGGU,UUUCGUUGAUCACCGACU
siNIX	AAAUCGACAUCGUACAUGC,AUUACCGUUGCCAUUGCUG,AAUGACGCCAGUGCUGACG,ACUCGUUCCAAGUCUCUUC

2.1.7 Plasmids

Table 2.11 List of plasmids.

Name	Usage	Origin	Reference
pEGFP-C1-rLC3	Visualization of autophagosome formation	<i>T. Yoshimori, Osaka, Japan</i>	<i>(Kabeya et al. 2000)</i>
pmCherry-Parkin	Visualization of Parkin dynamics	<i>R.J. Youle, Bethesda, USA</i>	<i>(Narendra et al. 2008)</i>
pcDNA3.1-mtGFP	Visualization of mitochondria via GFP	<i>AG Reichert, Frankfurt am Main</i>	<i>(Anand et al. 2016)</i>

2.1.8 Antibodies

Table 2.12 List of primary antibodies.

Name	Anti-gen	Type	Host	Source	Catalogue No.	Dilution	Band Size (kDa)
Atg5	hsa	p	ocu	<i>Sigma-Aldrich, Taufkirchen</i>	A0856	1:1000	56
Calreticulin	hsa	p	ocu	<i>Cell Signaling Technology, Danvers, USA</i>	2891	1:1000	55
Caspase 3	hsa	p	ocu	<i>Cell Signaling Technology, Danvers, USA</i>	9662	1:1000	17,19, 35
Cytochrome <i>c</i>	hsa	m	ocu	<i>Abcam, Cambridge, UK</i>	ab133504	1:2000	14
Cytochrome <i>c</i> , Alexa Fluor 488	mmu	m	mmu	<i>BD Bioscience, Heidelberg</i>	560263	1:500	14
Drp1	hsa	m	mmu	<i>Cell Signaling Technology, Danvers, USA</i>	14647	1:1000	80
GAPDH	ocu	m	mmu	<i>Sigma-Aldrich, Taufkirchen</i>	G8795	1:2000	45
GFP	A. victoria	m	mmu	<i>Sigma-Aldrich, Taufkirchen</i>	11814460001	1:1000	27
HO-1	hsa	m	ocu	<i>Abcam, Cambridge, UK</i>	ab52947	1:1000	33
Hsp60	hsa	p	ocu	<i>Sigma-Aldrich, Taufkirchen</i>	SAB4501464	1:1000	61
LC3	hsa	p	ocu	<i>Abcam, Cambridge, UK</i>	ab51520	1:1000	15, 18
NF- κ B p65	hsa	m	mmu	<i>BD Bioscience, Heidelberg</i>	610868	1:1000	65
OPA1	hsa	p	ocu	<i>AG Reichert, Frankfurt am Main</i>	-	1:1000	85,100
p616 Drp1	hsa	p	ocu	<i>Cell Signaling Technology, Danvers, USA</i>	3455	1:1000	80
p62	hsa	p	ocu	<i>Cell Signaling Technology, Danvers, USA</i>	5114	1:1000	62

p637 Drp1	hsa	p	ocu	<i>Cell Signaling Technology, Danvers, USA</i>	4867	1:1000	80
p70 S6 Kinase	hsa	p	ocu	<i>Cell Signaling Technology, Danvers, USA</i>	9202	1:1000	70, 85
Parkin	hsa	m	mmu	<i>Merck, Darmstadt</i>	05-882	1:1000	52
PARP	hsa	p	ocu	<i>Cell Signaling Technology, Danvers, USA</i>	9542	1:1000	89, 116
PGC-1 α	hsa	m	ocu	<i>Cell Signaling Technology, Danvers, USA</i>	2178	1:1000	130
PINK1	hsa	m	ocu	<i>Cell Signaling Technology, Danvers, USA</i>	6946	1:1000	50, 60
Qil1	hsa	p	ocu	<i>AG Reichert, Düsseldorf</i>	-	1:1000	13
TGM2	hsa	m	ocu	<i>Cell Signaling Technology, Danvers, USA</i>	3557	1:1000	78
Tim23	rno	m	mmu	<i>BD Bioscience, Heidelberg</i>	611222	1:1000	23
Tom20	hsa	p	ocu	<i>Proteintech, Manchester, UK</i>	11802-1- AP	1:1000	20
Ubiquitin	hsa	m	mmu	<i>Merck, Darmstadt</i>	05-944	1:1000	8
VDAC1	hsa	m	mmu	<i>Abcam, Cambridge, UK</i>	ab14734	1:1000	39
β -Actin	hsa	p	ocu	<i>Sigma-Aldrich, Taufkirchen</i>	A2103	1:1000	42
β -Tubulin	hsa	m	ocu	<i>Cell Signaling Technology, Danvers, USA</i>	2128	1:1000	55

p: polyclonal, m: monoclonal, ocu: rabbit, mmu: mouse, rno: rat, hsa: human.

Table 2.13 List of secondary antibodies.

Name	Antigen	Type	Host	Source	Catalogue No.	Dilution
Goat anti-mouse IgG (H+L), Alexa Fluor 488	mmu	p	goat	<i>Thermo Fisher Scientific, Langenselbold</i>	A-11001	1: 1000
Goat anti-mouse IgG (H+L) HRP conjugate	mmu	p	goat	<i>Abcam, Cambridge, UK</i>	ab97023	1:50000
Goat anti-rabbit IgG (H+L), Alexa Fluor 568	ocu	p	goat	<i>Thermo Fisher Scientific, Langenselbold</i>	A-11011	1: 1000
Goat anti-rabbit IgG (H+L) HRP conjugate	ocu	p	goat	<i>Dianova, Hamburg Santa Cruz</i>	DAB-087745	1:50000
Mouse anti-goat IgG-HRP	goat	m	mmu	<i>Biotechnology, Heidelberg</i>	sc2354	1:10000

p: polyclonal, m: monoclonal, ocu: rabbit, mmu: mouse.

2.1.9 Software

Table 2.14 List of software.

Name	Company
corelDRAW X7	<i>Corel Corporation, Ottawa, Canada</i>
EndNote X7	<i>Clarivate Analytics, London, UK</i>
FusionCapt Advance	<i>Vilber Lourmat, Eberhardzell</i>
iControl	<i>Tecan, Männedorf, Switzerland</i>
Illustrator CS3	<i>Adobe Systems, San Jose, USA</i>
ImageJ	<i>National Institutes of Health, Bethesda, USA</i>
Microsoft Office 2013	<i>Microsoft, Hamburg</i>
Photoshop CS3	<i>Adobe Systems, San Jose, USA</i>
Prism 7	<i>Graphpad, La Jolla, USA</i>
ProbeFinder Version 2.52	<i>Roche, Rotkreuz, Switzerland</i>
Rotor-Gene Q	<i>Qiagen, Hilden</i>
Volocity(64 bit)	<i>PerkinElmer, Solingen</i>
ZEN 2012	<i>Carl Zeiss, Jena</i>

2.1.10 Animal tissue lysates

In total, sixteen rat cortex lysate samples are kindly provided by Dr. Boris Görg, Dr. Hans-Jürgen Bidmon, and Prof. Dieter Häussinger's group.

The details of these samples are listed below:

Rats: Wistar, male,

Age: animals 1-8: 26 days, animals 13-20: 28 days,

Taurine: 5% in drinking water for 5 days,

Ammonium acetate: single intraperitoneal injection of ammonium acetate (4.5 mmol/kg BW),

Vehicle: NaCl (0.9%),

Duration of the experiment: 24 h.

Table 2.15 List of animal tissue samples.

Animal No.	Characteristics
1	Taurine + 0.9% NaCl
2	Taurine + 0.9% NaCl
3	Taurine + Ammonium acetate
4	Taurine + Ammonium acetate
5	Taurine + Ammonium acetate
6	Taurine + 0.9% NaCl
7	Taurine + Ammonium acetate
8	Taurine + 0.9% NaCl
13	Untreated + 0.9% NaCl
14	Untreated + 0.9% NaCl
15	Untreated + Ammonium acetate
16	Untreated + Ammonium acetate
17	Untreated + Ammonium acetate
18	Untreated + Ammonium acetate
19	Untreated + 0.9% NaCl
20	Untreated + 0.9% NaCl

2.2 Methods

2.2.1 Preparation and cultivation of primary rat astrocytes

All animal experimental protocols have been approved by Institutional Animal Care and Use Committee, Heinrich Heine University Düsseldorf. Primary rat astrocytes were prepared by Dr. Boris Görg and Prof. Dieter Häussinger's group, from the cerebral cortex of newborn Wistar rats as described (Matthiessen et al. 1989). Briefly, after decapitation, the scalp was removed and the skull was opened by scissors. The brain was taken out and the hemispheres were separated by tweezers. With the scalpel, the cerebral cortex of both hemispheres was prepared and the meninges were then taken away. Subsequently, the cortex was coarse crushed with a scalpel in 10 mL DMEM (supplemented by 10% (v/v) penicillin/streptomycin and 10% (v/v) FBS) and centrifuged for 1 minute at 1500 rpm. After mixing with 20 mL DMEM culture medium via a Pasteur pipette, the tissue suspension was filtered via a sterile nylon mesh (60 µm). The suspension was then split into cell culture flasks and cultured in an incubator (10% CO₂, 37 °C) for 7 days. To further purify astrocytes, flasks were shaken at 200 rpm for 12 h to reduce the residual microglia cells, oligodendrocytes and neurons (Booher and Sensenbrenner 1972). Later, the cultures were split into flasks again in a ratio of 1: 3 and cultured in an incubator (5% CO₂, 37 °C) to reach confluency. For experiments, the cells were split again on cell culture dishes and cultured in DMEM culture medium (supplemented with 10% (v/v) penicillin/streptomycin, 10% (v/v) FBS, and 2 mM GlutaMAX). Trypsinization was performed using PBS without Ca²⁺ and Mg²⁺. DMEM culture medium was changed every two days and cell growth was monitored via an Eclipse TS100 microscope (Nikon). Generally, primary rat astrocytes were cultured for 4-6 weeks before experiments.

2.2.2 Cultivation of human cell lines

Besides primary rat astrocytes, six human cell lines were also used in this study, as described

in Table 2.7. Cells were maintained in DMEM culture medium (supplemented with 10% (v/v) penicillin/streptomycin, 10% (v/v) FBS, and 2 mM GlutaMAX) in an incubator (5% CO₂, 37 °C) under water vapor saturation. When the cells reached 80% confluency, they were split on new cell culture dishes in a ratio of 1:10. To avoid contamination, a mycoplasma test was conducted at regular intervals according to the manufacturer's protocol (Minerva Biolabs). Cell lines were preserved using cryopreservation medium (50% DMEM with 40% FBS, 10% DMSO, (v/v)).

2.2.3 MTT assay

Primary rat astrocytes were seeded into 96 well plates at a density of around 3500/well. Cells were then incubated in DMEM culture medium (supplemented with 10% (v/v) penicillin/streptomycin, 10% (v/v) FBS, and 2 mM GlutaMAX) in an incubator (5% CO₂, 37 °C) for 24 h. The old medium was then removed and the experiments were carried out with indicated treatments for indicated time periods. At the scheduled time points, cells were washed with PBS once and incubated with medium containing 0.5 mg/mL MTT in an incubator (5% CO₂, 37 °C) for 4 h. Finally, the medium was removed and 100 µL DMSO was added to each well to extract the purple formazan (1-(4,5-Dimethylthiazol-2-yl)-3,5-diphenylformazan). The plates were then being processed by the Microplate reader infinite 200 PRO spectrophotometer (Tecan). The absorbance at the wavelength of 570 nm was measured with the reference wavelength of 650 nm. Data were obtained in triplicates and the mean absorbance was presented for each experiment.

2.2.4 Trypan blue staining

Trypan blue staining was used to check the cell viability after NH₄Cl treatment. Trypan blue can only pass through the cell membrane of dead cells, thus makes dead cells distinguished from living cells. After treatment, cells were trypsinized and resuspended in DMEM culture

medium. 0.8 mM trypan blue was dissolved in PBS and mixed with cell suspension in a ratio of 1:1 (v/v). 10 μ L suspension mixture was taken out for each sample and cells were counted manually with Neubauer chamber (Brand) or automatically by the Countess automated cell counter (Invitrogen). Data were produced in triplicate for each sample and the mean cell viability was presented.

2.2.5 Preparation of plasmids from *E. coli* cells

Chemically competent *E. coli* cells were prepared as follows: *E. coli* strain was cultivated to mid-log phase (OD₆₀₀ 0.25-0.3) in 100 mL LB medium (37 °C, vigorous shaking). Cells were then centrifuged at 3300 x g for 10 min at 4 °C. Afterward, cells were resuspended in 40 mL ice-cold 0.1 M calcium chloride for 30 min. Cells were then collected and kept in cold 0.1 M calcium chloride solution plus 15% glycerol at -80 °C. Transformation of *E. coli* cells was carried out using the heat shock method. Briefly, 100 μ L chemically competent *E. coli* cells were mixed carefully with 50 ng of plasmids, the mixture was then incubated on ice for 30 min followed by a heat shock at 42 °C for 1.5 min. After adding 1 mL LB medium, cells were recovered by shaking at 37 °C for 30 min. Cells were then collected and spread on LB_{Amp} agar plates. Colonies were picked after overnight incubation at 37 °C. Isolation of plasmid DNA from *E. coli* cells was based on the alkaline lysis method (Birnboim and Doly 1979). Plasmid extraction was executed with either QIAprep spin miniprep kit (Qiagen) or PureLink HiPure plasmid midiprep kit (Life Technology) following the manufacturer's protocols. DNA concentration was determined by the absorbance at 260 nm and DNA purity was indicated by the ratio of absorbance at 260 nm and 280 nm, using the Biospectrometer basic (Eppendorf). Agarose gel electrophoresis (1%, in 1X TAE buffer) was used to confirm the amplified plasmid size.

2.2.6 siRNA transfection

siRNA used in this study are listed in Table 2.9. Cultured astrocytes were plated on a dish before transfection. When cells reached around 80% confluency, overnight transfection was performed with either siRNA against rat Atg5 (Dharmacon Research, M-095125-01-0005), Parkin (Dharmacon Research, L-090709-02-0005), PINK1 (Ambion, ID#180640) or with a scrambled control siRNA (Ambion, AM4611). 100 nM final concentration was used for each of these siRNAs. Transfection was done with Lipofectamine RNAiMax (Invitrogen) or HiPerFect transfection reagent (Qiagen), according to the manufacturer's protocols. The samples were collected or assayed after 48-96 h of transfection, the efficiencies of gene knockdown were verified using western blot analysis.

2.2.7 Crude mitochondria isolation

Crude mitochondrial isolation was performed as previously described (Anand et al. 2016). After treatment, the cells were washed with 10 mL PBS and harvested by scraping. Cell pellets were obtained by centrifuge at 500 x g for 5 min. Cells were then resuspended in ice-cold mitoisolation buffer for 10 min on ice. The suspension was homogenized by repeatedly passing through a syringe needle of 26G cannula for 25 times. Then the suspension was first centrifuged at 1000 x g, 4 °C for 5 min, after which the turbidity of the supernatant was checked. The needle-mediated mechanical rupture process was repeated if the supernatant was almost clear. After turbidity check, the suspension was centrifuged again at 1000 x g, 4 °C for another 10 min to pellet the cell debris and nuclei. The supernatant containing heavy membranes was further centrifuged at 7000 x g, 4 °C for another 15 min to pellet crude mitochondria. The protein concentration was then determined using Bradford reagent (Sigma-Aldrich), according to the manufacturer's protocol. The mitochondrial fraction was frozen in mitoiso freezing medium and kept at -80 °C.

2.2.8 TCA precipitation

TCA precipitation was used to concentrate protein content in the samples. One volume of 72% TCA stock solution was mixed with five volumes of protein sample to reduce the TCA concentration to 12%. The mixed aqueous solution was incubated on ice for 30 min and then centrifuged at 14000 rpm for 5 min. The supernatant was carefully removed from the whitish, fluffy pellet. 0.5 mL cold acetone (-20 °C) was then slowly added to wash the pellet. The samples were centrifuged again at 14000 rpm for 5 min and the pellet was air-dried for 15 min to drive off acetone. The pellet was dissolved in 2x Lämmli buffer and cooked at 95 °C for 5 min before analysis. Tris was added to neutralize the pH when the color of samples became yellowish.

2.2.9 SDS-PAGE

SDS-PAGE gels containing a 5% stacking gel and different percentage of resolving gels were cast according to Table 2.16.

Table 2.16 Composition of the SDS-PAGE gels.

Component	Resolving gel (15 mL), mL				Stacking gel (5 mL), mL
	8%	10%	12%	14%	
MiliQ H ₂ O	7.9	7.15	6.4	5.65	3.6075
Rotiphorese gel 40 (AA/BAA = 37.5/1) (w/v)	3	3.75	4.5	5.25	0.6225
1.5 M Tris-HCl buffer (pH 8.8)	3.8	3.8	3.8	3.8	-
1.0 M Tris-HCl buffer (pH 6.8)	-	-	-	-	0.63
10% (w/v) SDS	0.15	0.15	0.15	0.15	0.05
10% (w/v) APS	0.15	0.15	0.15	0.15	0.05
TEMED	0.009	0.009	0.009	0.009	0.005

After experiments, cells were harvested and lysed in appropriate lysis buffers for 1 h on ice.

Then the lysates were centrifuged at 10000 rpm for 5 min at 4 °C, only the supernatants were kept. The protein concentration in the supernatant was then determined using Bradford reagent (Sigma-Aldrich), according to the manufacturer's protocol. Serial-diluted BSA solution was used to generate the standard curve. The absorbance at 595 nm was measured and the protein concentration was determined using the standard curve. An equal amount of protein lysates were then mixed with an appropriate amount of 4x Lämmli buffer and lysis buffer, before cooking at 95 °C for 5 min. After cooking, samples were briefly centrifuged and loaded into gels. Gels were run in 1X SDS running buffer, first at a constant voltage of 80 V and later at a constant voltage of 100 V when the bromophenol blue line had become condense and even. The proteins were then separated according to their molecular weights.

2.2.10 Western blot

Western blots were performed on a semidry blotting machine (P. Reiser). Whatman papers, nitrocellulose membranes or methanol-activated PVDF membranes were soaked in ice-cold 1X blotting buffer before use. The SDS-PAGE gel was also immersed in ice-cold 1X blotting buffer to get equilibrated. Papers and the membrane were arranged in the following order: the anode, Whatman papers, the membrane, the gel, Whatman papers, the cathode. The protein transfer was carried out at a constant current of 200 mA for 1.5 h. After transfer, Ponceau S solution was used to stain the membrane for 1 min to confirm the successful transfer of proteins. The membrane was then blocked in blocking solution for 30 min. Primary and secondary antibodies were diluted in 5% milk TBST solution (Table 2.12 & 2.13). The membrane was incubated with primary antibody at 4 °C overnight or at room temperature for 1-2 h. Subsequently, the membrane was washed three times with 1X TBST buffer for 5 min. Afterward the membrane was incubated with secondary antibody at room temperature for 30 min. Next, the membrane was washed three times with 1X TBST buffer for 10 min. The membrane was then developed with SignalFire ECL reagent (Cell Signaling Technology) and documented by FUSION SL chemiluminescence system (Vilber Lourmat). If necessary, the membrane was stripped in

stripping buffer at 50 °C for 30 min after which the membrane was re-blocked in fresh blocking solution. Densitometric quantification of at least three independent experiments was conducted with ImageJ (National Institutes of Health)/FusionCapt Advance (Vilber Lourmat). GAPDH, β -tubulin, β -actin and Ponceau S staining were used as loading controls.

2.2.11 Immunofluorescence

Immunofluorescence analysis was carried out to visualize the expression and intracellular localization of specific proteins. For rat astrocytes, astrocytes were plated on MatTek dishes and treated as indicated in experimental conditions. Subsequently, cells were washed by PBS (10 min) twice and fixed by 1 mL 4% (v/v) paraformaldehyde in PBS for 20 min at 37 °C. After washing with PBS (10 min) thrice, cells were permeabilized by 1 mL 0.15% (v/v) Triton-X in PBS for 15 min at room temperature. Following washing with PBS (10 min) thrice, 1 mL of blocking solution (3% (w/v) BSA in PBS) was added into the dish and incubated for 1 h at room temperature. Next cells were incubated with 300 μ L primary antibodies diluted in blocking solution overnight at 4 °C (dilution factor: 50-100). Cells were then washed three times with PBS (10 min) before they were incubated with 500 μ L secondary antibodies conjugated with specific fluorochromes for 2 h at room temperature (dilution factor: 1000-2000). After another PBS (10 min) wash for three times, cell nuclei were stained with 150 μ L DAPI (1:1000) for 10 min at room temperature. Finally, cells were again washed three times with PBS (10 min) and maintained in 2 mL PBS, fluorescence observation was then carried out using the Axio observer D1 fluorescence microscopy (Carl Zeiss) or Eclipse Ti microscope (Nikon) in combination with UltraVIEW VoX spinning disk confocal system (PerkinElmer).

2.2.12 Evaluation of mitochondrial membrane potential via TMRM

The mitochondrial membrane potential was measured using the voltage-sensitive dye TMRM.

Rat astrocytes were transfected with pcDNA3.1-mtGFP 48 h before treatment, using Effectene transfection reagent (Qiagen). After treatment with the indicated amount of NH₄Cl for 72 h, cells were stained with 50 nM TMRM for 30 min at 37 °C. For the positive control group, 10 μM CCCP was added after cells were treated without NH₄Cl for 66 h. After washing with PBS (10 min) three times, cells were imaged using the Axio observer D1 fluorescent microscope (Carl Zeiss). mtGFP was used to localize and focus the cells, untreated stained cells and CCCP-treated cells served as negative control and positive control for optimizing laser power, exposure time and sensitivity. Once the optimal exposure time was fixed, the same setting for the red channel was used for the whole experiment. Semiquantification of red fluorescence intensity was carried out in 10-15 randomly selected areas using the ZEN 2012 software (Carl Zeiss). Quantification was expressed as the mean of red fluorescence ratios, compared to untreated control group which was set to 100%.

2.2.13 Fluorescence microscopy

Fluorescence microscopy was used to visualize the mitochondrial dynamics and the colocalization between Parkin with mitochondria. Cells were cotransfected with an appropriate amount of pcDNA3.1-mtGFP and pmCherry-Parkin using Effectene transfection reagent (Qiagen), according to the manufacturer's protocol. 24 h after transfection, cells were seeded onto MatTek dishes. 48 h after transfection, cells were treated with sterilized H₂O or 5 mM NH₄Cl for indicated time periods. Treatment with 10 μM CCCP for 6 hours served as a positive control. Imaging at different time points was done using the Axio observer D1 fluorescent microscope (Carl Zeiss) with a 63X objective. For mitochondrial morphology and Parkin colocalization, ZEN 2012 software (Carl Zeiss) was used to prepare the images.

2.2.14 Spinning disk confocal microscopy

The spinning disk confocal microscopy is a combination of Eclipse Ti microscope (Nikon) and UltraVIEW VoX spinning disk confocal system (PerkinElmer). This system was used in several experiments including measurement of mitochondrial membrane potential and immunostaining. For measurement of mitochondrial membrane potential, MatTek/Ibidi dishes were put into the live imaging chamber (5% CO₂, 37 °C) at the scheduled time point and stay there for the whole imaging period. Laser power, exposure time and sensitivity were adjusted to get the optimal image quality. Once these parameters were fixed, images were acquired and analyzed by Volocity (64 bit) (PerkinElmer) in video mode with the 60X objective.

2.2.15 Transmission electron microscopy

Cells with 80% confluence were cultured in a petri dish and fixed using 3% glutaraldehyde buffered in 0.1 M sodium cacodylate buffer (pH 7.2). After fixation, cells were harvested by scraping and centrifugation. The cell pellet was then washed with 0.1 M sodium cacodylate buffer (pH 7.2) and embedded in 2% agarose. Subsequently, cells were stained with 1% osmium tetroxide for 50 min, followed by 1% uranyl acetate/1% phosphotungstic acid staining for 1 h. After that, samples were dehydrated using the graded acetone series and specimen were embedded in spur epoxy resin for polymerization (65°C, 24 h). The microtome was then employed to prepare the ultrathin sections and images were acquired using the H600 transmission electron microscope (Hitachi, 75V) and Bioscan model 792 (Gatan). Images were analyzed using ImageJ (National Institute of Health).

2.2.16 Validation of paNP functionality by pH measurement

pH measurement was conducted in water solution with or without 10% (v/v) FBS, 125 µL paNP (25 mg/mL) was added into 1 mL water solution together with 0.25 µL 1 M NaOH. Water solution with or without 10% (v/v) FBS were strictly kept in the dark (aluminum foil cover,

avoid light when opened), room temperature for 24 h and pH was measured at 0 h, 1 h, 2 h, 4 h and 24 h. At 24 h, the solutions were directly exposed to a continuous three sections of 10 min UV exposure (366 nm, 4W), pH was measured after each section (UV exposure for 10 min, 20 min, and 30 min). After 30 min UV exposure, the solutions were again kept in the dark at room temperature for another 24 h and pH was measured again at 24.5 h (0 h after 30 min UV exposure), 25.5 h, 26.5 h, 28.5 h and 48.5 h post UV exposure.

2.2.17 LysoSensor™ staining and image analysis

Astrocytes were seeded in MatTek dishes 48 h before experiments. Where indicated, paNP (25 µg/mL) were applied 4 h before NH₄Cl treatment (5 mM, 72 h). After treatment, cells were stained with 1 µM LysoSensor™ Green DND-189 (Invitrogen) for 30 min, for the NH₄Cl-treated group, 5 mM NH₄Cl was present during the staining procedure. Astrocytes were then imaged with the same setting using the spinning disk confocal microscopy (Eclipse Ti microscope (Nikon) and UltraVIEW VoX spinning disk confocal system (PerkinElmer)). Around 50 cells were analyzed for each group.

2.2.18 Magic red cathepsin L activity assay

Cultured rat astrocytes were treated with 25 µg/mL paNP 4 h before NH₄Cl/CH₃NH₃Cl treatment. The UV exposure group received a 5 min UV exposure (365 nm, 4 W) after being treated with NH₄Cl for 48 h. The positive control group was treated with H₂O₂ (1.5 mM, 72 h). 72 h after NH₄Cl/CH₃NH₃Cl treatment, cathepsin L activity was analyzed via magic red cathepsin L assay kit (Immunochemistry technology), according to the manufacturer's manual (protocol 15). Red (excitation: 592 nm; emission: 628 nm) fluorescence was detected by microplate reader infinite 200 PRO (Tecan).

2.2.19 Nanoparticle treatment and UV exposure

For autophagic activity and relevant MTT assay, paNP were applied in cell culture 4 h before $\text{NH}_4\text{Cl}/\text{CH}_3\text{NH}_3\text{Cl}$ treatment to reach a final concentration of 25 $\mu\text{g}/\text{mL}$. The UV exposure group received a UV exposure (365 nm, 4 W, 5 min) after being treated with $\text{NH}_4\text{Cl}/\text{CH}_3\text{NH}_3\text{Cl}$ for 48 h. After another 24 h, cells were harvested for western blot analysis or assayed via MTT. For determination of cytotoxicity due to paNP concentration, cells were treated with various concentration of paNP 4 h before UV exposure (365 nm, 4 W, 5 min), after UV exposure, cells were kept in the dark for another 21 h before MTT assay. For determination of cytotoxicity due to UV exposure duration, cells were treated with paNP (25 $\mu\text{g}/\text{mL}$) 4 h before indicated UV exposure (365 nm, 4W), cells were kept in the dark for another 21 h before MTT assay. UV exposure was conducted as follows: plates were strictly kept in dark before UV exposure, during UV exposure, plates were directly placed under UV lamp without the protection of lid. After UV exposure, the plates were again covered with aluminum foil until further measurement.

2.2.20 Rat models of acute ammonium intoxication

Rat cortex lysate samples from a model of acute ammonium intoxication were obtained from Dr. Boris Görg, Dr. Hans-Jürgen Bidmon, and Prof. Dieter Häussinger's group. Detailed information of these samples is listed in Table 2.15. Acute ammonium acetate intoxication in rats was done via administration of ammonium acetate (NH_4Ac) at a dose of 4.5 mmol/kg BW. Samples were obtained and prepared as previously described (Schliess et al. 2002). To test the effect of taurine on NH_4Ac -induced acute ammonium intoxication, rats were supplied with drinking water containing 5% taurine (w/v) for 5 days before NH_4Ac administration.

2.2.21 *Post Mortem* human brain tissue

Post mortem human tissue were obtained by Dr. Boris Görg, Dr. Hans-Jürgen Bidmon, and Prof. Dieter Häussinger's group from the Department of Anatomy at the University of Düsseldorf or the Australian Brain Donor Programs NSW Tissue Resource Centre. Patient characteristics and histories have been described previously (Görg et al. 2013).

2.2.22 Array-based human transcriptome analysis

Data of Agilent microarray analysis for TGM2 gene expression in HE patients were prepared by Dr. Boris Görg. Briefly, two human transcriptome analyses were done using Agilent™ whole human genome microarray analysis (Agilent) by Miltenyi-Biotech (Bergisch Gladbach, Germany) (Görg et al. 2013, Sobczyk et al. 2015). Human samples in the first analysis included *post mortem* brain tissues of the intersection parietal to occipital cortex area from eight control subjects and eight patients with liver cirrhosis and accompanying HE (the Düsseldorf cohort). Additional *post mortem* brain tissues from three patients with liver cirrhosis without HE were obtained from the Australian cohort. Detailed information on this microarray and statistical analysis was described previously (Görg et al. 2013). Human samples in the second analysis included *post mortem* brain samples of the fusiform gyrus from control subjects, patients with liver cirrhosis with or without HE (four cases in each group) (the Australian cohort). Detailed information of this microarray and statistical analysis was described previously (Sobczyk et al. 2015). Gene array data were deposited at the public genomic data repository “Gene Expression Omnibus” (GEO, accession No. GSE41919 and GSE57193) of the National Center for Biotechnology Information (NCBI).

2.2.23 Statistical analysis

Data are presented as mean \pm standard error of the mean (SEM) unless otherwise stated. For analysis, at least three independent experiments were used. For comparison between two groups, a two-tailed, unpaired *t*-test was used to evaluate the statistical significance. If more than two groups were compared, the statistical evaluation was carried out by a one-way ANOVA with *post hoc* Bonferroni's test. The analysis was performed using Excel (Microsoft) or Prism 7 (Graphpad). A *p* value less than 0.05 was considered to be statistically significant.

3. Results

3.1 Autophagy is partially inhibited by ammonia in cultured rat astrocytes

3.1.1 Dual role of ammonia on autophagy in cultured rat astrocytes

Although increasing evidence suggests that intracellular autophagy is altered by ammonia in various pathological conditions, the impact of ammonia on autophagy has not been evaluated so far in astrocytes and HE (Youle and Narendra 2011, Polletta et al. 2015).

To determine this, we first examined autophagy in a well-established cultured rat astrocytes model (Schliess et al. 2002, Görg et al. 2015, Oenarto et al. 2016). Rat astrocytes were transfected with pEGFP-LC3, 24 h after transfection, astrocytes were treated with or without NH_4Cl , after treatment with indicated concentrations of NH_4Cl for 72 h, cells were harvested and subjected to western blot analysis (Fig. 3.1A). The autophagosome formation marker, LC3-II, was remarkably increased in astrocytes treated with 5 mM NH_4Cl , together with robustly accumulated autophagic substrate p62, relative to control (Fig. 3.1A). Interesting to note, compared with astrocytes receiving no NH_4Cl treatment, astrocytes treated with 0.5 or 1 mM NH_4Cl showed an increased LC3-II level but decreased p62 accumulation, which is similar to that of rapamycin-treated astrocytes. This altered autophagy pattern was also evidenced by the dose-dependent accumulation of free GFP cleaved from GFP-LC3.

In parallel, cells receiving the same treatments were examined via fluorescence microscopy, as shown in Fig. 3.1B, treatments of various concentrations of NH_4Cl rendered a dose-dependent increase in the formation of GFP-LC3 puncta which was further enhanced by 10 μM chloroquine (CQ). Considering the fact that CQ is commonly used to completely block autophagic flux via neutralizing lysosomal pH, 5 mM NH_4Cl treatment only partially inhibits autophagic flux.

Together, these results suggest that NH_4Cl treatment at low concentrations induces autophagy

while NH_4Cl treatments at higher concentrations block autophagic flux. Interesting to note, both fluorescence microscopy and western blot data showed that compared with astrocytes treated with 5 mM NH_4Cl and 10 μM CQ, autophagy activity was still not fully inhibited in the 5 mM NH_4Cl -treated group, as evidenced by the relatively less increase in the GFP-LC3 puncta formation and the less accumulation of p62 (Fig. 3.1A, B).

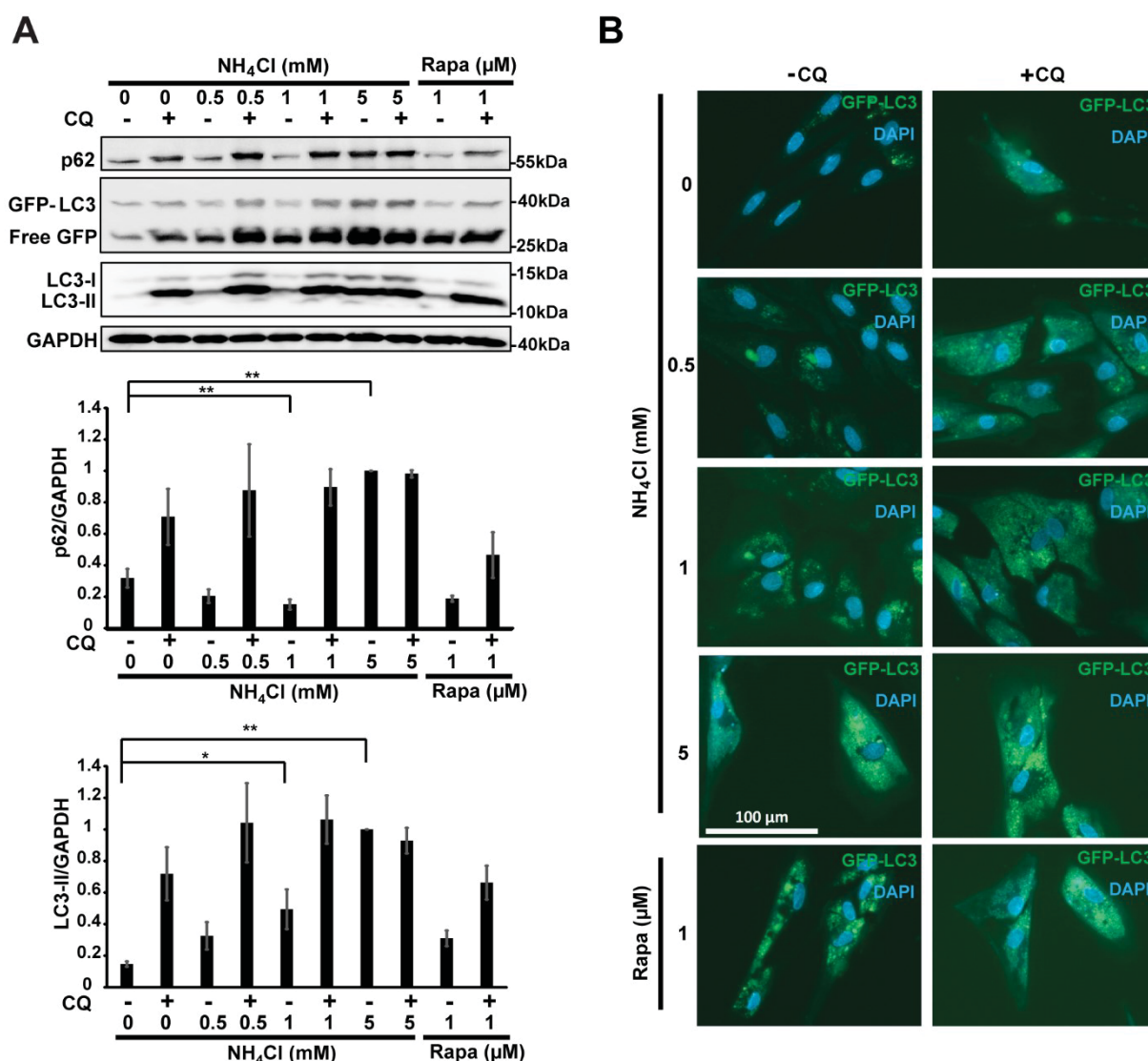


Fig. 3.1 Ammonium treatment inhibits autophagy in primary rat astrocytes. Astrocytes were transfected with pEGFP-LC3 for 24 h, after which, astrocytes were treated with various concentration of NH_4Cl with or without chloroquine (CQ, 10 μM) for 72 h. The positive control group was left untreated for 48 h and then autophagy was induced by addition of rapamycin (Rapa, 1 μM) for 24 h. After 72 h NH_4Cl treatment, intracellular autophagic activity was assayed via (A) western blot analysis and densitometric analysis of autophagy markers (n=3) and (B) fluorescence microscopy images of autophagosome (GFP-LC3 puncta) formation (scale bar: 100 μm). * $p < 0.05$, ** $p < 0.01$, compared with control group.

3.1.2 High concentrations of ammonium treatment inhibit autophagy in various cell lines

To test the hypothesis that the inhibitory effect of ammonia on autophagy is general rather than specific for astrocytes, we additionally evaluated the autophagy activity in various human cell lines after 5 mM NH₄Cl treatment. Although astrocytes were claimed to be the major target for ammonia-induced toxicity (Häussinger and Sies 2013), autophagy was shown to be consistently inhibited after a high concentration (5 mM) of ammonium treatment in various cell lines regardless of their tumorous states (Fig. 3.2). This result suggests that under hyperammonemic conditions, autophagy inhibition is present in various types of neuronal cells and thus possibly at a tissue level.

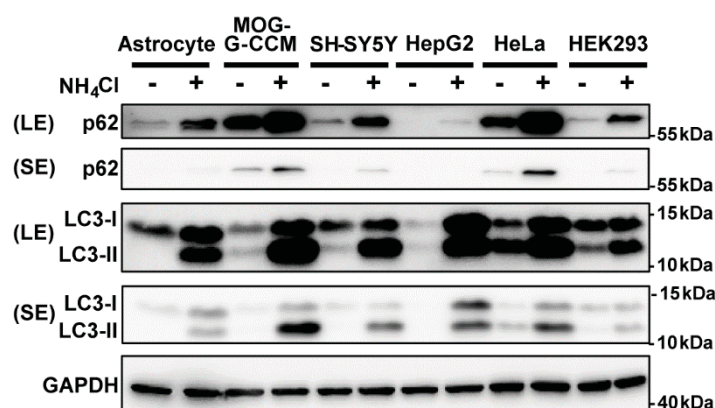


Fig. 3.2 Autophagy is inhibited by ammonium treatment in various cell lines. Western blot analysis of autophagy markers in primary rat astrocytes and various human cell lines with or without 5 mM NH₄Cl treatment for 72 h. LE: long exposure, SE: short exposure.

3.2 Inhibition of autophagy by ammonium is time- and dose-dependent, fast and reversible

We then proceeded to further characterize ammonia-induced autophagy inhibition in cultured rat astrocytes. As previous data indicated ammonia played a dual role in autophagy induction, we first sought to investigate the threshold concentration for NH₄Cl to place an inhibitory effect. As shown in Fig. 3.3A, from 2 mM onwards, the accumulation of autophagy substrate p62 and

autophagosome formation marker LC3-II began.

This accumulation of p62 and LC3-II in response to 5 mM NH_4Cl treatment was observed to be more prominent along with time (Fig. 3.3B). Relative to astrocytes left untreated for 24 h, the autophagosome-associated LC3-II was observed to be significantly increased in 5 mM NH_4Cl -treated groups after 24 h, 48 h and 72 h together with an insufficient clearance of autophagy substrate p62.

In cultured rat astrocytes, the alteration of autophagy activity happens very fast as evidenced by the obvious conversion of LC3-I to LC3-II after 1 h, however, the accumulation of p62 was more pronounced after 4 h (Fig. 3.3C).

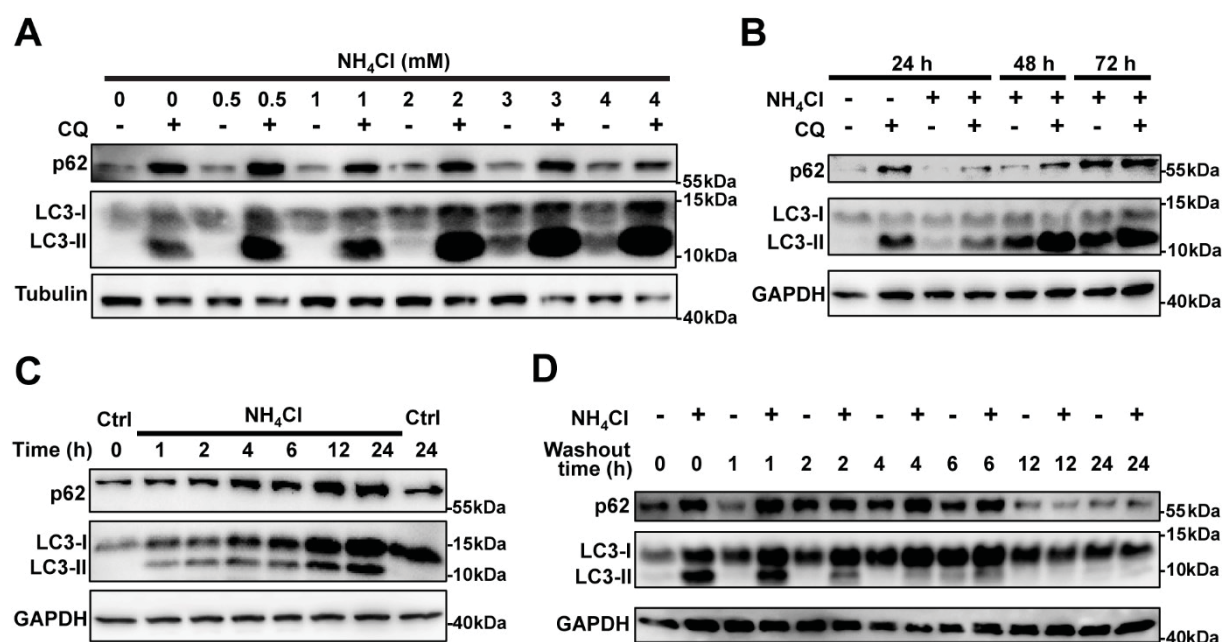


Fig. 3.3 Ammonia-induced autophagy inhibition is dose- and time-dependent, fast and reversible. Western blot analysis of autophagy activity in astrocytes treated with various concentrations of NH_4Cl with or without chloroquine (CQ, 10 μM) for the indicated amount of time, showing (A) threshold concentration of autophagy inhibition, (B) time dependence and (C) starting time point for autophagy inhibition. (D) Reversibility of autophagy inhibition induced by ammonia. Astrocytes treated with 5 mM NH_4Cl for 72 h, after which the old medium containing NH_4Cl was replaced with fresh medium for the indicated amount of time. Reversibility was then assayed via western blot analysis. Control group was treated with H_2O for the indicated amount of time.

Of note, ammonia-induced autophagy inhibition was proved to be reversible as evidenced by the clearance of p62 and LC3-II accumulation after a washout period of 12 h (Fig. 3.3D),

supporting the previous notion that HE symptoms were fully or partially reversible in patients receiving treatment (Atluri et al. 2010).

3.3 Inhibition of autophagy by ammonia is mainly mediated via pH alteration and is decreased by ROS scavengers

3.3.1 Autophagy inhibition induced by ammonium treatment is mainly mediated by pH alteration

As various studies pointed out ammonia treatment resulted in alkalization of intracellular pH (Bartolic et al. 2016), we first asked whether ammonia-induced autophagy inhibition is pH-dependent. Via electron microscopy (EM), compared with H₂O-treated controls, it was clear that 5 mM NH₄Cl treatment led to a dramatic increase in the number of darkly stained autophagosome/autolysosome structures (Fig. 3.4A). Quantification showed a 4.2 ± 3.2 fold increase ($p < 0.01$) in the number of autophagosome/autolysosome structures per area in 5 mM NH₄Cl-treated group, although a statistically significant increasing trend for the structure size was not observed (Fig. 3.4B, C, D). EM images also showed that in response to methylammonium chloride (CH₃NH₃Cl) treatment, astrocytic autophagosome/autolysosome number was increased to 5.1 ± 3.6 fold ($p < 0.01$), which was comparable to NH₄Cl treatment (Fig. 3.4B). Since the non-metabolizable CH₃NH₃Cl and NH₄Cl have a comparable capacity in altering intracellular pH, this result suggests that autophagy inhibition induced by ammonium treatment is mainly mediated by pH alteration.

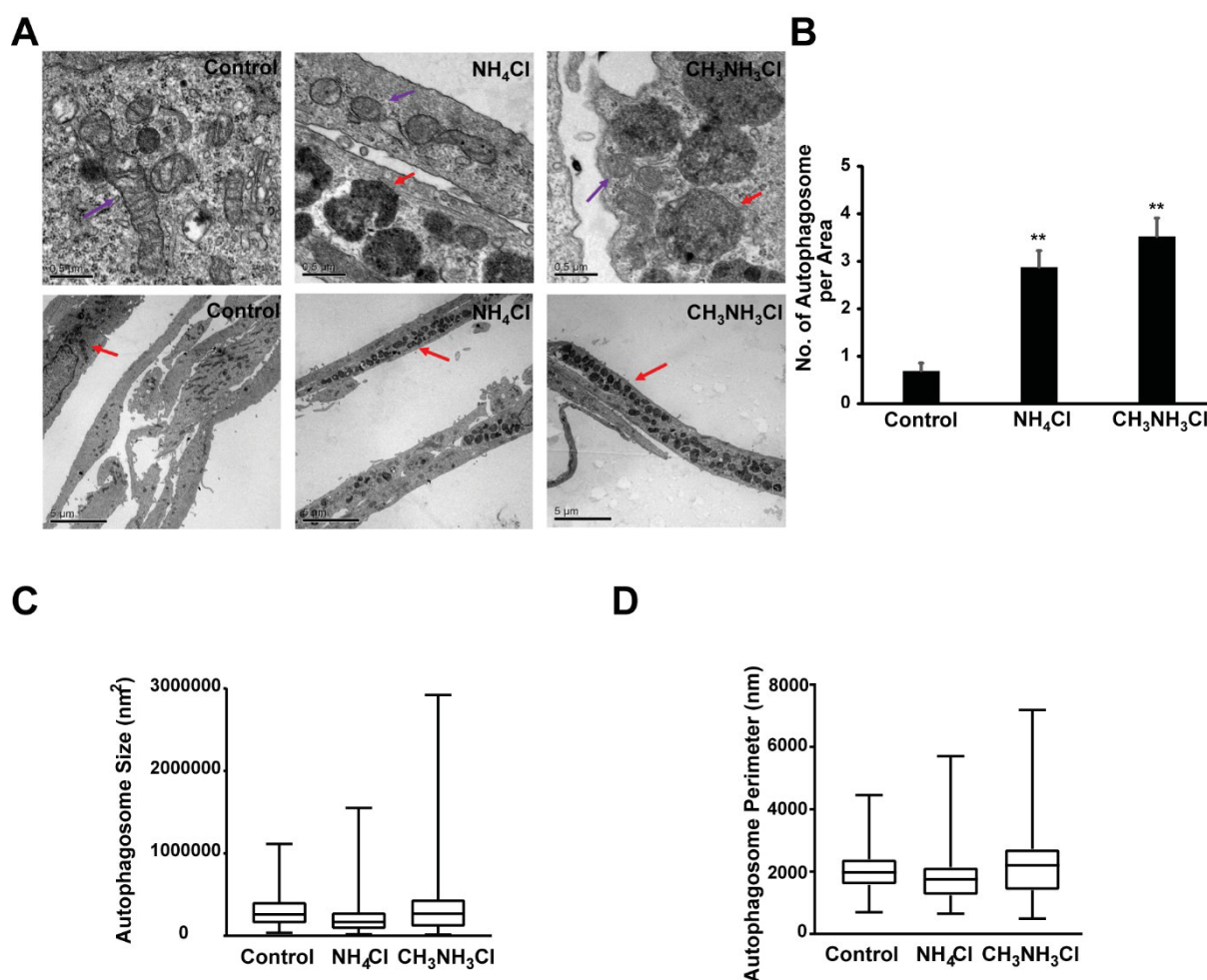


Fig. 3.4 Ammonia inhibits autophagy mainly via pH alteration. Astrocytes were treated with H₂O (control), NH₄Cl (5 mM) or CH₃NH₃Cl (5 mM) for 72 h. Autophagy was then assayed via electronic microscopy and quantification of autophagosomes. Representative EM images are shown in (A) (red arrows indicate autophagosomes/autolysosomes, purple arrows indicate mitochondria; scale bar: lower (5000X), 5 μ m; upper (50000X), 0.5 μ m). Quantification of autophagosome number per area (B), box plots of autophagosome size (C) and autophagosome perimeter (D) were analyzed from around 40 images per group, ** $p < 0.01$, compared with control group.

3.3.2 Inhibition of autophagy by methylammonium chloride is similar to that induced by ammonium chloride

We next asked whether CH₃NH₃Cl inhibits autophagy in a similar manner, compared with NH₄Cl. As shown in Fig. 3.5, characterization of the inhibitory effect that CH₃NH₃Cl placed on autophagy did prove that this inhibitory effect was also fast and reversible. Similar to NH₄Cl-induced LC3-II accumulation, CH₃NH₃Cl-induced LC3-II accumulation was also already

observable after 1 h (Fig. 3.5A). A washout period of 2 h already lead to dramatic clearance of the accumulated LC3-II and p62 while after a washout period of 6 h, the LC3-II level is comparable between control and CH₃NH₃Cl-treated group (Fig. 3.5B).

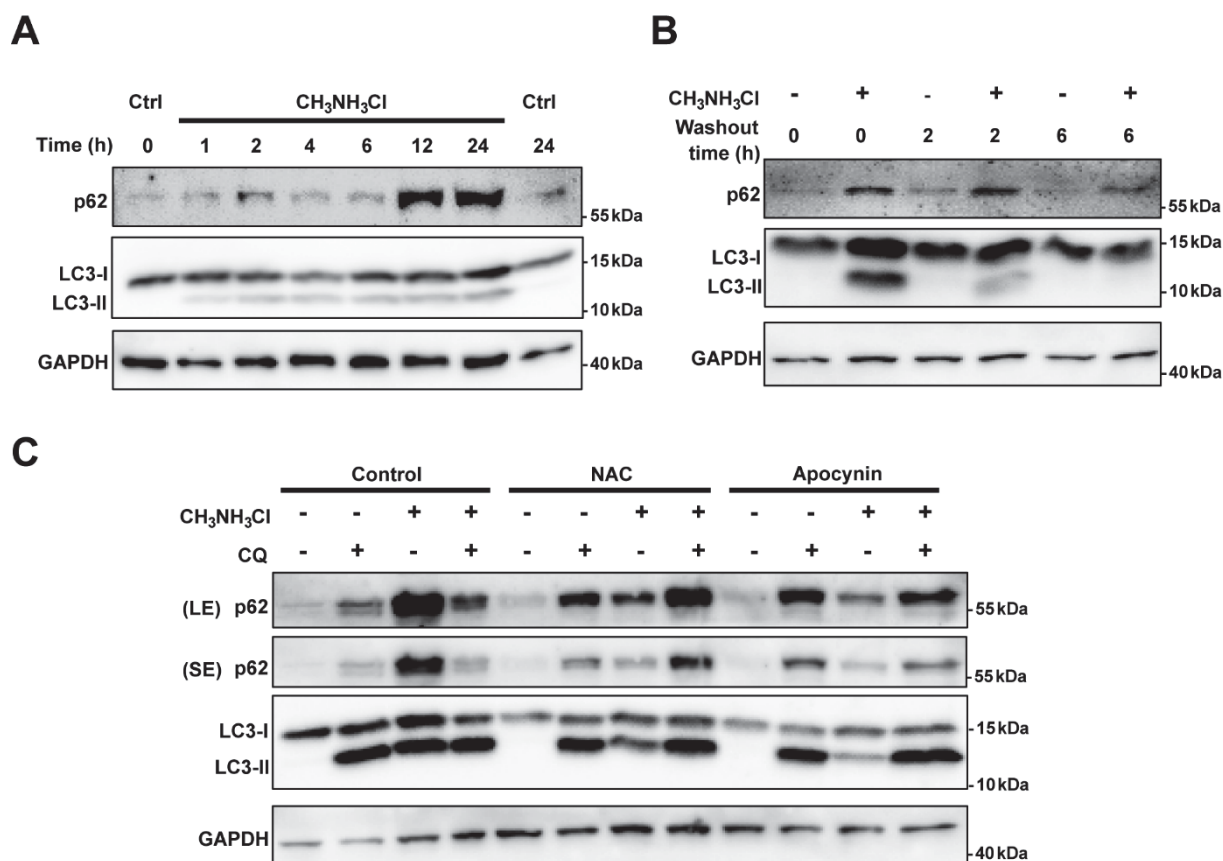


Fig. 3.5 Methylammonium chloride-induced autophagy inhibition is fast, dose-dependent and reversible. (A) Western blot analysis showing starting time point for CH₃NH₃Cl-induced autophagy inhibition in astrocytes treated with 5 mM CH₃NH₃Cl for the indicated amount of time. (B) Western blot analysis showing reversibility of CH₃NH₃Cl-induced autophagy inhibition. Astrocytes were treated with 5 mM CH₃NH₃Cl for 72 h, followed by a washout experiment for 0 h, 2 h or 6 h. (C) Pharmacological characterization of CH₃NH₃Cl-induced autophagy inhibition. Where indicated, NAC (2 mM) and apocynin (300 μM) were used to pre-treat astrocytes for 30 min and remained during the 72 h treatment of CH₃NH₃Cl (5 mM) with or without chloroquine (CQ, 10 μM). Autophagy inhibition was then assayed via western blot analysis. LE: long exposure, SE: short exposure.

3.3.3 Autophagy inhibition can be largely alleviated by intracellular ROS scavengers

Ammonia-induced formation of super anion radical in cultured rat astrocytes has been shown to be responsible for ammonia-induced toxic effects in several studies (Reinehr et al. 2007, Görg et al. 2015). To further address the question whether oxidative stress also makes a significant contribution towards ammonia-induced autophagy inhibition, multiple ROS decreasing agents were applied to cultured rat astrocytes before and during ammonium treatment.

Consistent with previous EM observations, western blot analysis revealed that treatment of 5 mM NH_4Cl or $\text{CH}_3\text{NH}_3\text{Cl}$ led to a similar degree of autophagy inhibition, as evidenced by the accumulation of LC3-II and p62 (Fig. 3.6A). In line with this, via immunostaining, the LC3 signal intensity was dramatically increased in both $\text{CH}_3\text{NH}_3\text{Cl}$ - and NH_4Cl -treated groups compared with control (Fig. 3.6B). These results further confirm that ammonia-induced autophagy inhibition is mainly mediated via altering the intracellular pH.

While pre-treatment of astrocytes with NAC (2 mM), a well acknowledged intracellular ROS scavenger (Warskulat et al. 2002), could dramatically block autophagy inhibition induced by ammonia to almost basal level (Fig. 3.6A). To a lesser extent, this alleviation effect on autophagy inhibition was also observed for the astrocytes pre-treated with apocynin (300 μM), as evidenced by the steady but less decrease in p62 and LC3-II levels (Fig. 3.6A). Compared with control group, the LC3-II conversion was also observed to be significantly decreased in the NAC- or apocynin-treated groups after 72 h along with a reduced accumulation of p62. Consistent with western blot analysis, immunostaining of LC3 also showed a decreased intensity in response to the combinational treatment of NAC and NH_4Cl (Fig. 3.6B). Together, these results indicate a direct role of antioxidants in blocking ammonia-induced autophagy inhibition.

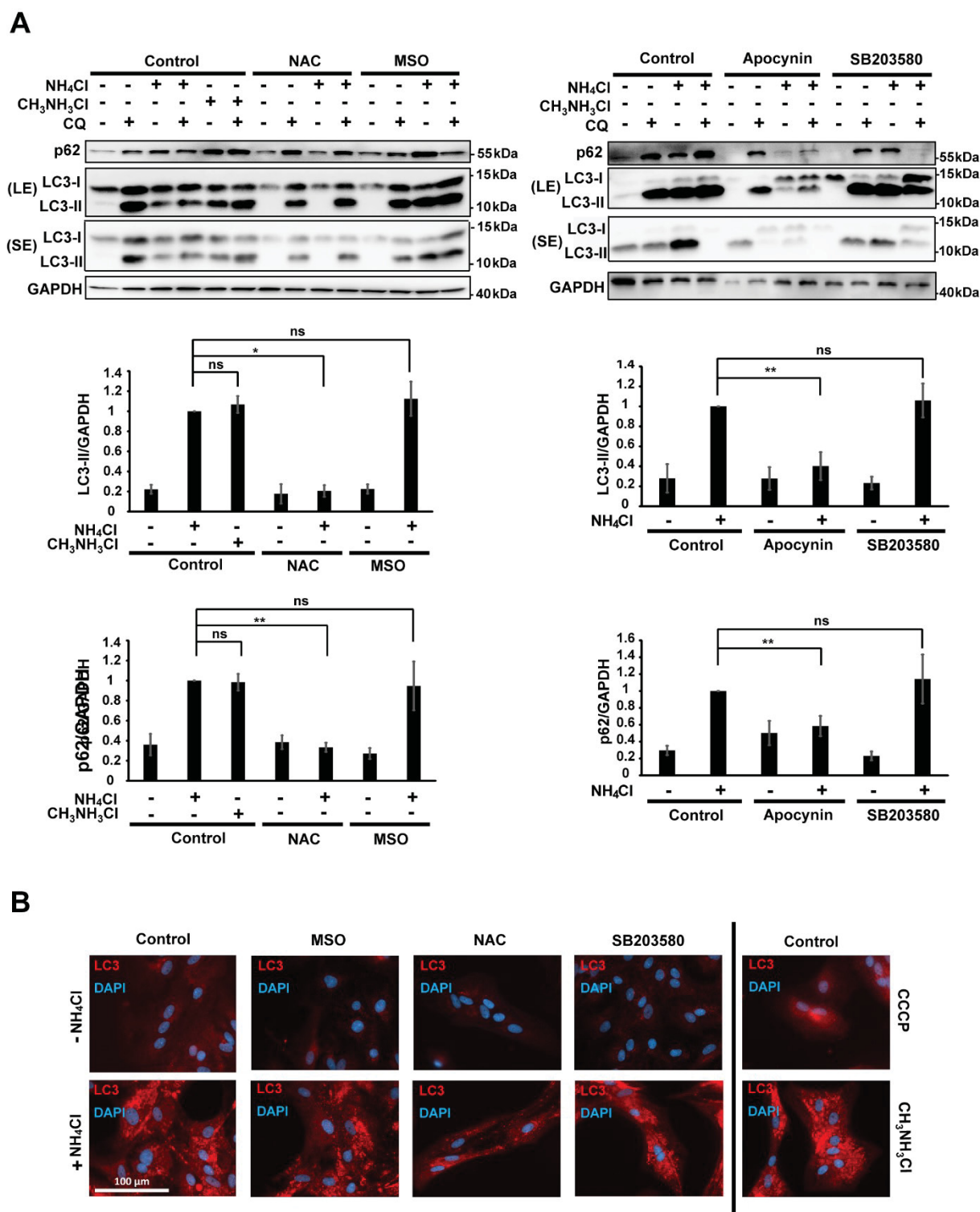


Fig. 3.6 Ammonia-induced autophagy inhibition is pH- and ROS-dependent but not GS- or p38MAPK-dependent. Where indicated, astrocytes were pre-treated with MSO (3 mM), NAC, (2 mM), apocynin (300 μ M), or SB203580 (10 μ M) for 30 min followed by a treatment of H₂O (control), NH₄Cl (5 mM) or CH₃NH₃Cl (5 mM) with or without chloroquine (CQ, 10 μ M) for 72 h. The pre-treatment chemicals were present throughout the treatment period. Autophagy was assayed via (A) western blot analysis and densitometric analysis of autophagic markers (n=3/4) and (B) fluorescence microscopy detection of LC3 immunostaining (red: LC3, blue: DAPI, scale bar: 100 μ m). * $p < 0.05$, ** $p < 0.01$, ns: no significance. LE: long exposure, SE: short exposure.

Moreover, the inhibitory effect of $\text{CH}_3\text{NH}_3\text{Cl}$ on autophagy was also shown to be blunted upon NAC or apocynin treatment in cultured rat astrocytes, indicating the crucial role of ROS in regulating this pH-dependent autophagy inhibition (Fig. 3.5C).

3.3.4 Autophagy inhibition is not dependent on glutamine synthetase or p38MAPK activity

As glutamine synthetase (GS) or p38MAPK activity was also reported to be responsible for regulating HE relevant pathological processes via generation of oxidative stress (Karababa et al. 2014, Görg et al. 2015), a pharmacological characterization was further conducted to determine their impact on ammonia-induced autophagy inhibition. Fig. 3.6A showed that treatment of the glutamine synthetase (GS) inhibitor MSO (3 mM), or the p38MAPK inhibitor SB203580 (10 μM), exhibited little regulatory effect on autophagic activity in presence of ammonia, as the relevant LC3-II conversion and p62 accumulation were maintained at similar levels for MSO- or SB203580-treated group, compared with that of the NH_4Cl -treated group. These results suggest ammonia-induced autophagy inhibition is GS- and p38MAPK-independent.

Likewise, fluorescence microscopy detection of LC3 immunostaining signal also showed a similar LC3 accumulation pattern as revealed by western blot analysis, confirming that ammonia-induced autophagy inhibition is a pH-dependent, but not a GS-, or p38MAPK-dependent process (Fig. 3.6B).

3.4 Autophagy is impaired in the brains of rats acutely intoxicated by ammonium acetate and the impairment is alleviated by taurine

3.4.1 Ammonium treatment results in autophagy inhibition in an *in vivo* model of HE

To verify the *in vivo* relevance of brain autophagy inhibition during HE, we used an established

rat model of acute hyperammonemia in which increases in blood and brain ammonia was induced by NH_4Ac administration (4.5 mmol/kg BW, 24 h) in male Wistar rats (26-28 days) (Warskulat et al. 2002).

After indicated treatment, *in vivo* autophagy activity was evaluated using lysates obtained from the cortex region from rats with or without acute ammonium intoxication. NH_4Ac administration for 24 h prominently induced conversion of LC3-I to LC3-II as well as accumulation of main autophagy substrate p62 (Fig. 3.7A). While LC3-II suggested increased autophagosome formation, p62 accumulation proved the blockage of degradation, these results suggested that consistent with what was found in cultured rat astrocytes, autophagy inhibition was also present *in vivo* on the tissue level. Together, these results suggest that autophagy inhibition is involved in the pathogenesis of HE.

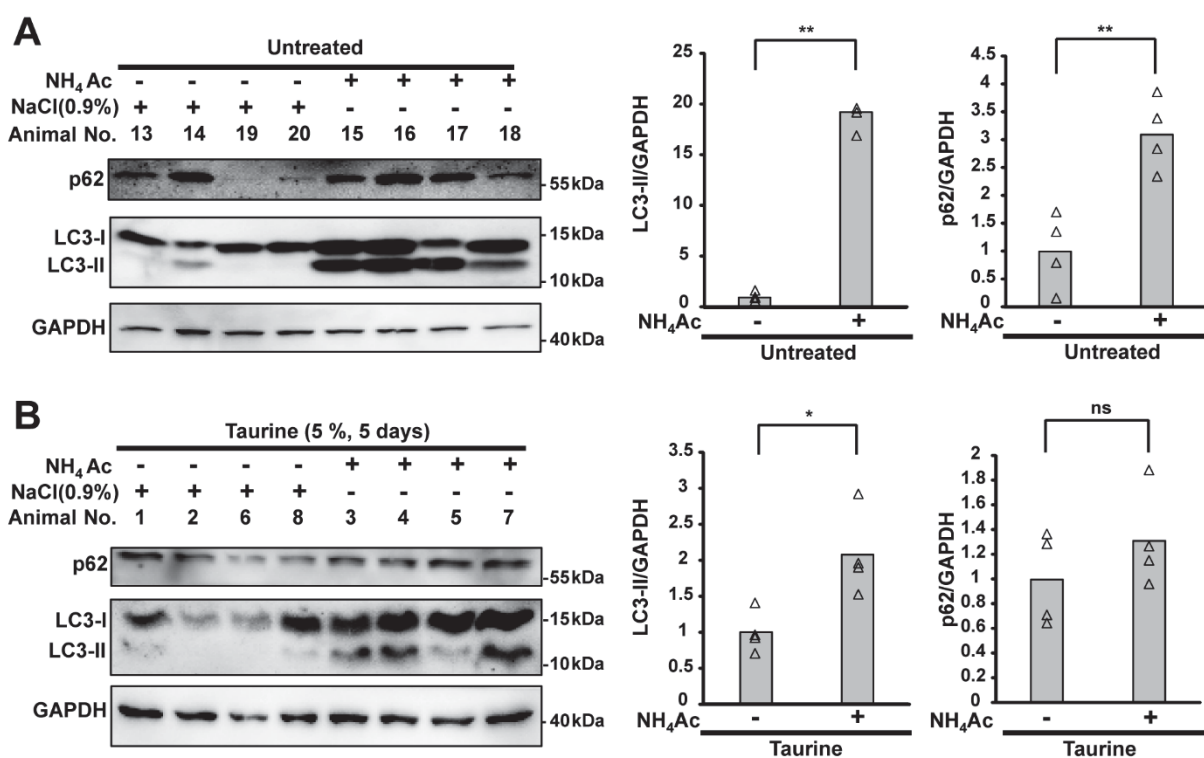


Fig. 3.7 Ammonium treatment results in autophagy inhibition in a rat model of HE. Western blot analysis and quantitative analysis of autophagy markers in cerebral cortex samples from a rat model of acute ammonium intoxication (NH_4Ac administration, 4.5 mmol/kg BW, 24 h) without (A) or with (B) pre-treatment of taurine supplement (5% taurine in drinking water, 5 days). LC3-II/GAPDH, p62/GAPDH are presented as bar charts which represent average fold change of these ratios. In addition, all data values from animal samples are plotted. * $p < 0.05$, ** $p < 0.01$, ns: no significance.

3.4.2 Taurine treatment reduces the degree of autophagy inhibition in a rat model of HE

Taurine, an amino acid with osmolyte, calcium modulator, neurotransmitter and antioxidant activities (Cooper and Jeitner 2016), has been demonstrated to be potent in rescuing various HE relevant defects including proliferation inhibition and senescence (Warskulat et al. 2002, Oenarto et al. 2016). The mechanisms of how taurine acts, however, is unclear. To examine whether taurine modulates autophagy inhibition in rat models of HE, we conducted western blot analysis of autophagic flux markers for rat cortex homogenates from control and NH₄Ac-intoxicated rats pre-treated with taurine supplement (5% taurine in drinking water, 5 days). Interesting to note, rat receiving taurine supplement showed a decreased degree of autophagy blockage in the cortex (Fig. 3.7B). Compared with untreated rats with NH₄Ac intoxication, decreased relative folds of LC3-II conversion (2.1 ± 0.6 fold; $p < 0.01$) and p62 accumulation (1.3 ± 0.4 fold; $p < 0.01$) were consistently detected in the brains of rats pre-treated with taurine (Fig. 3.7B).

3.4.3 Taurine treatment reduces the degree of autophagy inhibition induced by ammonia in cultured rat astrocytes

To further test this previous observation, we employed cultured rat astrocytes as the *in vitro* model for assaying the effect of taurine on ammonia-inhibited intracellular autophagy. In line with the *in vivo* data, in cultured rat astrocytes treated with ammonium, pre-treatment of taurine (5 mM) leads to a weaker blockage of autophagy. Compared with NH₄Cl-treated control group, relatively low amounts of LC3-II and p62 were observed in the taurine-treated group after ammonium treatment (Fig. 3.8).

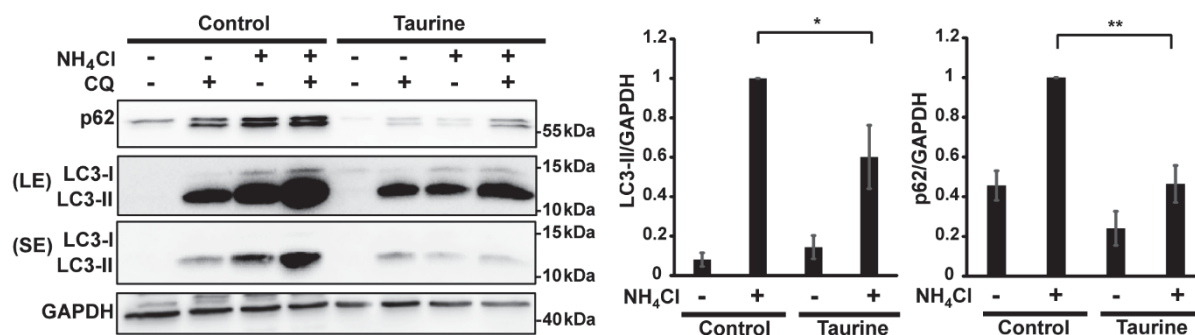


Fig. 3.8 Taurine supplement alleviates ammonia-induced autophagy inhibition in cultured rat astrocytes. Western blot analysis and densitometric analysis of autophagy markers in astrocytes pre-treated with 5 mM taurine in the presence of ammonia (n=4). * $p < 0.05$, ** $p < 0.01$. LE: long exposure, SE: short exposure.

Comparison of autophagic markers between *in vivo* and *in vitro* HE model indicated that the *in vivo* model exhibited a more severe inhibition as evidenced by the stronger increases in the relative fold change of LC3-II/GAPDH and p62/GAPDH (Fig. 3.9). Besides, the alleviation effect by taurine on ammonia-induced autophagy inhibition is also observed to be more pronounced in the *in vivo* HE model (Fig. 3.9), pointing out the therapeutic importance of taurine supplement.

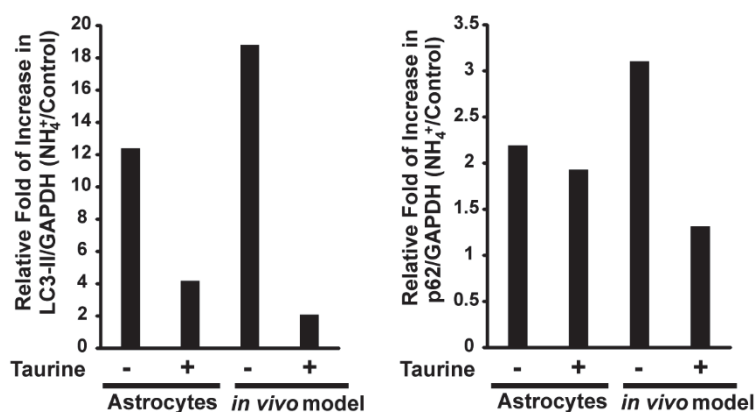


Fig. 3.9 Comparison of ammonia-induced autophagy inhibition between cultured rat astrocytes and a rat model of acute ammonium intoxication. Quantification of relative fold change of autophagy markers in cultured rat astrocytes and a rat model of acute ammonium intoxication. Relative folds were calculated using NH₄Cl- or NH₄Ac-treated group normalized to the untreated group.

3.5 TGM2 is upregulated in response to ammonia

3.5.1 Ammonium treatment leads to upregulation of TGM2 in cultured rat astrocytes

TGM2 is upregulated at high levels under various stress conditions including tissue injury, inflammation, and oxidative stress (Yeo et al. 2016). Recently, it was also demonstrated to positively regulate the late stages of autophagy processes (Yeo et al. 2016). As ammonia inhibits autophagy through pH alteration during late-stage degradation, we sought to determine the possible involvement of TGM2 as one of the defense mechanisms.

As shown in Fig. 3.10A, in cultured rat astrocytes, compared with untreated control, TGM2 was frequently seen to be upregulated in response to 5 mM NH₄Cl treatment. Compared with control at 24 h, treatment of 5 mM NH₄Cl also led to a time-dependent increase in the TGM2 expression at 24 h, 48 h and 72 h in cultured rat astrocytes (Fig. 3.10B).

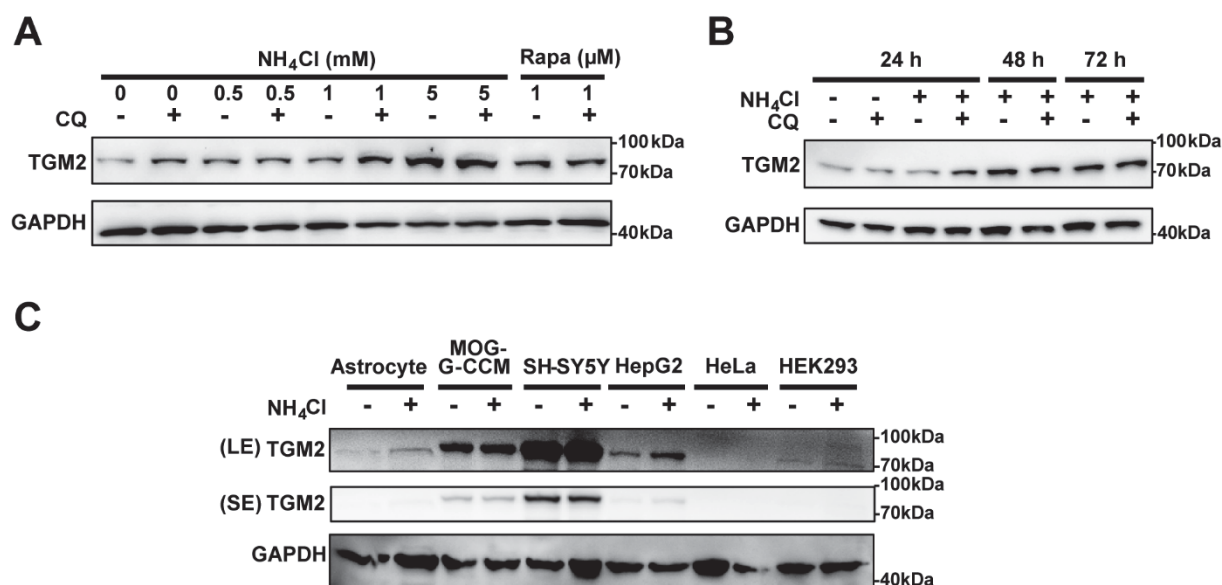


Fig. 3.10 Ammonium treatment leads to upregulation of TGM2 in cultured rat astrocytes. Western blot analysis of TGM2 in astrocytes treated with various concentrations of NH₄Cl for 72 h (A) or with 5 mM NH₄Cl for various time points (B). (C) Western blot analysis of TGM2 in primary rat astrocytes and various human cell lines after 5 mM NH₄Cl for 72 h. LE: long exposure, SE: short exposure.

3.5.2 Elevated expression level of TGM2 is observed in multiple cell lines

Moreover, Ammonia-induced TGM2 upregulation was not only observed in cultured rat astrocytes but also in HepG2 cells, suggesting TGM2 may also contribute to hepatic autophagy under hyperammonemic conditions (Fig. 3.10C). However, an upregulation by ammonia was not observed in astrocytoma cell line MOG-G-CCM or neuroblastoma cell line SH-SY5Y which both express a high amount of TGM2. Considering autophagy degradation was consistently blocked in all these cells, different expression levels of TGM2 are not likely to be due to a general blockage of TGM2 turnover but rather reflect different mechanisms for evoking stress response used by individual cell lines.

3.5.3 Elevated expression level of TGM2 is observed in a rat model of HE

To determine the *in vivo* relevance of TGM2 upregulation, TGM2 protein expression was evaluated in the cortex region of rat HE model. As shown in Fig. 3.11, TGM2 upregulation also happened in animals suffering hyperammonemia complications, as evidenced by the elevated TGM2 level in both rat acute ammonium intoxication model with or without taurine pre-treatment (1.9 ± 0.6 fold, $p < 0.05$; 2.0 ± 0.7 fold, $p < 0.05$, respectively). However, pre-treatment with taurine did not grossly affect the elevation of TGM2 levels (Fig. 3.11A, B).

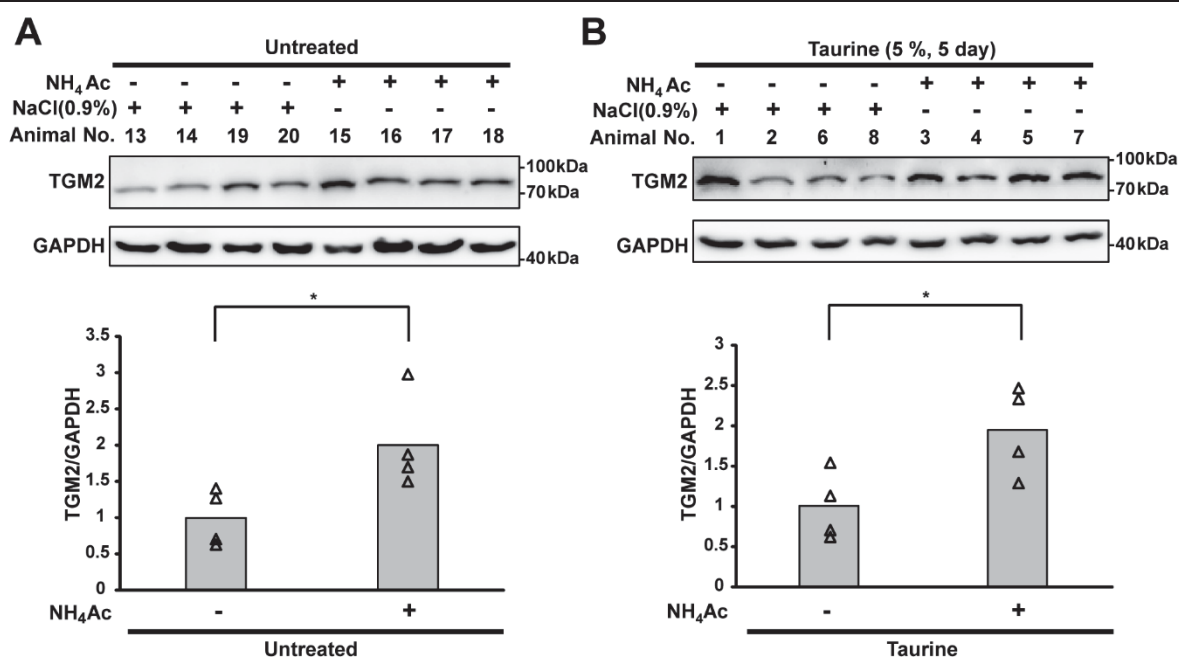


Fig. 3.11 Ammonium treatment leads to upregulation of TGM2 in a rat model of HE. Western blot analysis and quantitative analysis of TGM2 in cerebral cortex samples from rat model of acute ammonium intoxication (NH₄Ac administration, 4.5 mmol/kg BW, 24 h) without (A) or with (B) pre-treatment of taurine supplement (5% taurine in drinking water, 5 day). TGM2/GAPDH is presented as bar charts on which average fold change is plotted. In addition, all data values from animal samples are plotted. * $p < 0.05$, ** $p < 0.01$.

3.5.4 TGM2 mRNA is upregulated in the human cerebral cortex of patients with HE

Important to note, in two independent patient cohorts, via whole genome microarray analysis of mRNA isolated from the human cerebral cortex, Dr. Boris Görg confirmed that TGM2 mRNA was upregulated in cirrhosis patient co-diagnosed with HE compared with control patients with or without cirrhosis. As shown in Fig. 3.12, TGM2 gene expression levels were analyzed by two different sequences. From Dr. Boris Görg's analysis, in the Düsseldorf cohort, compared with control, both TGM2 sequences were upregulated by around 3 folds in HE patients with liver cirrhosis while they were downregulated by around 1.5 folds in non HE patients with liver cirrhosis. In line with this, the Australian cohort also showed that TGM2 mRNA was elevated by around 3 fold in HE patients compared with non HE patients with liver cirrhosis. These results indicate TGM2 upregulation is mainly a characteristic of HE but not a characteristic of liver cirrhosis.

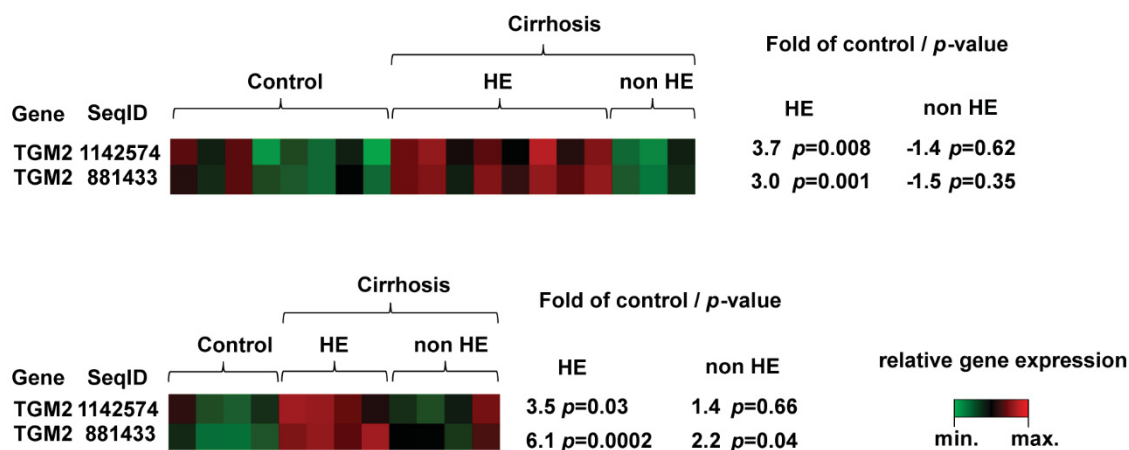


Fig. 3.12 TGM2 mRNA levels in the cerebral cortex of patients with liver cirrhosis with or without HE. Gene expression levels were measured by microarray analysis in two independent cohorts of HE patients and presented as heat maps. TGM2 expression level was determined by two different sequences. Relative fold changes and p values compared with control groups are indicated while enhanced or reduced gene expression levels are colored in red or green, respectively. (Done by Dr. Boris Görg)

Overall, we showed that TGM2 was upregulated not only in cultured rat astrocytes *in vitro* but also *in vivo* in a rat model of HE and in HE patients, thus TGM2 upregulation apparently represents a conservative stress response in mammals when autophagy degradation is impaired through the disturbance of intracellular pH by ammonia.

3.6 Mitochondrial dysfunction is increased by ammonia in cultured rat astrocytes

3.6.1 Ammonium treatment leads to mitochondrial fragmentation

As the activity of autophagy, a general process required for mQC, was shown to be blocked by ammonia in HE models, it is possible that during HE pathogenesis, removal of damaged and dysfunctional mitochondria is not efficient. Since mQC is essential for maintaining the proper mitochondrial function, compromised mitochondrial function may be a common phenomenon in HE. Indeed, various mitochondrial disorders have already been associated with HE including mitochondrial fragmentation and swelling as well as mitochondrial membrane potential loss

(Drewes and Leino 1985, Bai et al. 2001, Görg et al. 2015).

In the present study, rat astrocytes were transfected transiently with pcDNA3.1-mtGFP, the tubular and fragmented mitochondria were then observed via fluorescence microscopy. In line with previous publications reporting increased mitochondrial fragmentation after 24 h NH_4Cl treatment (Görg et al. 2015), we confirmed ammonia-induced mitochondrial fragmentation in cultured rat astrocytes after 72 h NH_4Cl treatment (Fig. 3.13A).

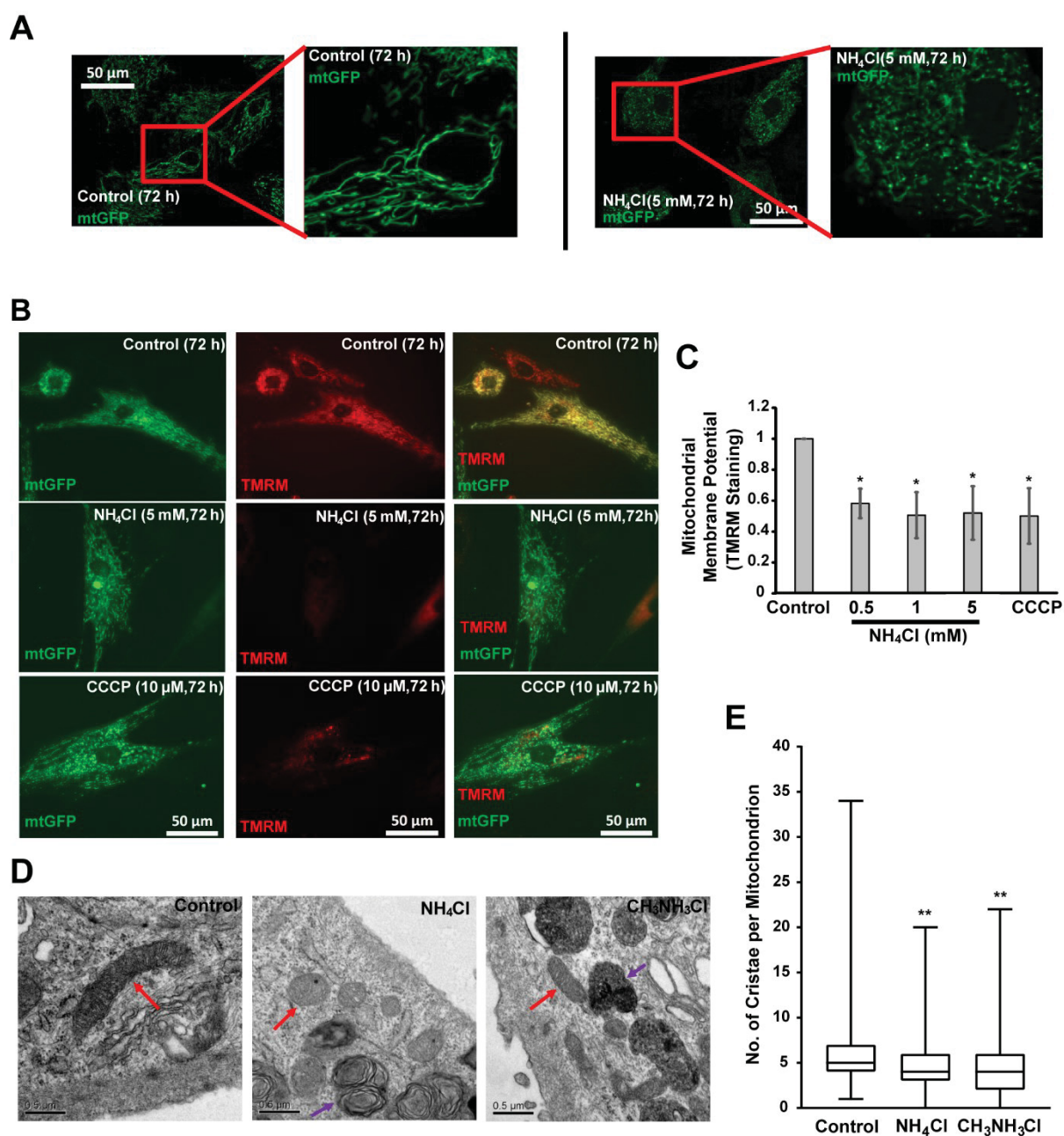


Fig. 3.13 Ammonium treatment impairs mitochondrial function in primary rat astrocytes. (A) Representative fluorescence microscopy images of mitochondrial morphology after 5 mM NH₄Cl treatment (72 h) in astrocytes transfected with pcDNA3.1-mtGFP (scale bar: 50 μm). Selected areas are magnified on the right side. (B) Representative fluorescence microscopy images (scale bar: 50 μm) and (C) analysis of mitochondrial TMRM staining after various concentrations of NH₄Cl treatment for 72 h. CCCP (10 μM, 6 h) treatment was employed as a positive control. Analysis was done by quantification of the red channel intensity normalized to that of control group. (D) Representative EM images of mitochondrial structure (red arrows indicate mitochondria, purple arrows indicate autophagosomes/autolysosomes, scale bar: 0.5 μm). (E) Box plot analysis of mitochondrial cristae number after 5 mM NH₄Cl/CH₃NH₃Cl treatment for 72 h. Around 150 mitochondria were analyzed for each group. ** $p < 0.01$, compared with control group.

3.6.2 Ammonium treatment results in loss of mitochondrial membrane potential

To investigate whether mitochondria in astrocytes treated with high concentrations of ammonia are in a dysfunctional status, mitochondrial membrane potential ($\Delta\psi_m$) in cultured primary rat astrocytes with or without various concentrations of NH₄Cl treatment (72 h) was measured. We employed Tetramethylrhodamine-Methylester (TMRM), a $\Delta\psi_m$ -dependent dye, to stain the mitochondria in live astrocytes after treatment. Intact mitochondria accumulate TMRM, thus exhibiting a high TMRM intensity while dysfunctional mitochondria with $\Delta\psi_m$ loss display a reduced TMRM intensity (Petrat et al. 2003), although they maintain mtGFP fluorescence. CCCP-treated astrocytes were used as a positive control for the $\Delta\psi_m$ loss.

Consistent with previous studies (Bai et al. 2001), mitochondria membrane potential was observed to be dramatically reduced by 5 mM NH₄Cl to a comparable level as the mitochondrial uncoupler CCCP (Fig 3.13B, C). Compared with the control group, 0.5 mM NH₄Cl treatment already resulted in dramatic decrease in the TMRM mean intensity (Fig 3.13C), confirming NH₄Cl treatment leads to accumulation of depolarized mitochondria.

3.6.3 High concentrations of ammonia decrease cristae number per mitochondrion

Mitochondrial dysfunction is often associated with changes in mitochondrial ultrastructure (Anand et al. 2016). Mitochondrial swelling was documented in astrocytes after 24 h 5 mM

NH₄Cl treatment (Görg et al. 2015), we therefore analyzed the effect of ammonia on mitochondrial structure via electron microscopy (EM).

Representative electron micrographs of mitochondrial structure after NH₄Cl or CH₃NH₃Cl treatment were shown in Fig. 3.13D. Compared with H₂O-treated control group (6.7 ± 5.4), we found that mitochondrial cristae number per mitochondrion was significantly decreased in the 5 mM NH₄Cl- ($4.8 \pm 3.2, p < 0.01$) or CH₃NH₃Cl-treated ($4.6 \pm 3.3, p < 0.01$) groups, suggesting NH₄Cl or CH₃NH₃Cl treatment may lead to deficient energy generation (Fig. 3.13E). No statistically significance was observed when NH₄Cl and CH₃NH₃Cl-treated groups were compared (Fig. 3.13E). However, mitochondrial swelling is not reflected in the EM data as other mitochondrial parameters (mitochondria number, size, perimeter, length of major and minor axis) remained rather unchanged among these examined groups (Fig. 3.14). This may be due to the fact that EM is not an ideal approach for examining mitochondrial swelling.

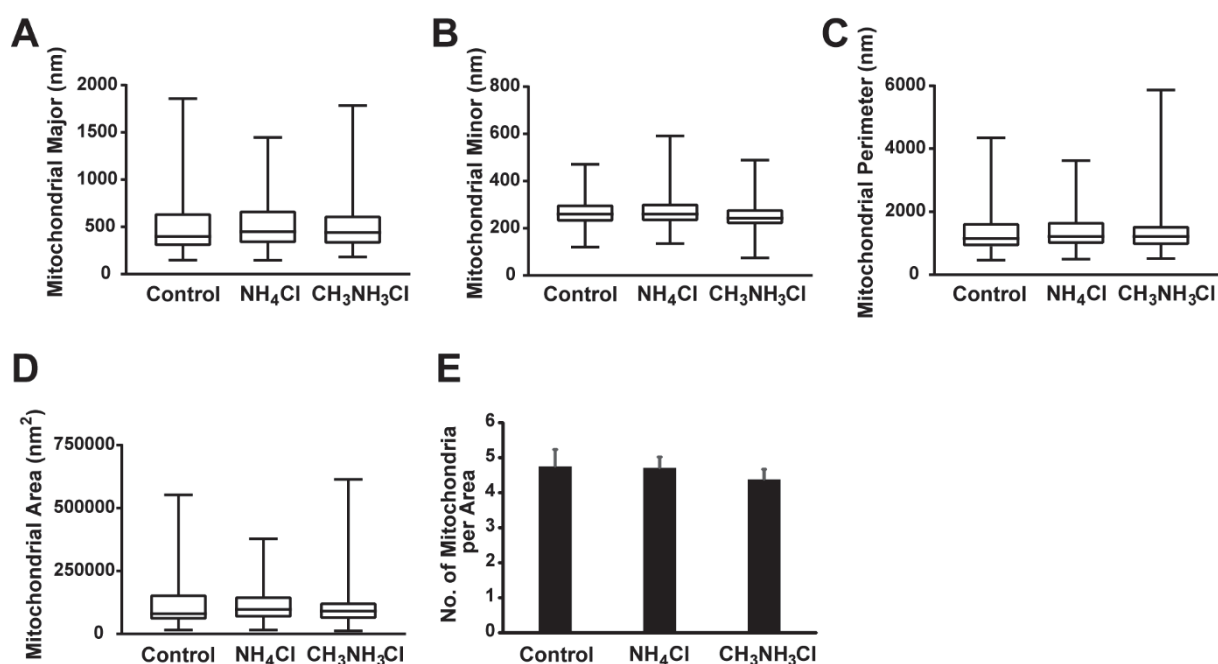


Fig. 3.14 Ammonium treatment does not affect the mitochondrial number and major mitochondrial morphological parameters. Astrocytes were treated with 5 mM NH₄Cl/CH₃NH₃Cl treatment for 72 h. Box plot analysis were conducted for major mitochondrial structure parameters: (A) length of major axis, (B) length of minor axis, (C) mitochondrial perimeter, and (D) mitochondrial area. (E) Analysis of mitochondrial numbers after 5 mM NH₄Cl/CH₃NH₃Cl treatment for 72 h. Around 150 mitochondria were analyzed for each group. Length of major axis: the longest length of mitochondria; length of minor axis: the shortest length of mitochondria.

3.6.4 Both l-OPA1 and s-OPA1 are accumulated after ammonium treatment

Since mitochondrial fragmentation is stimulated by ammonium treatment and OPA1 is a major player in mitochondria fusion and fission, we processed to examine the level of l-OPA1 and s-OPA1 upon various concentrations of NH_4Cl treatment. Both l-OPA1 and s-OPA1 were remarkably increased in astrocytes treated with 5 mM NH_4Cl relative to control (Fig. 3.15). Compared with 0.5 mM and 1 mM NH_4Cl -treated group, the effect of NH_4Cl on OPA1 accumulation was also demonstrated to be dose-dependent (Fig. 3.15). Of note, the ammonia-induced dose-dependent accumulation of s-OPA1 may partially explain the increased mitochondrial fragmentation previously observed (Fig. 3.13A). The dose-dependent accumulation of l-OPA1 may be a result of increased mitochondrial biogenesis, indicating a demand for maintaining healthy mitochondrial mass in response to ammonia-induced stress.

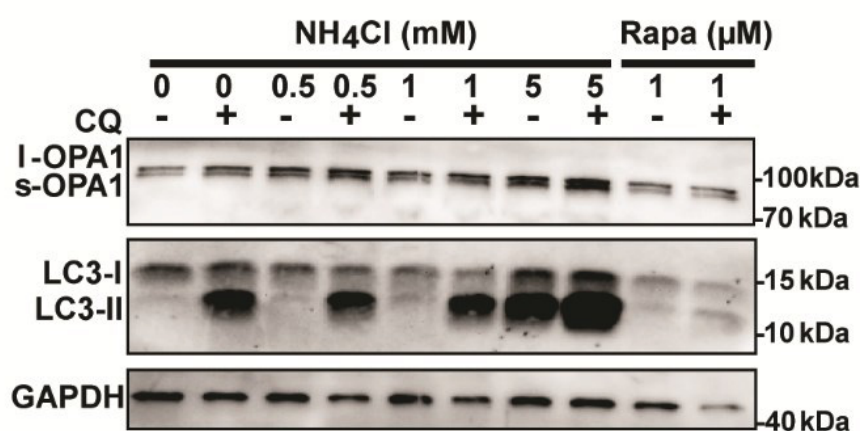


Fig. 3.15 Ammonium treatment leads to accumulation of both l-OPA1 and s-OPA1 in cultured rat astrocytes. Astrocytes were treated with various concentration of NH_4Cl with or without chloroquine (CQ, 10 μM) for 72 h. Rapamycin group was left untreated for 48 h and then autophagy was induced by treatment of rapamycin (Rapa, 1 μM) for 24 h. After 72 h NH_4Cl treatment, OPA1 expression levels were assayed via western blot analysis.

3.7 Ammonium treatment leads to enhanced Parkin-mediated mitophagy initiation in cultured rat astrocytes

Following the observation of ammonia-induced mitochondrial structure and function impairment, we next asked whether ammonia also led to specific degradation of dysfunctional mitochondria. Besides autophagy, damaged mitochondria could also be degraded via a set of specific degradation pathways termed mitophagy (Müller et al. 2015). Still, genetic- or chemical-induced loss of mitochondrial membrane potential alone was demonstrated to be not sufficient in stimulating mitophagy (Gilkerson et al. 2012).

To determine the possible involvement of mitophagy in the pathogenesis of HE, we used pharmacological administration and fluorescence microscopy detection of LC3 and Tim23 immunostaining signal to gain a general impression of overall mitophagy upon ammonia treatment. As shown in Fig. 3.16, compared with control group, increased colocalization signal was observed in NH_4Cl - or $\text{CH}_3\text{NH}_3\text{Cl}$ -treated groups as well as NH_4Cl -treated groups pre-treated with MSO or SB203580 while less colocalization signal was observed for NH_4Cl -treated groups pre-treated with NAC, suggesting that ammonia-induced mitophagy is pH-dependent, and can be reduced by NAC administration. We then focused on two distinct yet connected pathways, Parkin- and NIX-mediated mitophagy pathways.

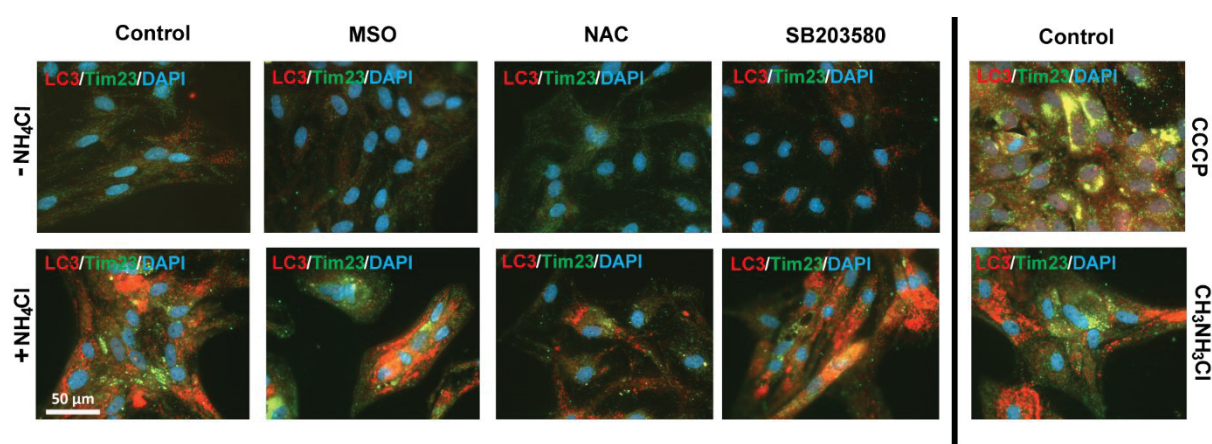


Fig. 3.16 Ammonium treatment induces mitophagy in cultured rat astrocytes. Fluorescence microscopy detections of LC3 and Tim23 immunostaining in cultured rat astrocytes treated with H_2O (control), NH_4Cl (5 mM) or $\text{CH}_3\text{NH}_3\text{Cl}$ (5 mM) for 72 h. Where indicated, astrocytes were pre-treated with MSO (3 mM) or NAC (2 mM) for 30 min. The pre-treatment chemicals were present throughout the cell culture period. (red: LC3, green: Tim23, blue: DAPI, scale bar: 50 μm).

3.7.1 Ammonium treatment induces Parkin-mediated mitophagy

As Parkin translocation onto mitochondria is regarded as a landmark for the initiation of Parkin-mediated mitophagy (Youle and Narendra 2011), we first processed to examine the Parkin translocation onto mitochondria via fluorescence microscopy in primary rat astrocytes and HeLa cells transfected with pmCherry-Parkin and pcDNA3.1-mtGFP. Quantification of the colocalized signal of Parkin and mtGFP after treatment revealed that upon co-incubation with 5 mM NH₄Cl for 72 h, mitochondrial translocated Parkin signal was increased to around 10 fold ($p < 0.01$) and 7 fold ($p < 0.01$) in HeLa cells and primary rat astrocytes, respectively (Fig. 3.17A).

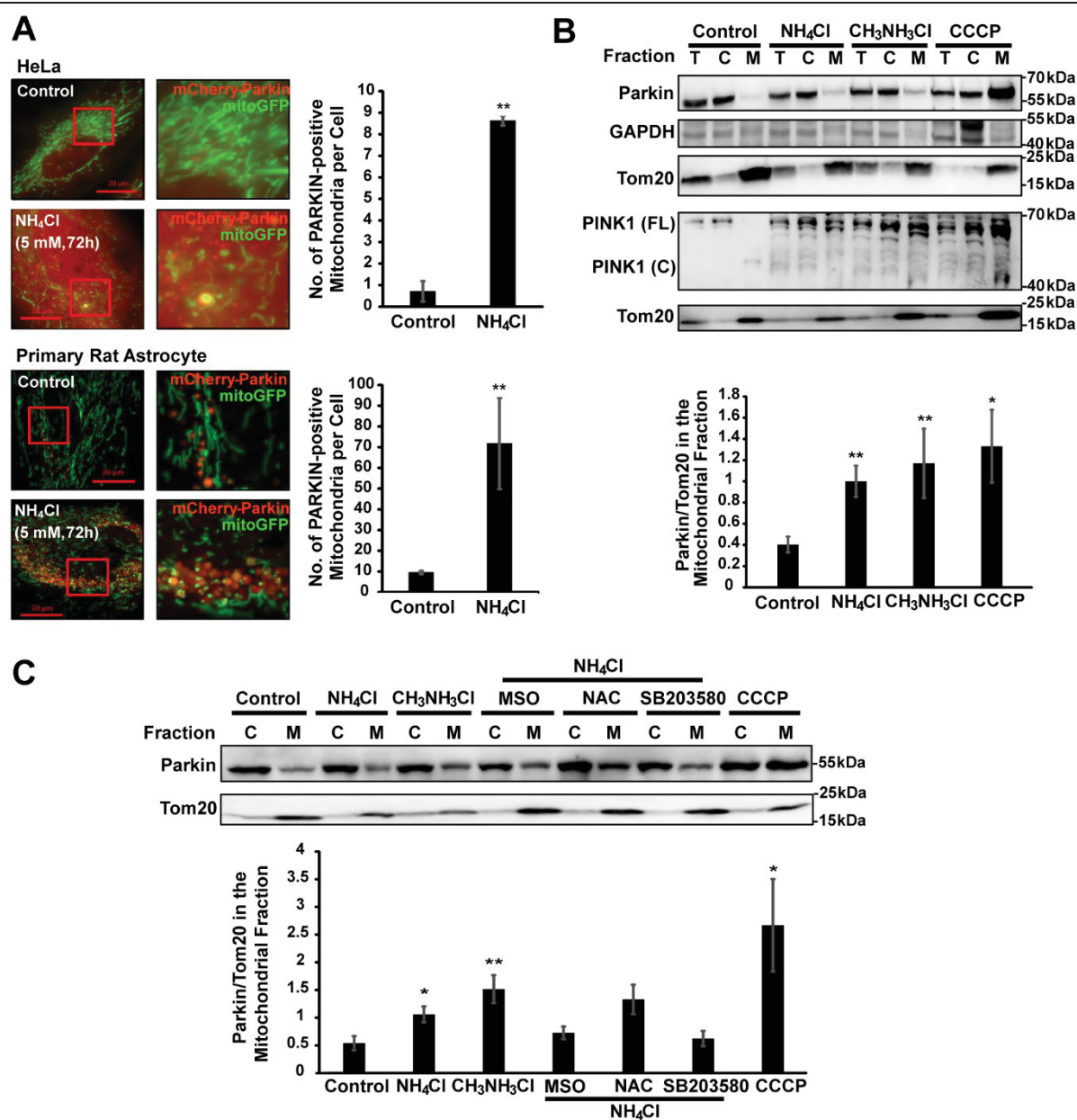


Fig. 3.17 Ammonium treatment induces Parkin-mediated mitophagy in primary rat astrocytes. (A) Fluorescence microscopy images and Quantifications of Parkin translocation on to mitochondria. HeLa or astrocytes were cotransfected with pcDNA3.1-mtGFP and pmCherry-Parkin 48 h before 5 mM NH₄Cl treatment (72 h). Around 50 cells were analyzed for each group (data were presented as mean \pm standard deviation, scale bar: 20 μ m). Selected areas are magnified in boxes. (B) Western blot analysis and densitometric analysis of Parkin translocation in astrocytes treated with 5 mM NH₄Cl/CH₃NH₃Cl for 72 h (n=4). (C) Western blot analysis and densitometric analysis of Parkin translocation in astrocytes pre-treated with indicated chemicals followed by NH₄Cl treatment (5 mM, 72 h) (n=4). CCCP (10 μ M, 6 h) treatment was employed as a positive control. T: total cell lysate, C: cytosol fraction, M: mitochondrial fraction. FL: full-length, C: cleaved. * $p < 0.05$, ** $p < 0.01$, compared with control group.

3.7.2 Parkin-mediated mitophagy can also be induced by methylammonium chloride

To elucidate the molecular mechanism underlying ammonia-induced Parkin-mediated mitophagy initiation, we also conducted a pharmacological characterization with western blot analysis of Parkin level in the cytosolic and mitochondrial fractions. Under control conditions, the majority of Parkin was located in the cytosol, upon loss of mitochondrial membrane potential, increased Parkin signal was observed in the mitochondrial fraction (Fig. 3.17B). When normalized to Tom20, compared with that of the control group, more abundant Parkin signal was observed in the mitochondrial fraction of NH_4Cl - and $\text{CH}_3\text{NH}_3\text{Cl}$ -treated group, although the Parkin expression was less than that of the CCCP-treated astrocytes (Fig. 3.17B).

As Parkin is recruited by full-length PINK1 in the OMM (Youle and Narendra 2011), we also evaluated the mitochondrial levels of full-length and cleaved PINK1 under NH_4Cl - and $\text{CH}_3\text{NH}_3\text{Cl}$ -treated conditions. Indeed, in the absence of ammonia, full-length PINK1 was barely detectable in the mitochondrial fraction, when the mitochondrial membrane potential was dissipated by CCCP, full-length PINK1 was strongly accumulated in the mitochondrial fraction, validating this assay for mitophagy induction (Fig. 3.17B). Both NH_4Cl and $\text{CH}_3\text{NH}_3\text{Cl}$ led to mitochondrial accumulation of PINK1 in primary rat astrocytes (Fig. 3.17B), indicating that transport of PINK1 into the IMS and/or PARL-mediated cleavage of PINK1 might be diminished by ammonia-induced intracellular pH alteration. These results suggest that ammonia-enhanced initiation of Parkin-mediated mitophagy is mainly mediated via intracellular pH alterations.

Furthermore, pre-treatment of astrocytes with the GS inhibitor MSO or the p38MAPK inhibitor SB203580 appeared to alleviate the effects of NH_4Cl , while NAC pre-treatment had less effect on decreasing mitochondrial Parkin levels, indicating a possible role of GS and p38MAPK, but not ROS, during ammonia-induced Parkin-mediated mitophagy (Fig. 3.17C). Future studies are still necessary to elucidate the detailed mechanisms underlying Parkin-mediated mitophagy stimulated by ammonia.

3.8 Ammonium treatment increases NIX-mediated mitophagy initiation in cultured rat astrocytes

Apart from the Parkin-mediated pathway which requires ubiquitination, mitophagy can also be induced via pathways mediated by various LC3-interacting receptor proteins on mitochondria, among which, NIX was recently linked to brain injury (Youle and Narendra 2011, Yuan et al. 2017). Besides, NIX was also reported to contribute to CCCP-induced mitochondrial translocation of Parkin (Ding et al. 2010).

3.8.1 Ammonium treatment induces NIX-mediated mitophagy in non-cancerous cells

We discovered that ammonia dramatically upregulated NIX expression in cultured rat astrocytes, notably, this upregulation was also observed in immortalized HEK293 cells but not in cancerous cell lines including MOG-G-CCM, SH-SY5Y, HeLa and HepG2, indicating ammonia increased initiation of NIX-mediated mitophagy via a mechanism that is inactivated or insensitive in tumors (Fig. 3.18A).

Interestingly, multiple forms of NIX were observed to be involved in the ammonia-induced upregulation in normal cells. Since the upregulation was not happening in cancerous cells where autophagy degradation was also largely blocked by ammonia, the accumulated expression level of NIX was not likely to be solely dependent on degradation deficiency. Later we also assayed the NIX expression level in both 5 mM NH₄Cl-treated and CQ-treated astrocytes via western blot analysis. CQ treatment was able to result in partial accumulation of two major forms of NIX (Fig. 3.18B), suggesting that in normal cells, ammonia-induced enhancement of NIX expression is more complex than the mere accumulation of NIX by autophagy inhibition.

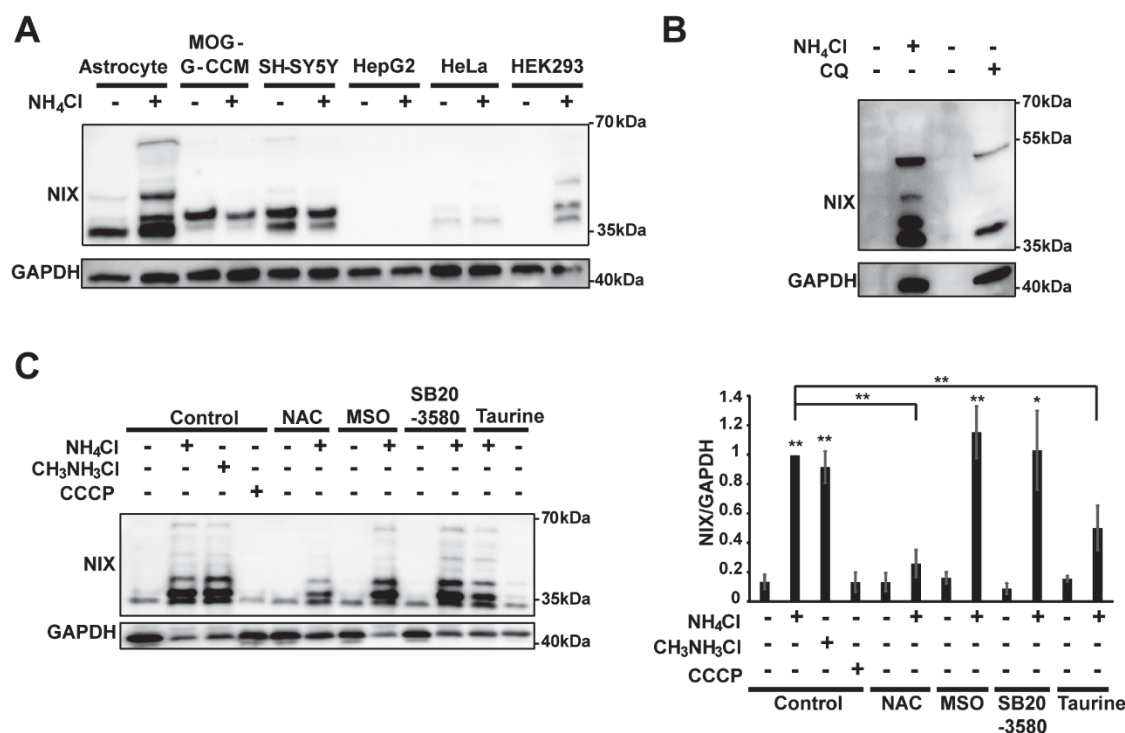


Fig. 3.18 Ammonium treatment induces NIX-mediated mitophagy in primary rat astrocytes. (A) Western blot analysis of NIX in primary rat astrocytes and various human cell lines after 5 mM NH₄Cl treatment for 72 h. (B) Western blot analysis of NIX in primary rat astrocytes treated with 5 mM NH₄Cl treatment or chloroquine (CQ) for 72 h. (C) Western blot analysis and densitometric analysis of NIX in astrocytes pre-treated with indicated chemicals followed by NH₄Cl treatment (5 mM, 72 h) (n=3). * $p < 0.05$, ** $p < 0.01$, compared with control group.

3.8.2 NIX accumulation is mainly dependent on pH and is affected by ROS level

We next examined the molecular mechanisms of NIX-mediated mitophagy in response to ammonium treatment. Through pharmacological characterization, intracellular pH alteration was also demonstrated to be the main factor responsible for elevated NIX level in response to ammonium treatment while neither GS nor p38MAPK activity was required for the NIX upregulation (Fig. 3.18C). Interestingly, treatment of antioxidant NAC (2 mM) or taurine (5 mM) was potent in blunting ammonia-induced NIX upregulation, indicating the critical role of ROS in regulating NIX-mediated mitophagy initiation.

Together, our data provide the first *in vitro* evidence that ammonia induces mitophagy initiation

in astrocytes via at least two different mitophagy pathways. The alterations of both the ubiquitin-dependent PINK1/Parkin pathway and the receptor-dependent NIX pathway in response to ammonia connect mitophagy with the pathobiology of HE.

3.9 Ammonia induces PGC-1 α -mediated mitochondrial biogenesis in cultured rat astrocytes

3.9.1 Elevation of PGC-1 α expression induced by ammonia is dose- and time-dependent

To investigate whether ammonia-induced mitophagy initiation also triggers relevant compensation mechanisms essential for mitochondrial homeostasis, we analyzed the expression level of PGC-1 α , the master gene controlling mitochondrial biogenesis, under various ammonium treatment conditions.

As shown in Fig. 3.19A, in response to NH₄Cl treatments at various concentrations, PGC-1 α expression was frequently seen to be elevated and exhibited a dose-dependency. Since NH₄Cl treatment at these concentrations represent different autophagy inducing or inhibition states, the PGC-1 α expression pattern indicates that in order to cope with ammonia-induced intracellular stresses, cells appear to have a consistent demand for *de novo* mitochondrial biogenesis.

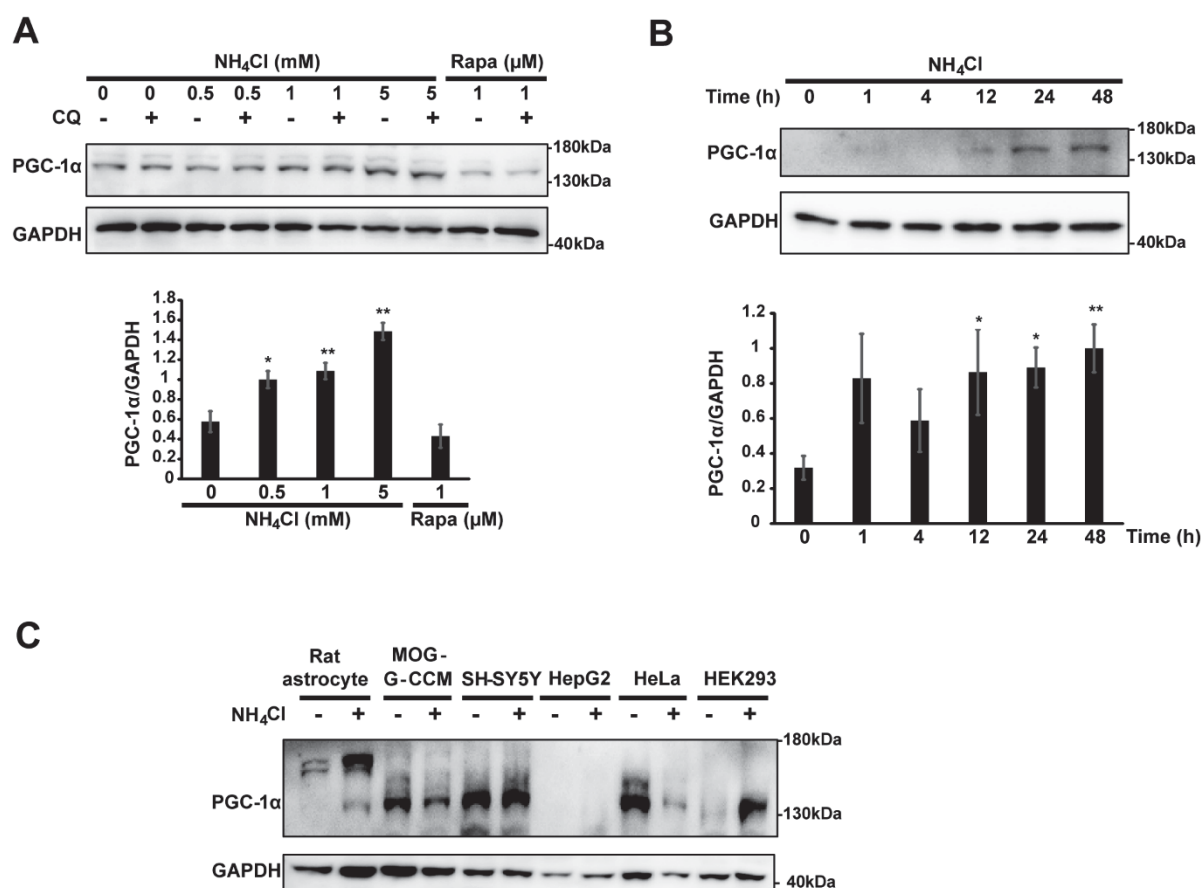


Fig. 3.19 Ammonium treatment enhances PGC-1 α expression level in primary rat astrocytes. (A) Western blot analysis and densitometric analysis of PGC-1 α in astrocytes treated with 5 mM NH₄Cl for various time points. (B) Western blot analysis and densitometric analysis of PGC-1 α in astrocytes treated with various concentrations of NH₄Cl with or without chloroquine (CQ, 10 μ M) for 72 h. Rapamycin group was left untreated for 48 h and then treated with rapamycin (Rapa, 1 μ M) for 24 h (n=3/4). (C) Western blot analysis of PGC-1 α in primary rat astrocytes and various human cell lines after 5 mM NH₄Cl treatment for 72 h. * $p < 0.05$, ** $p < 0.01$, compared with control group.

Besides, compared with control, ammonia-treated astrocytes exhibited progressively increased PGC-1 α levels over time (Fig. 3.19B), indicating a high bioenergetic demand in astrocytes after long-term ammonium treatment which rendered autophagy inhibition and mitochondrial dysfunction. The upregulated mitochondrial biogenesis may increase the proportion of healthy mitochondria and mask the loss of mitochondria due to degradation. Thus this at least partially contribute to the accumulation of l-OPA1 and the stable density of mitochondria in response to ammonium treatment (Fig. 3.14E, 3.15).

3.9.2 Elevated expression level of PGC-1 α is observed in non-cancerous cells

Moreover, Fig 3.19C showed that similar to NIX, NH₄Cl treatment (5 mM, 72 h) resulted in a prominent reduction in PGC-1 α level in the majority of cancerous cell lines tested. Elevated PGC-1 α expression level was observed only in primary rat astrocytes and HEK293 cells in response to ammonia, suggesting mitochondrial biogenesis, another essential mQC process, was activated by non-cancerous cells under hyperammonemic states to maintain the intracellular bioenergetics homeostasis.

Compared with human PGC-1 α , besides the validated molecular weight (130 kDa, done by Cell Signaling Technology), a large portion of rat PGC-1 α was observed with a much larger molecular weight (Fig. 3.19C). As there was only one entry for rat PGC-1 α isoform in UniProtKB ([Q9QYK2](#)) which shared a similar molecular weight of around 91 kDa with major human PGC-1 α isoforms ([Q9UBK2](#)), we suspected this was due to post-translational modifications or unknown rat isoforms.

3.10 Knockdown of key autophagy/mitophagy machinery genes sensitizes cells at high concentrations of ammonia

3.10.1 Ammonia reduces MTT assay activity in cultured rat astrocytes

To elucidate the biological consequence of ammonia-induced mitophagy initiation and autophagy inhibition, we mainly applied the 3-(4,5-dimethylthiazol-2-yl)-2,5-diphenyltetrazolium bromide (MTT) assay. MTT assay reflects the overall cellular metabolic activity and is commonly used as an indicator of cell viability (Ha and Snyder 1999, Lu et al. 2013, Rai et al. 2018).

First, cytotoxicity induced by various concentrations of ammonia was evaluated in cultured rat astrocytes. Compared with control groups, NH₄Cl treatment for 24 h or 48 h caused little cytotoxicity in astrocytes, however, 5 mM treatment for 72 h already resulted in a significant

decrease of around 15% ($p < 0.05$) in the MTT assay activity (Fig. 3.20A). At 72 h, a clear dose-dependency of ammonia-induced cytotoxicity was observed in astrocytes, MTT assay activity was consistently further reduced when NH_4Cl concentration increased (Fig. 3.20A). 40 mM treatment was demonstrated to render a decreased MTT assay activity of around 50% ($p < 0.05$), compared with that of the control group.

Results from trypan blue staining also demonstrated a similar dose-dependent cytotoxicity after 72 h NH_4Cl treatment (Fig. 3.20B), indicating long-term autophagy inhibition placed a harmful effect towards cell viability.

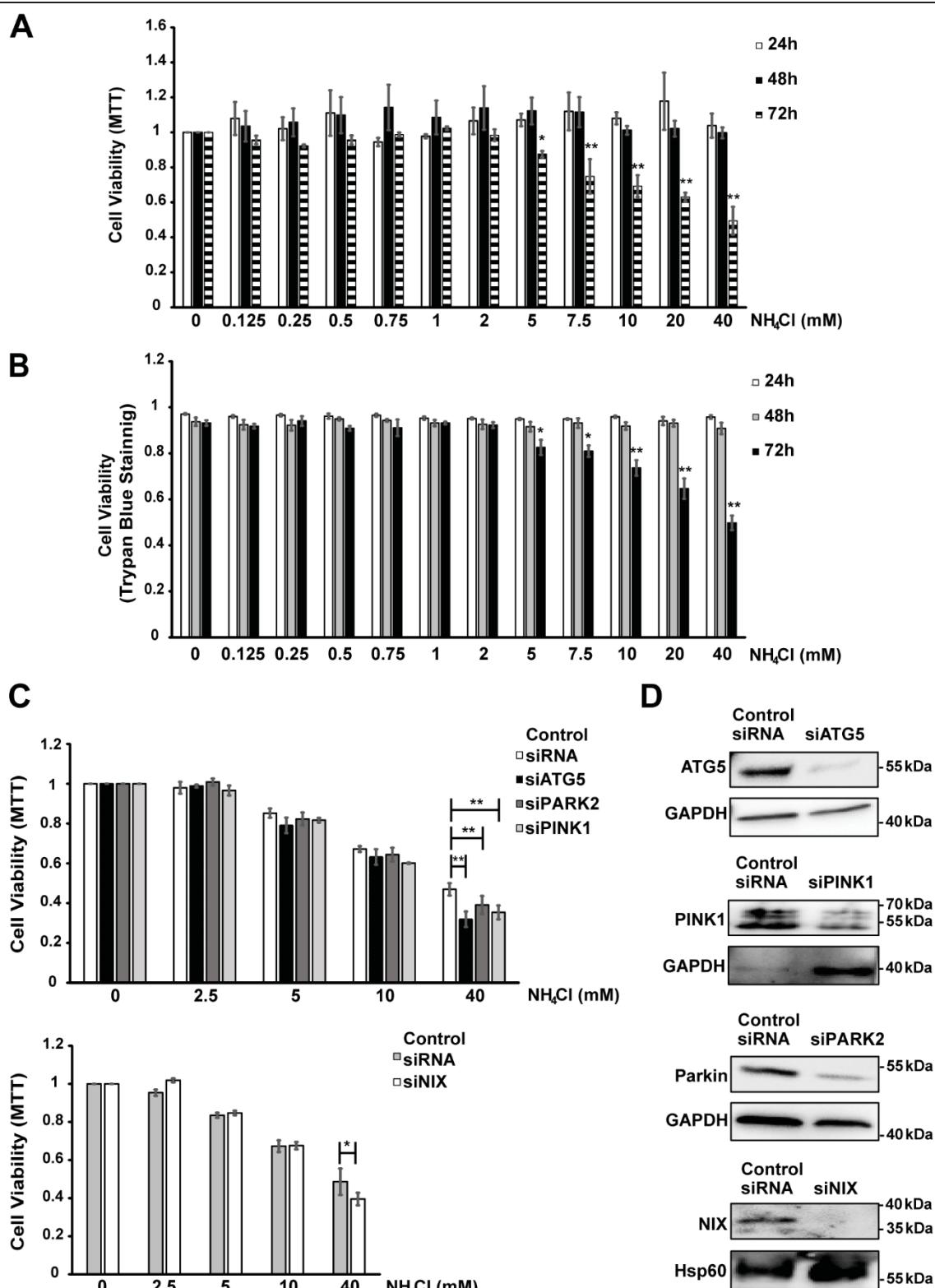


Fig. 3.20 Autophagy and mitophagy inhibition further sensitize astrocytes to cell death only after treatment of extremely high concentration of ammonium. (A) Cytotoxicity of NH₄Cl treatment (5 mM, 72 h) measured by MTT assays. * $p < 0.05$, ** $p < 0.01$, compared with respective control group at the same time ($n=3$). (B) Cytotoxicity of NH₄Cl treatment (5 mM, 72 h) measured by trypan blue staining. * $p < 0.05$, ** $p < 0.01$, compared

with respective control group at the same time (n=3). (C) Cytotoxicity of various NH₄Cl treatments (72 h) measured by MTT assays in astrocytes with deficient autophagy/mitophagy machinery. Atg5, Parkin, PINK1 and NIX were knocked down by their respective siRNAs (100 nM) 24 h before NH₄Cl treatments, the control group was transfected with a control siRNA (100 nM) for the same treatment period. * $p < 0.05$, ** $p < 0.01$, compared with respective control group at the same NH₄Cl concentration (n=4). (D) Representative western blot analysis of knockdown efficiency via RNAi (96 h post-transfection).

3.10.2 Autophagy and mitophagy inhibition do not further sensitize astrocytes to cell death after ammonium treatment

Modulation of autophagy/mitophagy machinery was then carried out via respective siRNA knockdown of Atg5, Parkin, PINK1, and NIX. Through western blot analysis, the knockdown efficiencies of respective genes were confirmed (Fig. 3.20D).

However, without ammonia treatment, knockdown of Atg5 and NIX alone had already led to a significant decrease in MTT assay activity. Surprisingly, after normalization, compared with the control siRNA transfected group, a significant decrease in cytotoxicity was only observed under extreme conditions (40 mM, 72 h) in astrocytes with autophagy/mitophagy defects (Fig. 3.20C). Upon 40 mM NH₄Cl treatment, compared with astrocytes transfected with negative control siRNA, astrocytes transfected with siAtg5 exhibited a significant decrease of around 30% in the MTT assay activity ($p < 0.01$) while astrocytes transfected with siPARK2, siPINK1, or siNIX showed a less decrease of around 20% in the MTT assay activity ($p < 0.01$, $p < 0.01$, $p < 0.05$, respectively).

These results suggested that additional knockdown of key autophagy and mitophagy genes only sensitize astrocytes to cell death under conditions with very high concentrations of ammonia while under moderate hyperammonemic conditions (5 mM, 10 mM), single knockdown of key autophagy/mitophagy genes did not further sensitize astrocytes to ammonia-induced cytotoxicity.

3.11 Photoactivatable acidifying nanoparticles (paNP) restore autophagic flux in cultured rat astrocytes

Recently, Trudeau et al. demonstrated that under lipid toxicity conditions, the lysosomal-localizing photoactivatable acidifying nanoparticles (paNP) could restore autophagic flux and insulin secretion in INS1 cells as well as mouse islets via specific acidification of impaired lysosomes (Trudeau et al. 2016). As our data showed ammonia-induced autophagy inhibition was mainly mediated via pH alteration, we further investigated the possible rescue effect of paNP on autophagy in cultured rat astrocytes, in collaboration with Dr. Anton Peterski and Prof. Orian Shirihai.

3.11.1 Quality control of paNP and optimization of treatment conditions

To test the functionality of paNPs, we first investigated the capacity of paNP in acidifying solution pH in the cell-free systems. paNP were added into water solution with and without 10% FBS and strictly kept in dark at room temperature for 24 h. Measurement of the solution pH showed that compared with the solution pH at 0 h, 24 h in the dark environment caused just a slight decrease in the solution pH while a UV exposure could lead to a much stronger pH decrease within 30 min ($p < 0.01$) in water solution without or with 10% FBS (Fig. 3.21A).

Cytotoxicity tests were then carried out to determine the optimal concentration and UV exposure duration for testing the rescue effect of paNP. As shown in Fig 3.15B, paNP treatments up to 25 $\mu\text{g}/\text{mL}$ were demonstrated to be safe for astrocyte under both UV-free and UV-exposed conditions, while 100 $\mu\text{g}/\text{mL}$ or 250 $\mu\text{g}/\text{mL}$ paNP treatment showed significant cytotoxicity in both conditions (Fig. 3.21B). Furthermore, in cultured rat astrocytes, UV exposure appeared to have an alleviation effect on the cytotoxicity induced by high concentrations of paNP (Fig. 3.21B). Besides, a UV exposure durations up to 5 min were shown to be not harmful to astrocytes while 7.5 min and 10 min exposure led to a decreased MTT assay activity of around 80% ($p < 0.01$) and 75% ($p < 0.01$), respectively (Fig. 3.21C). Thus for future experiments, a condition of 25 $\mu\text{g}/\text{mL}$ paNP, 5 min UV exposure was selected.

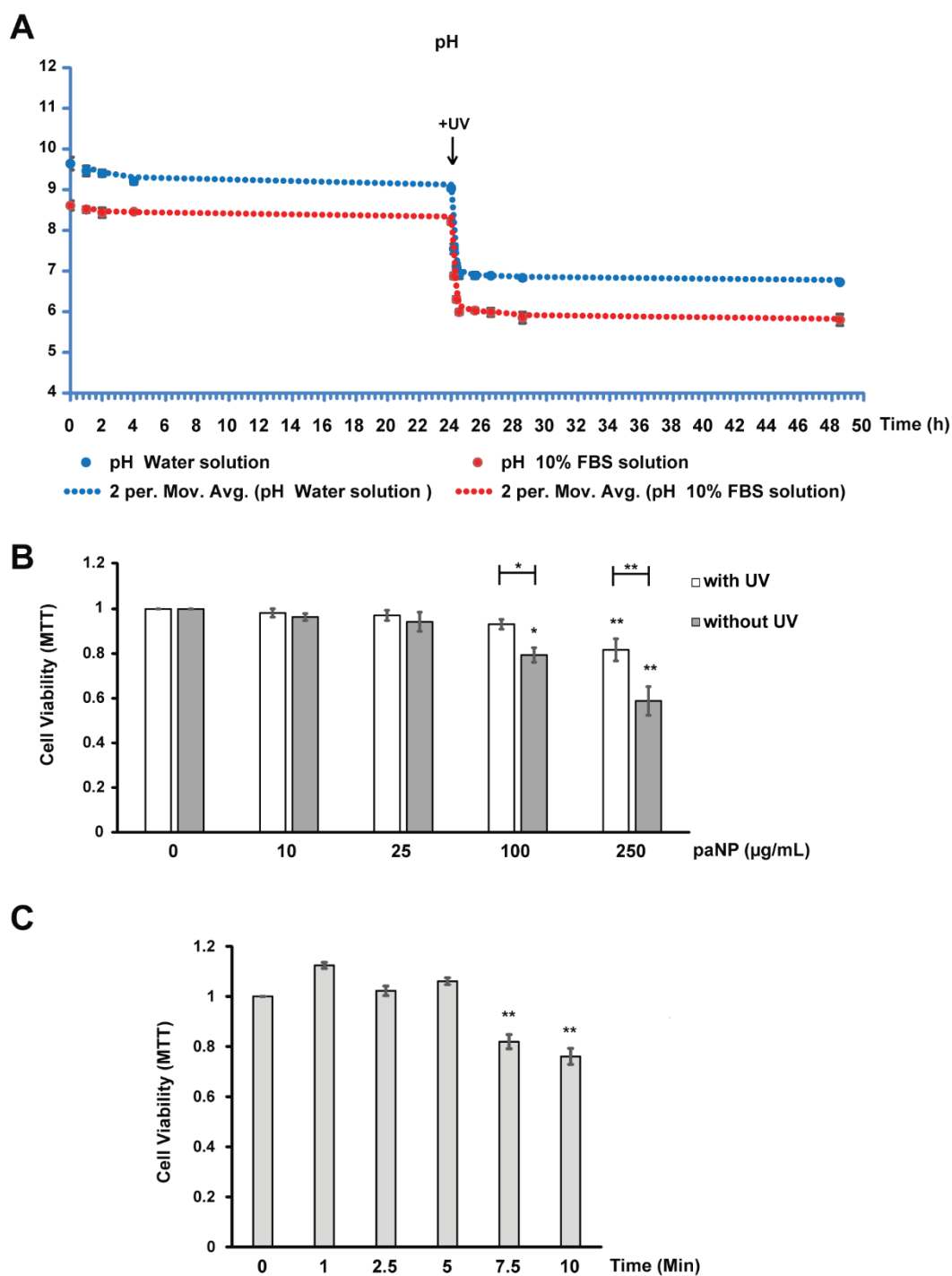


Fig. 3.21 Characterization of photoactivatable acidifying nanoparticle functionalities. (A) pH curves of deionized water containing paNP supplemented without or with 10% FBS ($n=3$). (B) Cytotoxicity measured by MTT assays in cultured rat astrocytes treated with various concentrations of paNP. Where indicated, cells were treated with a UV exposure (365 nm, 5 min, 4W) 21 h before MTT assay ($n=3$). * $p < 0.05$, ** $p < 0.01$, compared with respective control group with the same UV exposure. (C) Cytotoxicity measured by MTT assays in cultured rat astrocytes treated with various durations of UV exposure. Cells were treated with paNP (25 $\mu\text{g/mL}$) 4 h before indicated UV exposure (365 nm, 4W), cells were kept in dark for another 21 h before MTT assay ($n=3$). ** $p < 0.01$, compared with control.

3.11.2 paNP relieve ammonia-induced autophagy inhibition in cultured rat astrocytes

To evaluate whether paNP-mediated intracellular acidification could weaken ammonia-induced autophagy inhibition, an *in vitro* determination of the rescue effect by paNP on autophagic flux was then carried out in cultured rat astrocytes. As shown in Fig. 3.22A, without UV activation, the addition of paNP did not alleviate the autophagy inhibition induced by ammonia in astrocytes while upon UV exposure, paNP treatment led to much weaker accumulations of both LC3-II and p62 ($p < 0.01$, $p < 0.05$, respectively). Similar results were also observed for the $\text{CH}_3\text{NH}_3\text{Cl}$ -induced inhibition of autophagy (Fig. 3.22A). Of note, neither UV exposure alone nor paNP alone could relieve the autophagy inhibition induced by NH_4Cl or $\text{CH}_3\text{NH}_3\text{Cl}$ (Fig. 3.22A). These results thus indicate that the pH-mediated autophagy inhibition by ammonia could be reversed by activation of paNP by UV. However, under hyperammonemic conditions, no statistically significant increase in cell viability was observed in response to UV exposure (Fig. 3.22B).

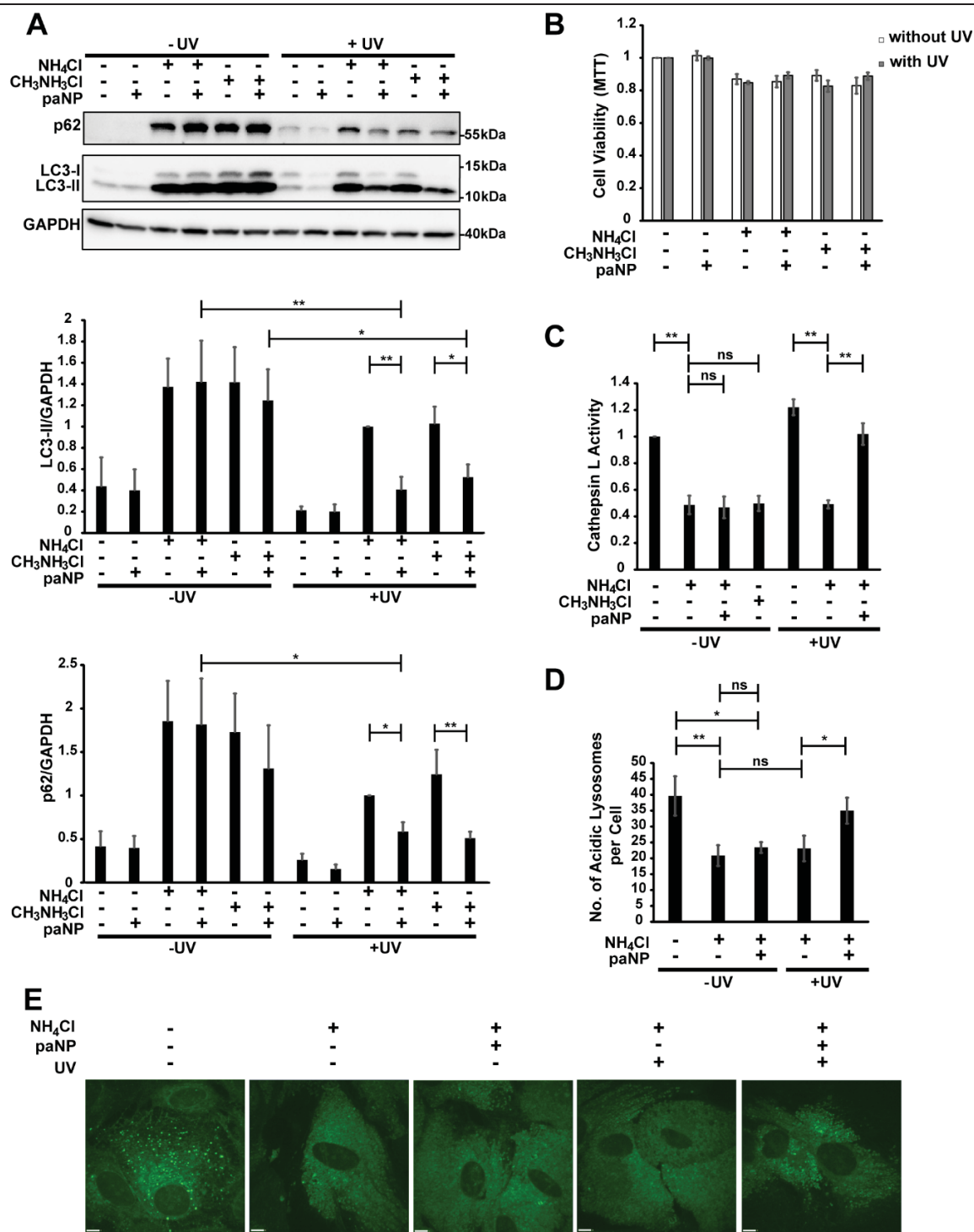


Fig. 3.22 Lysosome acidification by photoactivated nanoparticles restores autophagy under NH₄Cl treatment. (A) Western blot analysis and densitometric analysis of autophagy markers in astrocytes treated with paNP and NH₄Cl/CH₃NH₃Cl for 72 h. paNP were applied 4 h before NH₄Cl/CH₃NH₃Cl treatment. The UV exposure group was exposed to UV (365 nm, 5 min, 4W) after being treated with NH₄Cl/CH₃NH₃Cl for 48 h (n=4). (B) Cytotoxicity measured by MTT assays in cultured rat astrocytes treated with a combination of paNP and NH₄Cl/CH₃NH₃Cl (72 h). paNP were applied 4 h before NH₄Cl/CH₃NH₃Cl treatment. Where indicated, cells were treated with a UV exposure (365 nm, 5 min, 4W) 24 h before MTT assay (n=3). (C) Activity of lysosomal cathepsin L via magic red substrate assay in cultured rat astrocytes treated with paNP and NH₄Cl. paNP were

applied 4 h before $\text{NH}_4\text{Cl}/\text{CH}_3\text{NH}_3\text{Cl}$ treatment. The UV exposure group was exposed to UV (365 nm, 5 min, 4W) after being treated with NH_4Cl for 48 h ($n=3$). (D) Quantification and (E) fluorescence microscopy images of acidic lysosomes in cultured rat astrocytes treated with NH_4Cl and paNP. Where indicated, paNP were applied 4 h before NH_4Cl treatment (5 mM, 72 h). The UV exposure group was exposed to UV (365 nm, 5 min, 4W) after being treated with NH_4Cl for 48 h. After treatment, cells were stained with 1 μM LysoSensorTM Green DND-189 (Invitrogen) for 30 min, for NH_4Cl -treated group, 5 mM NH_4Cl was present during the staining procedure. Around 50 cells were analyzed for each group (scale bar: 9 μm). * $p < 0.05$, ** $p < 0.01$, ns: no significance.

3.11.3 paNP restore cathepsin L activity in cultured rat astrocytes treated with ammonium

As the intracellular autophagic flux was successfully restored by paNP, we speculated that paNP placed positive effects towards lysosome acidification and thus activity of enzymes involved in degradation. We first employed fluorescence microscopy and LysoSensorTM Green which labels lysosomes based on their acidity (Neuhaus and Soldati 2000). As shown in Fig. 3.22D, compared with astrocytes in the control group, NH_4Cl -treated astrocytes exhibited a much bigger area stained with LysoSensorTM Green but less bright dots, showing the area of lysosomal structures were increased but the number of acidic lysosomes was decreased upon NH_4Cl treatment. Without UV activation, paNP rendered no obvious change in the lysosome morphology while with UV exposure, paNP treatment increased the number of active lysosomes although their average fluorescent intensity was weaker than that of the control group. This indicates that combinational treatment of paNP and UV but not paNP alone was capable of causing lysosome acidification.

Cathepsin L had been used as a representative lysosomal degradation enzyme as its activity is pH-dependent (Trudeau et al. 2016). As shown in Fig. 3.22C, under UV-free conditions, NH_4Cl and $\text{CH}_3\text{NH}_3\text{Cl}$ could decrease the enzyme activity to $48.7 \pm 12.0\%$ ($p < 0.05$) and $49.7 \pm 9.8\%$ ($p < 0.05$), respectively. Addition of paNP did not enhance the activity of cathepsin L under these conditions. Interestingly, upon UV exposure, we discovered a rescue effect by paNP, as compared with NH_4Cl only groups, the enzyme activity of cathepsin L was increased by around 2 fold ($p < 0.05$). Overall, these results point out a potential of using paNP as a nanomedicine against HE via restoring lysosomal acidity and autophagic flux.

4. Discussion

4.1 Current model

In the present study, we analyzed the effects of ammonia on several mitochondrion-related cellular quality control mechanisms using *in vitro* or *in vivo* HE models. Fig. 4.1 depicts our current model elucidating the involvement of various mQC pathways in the pathogenesis of HE. In our model, ammonia plays a central role in the pathogenesis of HE. Our data establish that ammonia increases mitochondrial dysfunction which naturally leads to activation of various mQC processes (Fig. 3.13). For mQC degradation pathways, on the one hand, ammonia increases mitophagy initiation via both ubiquitination-dependent and receptor-mediated mitophagy pathways (Fig. 3.17, 3.18); on the other hand, ammonia blocks the final stage of autophagy degradation via autophagosome/autolysosome pH alteration which in turn promotes TGM2 upregulation and relevant defense mechanisms (Fig. 3.1, 3.9). Treatment of ROS scavengers such as NAC largely abrogates the inhibitory effect on autophagy induced by ammonia (Fig. 3.6), suggesting a critical role for ROS in regulating ammonia-induced alteration in mitophagy/autophagy activity. The resulting loss of functional mitochondria is further balanced by the increased PGC-1 α -mediated mitochondrial biogenesis (Fig. 3.19). Of note, using rats acutely intoxicated by ammonium acetate as HE models, autophagy was found to be inhibited by ammonia *in vivo* (Fig. 3.7). Interestingly, the TGM2 upregulation in response to high concentrations of ammonia was even observed in the brains of patients suffering from HE (Fig. 3.12), underlining the importance of autophagy efficiency in the pathobiology of HE. In addition, taurine was shown to be potent in reducing both ammonia-induced NIX accumulation and autophagy inhibition (Fig. 3.7B, 3.9, 3.18C). Photoactivatable acidifying nanoparticles were also shown to efficiently restore the intracellular autophagic activity via re-acidification of lysosomes (Fig. 3.22).

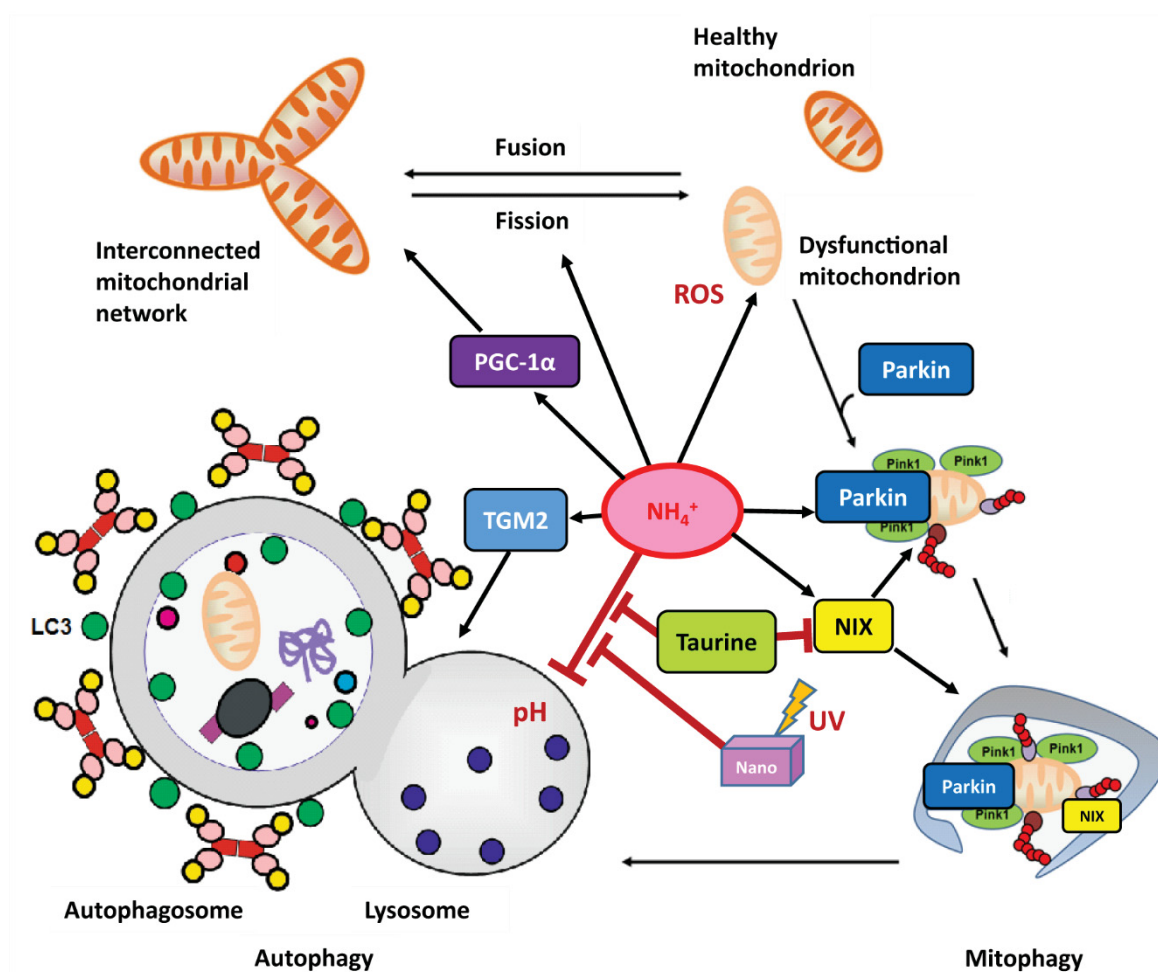


Fig. 4.1 Schematic drawing of the effect of ammonia on mitochondrial quality control pathways. In the pathogenesis of HE, high concentrations of ammonia affect at least three mQC processes, namely degradation through the autophagy pathway, initiation of mitophagy through ubiquitin-dependent and receptor-mediated pathways, and mitochondrial biogenesis mediated by PGC-1 α .

4.2 Ammonia aggravates mitochondrial dysfunction in the pathogenesis of HE

Defective mitochondrial dynamics and impaired mitophagy are associated with many pathological conditions including Parkinson's disease, Alzheimer's disease, various human cancers and certain mitochondrial diseases such as Barth syndrome (Schafer and Reichert 2009, Youle and Narendra 2011). Impaired respiratory chain activity as well as swollen and depolarized mitochondria were recently reported in the brain of bile duct ligated rats, which serve as an animal model for HE (Dhanda et al. 2018).

As previously mentioned, Ammonia is a major neurotoxin that dominates the etiology of HE (Häussinger and Sies 2013). In the present study, besides mitochondrial fragmentation and mitochondrial membrane potential loss, we also observed that ammonia induced a decrease in the number of mitochondrial cristae (Fig. 3.13). In addition, a dose-dependent accumulation of both l-OPA1 and s-OPA1 in response to ammonia treatment was observed (Fig. 3.15). However, different from a previous report claiming increased mitochondrial swelling in response to ammonia treatment (Görg et al. 2015), we did not observe alterations in other mitochondrial structural parameters using EM analysis (Fig. 3.14). This may be due to the low sensitivity of EM analysis. The number of mitochondria per area was also not changed after 5 mM NH₄Cl treatment (Fig. 3.14E).

As mitochondrial cristae host the electron transport chain which is responsible for ATP synthesis and their abnormalities are associated with many neurodegenerative diseases (Anand et al. 2016), decreased mitochondrial cristae number indicates an altered energy production efficiency during hyperammonemic conditions. This is in line with a recent report demonstrating that mitochondria exposed to ammonia experienced a severe ATP depletion (Niknahad et al. 2017).

The accumulation of s-OPA1 upon proteolytic processing of l-OPA1 has been well documented to be responsible for impaired mitochondrial fusion (Duvezin-Caubet et al. 2007, Griparic et al. 2007), thus ammonia-induced accumulation of s-OPA1 partially explains the increased mitochondrial fragmentation. Besides, the accumulation of s-OPA1 also confirms the functionality of the OPA1 processing machinery under long-term ammonium treatment. Interestingly, l-OPA1 which is responsible for mitochondrial fusion was also observed to be accumulated in response to ammonia treatment, this may represent a balancing attempt to maintain the homeostasis of functional mitochondria. It might also be a result of the observed increased PGC-1 α level which is known to promote mitochondrial biogenesis (Cannavino et al. 2015, Singh et al. 2016).

4.3 Various mQC degradation pathways are involved in the pathogenesis of HE

Defective mQC mechanisms are present in many pathological conditions including Parkinson's disease, Alzheimer's disease, various human cancers and several mitochondrial diseases such as Barth syndrome (Youle and Narendra 2011, Lu et al. 2013), however, they are not reported so far in the disease background of HE. Our current data suggest that besides enhanced fragmentation, ammonia could additionally have an impact on various intracellular QC processes including general autophagy, more specific mitophagy as well as mitochondrial biogenesis (Fig. 3.1, 3.16, 3.19).

In the present study, inhibition of autophagy degradation is demonstrated to be an early event in ammonia-triggered HE pathogenesis and its harmful effect can progressively increase over time (Fig. 3.3). As autophagy profoundly affects many HE relevant physiological and pathological processes such as inflammation, it is expected that long-term autophagy inhibition in the brain and liver will facilitate the pathogenesis and increase the lethality of HE (Yin et al. 2016). In line with this, decreased autophagosome biogenesis and inhibited autolysosome degradation were also observed in patient samples of various liver and neurodegenerative diseases including Alzheimer's disease and Parkinson's disease (Czaja et al. 2013, Wang et al. 2016).

Recently, a growing body of evidence suggested that in tumor cells, abnormal autophagic activity is a common phenomenon under various hyperammonemic conditions (Li et al. 2016). Detailed examination revealed the dual effect of ammonia on autophagy under these circumstances, on the one hand, ammonia elevated autophagosomal pH to block autophagic flux, on the other hand, ammonia also induced autophagy through the G protein-coupled receptor DRD3 (Dopamine receptor D3) which served as an ammonia sensor in the cell membrane (Li et al. 2016). Interesting to note, activity and lysosomal localization of mTOR were reported to be decreased in response to high concentrations of ammonia (Li et al. 2016). As the ammonia concentration tested is comparable to the pathophysiological concentrations found in tumor microenvironments (2–5 mM) and patients suffering from hyperammonemia complications (0.5–5 mM) (Li et al. 2016, Spinelli et al. 2017), manipulating autophagy can be

proposed as therapeutic strategies against these diseases. Recently, Soria et al. found hepatic autophagy was activated *in vivo* by hyperammonemia through an α -ketoglutarate-dependent inhibition of mTOR. Enhanced autophagy in liver increased ureagenesis and thus protected cells against hyperammonemia-induced various stresses (Soria et al. 2018). Consistent with these studies, our current data also suggest that ammonia induces autophagy at lower concentrations while it inhibits autophagy at high concentrations. However, whether mTOR activity is also inhibited by ammonia in astrocytes remains to be tested.

Although astrocytes are the major target of ammonia-induced toxicity during the pathogenesis of HE (Schliess et al. 2002, Häussinger and Sies 2013), ammonia-induced harmful effects, such as autophagy inhibition, could also be present in other neuronal cells and at a tissue level which may result in even worse systemic effects and thus facilitate the development of HE symptoms. Indeed, autophagy was observed to be consistently inhibited in various normal and cancerous cell lines as well as in a rat model of acute hyperammonemia intoxication (Fig. 3.2, 3.7). Thus ammonia-induced neuronal toxicity via autophagy inhibition not only consists of the direct autophagy inhibition in neuronal cells but also includes an indirect exacerbated effect by insufficient brain ammonia detoxification in astrocytes.

Besides autophagy inhibition, initiation of Parkin- and NIX-mediated mitophagy was found to be enhanced by ammonia in cultured rat astrocytes (Fig. 3.17, 3.18), possibly due to the accumulation of defects in mitochondrial structure and function as well as the lack of detoxification mechanisms clearing the toxic wastes. Although we cannot rule out that mitophagy is partially a consequence of impaired autophagy preventing the recycling of damaged mitochondria, we feel the induction of mQC is more likely a direct result of mitochondrial damage since mitochondrial function appears to be impaired rapidly and directly in our and others' studies (Drewes and Leino 1985, Bai et al. 2001, Görg et al. 2015). The observed upregulation of PGC-1 α , a master regulator of mitochondrial biogenesis (Fig. 3.19), further supports this view as this is known to occur as a response to mitochondrial damage in an attempt to maintain a healthy set of mitochondrial mass (Canto and Auwerx 2009, Jenning et al. 2010).

As Parkin- and NIX-mediated mitophagy pathways represent mitophagy pathways dependent either on ubiquitination or receptor proteins, ammonia seems to trigger different mitophagy pathways via their common upstream inducers. It is likely that other receptor-mediated pathways such as FUNDC1-mediated mitophagy or even cardiolipin-mediated mitophagy are also triggered under hyperammonemia conditions. The involvement of FUNDC1- and cardiolipin-mediated mitophagy has also been recently reported in various brain injuries (Liu et al. 2012, Chu et al. 2013, Zhao et al. 2016). Furthermore, increased Parkin translocation onto mitochondria is also observed in HeLa cells transfected with pmCherry-Parkin (Fig. 3.17A), indicating ammonia-induced mitophagy initiation could occur in various cell types and at tissue levels.

However, during HE pathogenesis, it is still unclear whether degradation of mitochondria is actually stimulated or blocked at the late stages as final clearance of mitochondria also requires active lysosomal proteases. It is also not clear in hyperammonemic complications, whether enhanced mitophagy initiation is present and plays a role during detoxification of ammonia in liver tissues.

In addition, ammonia-induced harmful effects such as intracellular pH alteration, toxic waste accumulation due to autophagy defect and increased oxidative/nitrosative stress may not only target mitochondria. It is possible that dysfunction and consequently specific autophagy of various organelles such as ER, ribosomes, peroxisomes will be enhanced in response to ammonia. As acidification of lysosomes is impaired at the same time under hyperammonemic conditions, possible protective effects of these selective types of autophagy thereof may be largely hampered, leading to amplification of ammonia-induced toxicity. With these in consideration, it is likely that hyperammonemia, together with other pathological factors may also increase dysfunction of other organelles besides mitochondria (e.g. ER) and thus initiation of respective selective degradation pathways (ER-phagy). Deficiency of those selective degradation pathways may contribute to severe defects and thus be involved in the pathogenesis of various hyperammonemic complications such as HE. Yet, in-depth studies are necessary for evaluating the involvement of other selective types of autophagy in HE pathogenesis.

As autophagy and mitophagy play crucial roles in cell survival, we first sought to determine the biological consequence of ammonia-altered autophagy and mitophagy by evaluating astrocyte viability via MTT assays (Fig. 3.20). Although target genes were successfully knocked down in our experiments, a further sensitization to cell death via RNAi of key autophagy or mitophagy genes was only observed under extreme high conditions of ammonium treatment (40 mM) (Fig. 3.20C, D). This rescue suggests that autophagy and mitophagy at least in part act to reduce ammonia-induced toxicity. Nevertheless, the fact that this rescue was not seen in astrocytes treated with 5 mM NH₄Cl indicates that 5 mM NH₄Cl may not be a harsh enough condition which demands autophagy or mitophagy for cell survival (Görg et al. 2015). This observation can also be attributed to the low sensitivity of the MTT assay or the fact that the strong inhibition of autophagy by ammonia simply masks the effect of any additional depletion of these factors. It is also possible that upon impairing one pathway, one or more other pathways are still there or even stimulated and by this allow additional compensation. Following the latter interpretation, only at high ammonia concentrations, the lack of one pathway may not be compensated in a sufficient manner.

Although we do not observe severe cell death under treatment of ammonia at pathophysiologically relevant concentrations, autophagy and/or mitophagy insufficiency might be still responsible for other pathological conditions frequently observed in HE and other neurodegenerative diseases such as inflammation, proliferation inhibition, senescence and ATP depletion. For example, cognitive impairment and memory loss are frequently observed in patients with hepatic encephalopathy (Riggio et al. 2011). Postsynaptic protein synthesis is a process critically involved in learning and memory consolidation. Ammonia-induced autophagy inhibition may impair this process via limiting both nutrient and energy supply, thus autophagy inhibition provides a novel explanation for various disturbances of neurotransmitter systems and subsequent cognitive deficits. Future studies will have to decipher the involvement and the interplay of distinct stress response or mQC pathways.

4.4 Common regulatory mechanisms are underlying ammonia-altered autophagy and mitophagy

Ammonia-induced autophagy inhibition and mitophagy initiation share a similarity in their mode of action. First, the influences on autophagy and mitophagy by NH_4Cl can both be mimicked by $\text{CH}_3\text{NH}_3\text{Cl}$ (Fig. 3.4, 3.17B, 3.18C), indicating the fundamental role of pH in maintaining the functionalities of both autolysosomes and mitochondria.

The intricate effects of ammonia on pH have been previously documented. The majority of studies found that high concentrations of ammonia-induced intracellular alkalinization in various cell lines and animal models (Swain et al. 1991, Boyarsky et al. 1993, Busch et al. 1996, Bai et al. 2001), possibly due to the generation of membrane permeable NH_3 . Yet opposite evidence exists, showing acidification was also induced in mouse astrocytes after ammonia treatment (Nagaraja and Brookes 1998). Regarding HE, recently, utilizing fluorescence microscopy, Bartolic et al. again proved that application of NH_4Cl led to a rapid dose-dependent alkalinization of the cytoplasm followed by a slow recovery in both astrocytes and endothelial cells (Bartolic et al. 2016). The negative impact of pH alteration on autophagy thus is easy to understand since intracellular alkalinization can decrease lysosome protease activities (Kappler et al. 2012, Bartolic et al. 2016, Li et al. 2016) while connections between mitochondrial quality and pH are not well studied. One possible connection may be that, similar to that of lysosomal proteases, the activity of mitochondrial proteases, such as PARL, are likely to be influenced by NH_4Cl -induced intracellular pH change. Ammonia induces mitochondrial membrane potential loss and thus mitochondrial pH alkalinization, these further interfere with the internal transport and/or the cleavage of full-length PINK1 (Youle and Narendra 2011).

Alteration of intracellular pH homeostasis have been linked to a variety of human diseases and decreased physical performance (Aoi and Marunaka 2014). As hypoxia-inducible factor-1 α (HIF-1 α) is the master regulator for maintaining intracellular pH homeostasis, future studies are desirable to elucidate the contribution of HIF-1 α pathway in the pathogenesis of HE which will be discussed later (Fig. 4.2).

Another major discovery about the regulatory mechanisms is that decreasing ROS level is demonstrated to be able to reverse ammonia-altered autophagy and mitophagy. In the disease background of HE, increased oxidative/nitrosative stress has been well documented in ammonia-treated rat astrocytes (Görg et al. 2008, Görg et al. 2015), in animal models of HE (Görg et al. 2008), as well as in *post mortem* brain samples of cirrhosis patients with HE (Görg et al. 2013, Görg et al. 2013, Görg et al. 2015). Especially, the expression of heme oxygenase I (HO-1), a key enzyme involved in the maintenance of redox homeostasis, was also reported to be stimulated in response to ammonia (Warskulat et al. 2002, Oenarto et al. 2016), indicating its participation in a ROS regulatory network regulating the pathogenesis of HE. However, the effects of ammonia on other Nrf2 pathway components and the relevant contribution of mitochondria in this scenario remain unclear.

In the current study, it was shown that ammonia-induced autophagy inhibition and mitophagy initiation are sensitive to the intracellular ROS scavenger NAC, the NADPH oxidase inhibitor apocynin or oxidative stress reducer taurine (Fig. 3.6, 3.9, 3.16). Ammonia-induced NIX-mediated mitophagy could also be reduced by NAC and taurine (Fig. 3.18C). Among all these drugs, NAC was the most potent. This is in line with many previous publications showing that ammonia-induced toxicity was partially or completely mediated via formation of ROS/RNS in astrocytes (Schliess et al. 2002, Görg et al. 2008, Görg et al. 2015, Oenarto et al. 2016). However, neither the autophagy inhibition nor mitophagy initiation was shown to be reversed by the GS inhibitor MSO or the p38MAPK inhibitor SB203580. As MSO and SB203580 were reported to act further upstream in the oxidative stress generation (Schliess et al. 2002), this result indicates that the effects of ROS placed on ammonia-altered autophagy or mitophagy is cumulative and rather at a late stage. One possible explanation could be that in hyperammonemic conditions, independent of GS and p38MAPK, increased environmental ROS levels may result in the oxidation and inactivation of active degradation enzymes which further lead to deficiencies in the autophagic clearance. This, at least partially, explains the phenomenon that various antioxidants were potent in attenuating ammonia-induced autophagy inhibition. Decreased ROS levels are frequently associated with an improved mitochondrial function (Görg et al. 2015, Niknahad et al. 2017), and thus result in less initiation of mitophagy

and autophagy.

Previous studies revealed that autophagy and mitophagy induction could be rather separated processes as enhanced mitophagy do not necessarily lead to the corresponding elevated autophagy (Frank et al. 2012). Along with this, through immunostaining, we also observed mitophagy and autophagy were still maintained in distinct regions inside astrocytes (Fig. 3.16), however, the similar molecular mechanisms mentioned in this study suggest the existence of a connected regulatory network coordinating both autophagy and mitophagy during hyperammonemia.

In the pathogenesis of HE, it is possible that these two degradation pathways are directly connected to each other via multiple linkages, forming a self-amplifying cycle. For example, besides promoting Parkin translocation on to mitochondria, NIX was found to be required for ROS-mediated autophagy induction (Ding et al. 2010). BNIP3 or NIX could compete with BECN1 for binding to BCL2 or BCL2L1, thus the increased expression of BNIP3 or NIX will release BECN1 from BCL2 or BCL2L1 to activate autophagy and mitophagy (Zhang and Ney 2009). Also, insufficient autophagy could result in a higher energy demand compensated by increased mitochondrial respiration which could generate more ROS and dysfunctional mitochondria, if proper homeostasis is not maintained. Increased oxidative stress then can further induce mitophagy and block autophagic flux.

4.5 Compensatory mechanisms are possibly triggered in response to ammonia

It is well established that neuronal tissue needs to fight against age- and stress-induced neurodegeneration throughout life which is highly dependent on their capacity in maintaining the intracellular homeostasis (Komatsu et al. 2006). To compensate for alterations in autophagy and mitophagy degradation pathways, cells may evoke other quality control mechanisms (e.g. UPS, NF- κ B signaling) to minimize stresses (Widmer et al. 2007).

As TGM2 is a stress response gene, its upregulation represents a decrease in vulnerability towards hyperammonemic stress. TGM2 is also known to enhance mitochondrial complex I activity and relevant ATP synthesis which might be helpful under ammonia-induced mitophagy initiation and autophagy inhibition (Battaglia et al. 2007). Also, it was recently demonstrated that TGM2 placed a positive regulatory effect on autophagosome maturation and cargo degradation (D'Eletto et al. 2009, Yeo et al. 2016). The upregulation of TGM2 also represents a negative feedback defense response specifically aiming to repair the dysfunctional autophagosome/autolysosome in the later stages of degradation.

The observation that TGM2 was mainly upregulated in normal cells might be explained by the fact that TGM2 is a downstream target gene of tumor suppressor protein 53 (TP53) which was observed to be activated for transcription in cultured astrocytes under NH₄Cl treatment (Fig. 3.10C) (Görg et al. 2015, Yeo et al. 2016). Moreover, TGM2 was frequently seen to form a self-amplifying loop with NF- κ B (Ai et al. 2012, Zhang et al. 2016). Consequently, upregulation of TGM2 could also be a result of the previously observed activation of NF- κ B due to ammonia treatment (Albrecht and Norenberg 2006, Häussinger and Görg 2010).

Important to note, elevated mRNA expression levels of TGM2 were found in *post mortem* brain biopsies of liver cirrhosis patients with HE but not in cirrhosis patients without HE (Fig. 3.12), indicating that insufficient autophagy and relevant defense mechanisms are associated with HE. However, it remains to be elucidated to what extent, TGM2 upregulation contributes to the suppression of autophagy defect and development of HE symptoms.

Besides TGM2 upregulation, ammonia-induced upregulation of PGC-1 α has also been observed in cultured rat astrocytes (Fig. 3.19). This represented a demand to balance the deficiency of energy and other essential mitochondrial functions. Indeed, via EM, we did not observe a significant decrease in mitochondrial number per area or other major mitochondrial parameters (Fig. 3.14), indicating the mitochondrial mass was not much affected even when initiation of various mitophagy pathways was demonstrated to be enhanced. This might be partially explained by the balance between the increased PGC-1 α -mediated mitochondrial biogenesis and the enhanced mitophagy initiation.

Previous studies have also proved that mitochondrial biogenesis is tightly controlled within a cell and there is crosstalk between mitochondrial biogenesis and mitochondrial degradation pathways. For example, Parkin was demonstrated to ubiquitylate and trigger the proteolytic breakdown of the Parkin interacting substrate (PARIS), thus releasing the repression on PGC-1 α and resulting in boosted mitochondrial biogenesis in neurons (Shin et al. 2011).

Interestingly, PGC-1 α was also reported to be an upstream regulator of HO-1 in mouse adipocytes (Singh et al. 2016), thus upregulation of HO-1 in cultured rat astrocytes induced by ammonia may also be partially attributed to enhanced expression of PGC-1 α . However, future investigations are still needed for the question whether enhancing mitochondrial biogenesis can serve as a therapeutic strategy towards HE.

Another interesting observation of current study is that there is a similar expression pattern of TGM2, NIX, and PGC-1 α in response to high concentration of ammonium treatment. Under hyperammonemic conditions, all three proteins were shown to be upregulated in primary rat astrocytes and immortalized cell line HEK293, however, they were unchanged or even downregulated in cancerous cell lines MOG-G-CCM, SH-SY5Y, and HeLa (Fig. 3.10C, 3.18A, 3.19C). It is possible that a common regulatory network is responsible for the cooperated upregulation of TGM2, NIX, and PGC-1 α in cultured rat astrocytes. TGM2 was shown to constitutively activate HIF-1 α , the master regulator for intracellular pH homeostasis, under various stress conditions, leading to amplification of many HIF-1 α target genes (Kappler et al. 2012, Kumar and Mehta 2012). Interestingly, PGC-1 α also showed capacity in stabilizing the HIF-1 α protein and thus induce HIF-1 α target gene expressions in response to hypoxia (O'Hagan et al. 2009). Thus under hyperammonemic conditions, TGM2 and PGC-1 α may act synergistically to enhance the regulation by HIF-1 α on intracellular pH homeostasis and consequent stress response mediated by HIF-1 α target genes. Indeed, NIX, another gene upregulated only in normal cells in response to ammonia, was shown to be a target gene of HIF-1 α (Fig. 3.18A) (Bakker et al. 2007). Along these lines, via immunostaining, Tallis et al. have observed enhanced expression levels of HIF-1 α as well as its downstream target genes P-glycoprotein (P-gp) and erythropoietin receptor (Epo-R) in cortical neurons of rats developing minimal HE (MHE) (Tallis et al. 2014).

Together, the similar patterns of TGM2, PGC-1 α , and NIX upregulation indicate a coordinated regulatory network via modulating HIF-1 α , the master regulator of intracellular pH homeostasis, in response to ammonia treatment (Fig. 4.2). As HIF-1 α , TGM2, PGC-1 α , and NIX are also involved in the ROS-signaling pathways, this network may also reveal a connection responsible for the coordination between intracellular pH and redox homeostasis. Future studies are necessary to demonstrate the existence of such network in various hyperammonemia complications.

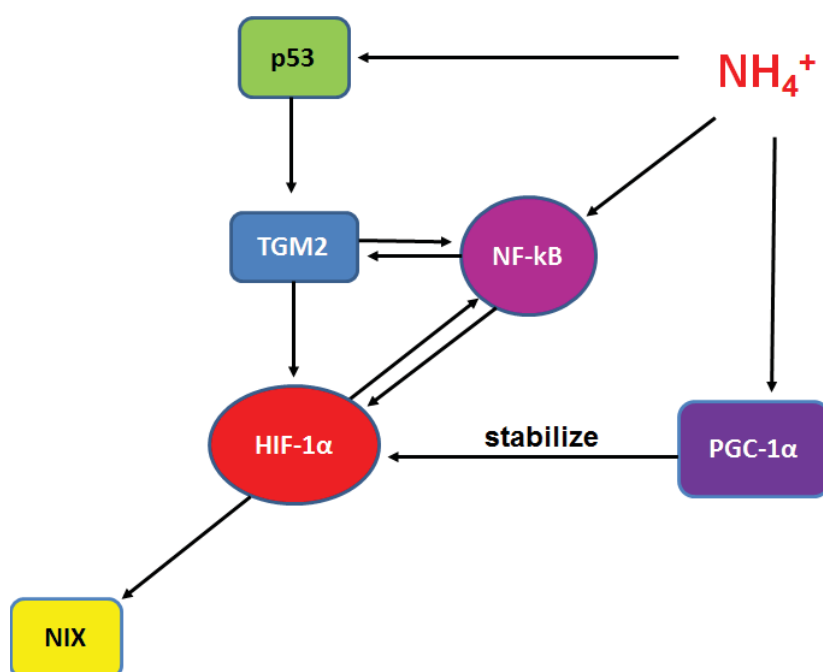


Fig. 4.2 Schematic drawing of a regulatory network centered by HIF-1 α for defensive mechanisms evoked by hyperammonemia. TGM2 upregulation, NIX-mediated mitophagy, PGC-1 α -mediated mitochondrial biogenesis represent three perspectives in the defense against hyperammonemic stress. High concentration of ammonia may upregulate NIX through multiple pathways involving HIF-1 α . TGM2 can also be induced via ammonia-activated TP53 as well as NF- κ B which forms a self-amplifying loop with HIF-1 α . Additionally, ammonia-induced PGC-1 α may stabilize the HIF-1 α protein and thus enhance NIX expression levels.

4.6 Taurine, NAC, and paNP may serve as bases for future therapeutics against HE

Current therapies towards HE are often inadequate and largely target the production of ammonia in the intestine or the gut microbiome (Atluri et al. 2010, Riggio et al. 2011, Häussinger and Sies 2013). Therapeutic strategies directly aiming at the low-grade edema or the associated oxidative stress have not been incorporated into clinical treatment yet, although results of animal studies support the promising outcome of applying such strategies (Häussinger and Sies 2013). As autophagy and mitophagy alterations are possibly involved in the pathogenesis of HE, minimizing and repairing autophagic and mitochondrial defects are therefore proposed as novel therapeutic strategies.

Modulating ammonia-induced toxicity via reducing ROS has been proposed as a therapeutic strategy against HE for a long time. Via different pharmacological characterizations, many studies have proved the critical involvement of oxidative stress in formulating the major pathological symptoms of HE (Schliess et al. 2002, Häussinger and Görg 2010, Oenarto et al. 2016). Here similar to previous studies (Warskulat et al. 2002), we provide evidence that treatment of ROS scavenger NAC can alleviate the majority of ammonia-induced autophagy inhibition and NIX accumulation in cultured rat astrocytes (Fig. 3.6A, 3.18C).

Moreover, in this study we provide for the first time evidence that taurine, an amino acid widely acknowledged as a biomembrane stabilizer and oxidative stress mitigator (Huxtable 1992), largely abolished ammonia-induced autophagy inhibition and NIX-mediated mitophagy initiation in *in vitro* or *in vivo* models of HE (Fig. 3.7B, 3.8, 3.18C). Apart from efficiently abolishing ammonia-induced toxicity such as proliferation inhibition and senescence (Warskulat et al. 2002, Oenarto et al. 2016), taurine was also reported to promote mitochondrial function, prevent mitochondrial swelling, or improve mitochondrial membrane potential and respiration efficiency under conditions of high ammonia (Niknahad et al. 2017). Furthermore, a deficiency in taurine transporters (TauT) results in reduced life expectancy and increased mitochondrial dysfunction *in vivo* (Warskulat et al. 2006, Ito et al. 2014). Recently, serum taurine levels prior treatment with L-carnitine were reported to be an amelioration predictor in patients suffering from minimal HE (Saito et al. 2016). In view of these, we propose that these

reported beneficial effects of taurine are at least partially caused by improving the efficiency of autophagy and mQC.

It is important to note that antioxidants such as taurine supplement could act systematically at multiple levels against hyperammonemic complications. Still, in-depth studies are necessary for evaluating the potential of such therapeutic approaches aiming at the increased systemic oxidative stress in HE.

Lysosome re-acidification has been investigated as a promising therapeutic strategy towards various neurodegenerative lysosomal storage disorders caused by lipid-induced alkalization of lysosomal pH (Folts et al. 2016). Recent studies have shown nanoparticles, especially paNP, could specifically acidify lysosomes and thus restore autophagic flux and insulin secretion in INS1 insulinoma line and primary mouse islets, providing a novel strategy against lipid toxicity-associated diseases such as diabetes (Trudeau et al. 2016). However, the potential of nanomedicine as a novel therapy strategy combating HE has not been tested so far.

In this study, paNP was introduced for the first time as a lysosomal acidifying agent in models of hyperammonemia complications. As shown in Fig. 3.22A, upon 5 min of UV exposure, photoactivatable acidifying nanoparticles were demonstrated to restore a large portion of intracellular autophagic activity without causing severe cytotoxicity. This is possibly achieved via re-acidification of lysosomes and improvement of lysosomal degradation enzymes such as cathepsin L (Fig. 3.22C). Our data thus suggest that restoring lysosomal acidity via nanomedicine could be a novel strategy to treat hyperammonemia complications in which autophagosome/autolysosome function is impaired. Future *in vivo* studies are definitely needed to further evaluate the efficiency of such strategies.

Nevertheless, cautions should be raised when applying paNP as they might place much severer cytotoxic effects towards other neuronal cells. Although paNP mainly accumulate in lysosomes (Trudeau et al. 2016), it is possible that they might also affect functionalities of other organelles among which mitochondria are of particular interest. Furthermore, the disruption of intracellular processes other than autophagy and mitophagy by paNP should also be carefully examined.

Finally, regarding possible therapeutics against HE, future efforts are desirable to solve the open question whether an improvement in the quality control of mitochondria has a positive effect towards the cure of HE in the case of liver damage. Systematic approaches such as proteomics and more specific mitochondrial proteomics will be required to reveal the key interactions in various hyperammonemia-induced dysfunctions, thus elucidating the contribution of mitochondrial defects during different stages of HE development.

To my knowledge, this study provides the first documented evidence that mitophagy initiation and autophagy inhibition due to ammonia toxicity are involved in the pathogenesis of HE. We observed that in the disease background of HE, hyperammonemia has pleiotropic effects. Besides its effect on modulating autophagy, ammonia also impairs mitochondrial function. The latter is demonstrated by alterations in mitochondrial network morphology, structure, and reduction in mitochondrial membrane potential upon treatment with ammonium chloride. We further observed a clear induction of two mitophagy pathways, the Parkin- and the NIX/Bnip3L-mediated pathways, by ammonia in primary rat astrocytes. This is notable as it is a first example that demonstrates a simultaneous induction of both pathways in a disease model. For the Parkin-mediated pathway this might be expected, given that mitochondrial membrane potential was reduced. For NIX/Bnip3L-mediated mitophagy, this rather points to the view that multiple pathways aim to improve mitochondrial function which is consistent with an earlier study suggesting an interplay between these two pathways (Ding et al. 2010). In summary, under hyperammonemic conditions, mQC is severely hampered as autophagy degradation is largely blocked, yet, it is also promoted by at least three processes, namely the induction of PINK1/Parkin-mediated mitophagy, NIX/Bnip3L-mediated mitophagy, and stimulation of mitochondrial biogenesis via PGC-1 α (Fig. 4.1). Furthermore, the present work also indicates taurine and paNP supplementation as possible bases for future therapeutic approaches against HE.

Summary

Hepatic encephalopathy (HE) is a frequent neuropsychiatric syndrome associated with various forms of liver dysfunction. Characterized by elevated levels of ammonia in both blood and brain, HE is proposed to be the accumulative result of astrocyte dysfunction evolving from cerebral osmotic disturbances and increased intracellular oxidative/nitrosative stress. Recent studies demonstrated that treatment of cultured astrocytes with ammonia could lead to mitochondrial dysfunction such as alteration of mitochondrial morphology and decrease of mitochondrial membrane potential, suggesting mitochondrial quality control (mQC) is involved in the pathogenesis of HE. However, the effects of ammonia, the major toxin of HE, on mitochondria and mQC in the disease background of HE remain largely unknown. The focus of this work was investigating the involvement of autophagy and mitophagy, two important cellular quality control processes, in the pathogenesis of HE.

Since astrocyte dysfunction is central to the pathogenesis of HE, the characterization of autophagy and mitophagy was performed mechanistically by analyzing various markers in cultured rat astrocytes stimulated with NH_4Cl . The *in vivo* relevance was then validated via assaying cortex samples obtained from acutely ammonia intoxicated rats.

Treatment of astrocytes with low concentrations of NH_4Cl induced autophagy while from 2 mM onwards, NH_4Cl inhibited autophagy in astrocytes in a time- and dose-dependent manner. Characterization of the autophagy-inhibitory effect of ammonia showed that the blockage was mainly mediated via intracellular pH alteration and could be largely alleviated by decreasing the intracellular ROS level, while inhibition of GS or p38MAPK activity did not have a significant effect on this inhibition. Taurine supplement was shown to be able to decrease the degree of autophagy inhibition in cultured rat astrocytes as well as in the acute NH_4Ac -intoxicated rat model. This autophagy inhibitory effect was also shown to be reversible in cultured rat astrocytes. In addition, TGM2, a gene promoting the fusion between autophagosome and lysosome as well as the autolysosomal degradation, was shown to be increased at the protein level in response to ammonia treatment in both cultured rat astrocytes

and brain samples from a rat model of HE, indicating that relevant defense mechanisms may be triggered to protect the astrocytes against the ammonia-induced stress. Interesting to note, result from our cooperation partners, Prof. Dr. Dieter Haüssinger and Dr. Boris Görg, also showed an elevated TGM2 mRNA level in the cerebral cortex of patients suffering from HE.

In cultured rat astrocytes, 5 mM NH₄Cl was shown to induce mitochondrial dysfunction as evidenced by increased mitochondrial fragmentation, decreased mitochondrial membrane potential and reduced cristae number per mitochondrion. Likely as a reaction to the mitochondrial damage, a marked increase was observed for the colocalization between TIM23 and LC3 after ammonia treatment, indicating that there was an increased mitophagy induction. This increase was also observed in the CH₃NH₃Cl-treated samples but was much less in the NAC-treated samples, suggesting that ammonia-induced mitophagy induction was pH-dependent and could be decreased by reducing the intracellular ROS level.

Further examination of major mitophagy pathways revealed that ammonia induced Parkin-mediated mitophagy in astrocytes and this induction was largely dependent on pH as CH₃NH₃Cl treatment also led to a similar increase in the mitochondrial-translocated Parkin signal. This is likely a direct result of the stabilization of full-length PINK1 on the OMM. Besides, ammonia also induced NIX-mediated mitophagy as evidenced by the accumulation of various forms of NIX. The induction of NIX-mediated mitophagy was also mainly dependent on intracellular pH alteration while decreasing ROS levels by NAC or taurine rendered a much weaker accumulation of NIX. Moreover, we discovered that ammonia not only enhanced the initiation of different mitophagy pathways but also increased PGC-1 α -mediated mitochondrial biogenesis, demonstrating the critical participation of various mQC mechanisms in response to ammonia-induced stress.

Regarding biological consequence, we discovered under 5 mM NH₄Cl treatment, knockdown of autophagy/mitophagy machinery did not further sensitize astrocytes while at very high levels of ammonia, knockdown of Atg5 led to a significant decrease in cell viability and knockdown of Parkin, PINK1 or NIX led to a less severe decrease, suggesting that autophagy and mitophagy play a pro-survival role under extreme conditions.

For possible therapeutic strategies, we found that various ROS decreasing reagents (e.g. NAC and taurine) can lift the autophagy inhibition by ammonia to a large extent, in astrocytes or in animal models of HE. Photoactivatable acidic nanoparticles (paNP) were also proven to be potent in restoring intracellular autophagic activity via lysosome re-acidification in cultured rat astrocytes. This is possibly through improving the activity of lysosome enzymes such as cathepsin L, indicating the potential of novel nanomedicine therapeutics against HE.

In conclusion, the work presented here suggests that initiation of Parkin- and NIX-mediated mitophagy as well as insufficient progression of autophagy are involved in the pathogenesis of HE and as such, these are promising targets for the development of future therapies.

Zusammenfassung

Die hepatische Enzephalopathie (HE) ist ein häufiges neuropsychiatrisches Krankheitsbild, das mit verschiedenen Formen von Leberfunktionsstörungen einhergeht. Durch erhöhte Konzentrationen von Ammoniak sowohl im Blut als auch im Gehirn charakterisiert, wird HE als das kumulative Ergebnis einer Astrozytendysfunktion angesehen, die sich aus zerebralen osmotischen Störungen und erhöhtem intrazellulärem oxidativem/nitrosativem Stress entwickelt. Jüngste Studien haben gezeigt, dass die Behandlung von kultivierten Astrozyten mit Ammoniak, einem *In-vitro*-Modell für HE, zu mitochondrialen Störungen wie einer Veränderung der Mitochondrienmorphologie und einem Rückgang des mitochondrialen Membranpotentials führen kann, was darauf hindeutet, dass die mitochondriale Qualitätskontrolle (mQC) an der Pathogenese der HE beteiligt ist. Die Auswirkungen von Ammoniak, dem wesentlichen Toxin der HE, auf Mitochondrien und mQC im Krankheitshintergrund der HE sind jedoch weitgehend unbekannt. Der Fokus dieser Arbeit lag auf der Untersuchung der Beteiligung von Autophagie und Mitophagie, zwei wichtigen zellulären Qualitätskontrollprozessen, an der Pathogenese von HE.

Da die Dysfunktion von Astrozyten für die Pathogenese von HE von zentraler Bedeutung ist, wurde die Charakterisierung von Autophagie und Mitophagie mechanistisch durch Analyse verschiedener Marker in kultivierten Rattenastrozyten, die mit NH_4Cl stimuliert wurden, durchgeführt. Die *In-vivo*-Relevanz wurde dann durch die Untersuchung von Ratten-Kortexproben validiert, die aus einem akuten Ammoniakintoxikationsmodell von HE erhalten wurden.

Die Behandlung von Astrozyten mit niedrigen NH_4Cl -Konzentrationen induzierte Autophagie, während Mengen ab 2 mM NH_4Cl die Autophagie in Astrozyten zeit- und dosisabhängig hemmten. Die Charakterisierung der Autophagie-hemmenden Wirkung von Ammoniak zeigte, dass die Inhibition hauptsächlich über intrazelluläre pH-Veränderung vermittelt wurde und durch Verminderung des intrazellulären ROS-Spiegels weitgehend abgeschwächt werden konnte, während eine Hemmung der GS- oder p38MAPK-Aktivität keinen signifikanten

Einfluss auf diese Inhibition hatte. Es wurde gezeigt, dass Taurin-Supplementation in der Lage ist, den Grad der Autophagie-Inhibierung in kultivierten Rattenastrozyten sowie in einem akut mit NH_4Ac behandelten Rattenmodell zu verringern. Diese Autophagie-Hemmwirkung wurde auch in kultivierten Rattenastrozyten als reversibel nachgewiesen. Zusätzlich wurde gezeigt, dass TGM2, ein Gen, das die Fusion zwischen Autophagosom und Lysosom und den autolysosomalen Abbau fördert, einen erhöhten Proteinlevel in Reaktion auf Ammoniakbehandlung in kultivierten Rattenastrozyten und Gehirnproben aus einem Rattenmodell von HE zeigt. Dies weist darauf hin, dass relevante Abwehrmechanismen ausgelöst werden können, um Astrozyten vor dem Ammoniak-induzierten Stress zu schützen. In diesem Zusammenhang bemerkenswert ist das Ergebnis unserer Kooperationspartner Prof. Dr. Dieter Haüssinger und Dr. Boris Görg, welches ebenfalls eine erhöhte Menge TGM2-mRNA in der Großhirnrinde von Patienten mit HE zeigte.

Es konnte gezeigt werden, dass 5 mM NH_4Cl in kultivierten Rattenastrozyten mitochondriale Dysfunktion induzieren, was sich durch eine erhöhte mitochondriale Fragmentierung, ein verringertes mitochondriales Membranpotential und eine reduzierte Cristae-Zahl pro Mitochondrion äußert. Wahrscheinlich als Reaktion auf die mitochondrialen Schäden wurde ein deutlicher Anstieg der Kolokalisation zwischen TIM23 und LC3 nach Ammoniakbehandlung beobachtet, was auf eine erhöhte Mitophagie-Induktion hinweist. Dieser Anstieg wurde auch in den mit $\text{CH}_3\text{NH}_3\text{Cl}$ behandelten Proben beobachtet, war jedoch in den NAC-behandelten Proben viel geringer, was darauf hindeutet, dass die durch Ammonium induzierte Mitophagie-Induktion pH-abhängig war und durch Verringerung des intrazellulären ROS-Spiegels abgeschwächt werden konnte.

Eine weitere Untersuchung der Hauptwege der Mitophagie ergab, dass Ammoniak die Parkin-vermittelte Mitophagie in Astrozyten induzierte und diese Induktion stark vom pH-Wert abhängig war, da die $\text{CH}_3\text{NH}_3\text{Cl}$ -Behandlung ebenfalls zu einem ähnlichen Anstieg des mitochondrial-translozierten Parkin-Signals führte. Dies ist wahrscheinlich eine direkte Folge der Stabilisierung von Vollängen-PINK1 auf der OMM. Außerdem induzierte Ammoniak auch NIX-vermittelte Mitophagie, wie durch die Akkumulation verschiedener Formen von NIX gezeigt wird. Die Induktion von NIX-vermittelter Mitophagie war auch hauptsächlich abhängig

von der intrazellulären pH-Änderung, während die Verringerung des ROS-Spiegels durch NAC oder Taurin eine viel schwächere Akkumulation von NIX erreichte. Darüber hinaus haben wir entdeckt, dass Ammoniak nicht nur die Initiierung verschiedener Mitophagiewege verstärkt, sondern auch die PGC-1 α -vermittelte mitochondriale Biogenese verstärkt, was die kritische Beteiligung verschiedener mQC-Mechanismen als Reaktion auf Ammoniak-induzierten Stress zeigt.

Werden nachgeschaltete biologische Parameter betrachtet, so zeigt sich, dass bei 5 mM NH₄Cl-Behandlung der Knockdown von Bestandteilen der Autophagie- und Mitophagie -Maschinerie die Astrozyten nicht weiter sensibilisierte. Bei sehr hohen Konzentrationen an Ammonium führte der Knockdown von Atg5 jedoch zu einer signifikanten Abnahme der Zellebensfähigkeit und der Knockdown von Parkin, PINK1 oder NIX hatten einen geringeren Rückgang zur Folge, was darauf hindeutet, dass Autophagie und Mitophagie unter extremen Bedingungen eine überlebensnotwendige Rolle spielen.

Die von uns erzielten Ergebnisse, dass ROS-verringernde Reagenzien (z. B. NAC und Taurin) die Autophagie-Hemmung durch Ammoniak in Astrozyten oder in Tiermodellen von HE zum Großteil aufheben können, betrachten wir als vielversprechenden Ansatz für mögliche Therapien. Photoaktivierbare, saure Nanopartikel (paNP) erwiesen sich auch als wirksam bei der Wiederherstellung der intrazellulären autophagischen Aktivität durch Lysosomen-Reacidifizierung in kultivierten Rattenastrozyten. Dies liegt möglicherweise an der Verbesserung der Aktivität von lysosomalen Enzymen wie Cathepsin L, was das Potenzial für neuartige nanomedizinische Therapeutika gegen HE hervorhebt.

Zusammengefasst legt die hier vorgestellte Arbeit nahe, dass die Initiierung von Parkin- und NIX-vermittelter Mitophagie sowie ein unzureichender Ablauf der Autophagie an der Pathogenese von HE beteiligt sind und somit vielversprechende Ansatzpunkte für die Entwicklung zukünftiger Therapien darstellen.

References

- Abeliovich, H., M. Zarei, K. T. Rigbolt, R. J. Youle and J. Dengjel (2013). "Involvement of mitochondrial dynamics in the segregation of mitochondrial matrix proteins during stationary phase mitophagy." *Nat Commun* **4**: 2789.
- Ai, L., R. R. Skehan, J. Saydi, T. Lin and K. D. Brown (2012). "Ataxia-Telangiectasia, Mutated (ATM)/Nuclear Factor kappa light chain enhancer of activated B cells (NFkappaB) signaling controls basal and DNA damage-induced transglutaminase 2 expression." *J Biol Chem* **287**(22): 18330-18341.
- Aihara, M., X. Jin, Y. Kurihara, Y. Yoshida, Y. Matsushima, M. Oku, Y. Hirota, T. Saigusa, Y. Aoki, T. Uchiumi, T. Yamamoto, Y. Sakai, D. Kang and T. Kanki (2014). "Tor and the Sin3-Rpd3 complex regulate expression of the mitophagy receptor protein Atg32 in yeast." *J Cell Sci* **127**(Pt 14): 3184-3196.
- Akar, U., B. Ozpolat, K. Mehta, J. Fok, Y. Kondo and G. Lopez-Berestein (2007). "Tissue transglutaminase inhibits autophagy in pancreatic cancer cells." *Mol Cancer Res* **5**(3): 241-249.
- Al Rawi, S., S. Louvet-Vallee, A. Djeddi, M. Sachse, E. Culetto, C. Hajjar, L. Boyd, R. Legouis and V. Galy (2011). "Postfertilization autophagy of sperm organelles prevents paternal mitochondrial DNA transmission." *Science* **334**(6059): 1144-1147.
- Albrecht, J. and M. D. Norenberg (2006). "Glutamine: a Trojan horse in ammonia neurotoxicity." *Hepatology* **44**(4): 788-794.
- Anand, R., V. Strecker, J. Urbach, I. Wittig and A. S. Reichert (2016). "Mic13 Is Essential for Formation of Crista Junctions in Mammalian Cells." *PLoS One* **11**(8): e0160258.
- Aoi, W. and Y. Marunaka (2014). "Importance of pH homeostasis in metabolic health and diseases: crucial role of membrane proton transport." *Biomed Res Int* **2014**: 598986.
- Aoki, Y., T. Kanki, Y. Hirota, Y. Kurihara, T. Saigusa, T. Uchiumi and D. Kang (2011). "Phosphorylation of Serine 114 on Atg32 mediates mitophagy." *Mol Biol Cell* **22**(17): 3206-3217.
- Araki, Y., W. C. Ku, M. Akioka, A. I. May, Y. Hayashi, F. Arisaka, Y. Ishihama and Y. Ohsumi (2013). "Atg38 is required for autophagy-specific phosphatidylinositol 3-kinase complex integrity." *J Cell Biol* **203**(2): 299-313.
- Ashford, T. P. and K. R. Porter (1962). "Cytoplasmic components in hepatic cell lysosomes." *J Cell Biol* **12**: 198-202.
- Ashrafi, G. and T. L. Schwarz (2013). "The pathways of mitophagy for quality control and clearance of mitochondria." *Cell Death Differ* **20**(1): 31-42.
- Atluri, D. K., M. Asgeri and K. D. Mullen (2010). "Reversibility of hepatic encephalopathy after liver transplantation." *Metab Brain Dis* **25**(1): 111-113.
- B'Chir, W., A. C. Maurin, V. Carraro, J. Averous, C. Jousse, Y. Muranishi, L. Parry, G. Stepien, P. Fournoux and A. Bruhat (2013). "The eIF2alpha/ATF4 pathway is essential for stress-induced autophagy gene expression." *Nucleic Acids Res* **41**(16): 7683-7699.
- Bai, G., K. V. Rama Rao, C. R. Murthy, K. S. Panickar, A. R. Jayakumar and M. D. Norenberg (2001). "Ammonia induces the mitochondrial permeability transition in primary cultures of rat astrocytes." *J Neurosci Res* **66**(5): 981-991.
- Baker, B. M. and C. M. Haynes (2011). "Mitochondrial protein quality control during biogenesis and aging." *Trends Biochem Sci* **36**(5): 254-261.
- Bakker, W. J., I. S. Harris and T. W. Mak (2007). "FOXO3a is activated in response to hypoxic stress and inhibits HIF1-induced apoptosis via regulation of CITED2." *Mol Cell* **28**(6): 941-953.
- Bartolic, M., A. Vovk and D. Suput (2016). "Effects of NH4CL application and removal on astrocytes and endothelial cells." *Cell Mol Biol Lett* **21**: 13.
- Battaglia, G., M. G. Farrace, P. G. Mastroberardino, I. Viti, G. M. Fimia, J. Van Beeumen, B. Devreese, G. Melino, G.

- Molinaro, C. L. Busceti, F. Biagioni, F. Nicoletti and M. Piacentini (2007). "Transglutaminase 2 ablation leads to defective function of mitochondrial respiratory complex I affecting neuronal vulnerability in experimental models of extrapyramidal disorders." *J Neurochem* **100**(1): 36-49.
- Bellot, G., R. Garcia-Medina, P. Gounon, J. Chiche, D. Roux, J. Pouyssegur and N. M. Mazure (2009). "Hypoxia-induced autophagy is mediated through hypoxia-inducible factor induction of BNIP3 and BNIP3L via their BH3 domains." *Mol Cell Biol* **29**(10): 2570-2581.
- Bhujabal, Z., A. B. Birgisdottir, E. Sjøttem, H. B. Brenne, A. Overvatn, S. Habisov, V. Kirkin, T. Lamark and T. Johansen (2017). "FKBP8 recruits LC3A to mediate Parkin-independent mitophagy." *EMBO Rep.*
- Bingol, B., J. S. Tea, L. Phu, M. Reichelt, C. E. Bakalarski, Q. Song, O. Foreman, D. S. Kirkpatrick and M. Sheng (2014). "The mitochondrial deubiquitinase USP30 opposes parkin-mediated mitophagy." *Nature* **510**(7505): 370-375.
- Birky, C. W., Jr. (1995). "Uniparental inheritance of mitochondrial and chloroplast genes: mechanisms and evolution." *Proc Natl Acad Sci U S A* **92**(25): 11331-11338.
- Birnboim, H. C. and J. Doly (1979). "A rapid alkaline extraction procedure for screening recombinant plasmid DNA." *Nucleic Acids Res* **7**(6): 1513-1523.
- Boer, L. A., J. P. Panatto, D. A. Fagundes, C. Bassani, I. C. Jeremias, J. F. Daufenbach, G. T. Rezin, L. Constantino, F. Dal-Pizzol and E. L. Streck (2009). "Inhibition of mitochondrial respiratory chain in the brain of rats after hepatic failure induced by carbon tetrachloride is reversed by antioxidants." *Brain Res Bull* **80**(1-2): 75-78.
- Boland, M. L., A. H. Chourasia and K. F. Macleod (2013). "Mitochondrial Dysfunction in Cancer." *Front Oncol* **3**: 292.
- Booher, J. and M. Sensenbrenner (1972). "Growth and cultivation of dissociated neurons and glial cells from embryonic chick, rat and human brain in flask cultures." *Neurobiology* **2**(3): 97-105.
- Boore, J. L. (1999). "Animal mitochondrial genomes." *Nucleic Acids Res* **27**(8): 1767-1780.
- Boyarsky, G., B. Ransom, W. R. Schlue, M. B. Davis and W. F. Boron (1993). "Intracellular pH regulation in single cultured astrocytes from rat forebrain." *Glia* **8**(4): 241-248.
- Buchan, J. R., R. M. Kolaitis, J. P. Taylor and R. Parker (2013). "Eukaryotic stress granules are cleared by autophagy and Cdc48/VCP function." *Cell* **153**(7): 1461-1474.
- Burman, C. and N. T. Ktistakis (2010). "Regulation of autophagy by phosphatidylinositol 3-phosphate." *FEBS Lett* **584**(7): 1302-1312.
- Busch, G. L., H. Wiesinger, E. Gulbins, H. J. Wagner, B. Hamprecht and F. Lang (1996). "Effect of astroglial cell swelling on pH of acidic intracellular compartments." *Biochim Biophys Acta* **1285**(2): 212-218.
- Butterworth, R. F. (2002). "Pathophysiology of hepatic encephalopathy: a new look at ammonia." *Metab Brain Dis* **17**(4): 221-227.
- Cannavino, J., L. Brocca, M. Sandri, B. Grassi, R. Bottinelli and M. A. Pellegrino (2015). "The role of alterations in mitochondrial dynamics and PGC-1alpha over-expression in fast muscle atrophy following hindlimb unloading." *J Physiol* **593**(8): 1981-1995.
- Canto, C. and J. Auwerx (2009). "PGC-1alpha, SIRT1 and AMPK, an energy sensing network that controls energy expenditure." *Curr Opin Lipidol* **20**(2): 98-105.
- Cao, J. and W. Huang (2016). "Compensatory Increase of Transglutaminase 2 Is Responsible for Resistance to mTOR Inhibitor Treatment." *PLoS One* **11**(2): e0149388.
- Cebollero, E., F. Reggiori and C. Kraft (2012). "Reticulophagy and ribophagy: regulated degradation of protein production factories." *Int J Cell Biol* **2012**: 182834.
- Cereghetti, G. M., A. Stangherlin, O. Martins de Brito, C. R. Chang, C. Blackstone, P. Bernardi and L. Scorrano (2008). "Dephosphorylation by calcineurin regulates translocation of Drp1 to mitochondria." *Proc Natl Acad Sci U S A* **105**(41): 15803-15808.

- Chen, G., Z. Han, D. Feng, Y. Chen, L. Chen, H. Wu, L. Huang, C. Zhou, X. Cai, C. Fu, L. Duan, X. Wang, L. Liu, X. Liu, Y. Shen, Y. Zhu and Q. Chen (2014). "A regulatory signaling loop comprising the PGAM5 phosphatase and CK2 controls receptor-mediated mitophagy." *Mol Cell* **54**(3): 362-377.
- Chen, Z., L. Liu, Q. Cheng, Y. Li, H. Wu, W. Zhang, Y. Wang, S. A. Sehgal, S. Siraj, X. Wang, J. Wang, Y. Zhu and Q. Chen (2017). "Mitochondrial E3 ligase MARCH5 regulates FUNDC1 to fine-tune hypoxic mitophagy." *EMBO Rep* **18**(3): 495-509.
- Chu, C. T., H. Bayir and V. E. Kagan (2014). "LC3 binds externalized cardiolipin on injured mitochondria to signal mitophagy in neurons: implications for Parkinson disease." *Autophagy* **10**(2): 376-378.
- Chu, C. T., J. Ji, R. K. Dagda, J. F. Jiang, Y. Y. Tyurina, A. A. Kapralov, V. A. Tyurin, N. Yanamala, I. H. Shrivastava, D. Mohammadyani, K. Z. Qiang Wang, J. Zhu, J. Klein-Seetharaman, K. Balasubramanian, A. A. Amoscato, G. Borisenko, Z. Huang, A. M. Gusdon, A. Cheikhi, E. K. Steer, R. Wang, C. Baty, S. Watkins, I. Bahar, H. Bayir and V. E. Kagan (2013). "Cardiolipin externalization to the outer mitochondrial membrane acts as an elimination signal for mitophagy in neuronal cells." *Nat Cell Biol* **15**(10): 1197-1205.
- Cipolat, S., T. Rudka, D. Hartmann, V. Costa, L. Serneels, K. Craessaerts, K. Metzger, C. Frezza, W. Annaert, L. D'Adamo, C. Derks, T. Dejaegere, L. Pellegrini, R. D'Hooge, L. Scorrano and B. De Strooper (2006). "Mitochondrial rhomboid PARL regulates cytochrome c release during apoptosis via OPA1-dependent cristae remodeling." *Cell* **126**(1): 163-175.
- Cohen-Kaplan, V., I. Livneh, N. Avni, B. Fabre, T. Ziv, Y. T. Kwon and A. Ciechanover (2016). "p62- and ubiquitin-dependent stress-induced autophagy of the mammalian 26S proteasome." *Proc Natl Acad Sci U S A* **113**(47): E7490-E7499.
- Cooper, A. J. and T. M. Jeitner (2016). "Central Role of Glutamate Metabolism in the Maintenance of Nitrogen Homeostasis in Normal and Hyperammonemic Brain." *Biomolecules* **6**(2).
- Cui, M., X. Tang, W. V. Christian, Y. Yoon and K. Tieu (2010). "Perturbations in mitochondrial dynamics induced by human mutant PINK1 can be rescued by the mitochondrial division inhibitor mdivi-1." *J Biol Chem* **285**(15): 11740-11752.
- Czaja, M. J., W. X. Ding, T. M. Donohue, Jr., S. L. Friedman, J. S. Kim, M. Komatsu, J. J. Lemasters, A. Lemoine, J. D. Lin, J. H. Ou, D. H. Perlmutter, G. Randall, R. B. Ray, A. Tsung and X. M. Yin (2013). "Functions of autophagy in normal and diseased liver." *Autophagy* **9**(8): 1131-1158.
- D'Eletto, M., M. G. Farrace, L. Falasca, V. Reali, S. Oliverio, G. Melino, M. Griffin, G. M. Fimia and M. Piacentini (2009). "Transglutaminase 2 is involved in autophagosome maturation." *Autophagy* **5**(8): 1145-1154.
- De Duve, C. and R. Wattiaux (1966). "Functions of lysosomes." *Annu Rev Physiol* **28**: 435-492.
- Deffieu, M., I. Bhatia-Kissova, B. Salin, A. Galinier, S. Manon and N. Camougrand (2009). "Glutathione participates in the regulation of mitophagy in yeast." *J Biol Chem* **284**(22): 14828-14837.
- Deosaran, E., K. B. Larsen, R. Hua, G. Sargent, Y. Wang, S. Kim, T. Lamark, M. Jauregui, K. Law, J. Lippincott-Schwartz, A. Brech, T. Johansen and P. K. Kim (2013). "NBR1 acts as an autophagy receptor for peroxisomes." *J Cell Sci* **126**(Pt 4): 939-952.
- Deretic, V., T. Saitoh and S. Akira (2013). "Autophagy in infection, inflammation and immunity." *Nat Rev Immunol* **13**(10): 722-737.
- Dhanda, S., A. Sunkaria, A. Halder and R. Sandhir (2018). "Mitochondrial dysfunctions contribute to energy deficits in rodent model of hepatic encephalopathy." *Metab Brain Dis* **33**(1): 209-223.
- Ding, W. X., H. M. Ni, M. Li, Y. Liao, X. Chen, D. B. Stolz, G. W. Dorn, 2nd and X. M. Yin (2010). "Nix is critical to two distinct phases of mitophagy, reactive oxygen species-mediated autophagy induction and Parkin-ubiquitin-p62-mediated mitochondrial priming." *J Biol Chem* **285**(36): 27879-27890.
- Drewes, L. R. and R. L. Leino (1985). "Neuron-specific mitochondrial degeneration induced by hyperammonemia

- and octanoic acidemia." *Brain Res* **340**(2): 211-218.
- Duvezin-Caubet, S., M. Koppen, J. Wagener, M. Zick, L. Israel, A. Bernacchia, R. Jagasia, E. I. Rugarli, A. Imhof, W. Neupert, T. Langer and A. S. Reichert (2007). "OPA1 processing reconstituted in yeast depends on the subunit composition of the m-AAA protease in mitochondria." *Mol Biol Cell* **18**(9): 3582-3590.
- Escobar-Henriques, M. and T. Langer (2014). "Dynamic survey of mitochondria by ubiquitin." *EMBO Rep* **15**(3): 231-243.
- Farre, J. C., A. Burkenroad, S. F. Burnett and S. Subramani (2013). "Phosphorylation of mitophagy and pexophagy receptors coordinates their interaction with Atg8 and Atg11." *EMBO Rep* **14**(5): 441-449.
- Farre, J. C., R. Manjithaya, R. D. Mathewson and S. Subramani (2008). "PpAtg30 tags peroxisomes for turnover by selective autophagy." *Dev Cell* **14**(3): 365-376.
- Feng, J. F., K. M. Zhang, J. Y. Jiang, G. Y. Gao, X. Fu and Y. M. Liang (2010). "Effect of therapeutic mild hypothermia on the genomics of the hippocampus after moderate traumatic brain injury in rats." *Neurosurgery* **67**(3): 730-742.
- Feng, Y., Z. Yao and D. J. Klionsky (2015). "How to control self-digestion: transcriptional, post-transcriptional, and post-translational regulation of autophagy." *Trends Cell Biol* **25**(6): 354-363.
- Fiesel, F. C., E. L. Moussaud-Lamodiere, M. Ando and W. Springer (2014). "A specific subset of E2 ubiquitin-conjugating enzymes regulate Parkin activation and mitophagy differently." *J Cell Sci* **127**(Pt 16): 3488-3504.
- Finsterer, J. and M. Frank (2013). "Haematological features in Barth syndrome." *Current Opinion in Hematology* **20**(1): 36-40.
- Folts, C. J., N. Scott-Hewitt, C. Proschel, M. Mayer-Proschel and M. Noble (2016). "Lysosomal Re-acidification Prevents Lysosphingolipid-Induced Lysosomal Impairment and Cellular Toxicity." *PLoS Biol* **14**(12): e1002583.
- Frank, M., S. Duvezin-Caubet, S. Koob, A. Occhipinti, R. Jagasia, A. Petcherski, M. O. Ruonala, M. Priault, B. Salin and A. S. Reichert (2012). "Mitophagy is triggered by mild oxidative stress in a mitochondrial fission dependent manner." *Biochim Biophys Acta* **1823**(12): 2297-2310.
- Fu, M., P. St-Pierre, J. Shankar, P. T. Wang, B. Joshi and I. R. Nabi (2013). "Regulation of mitophagy by the Gp78 E3 ubiquitin ligase." *Mol Biol Cell* **24**(8): 1153-1162.
- Gao, M., P. Monian, Q. Pan, W. Zhang, J. Xiang and X. Jiang (2016). "Ferroptosis is an autophagic cell death process." *Cell Res* **26**(9): 1021-1032.
- Gaspard, G. J. and C. R. McMaster (2015). "The mitochondrial quality control protein Yme1 is necessary to prevent defective mitophagy in a yeast model of Barth syndrome." *J Biol Chem* **290**(14): 9284-9298.
- Geisler, S., K. M. Holmstrom, D. Skujat, F. C. Fiesel, O. C. Rothfuss, P. J. Kahle and W. Springer (2010). "PINK1/Parkin-mediated mitophagy is dependent on VDAC1 and p62/SQSTM1." *Nat Cell Biol* **12**(2): 119-131.
- Gerbitz, K. D., J. M. van den Ouweland, J. A. Maassen and M. Jaksch (1995). "Mitochondrial diabetes mellitus: a review." *Biochim Biophys Acta* **1271**(1): 253-260.
- Giatakis, C. and V. Papadopoulos (2004). "Differential utilization of the promoter of peripheral-type benzodiazepine receptor by steroidogenic versus nonsteroidogenic cell lines and the role of Sp1 and Sp3 in the regulation of basal activity." *Endocrinology* **145**(3): 1113-1123.
- Gilkerson, R. W., R. L. De Vries, P. Lebot, J. D. Wikstrom, E. Torgykes, O. S. Shirihai, S. Przedborski and E. A. Schon (2012). "Mitochondrial autophagy in cells with mtDNA mutations results from synergistic loss of transmembrane potential and mTORC1 inhibition." *Hum Mol Genet* **21**(5): 978-990.
- Gomez-Sanchez, J. A., L. Carty, M. Iruarrizaga-Lejarreta, M. Palomo-Irigoyen, M. Varela-Rey, M. Griffith, J. Hantke, N. Macias-Camara, M. Azkargorta, I. Aurrekoetxea, V. G. De Juan, H. B. Jefferies, P. Aspichueta, F. Elortza, A. M. Aransay, M. L. Martinez-Chantar, F. Baas, J. M. Mato, R. Mirsky, A. Woodhoo and K. R. Jessen (2015). "Schwann cell autophagy, myelinophagy, initiates myelin clearance from injured nerves." *J Cell Biol* **210**(1): 153-168.
- Görg, B., H. J. Bidmon and D. Häussinger (2013). "Gene expression profiling in the cerebral cortex of patients with

- cirrhosis with and without hepatic encephalopathy." *Hepatology* **57**(6): 2436-2447.
- Görg, B., A. Karababa, A. Shafiqullina, H. J. Bidmon and D. Häussinger (2015). "Ammonia-induced senescence in cultured rat astrocytes and in human cerebral cortex in hepatic encephalopathy." *Glia* **63**(1): 37-50.
- Görg, B., N. Qvartskhava, V. Keitel, H. J. Bidmon, O. Selbach, F. Schliess and D. Häussinger (2008). "Ammonia induces RNA oxidation in cultured astrocytes and brain in vivo." *Hepatology* **48**(2): 567-579.
- Görg, B., F. Schliess and D. Häussinger (2013). "Osmotic and oxidative/nitrosative stress in ammonia toxicity and hepatic encephalopathy." *Arch Biochem Biophys* **536**(2): 158-163.
- Grasso, D., A. Ropolo, A. Lo Re, V. Boggio, M. I. Molejon, J. L. Iovanna, C. D. Gonzalez, R. Urrutia and M. I. Vaccaro (2011). "Zymophagy, a novel selective autophagy pathway mediated by VMP1-USP9x-p62, prevents pancreatic cell death." *J Biol Chem* **286**(10): 8308-8324.
- Griparic, L., T. Kanazawa and A. M. van der Bliek (2007). "Regulation of the mitochondrial dynamin-like protein Opa1 by proteolytic cleavage." *J Cell Biol* **178**(5): 757-764.
- Guo, H., M. Chitiprolu, D. Gagnon, L. Meng, C. Perez-Iratxeta, D. Lagace and D. Gibbins (2014). "Autophagy supports genomic stability by degrading retrotransposon RNA." *Nat Commun* **5**: 5276.
- Ha, H. C. and S. H. Snyder (1999). "Poly(ADP-ribose) polymerase is a mediator of necrotic cell death by ATP depletion." *Proc Natl Acad Sci U S A* **96**(24): 13978-13982.
- Hara, T. and N. Mizushima (2009). "Role of ULK-FIP200 complex in mammalian autophagy: FIP200, a counterpart of yeast Atg17?" *Autophagy* **5**(1): 85-87.
- Hasson, S. A., L. A. Kane, K. Yamano, C. H. Huang, D. A. Sliter, E. Buehler, C. Wang, S. M. Heman-Ackah, T. Hessa, R. Guha, S. E. Martin and R. J. Youle (2013). "High-content genome-wide RNAi screens identify regulators of parkin upstream of mitophagy." *Nature* **504**(7479): 291-295.
- Häussinger, D. and B. Görg (2010). "Interaction of oxidative stress, astrocyte swelling and cerebral ammonia toxicity." *Curr Opin Clin Nutr Metab Care* **13**(1): 87-92.
- Häussinger, D., J. Laubenberger, S. vom Dahl, T. Ernst, S. Bayer, M. Langer, W. Gerok and J. Hennig (1994). "Proton magnetic resonance spectroscopy studies on human brain myo-inositol in hypo-osmolarity and hepatic encephalopathy." *Gastroenterology* **107**(5): 1475-1480.
- Häussinger, D. and F. Schliess (2008). "Pathogenetic mechanisms of hepatic encephalopathy." *Gut* **57**(8): 1156-1165.
- Häussinger, D. and H. Sies (2013). "Hepatic encephalopathy: clinical aspects and pathogenetic concept." *Arch Biochem Biophys* **536**(2): 97-100.
- Heitman, J., N. R. Movva and M. N. Hall (1991). "Targets for cell cycle arrest by the immunosuppressant rapamycin in yeast." *Science* **253**(5022): 905-909.
- Hirota, Y., D. Kang and T. Kanki (2012). "The physiological role of mitophagy: new insights into phosphorylation events." *Int J Cell Biol* **2012**: 354914.
- Hoppins, S., L. Lackner and J. Nunnari (2007). "The machines that divide and fuse mitochondria." *Annu Rev Biochem* **76**: 751-780.
- Hosokawa, N., T. Hara, T. Kaizuka, C. Kishi, A. Takamura, Y. Miura, S. Iemura, T. Natsume, K. Takehana, N. Yamada, J. L. Guan, N. Oshiro and N. Mizushima (2009). "Nutrient-dependent mTORC1 association with the ULK1-Atg13-FIP200 complex required for autophagy." *Mol Biol Cell* **20**(7): 1981-1991.
- Huxtable, R. J. (1992). "Physiological actions of taurine." *Physiol Rev* **72**(1): 101-163.
- Itakura, E., C. Kishi, K. Inoue and N. Mizushima (2008). "Beclin 1 forms two distinct phosphatidylinositol 3-kinase complexes with mammalian Atg14 and UVRAG." *Mol Biol Cell* **19**(12): 5360-5372.
- Ito, T., N. Yoshikawa, T. Inui, N. Miyazaki, S. W. Schaffer and J. Azuma (2014). "Tissue depletion of taurine accelerates skeletal muscle senescence and leads to early death in mice." *PLoS One* **9**(9): e107409.

- Jayakumar, A. R., M. Liu, M. Moriyama, R. Ramakrishnan, B. Forbush, 3rd, P. V. Reddy and M. D. Norenberg (2008). "Na-K-Cl Cotransporter-1 in the mechanism of ammonia-induced astrocyte swelling." *J Biol Chem* **283**(49): 33874-33882.
- Jayakumar, A. R., K. V. Rama Rao, A. Schousboe and M. D. Norenberg (2004). "Glutamine-induced free radical production in cultured astrocytes." *Glia* **46**(3): 296-301.
- Jeninga, E. H., K. Schoonjans and J. Auwerx (2010). "Reversible acetylation of PGC-1: connecting energy sensors and effectors to guarantee metabolic flexibility." *Oncogene* **29**(33): 4617-4624.
- Jiang, S., C. D. Wells and P. J. Roach (2011). "Starch-binding domain-containing protein 1 (Stbd1) and glycogen metabolism: Identification of the Atg8 family interacting motif (AIM) in Stbd1 required for interaction with GABARAPL1." *Biochem Biophys Res Commun* **413**(3): 420-425.
- Jiang, X. and X. Wang (2004). "Cytochrome C-mediated apoptosis." *Annu Rev Biochem* **73**: 87-106.
- Jin, S. M., M. Lazarou, C. Wang, L. A. Kane, D. P. Narendra and R. J. Youle (2010). "Mitochondrial membrane potential regulates PINK1 import and proteolytic destabilization by PARL." *J Cell Biol* **191**(5): 933-942.
- Jung, C. H., C. B. Jun, S. H. Ro, Y. M. Kim, N. M. Otto, J. Cao, M. Kundu and D. H. Kim (2009). "ULK-Atg13-FIP200 complexes mediate mTOR signaling to the autophagy machinery." *Mol Biol Cell* **20**(7): 1992-2003.
- Kabeya, Y., N. Mizushima, T. Ueno, A. Yamamoto, T. Kirisako, T. Noda, E. Kominami, Y. Ohsumi and T. Yoshimori (2000). "LC3, a mammalian homologue of yeast Apg8p, is localized in autophagosome membranes after processing." *EMBO J* **19**(21): 5720-5728.
- Kane, L. A., M. Lazarou, A. I. Fogel, Y. Li, K. Yamano, S. A. Sarraf, S. Banerjee and R. J. Youle (2014). "PINK1 phosphorylates ubiquitin to activate Parkin E3 ubiquitin ligase activity." *J Cell Biol* **205**(2): 143-153.
- Kanki, T. and D. J. Klionsky (2008). "Mitophagy in yeast occurs through a selective mechanism." *J Biol Chem* **283**(47): 32386-32393.
- Kanki, T., Y. Kurihara, X. Jin, T. Goda, Y. Ono, M. Aihara, Y. Hirota, T. Saigusa, Y. Aoki, T. Uchiumi and D. Kang (2013). "Casein kinase 2 is essential for mitophagy." *EMBO Rep* **14**(9): 788-794.
- Kanki, T., K. Wang, M. Baba, C. R. Bartholomew, M. A. Lynch-Day, Z. Du, J. Geng, K. Mao, Z. Yang, W. L. Yen and D. J. Klionsky (2009). "A genomic screen for yeast mutants defective in selective mitochondria autophagy." *Mol Biol Cell* **20**(22): 4730-4738.
- Kanki, T., K. Wang, Y. Cao, M. Baba and D. J. Klionsky (2009). "Atg32 is a mitochondrial protein that confers selectivity during mitophagy." *Dev Cell* **17**(1): 98-109.
- Kappler, M., H. Taubert, J. Schubert, D. Vordermark and A. W. Eckert (2012). "The real face of HIF1alpha in the tumor process." *Cell Cycle* **11**(21): 3932-3936.
- Karababa, A., B. Görg, F. Schliess and D. Häussinger (2014). "O-GlcNAcylation as a novel ammonia-induced posttranslational protein modification in cultured rat astrocytes." *Metab Brain Dis* **29**(4): 975-982.
- Karababa, A., K. Groos-Sahr, U. Albrecht, V. Keitel, A. Shafiqullina, B. Görg and D. Häussinger (2017). "Ammonia Attenuates LPS-Induced Upregulation of Pro-Inflammatory Cytokine mRNA in Co-Cultured Astrocytes and Microglia." *Neurochem Res* **42**(3): 737-749.
- Karbowsky, M. and R. J. Youle (2011). "Regulating mitochondrial outer membrane proteins by ubiquitination and proteasomal degradation." *Curr Opin Cell Biol* **23**(4): 476-482.
- Kaushik, S. and A. M. Cuervo (2012). "Chaperone-mediated autophagy: a unique way to enter the lysosome world." *Trends Cell Biol* **22**(8): 407-417.
- Keitel, V., B. Görg, H. J. Bidmon, I. Zemtsova, L. Spomer, K. Zilles and D. Häussinger (2010). "The bile acid receptor TGR5 (Gpbar-1) acts as a neurosteroid receptor in brain." *Glia* **58**(15): 1794-1805.
- Kelly, T., K. W. Kafitz, C. Roderigo and C. R. Rose (2009). "Ammonium-evoked alterations in intracellular sodium and pH reduce glial glutamate transport activity." *Glia* **57**(9): 921-934.

- Khaminets, A., C. Behl and I. Dikic (2016). "Ubiquitin-Dependent And Independent Signals In Selective Autophagy." *Trends Cell Biol* **26**(1): 6-16.
- Khaminets, A., T. Heinrich, M. Mari, P. Grumati, A. K. Huebner, M. Akutsu, L. Liebmann, A. Stolz, S. Nietzsche, N. Koch, M. Mauthe, I. Katona, B. Qualmann, J. Weis, F. Reggiori, I. Kurth, C. A. Hubner and I. Dikic (2015). "Regulation of endoplasmic reticulum turnover by selective autophagy." *Nature* **522**(7556): 354-358.
- Kim, J., M. Kundu, B. Viollet and K. L. Guan (2011). "AMPK and mTOR regulate autophagy through direct phosphorylation of Ulk1." *Nat Cell Biol* **13**(2): 132-141.
- Kim, J. Y., H. Zhao, J. Martinez, T. A. Doggett, A. V. Kolesnikov, P. H. Tang, Z. Ablonczy, C. C. Chan, Z. Zhou, D. R. Green and T. A. Ferguson (2013). "Noncanonical autophagy promotes the visual cycle." *Cell* **154**(2): 365-376.
- Kim, Y., J. Park, S. Kim, S. Song, S. K. Kwon, S. H. Lee, T. Kitada, J. M. Kim and J. Chung (2008). "PINK1 controls mitochondrial localization of Parkin through direct phosphorylation." *Biochem Biophys Res Commun* **377**(3): 975-980.
- Kircheis, G., A. Knoche, N. Hilger, F. Manhart, A. Schnitzler, H. Schulze and D. Häussinger (2009). "Hepatic encephalopathy and fitness to drive." *Gastroenterology* **137**(5): 1706-1715 e1701-1709.
- Kissova, I., M. Deffieu, S. Manon and N. Camougrand (2004). "Uth1p is involved in the autophagic degradation of mitochondria." *J Biol Chem* **279**(37): 39068-39074.
- Kissova, I., B. Salin, J. Schaeffer, S. Bhatia, S. Manon and N. Camougrand (2007). "Selective and non-selective autophagic degradation of mitochondria in yeast." *Autophagy* **3**(4): 329-336.
- Knott, A. B., G. Perkins, R. Schwarzenbacher and E. Bossy-Wetzel (2008). "Mitochondrial fragmentation in neurodegeneration." *Nat Rev Neurosci* **9**(7): 505-518.
- Koike, M., M. Shibata, S. Waguri, K. Yoshimura, I. Tanida, E. Kominami, T. Gotow, C. Peters, K. von Figura, N. Mizushima, P. Saftig and Y. Uchiyama (2005). "Participation of autophagy in storage of lysosomes in neurons from mouse models of neuronal ceroid-lipofuscinoses (Batten disease)." *Am J Pathol* **167**(6): 1713-1728.
- Komatsu, M., E. Kominami and K. Tanaka (2006). "Autophagy and neurodegeneration." *Autophagy* **2**(4): 315-317.
- Kondo-Okamoto, N., N. N. Noda, S. W. Suzuki, H. Nakatogawa, I. Takahashi, M. Matsunami, A. Hashimoto, F. Inagaki, Y. Ohsumi and K. Okamoto (2012). "Autophagy-related protein 32 acts as autophagic degron and directly initiates mitophagy." *J Biol Chem* **287**(13): 10631-10638.
- Koyano, F., K. Okatsu, H. Kosako, Y. Tamura, E. Go, M. Kimura, Y. Kimura, H. Tsuchiya, H. Yoshihara, T. Hirokawa, T. Endo, E. A. Fon, J. F. Trempe, Y. Saeki, K. Tanaka and N. Matsuda (2014). "Ubiquitin is phosphorylated by PINK1 to activate parkin." *Nature* **510**(7503): 162-166.
- Kraft, C., A. Deplazes, M. Sohrmann and M. Peter (2008). "Mature ribosomes are selectively degraded upon starvation by an autophagy pathway requiring the Ubp3p/Bre5p ubiquitin protease." *Nat Cell Biol* **10**(5): 602-610.
- Kruczek, C., B. Görg, V. Keitel, E. Pirev, K. D. Kroncke, F. Schliess and D. Häussinger (2009). "Hypoosmotic swelling affects zinc homeostasis in cultured rat astrocytes." *Glia* **57**(1): 79-92.
- Kumar, S. and K. Mehta (2012). "Tissue transglutaminase constitutively activates HIF-1alpha promoter and nuclear factor-kappaB via a non-canonical pathway." *PLoS One* **7**(11): e49321.
- Kuo, T. C., C. T. Chen, D. Baron, T. T. Onder, S. Loewer, S. Almeida, C. M. Weismann, P. Xu, J. M. Houghton, F. B. Gao, G. Q. Daley and S. Doxsey (2011). "Midbody accumulation through evasion of autophagy contributes to cellular reprogramming and tumorigenicity." *Nat Cell Biol* **13**(10): 1214-1223.
- Lachmann, V., B. Görg, H. J. Bidmon, V. Keitel and D. Häussinger (2013). "Precipitants of hepatic encephalopathy induce rapid astrocyte swelling in an oxidative stress dependent manner." *Arch Biochem Biophys* **536**(2): 143-151.
- Lai, T. S. and C. S. Greenberg (2013). "TGM2 and implications for human disease: role of alternative splicing." *Front Biosci (Landmark Ed)* **18**: 504-519.
- Lamb, C. A., S. Nuhlen, D. Judith, D. Frith, A. P. Snijders, C. Behrends and S. A. Tooze (2016). "TBC1D14 regulates

- autophagy via the TRAPP complex and ATG9 traffic." *EMBO J* **35**(3): 281-301.
- Lane, N. and W. Martin (2010). "The energetics of genome complexity." *Nature* **467**(7318): 929-934.
- Lazarou, M. (2015). "Keeping the immune system in check: a role for mitophagy." *Immunol Cell Biol* **93**(1): 3-10.
- Lazarou, M., D. A. Sliter, L. A. Kane, S. A. Sarraf, C. Wang, J. L. Burman, D. P. Sideris, A. I. Fogel and R. J. Youle (2015). "The ubiquitin kinase PINK1 recruits autophagy receptors to induce mitophagy." *Nature* **524**(7565): 309-314.
- Leadsham, J. E., K. Miller, K. R. Ayscough, S. Colombo, E. Martegani, P. Sudbery and C. W. Gourlay (2009). "Whi2p links nutritional sensing to actin-dependent Ras-cAMP-PKA regulation and apoptosis in yeast." *J Cell Sci* **122**(Pt 5): 706-715.
- Lee, I. H. and T. Finkel (2009). "Regulation of autophagy by the p300 acetyltransferase." *J Biol Chem* **284**(10): 6322-6328.
- Lee, J. Y., Y. Nagano, J. P. Taylor, K. L. Lim and T. P. Yao (2010). "Disease-causing mutations in parkin impair mitochondrial ubiquitination, aggregation, and HDAC6-dependent mitophagy." *J Cell Biol* **189**(4): 671-679.
- Lemasters, J. J. (2005). "Selective mitochondrial autophagy, or mitophagy, as a targeted defense against oxidative stress, mitochondrial dysfunction, and aging." *Rejuvenation Res* **8**(1): 3-5.
- Li, Z., X. Ji, W. Wang, J. Liu, X. Liang, H. Wu, J. Liu, U. S. Eggert, Q. Liu and X. Zhang (2016). "Ammonia Induces Autophagy through Dopamine Receptor D3 and MTOR." *PLoS One* **11**(4): e0153526.
- Lill, R. and G. Kispal (2000). "Maturation of cellular Fe-S proteins: an essential function of mitochondria." *Trends Biochem Sci* **25**(8): 352-356.
- Liu, L., D. Feng, G. Chen, M. Chen, Q. Zheng, P. Song, Q. Ma, C. Zhu, R. Wang, W. Qi, L. Huang, P. Xue, B. Li, X. Wang, H. Jin, J. Wang, F. Yang, P. Liu, Y. Zhu, S. Sui and Q. Chen (2012). "Mitochondrial outer-membrane protein FUNDC1 mediates hypoxia-induced mitophagy in mammalian cells." *Nat Cell Biol* **14**(2): 177-185.
- Liu, Z., P. Chen, H. Gao, Y. Gu, J. Yang, H. Peng, X. Xu, H. Wang, M. Yang, X. Liu, L. Fan, S. Chen, J. Zhou, Y. Sun, K. Ruan, S. Cheng, M. Komatsu, E. White, L. Li, H. Ji, D. Finley and R. Hu (2014). "Ubiquitylation of autophagy receptor Optineurin by HACE1 activates selective autophagy for tumor suppression." *Cancer Cell* **26**(1): 106-120.
- Llansola, M., H. Ahabrach, M. Errami, A. Cabrera-Pastor, K. Addaoudi and V. Felipo (2013). "Impaired release of corticosterone from adrenals contributes to impairment of circadian rhythms of activity in hyperammonemic rats." *Arch Biochem Biophys* **536**(2): 164-170.
- Loson, O. C., Z. Song, H. Chen and D. C. Chan (2013). "Fis1, Mff, MiD49, and MiD51 mediate Drp1 recruitment in mitochondrial fission." *Mol Biol Cell* **24**(5): 659-667.
- Lu, H., G. Li, L. Liu, L. Feng, X. Wang and H. Jin (2013). "Regulation and function of mitophagy in development and cancer." *Autophagy* **9**(11): 1720-1736.
- Lu, K., M. Han, H. L. Ting, Z. Liu and D. Zhang (2013). "Scutellarin from *Scutellaria baicalensis* suppresses adipogenesis by upregulating PPARalpha in 3T3-L1 cells." *J Nat Prod* **76**(4): 672-678.
- Lu, K., I. Psakhye and S. Jentsch (2014). "Autophagic clearance of polyQ proteins mediated by ubiquitin-Atg8 adaptors of the conserved CUET protein family." *Cell* **158**(3): 549-563.
- Maiuri, M. C., E. Zalckvar, A. Kimchi and G. Kroemer (2007). "Self-eating and self-killing: crosstalk between autophagy and apoptosis." *Nat Rev Mol Cell Biol* **8**(9): 741-752.
- Mancias, J. D., X. Wang, S. P. Gygi, J. W. Harper and A. C. Kimmelman (2014). "Quantitative proteomics identifies NCOA4 as the cargo receptor mediating ferritinophagy." *Nature* **509**(7498): 105-109.
- Mandell, M. A., A. Jain, J. Arko-Mensah, S. Chauhan, T. Kimura, C. Dinkins, G. Silvestri, J. Munch, F. Kirchhoff, A. Simonsen, Y. Wei, B. Levine, T. Johansen and V. Deretic (2014). "TRIM proteins regulate autophagy and can target autophagic substrates by direct recognition." *Dev Cell* **30**(4): 394-409.
- Mannella, C. A., M. Marko and K. Buttle (1997). "Reconsidering mitochondrial structure: new views of an old organelle." *Trends Biochem Sci* **22**(2): 37-38.

- Mao, K., K. Wang, M. Zhao, T. Xu and D. J. Klionsky (2011). "Two MAPK-signaling pathways are required for mitophagy in *Saccharomyces cerevisiae*." *J Cell Biol* **193**(4): 755-767.
- Margulis, L. (1971). "Symbiosis and evolution." *Sci Am* **225**(2): 48-57.
- Marshall, R. S., F. Li, D. C. Gemperline, A. J. Book and R. D. Vierstra (2015). "Autophagic Degradation of the 26S Proteasome Is Mediated by the Dual ATG8/Ubiquitin Receptor RPN10 in *Arabidopsis*." *Mol Cell* **58**(6): 1053-1066.
- Marshall, R. S., F. McLoughlin and R. D. Vierstra (2016). "Autophagic Turnover of Inactive 26S Proteasomes in Yeast Is Directed by the Ubiquitin Receptor Cue5 and the Hsp42 Chaperone." *Cell Rep* **16**(6): 1717-1732.
- Martinez-Hernandez, A., K. P. Bell and M. D. Norenberg (1977). "Glutamine synthetase: glial localization in brain." *Science* **195**(4284): 1356-1358.
- Matilainen, O., P. M. Quiros and J. Auwerx (2017). "Mitochondria and Epigenetics - Crosstalk in Homeostasis and Stress." *Trends Cell Biol*.
- Matsunaga, K., T. Saitoh, K. Tabata, H. Omori, T. Satoh, N. Kurotori, I. Maejima, K. Shirahama-Noda, T. Ichimura, T. Isobe, S. Akira, T. Noda and T. Yoshimori (2009). "Two Beclin 1-binding proteins, Atg14L and Rubicon, reciprocally regulate autophagy at different stages." *Nat Cell Biol* **11**(4): 385-396.
- Matthiessen, H. P., C. Schmalenbach and H. W. Muller (1989). "Astroglia-released neurite growth-inducing activity for embryonic hippocampal neurons is associated with laminin bound in a sulfated complex and free fibronectin." *Glia* **2**(3): 177-188.
- Mayr, J. A., F. A. Zimmermann, C. Fauth, C. Bergheim, D. Meierhofer, D. Radmayr, J. Zschocke, J. Koch and W. Sperl (2011). "Lipoic Acid Synthetase Deficiency Causes Neonatal-Onset Epilepsy, Defective Mitochondrial Energy Metabolism, and Glycine Elevation." *American Journal of Human Genetics* **89**(6): 792-797.
- Mendl, N., A. Occhipinti, M. Müller, P. Wild, I. Dikic and A. S. Reichert (2011). "Mitophagy in yeast is independent of mitochondrial fission and requires the stress response gene WHI2." *J Cell Sci* **124**(Pt 8): 1339-1350.
- Mercer, C. A., A. Kaliappan and P. B. Dennis (2009). "A novel, human Atg13 binding protein, Atg101, interacts with ULK1 and is essential for macroautophagy." *Autophagy* **5**(5): 649-662.
- Mijaljica, D. and R. J. Devenish (2013). "Nucleophagy at a glance." *J Cell Sci* **126**(Pt 19): 4325-4330.
- Mitchell, P. (1961). "Coupling of phosphorylation to electron and hydrogen transfer by a chemi-osmotic type of mechanism." *Nature* **191**: 144-148.
- Mizushima, N., B. Levine, A. M. Cuervo and D. J. Klionsky (2008). "Autophagy fights disease through cellular self-digestion." *Nature* **451**(7182): 1069-1075.
- Mochida, K., Y. Oikawa, Y. Kimura, H. Kirisako, H. Hirano, Y. Ohsumi and H. Nakatogawa (2015). "Receptor-mediated selective autophagy degrades the endoplasmic reticulum and the nucleus." *Nature* **522**(7556): 359-362.
- Mokranjac, D. and W. Neupert (2009). "Thirty years of protein translocation into mitochondria: unexpectedly complex and still puzzling." *Biochim Biophys Acta* **1793**(1): 33-41.
- Motley, A. M., J. M. Nuttall and E. H. Hettema (2012). "Pex3-anchored Atg36 tags peroxisomes for degradation in *Saccharomyces cerevisiae*." *EMBO J* **31**(13): 2852-2868.
- Müller, M., P. Kotter, C. Behrendt, E. Walter, C. Q. Scheckhuber, K. D. Entian and A. S. Reichert (2015). "Synthetic quantitative array technology identifies the Ubp3-Bre5 deubiquitinase complex as a negative regulator of mitophagy." *Cell Rep* **10**(7): 1215-1225.
- Müller, M., K. Lu and A. S. Reichert (2015). "Mitophagy and mitochondrial dynamics in *Saccharomyces cerevisiae*." *Biochim Biophys Acta* **1853**(10 Pt B): 2766-2774.
- Müller, M. and A. S. Reichert (2011). "Mitophagy, mitochondrial dynamics and the general stress response in yeast." *Biochem Soc Trans* **39**(5): 1514-1519.
- Nagaraja, T. N. and N. Brookes (1998). "Intracellular acidification induced by passive and active transport of ammonium ions in astrocytes." *Am J Physiol* **274**(4 Pt 1): C883-891.

- Narendra, D., A. Tanaka, D. F. Suen and R. J. Youle (2008). "Parkin is recruited selectively to impaired mitochondria and promotes their autophagy." *J Cell Biol* **183**(5): 795-803.
- Narendra, D. P., S. M. Jin, A. Tanaka, D. F. Suen, C. A. Gautier, J. Shen, M. R. Cookson and R. J. Youle (2010). "PINK1 is selectively stabilized on impaired mitochondria to activate Parkin." *PLoS Biol* **8**(1): e1000298.
- Neuhaus, E. M. and T. Soldati (2000). "A myosin I is involved in membrane recycling from early endosomes." *J Cell Biol* **150**(5): 1013-1026.
- Neupert, W. (1997). "Protein import into mitochondria." *Annu Rev Biochem* **66**: 863-917.
- Newmeyer, D. D. and S. Ferguson-Miller (2003). "Mitochondria: releasing power for life and unleashing the machineries of death." *Cell* **112**(4): 481-490.
- Ni, H. M., J. A. Williams and W. X. Ding (2015). "Mitochondrial dynamics and mitochondrial quality control." *Redox Biol* **4**: 6-13.
- Niknahad, H., A. Jamshidzadeh, R. Heidari, M. Zarei and M. M. Ommati (2017). "Ammonia-induced mitochondrial dysfunction and energy metabolism disturbances in isolated brain and liver mitochondria, and the effect of taurine administration: relevance to hepatic encephalopathy treatment." *Clin Exp Hepatol* **3**(3): 141-151.
- Niknahad, H., A. Jamshidzadeh, R. Heidari, M. Zarei and M. M. Ommati (2017). "Ammonia-induced mitochondrial dysfunction and energy metabolism disturbances in isolated brain and liver mitochondria, and the effect of taurine administration: relevance to hepatic encephalopathy treatment." *Clinical and Experimental Hepatology* **3**(3): 141-151.
- Nixon, R. A., J. Wegiel, A. Kumar, W. H. Yu, C. Peterhoff, A. Cataldo and A. M. Cuervo (2005). "Extensive involvement of autophagy in Alzheimer disease: an immuno-electron microscopy study." *J Neuropathol Exp Neurol* **64**(2): 113-122.
- Nowikovsky, K., S. Reipert, R. J. Devenish and R. J. Schweyen (2007). "Mdm38 protein depletion causes loss of mitochondrial K⁺/H⁺ exchange activity, osmotic swelling and mitophagy." *Cell Death Differ* **14**(9): 1647-1656.
- Nunnari, J. and A. Suomalainen (2012). "Mitochondria: in sickness and in health." *Cell* **148**(6): 1145-1159.
- O'Hagan, K. A., S. Cocchiglia, A. V. Zhdanov, M. M. Tambuwala, E. P. Cummins, M. Monfared, T. A. Agbor, J. F. Garvey, D. B. Papkovsky, C. T. Taylor and B. B. Allan (2009). "PGC-1alpha is coupled to HIF-1alpha-dependent gene expression by increasing mitochondrial oxygen consumption in skeletal muscle cells." *Proc Natl Acad Sci U S A* **106**(7): 2188-2193.
- Oenarto, J., A. Karababa, M. Castoldi, H. J. Bidmon, B. Görg and D. Häussinger (2016). "Ammonia-induced miRNA expression changes in cultured rat astrocytes." *Sci Rep* **6**: 18493.
- Ohara, K., M. Aoyama, M. Fujita, K. Sobue and K. Asai (2009). "Prolonged exposure to ammonia increases extracellular glutamate in cultured rat astrocytes." *Neurosci Lett* **462**(2): 109-112.
- Ohsumi, Y. (2001). "Molecular dissection of autophagy: two ubiquitin-like systems." *Nat Rev Mol Cell Biol* **2**(3): 211-216.
- Okamoto, K. (2014). "Organellophagy: eliminating cellular building blocks via selective autophagy." *J Cell Biol* **205**(4): 435-445.
- Okamoto, K., N. Kondo-Okamoto and Y. Ohsumi (2009). "Mitochondria-anchored receptor Atg32 mediates degradation of mitochondria via selective autophagy." *Dev Cell* **17**(1): 87-97.
- Orvedahl, A., R. Sumpter, Jr., G. Xiao, A. Ng, Z. Zou, Y. Tang, M. Narimatsu, C. Gilpin, Q. Sun, M. Roth, C. V. Forst, J. L. Wrana, Y. E. Zhang, K. Luby-Phelps, R. J. Xavier, Y. Xie and B. Levine (2011). "Image-based genome-wide siRNA screen identifies selective autophagy factors." *Nature* **480**(7375): 113-117.
- Otsu, K., T. Murakawa and O. Yamaguchi (2015). "BCL2L13 is a mammalian homolog of the yeast mitophagy receptor Atg32." *Autophagy* **11**(10): 1932-1933.
- Palade, G. E. (1953). "An electron microscope study of the mitochondrial structure." *J Histochem Cytochem* **1**(4):

188-211.

- Panickar, K. S., A. R. Jayakumar, K. V. Rao and M. D. Norenberg (2009). "Ammonia-induced activation of p53 in cultured astrocytes: role in cell swelling and glutamate uptake." *Neurochem Int* **55**(1-3): 98-105.
- Pankiv, S., T. H. Clausen, T. Lamark, A. Brech, J. A. Bruun, H. Outzen, A. Overvatn, G. Bjorkoy and T. Johansen (2007). "p62/SQSTM1 binds directly to Atg8/LC3 to facilitate degradation of ubiquitinated protein aggregates by autophagy." *J Biol Chem* **282**(33): 24131-24145.
- Petrat, F., S. Pindiur, M. Kirsch and H. de Groot (2003). ""Mitochondrial" photochemical drugs do not release toxic amounts of 1O(2) within the mitochondrial matrix space." *Arch Biochem Biophys* **412**(2): 207-215.
- Pflieger, D., J. P. Le Caer, C. Lemaire, B. A. Bernard, G. Dujardin and J. Rossier (2002). "Systematic identification of mitochondrial proteins by LC-MS/MS." *Anal Chem* **74**(10): 2400-2406.
- Pietrowsky, R., D. Braun, H. L. Fehm, P. Pauschinger and J. Born (1991). "Vasopressin and oxytocin do not influence early sensory processing but affect mood and activation in man." *Peptides* **12**(6): 1385-1391.
- Polletta, L., E. Vernucci, I. Carnevale, T. Arcangeli, D. Rotili, S. Palmerio, C. Steegborn, T. Nowak, M. Schutkowski, L. Pellegrini, L. Sansone, L. Villanova, A. Runci, B. Pucci, E. Morgante, M. Fini, A. Mai, M. A. Russo and M. Tafani (2015). "SIRT5 regulation of ammonia-induced autophagy and mitophagy." *Autophagy* **11**(2): 253-270.
- Popovic, D. and I. Dikic (2014). "TBC1D5 and the AP2 complex regulate ATG9 trafficking and initiation of autophagy." *EMBO Rep* **15**(4): 392-401.
- Priault, M., B. Salin, J. Schaeffer, F. M. Vallette, J. P. di Rago and J. C. Martinou (2005). "Impairing the bioenergetic status and the biogenesis of mitochondria triggers mitophagy in yeast." *Cell Death Differ* **12**(12): 1613-1621.
- Qu, D., A. Hage, K. Don-Carolis, E. Huang, A. Joselin, F. Safarpour, P. C. Marcogliese, M. W. Rousseaux, S. J. Hewitt, T. Huang, D. S. Im, S. Callaghan, D. Dewar-Darch, D. Figeys, R. S. Slack and D. S. Park (2015). "BAG2 Gene-mediated Regulation of PINK1 Protein Is Critical for Mitochondrial Translocation of PARKIN and Neuronal Survival." *J Biol Chem* **290**(51): 30441-30452.
- Quinsay, M. N., R. L. Thomas, Y. Lee and A. B. Gustafsson (2010). "Bnip3-mediated mitochondrial autophagy is independent of the mitochondrial permeability transition pore." *Autophagy* **6**(7): 855-862.
- Rai, Y., R. Pathak, N. Kumari, D. K. Sah, S. Pandey, N. Kalra, R. Soni, B. S. Dwarakanath and A. N. Bhatt (2018). "Mitochondrial biogenesis and metabolic hyperactivation limits the application of MTT assay in the estimation of radiation induced growth inhibition." *Sci Rep* **8**(1): 1531.
- Rama Rao, K. V. and M. D. Norenberg (2012). "Brain energy metabolism and mitochondrial dysfunction in acute and chronic hepatic encephalopathy." *Neurochem Int* **60**(7): 697-706.
- Reichert, A. S. and W. Neupert (2004). "Mitochondriomics or what makes us breathe." *Trends Genet* **20**(11): 555-562.
- Reinehr, R., B. Görg, S. Becker, N. Qvartskhava, H. J. Bidmon, O. Selbach, H. L. Haas, F. Schliess and D. Häussinger (2007). "Hypoosmotic swelling and ammonia increase oxidative stress by NADPH oxidase in cultured astrocytes and vital brain slices." *Glia* **55**(7): 758-771.
- Riggio, O., L. Ridola, C. Pasquale, S. Nardelli, I. Pentassuglio, F. Moscucci and M. Merli (2011). "Evidence of persistent cognitive impairment after resolution of overt hepatic encephalopathy." *Clin Gastroenterol Hepatol* **9**(2): 181-183.
- Rizzuto, R., M. R. Duchen and T. Pozzan (2004). "Flirting in little space: the ER/mitochondria Ca²⁺ liaison." *Sci STKE* **2004**(215): re1.
- Ropolo, A., D. Grasso, R. Pardo, M. L. Sacchetti, C. Archange, A. Lo Re, M. Seux, J. Nowak, C. D. Gonzalez, J. L. Iovanna and M. I. Vaccaro (2007). "The pancreatitis-induced vacuole membrane protein 1 triggers autophagy in mammalian cells." *J Biol Chem* **282**(51): 37124-37133.
- Rubinsztein, D. C., G. Marino and G. Kroemer (2011). "Autophagy and aging." *Cell* **146**(5): 682-695.

- Russell, R. C., H. X. Yuan and K. L. Guan (2014). "Autophagy regulation by nutrient signaling." *Cell Res* **24**(1): 42-57.
- Saito, M., H. Hirano, Y. Yano, K. Momose, M. Yoshida and T. Azuma (2016). "Serum level of taurine would be associated with the amelioration of minimal hepatic encephalopathy in cirrhotic patients." *Hepatol Res* **46**(2): 215-224.
- Sancak, Y., L. Bar-Peled, R. Zoncu, A. L. Markhard, S. Nada and D. M. Sabatini (2010). "Ragulator-Rag complex targets mTORC1 to the lysosomal surface and is necessary for its activation by amino acids." *Cell* **141**(2): 290-303.
- Sandilands, E., B. Serrels, D. G. McEwan, J. P. Morton, J. P. Macagno, K. McLeod, C. Stevens, V. G. Brunton, W. Y. Langdon, M. Vidal, O. J. Sansom, I. Dikic, S. Wilkinson and M. C. Frame (2011). "Autophagic targeting of Src promotes cancer cell survival following reduced FAK signalling." *Nat Cell Biol* **14**(1): 51-60.
- Saraste, M. (1999). "Oxidative phosphorylation at the fin de siecle." *Science* **283**(5407): 1488-1493.
- Sarraf, S. A., M. Raman, V. Guarani-Pereira, M. E. Sowa, E. L. Huttlin, S. P. Gygi and J. W. Harper (2013). "Landscape of the PARKIN-dependent ubiquitylome in response to mitochondrial depolarization." *Nature* **496**(7445): 372-376.
- Schafer, A. and A. S. Reichert (2009). "Emerging roles of mitochondrial membrane dynamics in health and disease." *Biol Chem* **390**(8): 707-715.
- Scheffler, I. E. (1999). *Metabolic Pathways Inside Mitochondria*. *Mitochondria*, John Wiley & Sons, Inc.: 246-272.
- Schliess, F., N. Foster, B. Görg, R. Reinehr and D. Häussinger (2004). "Hypoosmotic swelling increases protein tyrosine nitration in cultured rat astrocytes." *Glia* **47**(1): 21-29.
- Schliess, F., B. Görg, R. Fischer, P. Desjardins, H. J. Bidmon, A. Herrmann, R. F. Butterworth, K. Zilles and D. Häussinger (2002). "Ammonia induces MK-801-sensitive nitration and phosphorylation of protein tyrosine residues in rat astrocytes." *FASEB J* **16**(7): 739-741.
- Schmidt, O., N. Pfanner and C. Meisinger (2010). "Mitochondrial protein import: from proteomics to functional mechanisms." *Nat Rev Mol Cell Biol* **11**(9): 655-667.
- Schweers, R. L., J. Zhang, M. S. Randall, M. R. Loyd, W. Li, F. C. Dorsey, M. Kundu, J. T. Opferman, J. L. Cleveland, J. L. Miller and P. A. Ney (2007). "NIX is required for programmed mitochondrial clearance during reticulocyte maturation." *Proc Natl Acad Sci U S A* **104**(49): 19500-19505.
- Settembre, C., C. Di Malta, V. A. Polito, M. Garcia Arencibia, F. Vetrini, S. Erdin, S. U. Erdin, T. Huynh, D. Medina, P. Colella, M. Sardiello, D. C. Rubinsztein and A. Ballabio (2011). "TFEB links autophagy to lysosomal biogenesis." *Science* **332**(6036): 1429-1433.
- Sha, D., L. S. Chin and L. Li (2010). "Phosphorylation of parkin by Parkinson disease-linked kinase PINK1 activates parkin E3 ligase function and NF-kappaB signaling." *Hum Mol Genet* **19**(2): 352-363.
- Shah, N. J., H. Neeb, G. Kircheis, P. Engels, D. Häussinger and K. Zilles (2008). "Quantitative cerebral water content mapping in hepatic encephalopathy." *Neuroimage* **41**(3): 706-717.
- Shibata, M., T. Lu, T. Furuya, A. Degterev, N. Mizushima, T. Yoshimori, M. MacDonald, B. Yankner and J. Yuan (2006). "Regulation of intracellular accumulation of mutant Huntingtin by Beclin 1." *J Biol Chem* **281**(20): 14474-14485.
- Shin, J. H., H. S. Ko, H. Kang, Y. Lee, Y. I. Lee, O. Pletinkova, J. C. Troconso, V. L. Dawson and T. M. Dawson (2011). "PARIS (ZNF746) repression of PGC-1alpha contributes to neurodegeneration in Parkinson's disease." *Cell* **144**(5): 689-702.
- Shpilka, T., E. Welter, N. Borovsky, N. Amar, F. Shimron, Y. Peleg and Z. Elazar (2015). "Fatty acid synthase is preferentially degraded by autophagy upon nitrogen starvation in yeast." *Proc Natl Acad Sci U S A* **112**(5): 1434-1439.
- Sickmann, A., J. Reinders, Y. Wagner, C. Joppich, R. Zahedi, H. E. Meyer, B. Schonfisch, I. Perschil, A. Chacinska, B. Guiard, P. Rehling, N. Pfanner and C. Meisinger (2003). "The proteome of *Saccharomyces cerevisiae*

- mitochondria." *Proc Natl Acad Sci U S A* **100**(23): 13207-13212.
- Singh, R., S. Kaushik, Y. Wang, Y. Xiang, I. Novak, M. Komatsu, K. Tanaka, A. M. Cuervo and M. J. Czaja (2009). "Autophagy regulates lipid metabolism." *Nature* **458**(7242): 1131-1135.
- Singh, R., Y. Xiang, Y. Wang, K. Baikati, A. M. Cuervo, Y. K. Luu, Y. Tang, J. E. Pessin, G. J. Schwartz and M. J. Czaja (2009). "Autophagy regulates adipose mass and differentiation in mice." *J Clin Invest* **119**(11): 3329-3339.
- Singh, S. P., J. Schragenheim, J. Cao, J. R. Falck, N. G. Abraham and L. Bellner (2016). "PGC-1 alpha regulates HO-1 expression, mitochondrial dynamics and biogenesis: Role of epoxyeicosatrienoic acid." *Prostaglandins Other Lipid Mediat* **125**: 8-18.
- Sinke, A. P., A. R. Jayakumar, K. S. Panickar, M. Moriyama, P. V. Reddy and M. D. Norenberg (2008). "NFkappaB in the mechanism of ammonia-induced astrocyte swelling in culture." *J Neurochem* **106**(6): 2302-2311.
- Sobczyk, K., M. S. Jordens, A. Karababa, B. Görg and D. Häussinger (2015). "Ephrin/Ephrin receptor expression in ammonia-treated rat astrocytes and in human cerebral cortex in hepatic encephalopathy." *Neurochem Res* **40**(2): 274-283.
- Soleimanpour, S. A., A. Gupta, M. Bakay, A. M. Ferrari, D. N. Groff, J. Fadista, L. A. Spruce, J. A. Kushner, L. Groop, S. H. Seeholzer, B. A. Kaufman, H. Hakonarson and D. A. Stoffers (2014). "The diabetes susceptibility gene Clec16a regulates mitophagy." *Cell* **157**(7): 1577-1590.
- Song, W. H., Y. J. Yi, M. Sutovsky, S. Meyers and P. Sutovsky (2016). "Autophagy and ubiquitin-proteasome system contribute to sperm mitophagy after mammalian fertilization." *Proc Natl Acad Sci U S A* **113**(36): E5261-5270.
- Soria, L. R., G. Allegri, D. Melck, N. Pastore, P. Annunziata, D. Paris, E. Polishchuk, E. Nusco, B. Thony, A. Motta, J. Haberle, A. Ballabio and N. Brunetti-Pierri (2018). "Enhancement of hepatic autophagy increases ureagenesis and protects against hyperammonemia." *Proc Natl Acad Sci U S A* **115**(2): 391-396.
- Soubannier, V., P. Rippstein, B. A. Kaufman, E. A. Shoubridge and H. M. McBride (2012). "Reconstitution of mitochondria derived vesicle formation demonstrates selective enrichment of oxidized cargo." *PLoS One* **7**(12): e52830.
- Spinelli, J. B., H. Yoon, A. E. Ringel, S. Jeanfavre, C. B. Clish and M. C. Haigis (2017). "Metabolic recycling of ammonia via glutamate dehydrogenase supports breast cancer biomass." *Science* **358**(6365): 941-946.
- Stojanovski, D., M. Bohnert, N. Pfanner and M. van der Laan (2012). "Mechanisms of protein sorting in mitochondria." *Cold Spring Harb Perspect Biol* **4**(10).
- Sutovsky, P., R. D. Moreno, J. Ramalho-Santos, T. Dominko, C. Simerly and G. Schatten (1999). "Ubiquitin tag for sperm mitochondria." *Nature* **402**(6760): 371-372.
- Suzuki, K., C. Kondo, M. Morimoto and Y. Ohsumi (2010). "Selective transport of alpha-mannosidase by autophagic pathways: identification of a novel receptor, Atg34p." *J Biol Chem* **285**(39): 30019-30025.
- Suzuki, K., Y. Kubota, T. Sekito and Y. Ohsumi (2007). "Hierarchy of Atg proteins in pre-autophagosomal structure organization." *Genes Cells* **12**(2): 209-218.
- Swain, M. S., A. T. Blei, R. F. Butterworth and R. P. Kraig (1991). "Intracellular pH rises and astrocytes swell after portacaval anastomosis in rats." *Am J Physiol* **261**(6 Pt 2): R1491-1496.
- Tal, R., G. Winter, N. Ecker, D. J. Klionsky and H. Abeliovich (2007). "Aup1p, a yeast mitochondrial protein phosphatase homolog, is required for efficient stationary phase mitophagy and cell survival." *J Biol Chem* **282**(8): 5617-5624.
- Tallis, S., L. R. Caltana, P. A. Souto, A. E. Delfante, N. R. Lago, A. Brusco and J. C. Perazzo (2014). "Changes in CNS cells in hyperammonemic portal hypertensive rats." *J Neurochem* **128**(3): 431-444.
- Tatsuta, T. and T. Langer (2008). "Quality control of mitochondria: protection against neurodegeneration and ageing." *EMBO J* **27**(2): 306-314.
- Teter, S. A., K. P. Eggerton, S. V. Scott, J. Kim, A. M. Fischer and D. J. Klionsky (2001). "Degradation of lipid vesicles

- in the yeast vacuole requires function of Cvt17, a putative lipase." *J Biol Chem* **276**(3): 2083-2087.
- Thurston, T. L., G. Ryzhakov, S. Bloor, N. von Muhlinen and F. Randow (2009). "The TBK1 adaptor and autophagy receptor NDP52 restricts the proliferation of ubiquitin-coated bacteria." *Nat Immunol* **10**(11): 1215-1221.
- Thurston, T. L., M. P. Wandel, N. von Muhlinen, A. Foeglein and F. Randow (2012). "Galectin 8 targets damaged vesicles for autophagy to defend cells against bacterial invasion." *Nature* **482**(7385): 414-418.
- Trifunovic, A., A. Wredenberg, M. Falkenberg, J. N. Spelbrink, A. T. Rovio, C. E. Bruder, Y. M. Bohlooly, S. Gidlof, A. Oldfors, R. Wibom, J. Tornell, H. T. Jacobs and N. G. Larsson (2004). "Premature ageing in mice expressing defective mitochondrial DNA polymerase." *Nature* **429**(6990): 417-423.
- Trudeau, K. M., A. H. Colby, J. Zeng, G. Las, J. H. Feng, M. W. Grinstaff and O. S. Shirihai (2016). "Lysosome acidification by photoactivated nanoparticles restores autophagy under lipotoxicity." *J Cell Biol* **214**(1): 25-34.
- Twig, G., A. Elorza, A. J. Molina, H. Mohamed, J. D. Wikstrom, G. Walzer, L. Stiles, S. E. Haigh, S. Katz, G. Las, J. Alroy, M. Wu, B. F. Py, J. Yuan, J. T. Deeney, B. E. Corkey and O. S. Shirihai (2008). "Fission and selective fusion govern mitochondrial segregation and elimination by autophagy." *EMBO J* **27**(2): 433-446.
- Twig, G. and O. S. Shirihai (2011). "The interplay between mitochondrial dynamics and mitophagy." *Antioxid Redox Signal* **14**(10): 1939-1951.
- van der Bliek, A. M., Q. Shen and S. Kawajiri (2013). "Mechanisms of mitochondrial fission and fusion." *Cold Spring Harb Perspect Biol* **5**(6).
- Van Humbeeck, C., T. Cornelissen, H. Hofkens, W. Mandemakers, K. Gevaert, B. De Strooper and W. Vandenberghe (2011). "Parkin interacts with Ambra1 to induce mitophagy." *J Neurosci* **31**(28): 10249-10261.
- van Vliet, A. R., T. Verfaillie and P. Agostinis (2014). "New functions of mitochondria associated membranes in cellular signaling." *Biochim Biophys Acta* **1843**(10): 2253-2262.
- Viscomi, C., E. Bottani, G. Civiletto, R. Cerutti, M. Moggio, G. Fagiolari, E. A. Schon, C. Lamperti and M. Zeviani (2011). "In vivo correction of COX deficiency by activation of the AMPK/PGC-1alpha axis." *Cell Metab* **14**(1): 80-90.
- Waagepetersen, H. S., U. Sonnewald, G. Gegelashvili, O. M. Larsson and A. Schousboe (2001). "Metabolic distinction between vesicular and cytosolic GABA in cultured GABAergic neurons using C-13 magnetic resonance spectroscopy." *Journal of Neuroscience Research* **63**(4): 347-355.
- Waizenegger, T., S. J. Habib, M. Lech, D. Mokranjac, S. A. Paschen, K. Hell, W. Neupert and D. Rapaport (2004). "Tob38, a novel essential component in the biogenesis of beta-barrel proteins of mitochondria." *EMBO Rep* **5**(7): 704-709.
- Wallace, D. C. (2005). "A mitochondrial paradigm of metabolic and degenerative diseases, aging, and cancer: a dawn for evolutionary medicine." *Annu Rev Genet* **39**: 359-407.
- Wang, B., N. Abraham, G. Gao and Q. Yang (2016). "Dysregulation of autophagy and mitochondrial function in Parkinson's disease." *Transl Neurodegener* **5**: 19.
- Wang, K., M. Jin, X. Liu and D. J. Klionsky (2013). "Proteolytic processing of Atg32 by the mitochondrial i-AAA protease Yme1 regulates mitophagy." *Autophagy* **9**(11): 1828-1836.
- Warskulat, U., E. Borsch, R. Reinehr, B. Heller-Stilb, I. Mönninghoff, D. Buchczyk, M. Donner, U. Flogel, G. Kappert, S. Soboll, S. Beer, K. Pfeffer, H. U. Marschall, M. Gabrielsen, M. Amiry-Moghaddam, O. P. Ottersen, H. P. Dienes and D. Häussinger (2006). "Chronic liver disease is triggered by taurine transporter knockout in the mouse." *FASEB J* **20**(3): 574-576.
- Warskulat, U., B. Görg, H. J. Bidmon, H. W. Müller, F. Schliess and D. Häussinger (2002). "Ammonia-induced heme oxygenase-1 expression in cultured rat astrocytes and rat brain in vivo." *Glia* **40**(3): 324-336.
- Westermann, B. (2010). "Mitochondrial fusion and fission in cell life and death." *Nat Rev Mol Cell Biol* **11**(12): 872-884.

- Widmer, R., B. Kaiser, M. Engels, T. Jung and T. Grune (2007). "Hyperammonemia causes protein oxidation and enhanced proteasomal activity in response to mitochondria-mediated oxidative stress in rat primary astrocytes." *Arch Biochem Biophys* **464**(1): 1-11.
- Wild, P., H. Farhan, D. G. McEwan, S. Wagner, V. V. Rogov, N. R. Brady, B. Richter, J. Korac, O. Waidmann, C. Choudhary, V. Dotsch, D. Bumann and I. Dikic (2011). "Phosphorylation of the autophagy receptor optineurin restricts Salmonella growth." *Science* **333**(6039): 228-233.
- Williams, E. G., Y. Wu, P. Jha, S. Dubuis, P. Blattmann, C. A. Argmann, S. M. Houten, T. Amariuta, W. Wolski, N. Zamboni, R. Aebersold and J. Auwerx (2016). "Systems proteomics of liver mitochondria function." *Science* **352**(6291): aad0189.
- Wong, Y. C. and E. L. Holzbaur (2014). "Optineurin is an autophagy receptor for damaged mitochondria in parkin-mediated mitophagy that is disrupted by an ALS-linked mutation." *Proc Natl Acad Sci U S A* **111**(42): E4439-4448.
- Wu, H., D. Xue, G. Chen, Z. Han, L. Huang, C. Zhu, X. Wang, H. Jin, J. Wang, Y. Zhu, L. Liu and Q. Chen (2014). "The BCL2L1 and PGAM5 axis defines hypoxia-induced receptor-mediated mitophagy." *Autophagy* **10**(10): 1712-1725.
- Yamano, K., A. I. Fogel, C. Wang, A. M. van der Bliek and R. J. Youle (2014). "Mitochondrial Rab GAPs govern autophagosome biogenesis during mitophagy." *Elife* **3**: e01612.
- Yang, Z., J. Huang, J. Geng, U. Nair and D. J. Klionsky (2006). "Atg22 recycles amino acids to link the degradative and recycling functions of autophagy." *Mol Biol Cell* **17**(12): 5094-5104.
- Yang, Z. and D. J. Klionsky (2010). "Mammalian autophagy: core molecular machinery and signaling regulation." *Curr Opin Cell Biol* **22**(2): 124-131.
- Yao, Z., E. Delorme-Axford, S. K. Backues and D. J. Klionsky (2015). "Atg41/Icy2 regulates autophagosome formation." *Autophagy* **11**(12): 2288-2299.
- Yeo, S. Y., Y. Itahana, A. K. Guo, R. Han, K. Iwamoto, H. T. Nguyen, Y. Bao, K. Kleiber, Y. J. Wu, B. H. Bay, M. Voorhoeve and K. Itahana (2016). "Transglutaminase 2 contributes to a TP53-induced autophagy program to prevent oncogenic transformation." *Elife* **5**: e07101.
- Yin, Z., C. Pascual and D. J. Klionsky (2016). "Autophagy: machinery and regulation." *Microb Cell* **3**(12): 588-596.
- Yogalingam, G. and A. M. Pendergast (2008). "Abl kinases regulate autophagy by promoting the trafficking and function of lysosomal components." *J Biol Chem* **283**(51): 35941-35953.
- Yoshii, S. R., C. Kishi, N. Ishihara and N. Mizushima (2011). "Parkin mediates proteasome-dependent protein degradation and rupture of the outer mitochondrial membrane." *J Biol Chem* **286**(22): 19630-19640.
- Youle, R. J. and D. P. Narendra (2011). "Mechanisms of mitophagy." *Nat Rev Mol Cell Biol* **12**(1): 9-14.
- Young, A. R., E. Y. Chan, X. W. Hu, R. Kochl, S. G. Crawshaw, S. High, D. W. Hailey, J. Lippincott-Schwartz and S. A. Tooze (2006). "Starvation and ULK1-dependent cycling of mammalian Atg9 between the TGN and endosomes." *J Cell Sci* **119**(Pt 18): 3888-3900.
- Yuan, Y., Y. Zheng, X. Zhang, Y. Chen, X. Wu, J. Wu, Z. Shen, L. Jiang, L. Wang, W. Yang, J. Luo, Z. Qin, W. Hu and Z. Chen (2017). "BNIP3L/NIX-mediated mitophagy protects against ischemic brain injury independent of PARK2." *Autophagy* **13**(10): 1754-1766.
- Yun, J., R. Puri, H. Yang, M. A. Lizzio, C. Wu, Z. H. Sheng and M. Guo (2014). "MUL1 acts in parallel to the PINK1/parkin pathway in regulating mitofusin and compensates for loss of PINK1/parkin." *Elife* **3**: e01958.
- Zhan, T. and W. Stremmel (2012). "The diagnosis and treatment of minimal hepatic encephalopathy." *Dtsch Arztebl Int* **109**(10): 180-187.
- Zhang, H., M. Bosch-Marce, L. A. Shimoda, Y. S. Tan, J. H. Baek, J. B. Wesley, F. J. Gonzalez and G. L. Semenza (2008). "Mitochondrial autophagy is an HIF-1-dependent adaptive metabolic response to hypoxia." *J Biol Chem* **283**(16): 10892-10903.
- Zhang, H., Z. Chen, R. N. Miranda, L. J. Medeiros and N. McCarty (2016). "TG2 and NF-kappaB Signaling

-
- Coordinates the Survival of Mantle Cell Lymphoma Cells via IL6-Mediated Autophagy." *Cancer Res* **76**(21): 6410-6423.
- Zhang, J. and P. A. Ney (2009). "Role of BNIP3 and NIX in cell death, autophagy, and mitophagy." *Cell Death Differ* **16**(7): 939-946.
- Zhao, Z., M. Wang, Y. Tian, T. Hilton, B. Salsbery, E. Z. Zhou, X. Wu, P. Thiagarajan, E. Boilard, M. Li, J. Zhang and J. F. Dong (2016). "Cardiolipin-mediated procoagulant activity of mitochondria contributes to traumatic brain injury-associated coagulopathy in mice." *Blood* **127**(22): 2763-2772.
- Zhou, C., K. Ma, R. Gao, C. Mu, L. Chen, Q. Liu, Q. Luo, D. Feng, Y. Zhu and Q. Chen (2017). "Regulation of mATG9 trafficking by Src- and ULK1-mediated phosphorylation in basal and starvation-induced autophagy." *Cell Res* **27**(2): 184-201.
- Zhu, Y., S. Massen, M. Terenzio, V. Lang, S. Chen-Lindner, R. Eils, I. Novak, I. Dikic, A. Hamacher-Brady and N. R. Brady (2013). "Modulation of serines 17 and 24 in the LC3-interacting region of Bnip3 determines pro-survival mitophagy versus apoptosis." *J Biol Chem* **288**(2): 1099-1113.
- Zunino, R., A. Schauss, P. Rippstein, M. Andrade-Navarro and H. M. McBride (2007). "The SUMO protease SENP5 is required to maintain mitochondrial morphology and function." *J Cell Sci* **120**(Pt 7): 1178-1188.

List of Figures

Figures	Page
Fig. 1.1 Ultrastructure of mitochondria.	3
Fig. 1.2 The major functions of mitochondria.	4
Fig. 1.3 Fusion and fission of mammalian mitochondria.	6
Fig. 1.4 Major types of autophagy in mammals.	14
Fig. 1.5 Two common modes of selective types of autophagy in mammals.	15
Fig. 1.6 The core machinery of mammalian autophagy.	21
Fig. 1.7 Regulation of TGM2 on autophagy.	27
Fig. 1.8 Major pathways underlying mammalian mitophagy.	31
Fig. 1.9 A schematic model of mitophagy in <i>S. cerevisiae</i> .	36
Fig. 1.10 The pathogenetic model of hepatic encephalopathy.	40
Fig. 1.11 Major functional consequences of osmotic and oxidative/nitrosative stress in astrocytes.	44
Fig. 1.12 Working hypothesis: involvement of mitochondrial quality control pathways in the pathogenesis of hepatic encephalopathy.	46
Fig. 3.1 Ammonium treatment inhibits autophagy in primary rat astrocytes.	75
Fig. 3.2 Autophagy is inhibited by ammonium treatment in various cell lines.	76
Fig. 3.3 Ammonia-induced autophagy inhibition is dose- and time-dependent, fast and reversible.	77
Fig. 3.4 Ammonia inhibits autophagy mainly via pH alteration.	79
Fig. 3.5 Methylammonium chloride-induced autophagy inhibition is fast, reversible and decreased by ROS reducers..	80
Fig. 3.6 Ammonia-induced autophagy inhibition is pH- and ROS-dependent but not GS- or p38MAPK-dependent.	82
Fig. 3.7 Ammonium treatment results in autophagy inhibition in a rat model of HE.	84
Fig. 3.8 Taurine supplement alleviates ammonia-induced autophagy inhibition in cultured rat astrocytes.	86
Fig. 3.9 Comparison of ammonia-induced autophagy inhibition between cultured rat astrocytes and a rat model of acute ammonium intoxication.	86
Fig. 3.10 Ammonium treatment leads to upregulation of TGM2 in cultured rat astrocytes.	87
Fig. 3.11 Ammonium treatment leads to upregulation of TGM2 in a rat model of HE.	89
Fig. 3.12 TGM2 mRNA levels in the cerebral cortex of patients with liver cirrhosis with or without HE.	90
Fig. 3.13 Ammonium treatment impairs mitochondrial function in primary rat astrocytes.	91-92
Fig. 3.14 Ammonium treatment does not affect the mitochondrial number and major mitochondrial morphological parameters.	93
Fig. 3.15 Ammonium treatment leads to accumulation of both l-OPA1 and s-OPA1	94

in cultured rat astrocytes.	
Fig. 3.16 Ammonium treatment induces mitophagy in cultured rat astrocytes.	95
Fig. 3.17 Ammonium treatment induces Parkin-mediated mitophagy in primary rat astrocytes.	97
Fig. 3.18 Ammonium treatment induces NIX-mediated mitophagy in primary rat astrocytes.	100
Fig. 3.19 Ammonium treatment enhances PGC-1 α expression level in primary rat astrocytes.	102
Fig. 3.20 Autophagy and mitophagy inhibition further sensitize astrocytes to cell death only after treatment of extremely high concentration of ammonium.	105
Fig. 3.21 Characterization of photoactivatable acidic nanoparticle functionalities.	108
Fig. 3.22 Lysosome acidification by photoactivated nanoparticles restores autophagy under NH ₄ Cl treatment.	110- 111
Fig. 4.1 Schematic drawing of ammonium's effect on mitochondrial quality control pathways.	113
Fig. 4.2 Schematic drawing of a regulatory network centered by HIF-1 α for defensive mechanisms evoked by hyperammonemia.	124

List of Tables

Tables	Page
Table 1.1 List of liver and brain diseases associated with mitochondrial dysfunction.	9-11
Table 1.2 List of selective types of autophagy.	16-17
Table 1.3 Severity-based classification of hepatic encephalopathy.	38
Table 2.1 List of chemicals, enzymes and kits.	48-50
Table 2.2 List of equipment.	50-52
Table 2.3 List of consumables.	52-53
Table 2.4 List of mammalian cell culture mediums.	53
Table 2.5 List of <i>E. coli</i> culture mediums.	53
Table 2.6 List of buffers.	54-55
Table 2.7 List of mammalian cells.	55
Table 2.8 List of <i>E. coli</i> strains.	55
Table 2.9 List of siRNAs.	56
Table 2.10 Sequences of siRNAs	56
Table 2.11 List of plasmids.	56
Table 2.12 List of primary antibodies.	57-58
Table 2.13 List of secondary antibodies.	59
Table 2.14 List of software.	59
Table 2.15 List of animal tissue samples.	60
Table 2.16 Composition of the SDS-PAGE gels.	65

Abbreviations

% [v/v]	volume/volume percent
% [w/v]	weight/volume percent
·OH	hydroxyl radical
8OH(d)G	8-OH-deoxyguanosine
AA	acrylamide
AD	Alzheimer's disease
ADP	adenosine diphosphate
AMP	adenosine monophosphate
Amp	ampicillin
AMPK	5' adenosine monophosphate-activated protein kinase
ANOVA	Analysis of variance
Ape1	aminopeptidase 1
APS	ammonium persulfate
ARE	antioxidant response element
ATG	autophagy-related
ATP	adenosine triphosphate
BAA	bisacrylamide
Bcl-2	B-cell lymphoma-2
BCL2L	Bcl-2 like
BDNF	brain derived neurotrophic factor
BFP	blue fluorescent protein
BNIP3	Bcl-2/adenovirus E1B 19 kDa protein-interacting protein 3
BN-PAGE	blue native polyacrylamide gel electrophoresis
bp	base pair
BrdU	bromodeoxyuridine
BSA	bovine serum albumin
BW	body weight
<i>C. elegans</i>	<i>Caenorhabditis elegans</i>
C12FDG	5-dodecanoylaminofluorescein di-β-D-galactopyransoide
cAMP	cyclic adenosine monophosphate
CCCP	carbonyl cyanide m-chlorophenylhydrazone
CDK	cyclin-dependent kinase
cDNA	complementary desoxyribonucleic acid
cGMP	cyclic guanosine monophosphate
CH ₃ NH ₃ Cl	methylammoniumchlorid
ChiMERA	construct helping in mitochondria-ER association
Cip/Kip	CDK inhibitory polypeptides/kinase inhibitory proteins
CJ	crista junction
CK2	casein kinase 2
CL	cardiolipin
CM	cristae membrane

CO	carbon monoxide
CoQ	coenzyme Q
Cox3	cytochrome <i>c</i> oxidase subunit III
CQ	chloroquine
Ct	threshold cycle
Cvt	cytoplasm-to-vacuole targeting
DAPI	4',6-diamidino-2-phenylindole
DMEM	Dulbecco's minimal essential medium
DMSO	dimethyl sulfoxide
DNA	deoxyribonucleic acid
dNTP	deoxyribonucleotide triphosphate
Drp1	dynamamin related protein 1
DsRed	Discosoma sp. red fluorescent protein
DTT	dithiothreitol
<i>E. coli</i>	<i>Escherichia coli</i>
ECL	enhanced chemiluminescence
EDTA	ethylenediaminetetraacetic acid
EGTA	ethyleneglycoltetraacetic acid
ELISA	<i>enzyme linked immunosorbent assay</i>
EM	electron microscopy
eNOS	endothelial NO synthase
ER	endoplasmic reticulum
Erk	extracellular signal-regulated kinase
ERMES	the ER mitochondria encountering structure
et al.	et alii, et aliae
ETC	electron transport chain
Ex/Em	excitation wavelength/emission wavelength
FBS	fetal bovine serum
Fis1	mitochondrial fission protein 1
GABARAP	gamma-aminobutyric acid receptor-associated protein
GADD45 α	growth-arrest and DNA damage-inducible protein 45 alpha
GAPDH	glyceraldehyde 3-phosphate dehydrogenase
GDH	glutamate dehydrogenase
GDP	guanosine diphosphate
GFP	green fluorescent protein
GLN	glutamine
GLT	glutamate transporter
GLU	glutamate
GS	glutamine synthetase
GST	glutathion-s-transferase
GTP	guanosine triphosphate
h	hour
hsa	<i>Homo sapiens</i> (human)
H ₂ DCF-DA	dichlorodihydrofluorescein-diacetate

H ₂ O ₂	hydrogen peroxide
HBSS	Hank's balanced salt solution
HCl	hydrochloric acid
HE	hepatic encephalopathy
HEPES	4-(2-hydroxyethyl)-piperazine-N'-ethane-2-sulfonic acid
HIF-1	hypoxia-inducible factor 1
HO-1	heme oxygenase-1
HPLC	high performance liquid chromatography
Hprt1	hypoxanthine ribosyl transferase 1
HRP	horseradish peroxidase
Hsp	heat shock protein
IBM	inner boundary membrane
IgG	immunoglobulin G
IMM	the inner mitochondrial membrane
IMS	intermembrane space
iNOS	inducible nitric oxide synthase
kb	kilobase
kDa	kilodalton
Keap1	kelch-like ECH-associated protein 1
KOH	potassium hydroxide
L	liter
Lamp1	lysosomal associated membrane protein 1
LB	Luria Bertani
LC3	microtubule-associated protein 1A/1B-light chain 3
LDH	laktatdehydrogenase
LE	long exposure
LIR	LC3 interacting region
MAM	mitochondria-associated membranes
MAPK	mitogen activated protein kinase
Mcp	Mdm10 complementing protein
MEF	murine embryonic fibroblasts
Mfn	mitofusin
Mgm	mitochondrial genome maintenance
MICO	mitochondrial contact site
min	minute
Mmm1	mitochondrial morphology maintenance 1
mmu	<i>Mus musculus</i> (mouse)
MOPS	3-(N-morpholino)propane sulphonic acid
mQC	mitochondrial quality control
mRNA	messenger ribonucleic acid
MSO	L-methionine-S-sulfoximine
mt	mitochondrial
mtDNA	mitochondrial DNA

mTORC1	mammalian target of rapamycin complex 1
MTT	3-(4,5-dimethylthiazol-2-yl)-2,5-diphenyltetrazolium bromide
n	number of independent experiments
ns	not significant
NAC	N-acetyl-L-cysteine
NADH	nicotinamide adenine dinucleotide
NADPH	nicotinamide adenine dinucleotide phosphate
NaOH	sodium hydroxide
Ndufv1	NADH:ubiquinone oxidoreductase core subunit V1
NF- κ B	nuclear factor- κ B
NH ₃	ammonia
NH ₄ ⁺	ammonium
NH ₄ Cl	ammonium chlorid
NIX	nip3-like protein X
NMDA	N-methyl-D-aspartate
nNOS	neuronal-type nitric oxide synthase
NO	nitric oxide
No.	number
Nrf2	nuclear factor (erythroid derived 2)-like 2
O ₂ ⁻	superoxide
ocu	<i>Oryctolagus cuniculus</i> (rabbit)
OMM	the outer mitochondrial membrane
ONOO-	peroxynitrite
Opa1	optic atrophy 1
OPTN	optineurin
ORF	open reading frame
OXPPOS	mitochondrial oxidative phosphorylation system
p38MAPK	p38 mitogen-activated protein kinase
PAGE	polyacrylamide gel electrophoresis
paNP	photoactivatable acidifying nanoparticles
PARL	presenilin associated rhomboid like
PARP	poly ADP-ribose polymerase
PAS	phagophore assembly site
PBS	phosphate buffered saline
PCR	polymerase chain reaction
PD	Parkinson`s disease
PE	phosphatidylethanolamine
PEG	polyethylene glycol
PGC-1 α	Peroxisome proliferator-activated receptor gamma coactivator 1-alpha
pH	potential of hydrogen
PI3K	phosphatidylinositol-3-kinase
PINK1	PTEN-induced putative kinase 1

PIPES	1,4-piperazinediethanesulfonic acid
PKA	protein kinase A
PMSF	phenylmethane sulfonyl fluoride
p-p53	phosphoprotein p53
PTN	protein tyrosine nitration
PVDF	polyvinylidene difluoride
qPCR	quantitative polymerase chain reaction
Rapa	rapamycin
RNA	ribonucleic acid
rno	<i>Rattus norvegicus</i> (rat)
RNS	reactive nitrogen species
ROS	reactive oxygen species
rpm	revolutions per minute
rRNA	ribosomal RNA
RT	reverse transcription
Rubicon	RUN domain and cysteine-rich domain containing, Beclin 1-interacting
<i>S. cerevisiae</i>	<i>Saccharomyces cerevisiae</i>
SA- β -Gal	senescence associated β -galactosidase
SDS	sodium dodecyl sulfate
SE	short exposure
SEM	standard error of the mean
SNARE	soluble N-ethylmaleimide-sensitive factor attachment receptor
SOD	superoxide dismutase
SQSTM1	sequestosome 1
STD	standard deviation
TAE	tris acetate EDTA
TauT	taurin transporter
TBS	tris-buffered saline
TBST	tris-buffered saline tween-20
TCA	trichloroacetic acid
TEMED	tetramethylethylenediamine
Tgm2	transglutaminase 2
TIM	translocase of the inner mitochondrial membrane
TMD	transmembrane domain
TMRM	tetramethylrhodamine, methyl ester
TNF	tumor necrosis factor
TOB	topogenesis of mitochondrial outer-membrane beta-barrel proteins
TOM	translocase of the outer mitochondrial membrane
TP53	tumor suppressor protein 53
Tris	tris-hydroxymethyl-aminomethane
tRNA	transfer RNA
Ub	ubiquitin

UPS	ubiquitin-proteasome system
UTR	untranslated region
UV	ultraviolet
V	voltage
VDAC	voltage-dependent anion channel
WB	western blot
x g	acceleration relative to g (standard gravity)

Acknowledgements

First, my special thanks go to Prof. Dr. Andreas Reichert, for his willingness to take me as a doctoral student and the continuous support and guidance throughout my doctoral study. During these three and a half years, I had opportunities to participate in yeast genetics-, human disease- and nanomedicine-related projects and got meaningful scientific training in biomedical research. I would like to thank our collaborators Prof. Dr. Dieter Häussinger, Dr. Boris Görg, Dr. Hans-Jürgen Bidmon and Prof. Orian Shirihai for their continuous help, valuable suggestions and precious materials during these years' cooperation. Without these, this project will be much more difficult. I would also like to express my gratitude to my PhD mentor, Prof. Dr. Lutz Schmitt, for his useful suggestions and continuous help. Besides, my sincere thanks also go to Prof. Dr. Helmut Sies, Prof. Dr. William Stahl, and Prof. Dr. Klaus-Dietrich Kröncke, for their support and encourage, inspiring discussions and many helpful suggestions.

Furthermore, my sincere thanks go to my colleagues at the Institute of Biochemistry and Molecular Biology I for the pleasant working atmosphere, the constructive discussions and the happy time we spent together. Especially, I would like to thank Tan Tao, Ruchika, Katja, Marcel, Arun, Jennifer, David, Leonie, Anna, Lisa, and Solongo. I would also like to thank Ayse and Torsten from Clinic for Gastroenterology, Hepatology, and Infectiology as well as Anton from UCLA. My thanks also go to our technicians and secretaries, particularly, Andrea, Thomas, Tanja, Peter, and Laura, for their constant professional support. In addition, I would like to acknowledge previous lab members of AG Reichert in Frankfurt, for their valuable information and suggestions.

I would also like to express my gratitude to the Collaborative Research Center 974 "Communication and Systems Relevance in Liver Injury and Regeneration (SFB974, Düsseldorf)" supported by the German Research Foundation (Deutsche Forschungsgemeinschaft, DFG), for providing the financial support as well as helpful training for my project. My thanks also go to iGRAD/iGK for their excellent courses and workshops.

I'm also grateful for tissue samples provided by the Department of Anatomy, Heinrich Heine University Düsseldorf and the New South Wales Tissue Resource Center at the University of Sydney which is supported by the National Health and Medical Research Council of Australia, Schizophrenia Research Institute, National Institute of Alcohol Abuse and Alcoholism (NIH (NIAAA)R24AA012725).

Last but not least, my big thanks go to my parents for their tremendous sacrifice, great love as well as unselfish support throughout my life, especially during these four years, without which this journey will never be possible.

Eidesstattliche Erklärung

Die hier vorgelegte Dissertation habe ich eigenständig und ohne unerlaubte Hilfe unter Beachtung der „Grundsätze zur Sicherung guter wissenschaftlicher Praxis an der Heinrich-Heine-Universität Düsseldorf“ angefertigt. Die Dissertation wurde in der vorgelegten oder in ähnlicher Form noch bei keiner anderen Institution eingereicht. Ich habe bisher keine erfolglosen Promotionsversuche unternommen.

Ort, Datum

Unterschrift

